RNA METABOLISM AND A NEW MODE OF DEVELOPMENT IN *STREPTOMYCES*

RNA METABOLISM AND A NEW MODE OF DEVELOPMENT IN *STREPTOMYCES*

By STEPHANIE ERIN JONES, B.Sc.

A Thesis Submitted to the School of Graduate Studies in Partial Fulfilment of the Requirements for the Degree of Doctor of Philosophy

McMaster University
Hamilton, Ontario

Doctor of Philosophy
Biology

TITLE: RNA metabolism and a new mode of development in *Streptomyces*

AUTHOR: Stephanie E. Jones, B.Sc. (Syracuse University)

SUPERVISOR: Professor Marie A. Elliot

Number of pages: 159

LAY ABSTRACT

Streptomyces are soil bacteria that produce most clinically used antibiotics. Many regulatory systems control *Streptomyces* growth and antibiotic production. In all cells, molecular blueprints called DNA are converted into RNA, and RNA is converted into proteins. In this work, we investigated how RNA regulators affect *Streptomyces*. We found RNA regulators are important for antibiotic production and for the activities of protein assembly factories. It is possible to manipulate these RNA regulators to better understand how *Streptomyces* produce antibiotics. We also investigated how *Streptomyces* grow. While it had always been thought *Streptomyces* grow rooted in place like plants, we found *Streptomyces* can sometimes rapidly explore their environments. Remarkably, these 'explorer' *Streptomyces* can communicate with other bacteria using airborne signals. This work reveals new ways that bacteria can interact and communicate, and demonstrates that airborne signaling is an important language of communication in microbial communities.

ABSTRACT

Streptomyces are soil bacteria best known for their ability to produce medicinally useful compounds and for their complex life cycle. RNA processing represents a critical layer of regulatory control in bacteria, and RNA cleavage is mediated by ribonucleases (RNases). We probed the roles of RNase III and RNase J in the emerging model system *Streptomyces venezuelae*. We found both RNases impact the development and metabolism of *S. venezuelae*, and are essential for ribosome activity and assembly.

While investigating the metabolic changes associated with the RNase mutants, we made a discovery that shifted the focus of my Ph.D. work. For the past 70 years, it had been thought that *Streptomyces* grow as static colonies. We discovered that when *S. venezuelae* is grown beside yeast, *S. venezuelae* grows in a completely novel way termed 'exploration'. Exploring colonies can rapidly traverse surfaces. Remarkably, exploring colonies release an airborne volatile organic compound (VOC) that serves to induce exploration in physically separated streptomycetes. We identified the VOC as being trimethylamine (TMA), and discovered that this VOC induces *Streptomyces* exploration by raising the pH of the surrounding environment.

VOCs have important roles in influencing microbial community dynamics, and we analyzed how TMA produced by exploring *Streptomyces* impacts other soil microbes. We found TMA inhibits the growth of other microbes by raising environmental pH and altering iron availability. Exploring *Streptomyces* overcome this iron deficiency by producing siderophores, and by upregulating siderophore uptake clusters.

Streptomyces exploration is rapid, and we sought to identify the cellular factors driving exploration. Previous work has shown *Streptomyces* grow by hyphal tip extension governed by the protein DivIVA. In contrast, many rod-shaped bacteria grow using the protein MreB. We demonstrate that exploratory growth requires contributions from both DivIVA and MreB. Employing two distinct growth mechanisms in this manner is unprecedented in bacteria.

ACKNOWLEDGEMENTS

First and foremost, thank you to Marie. I had no idea what I wanted to do or what I wanted to study when I finished undergrad. I think I accidentally stumbled into your lab, and I can't believe how lucky I am to have found such a supportive supervisor. Thank you for taking a chance on me, and for letting me stay in the lab following the most embarrassing incident of my life in February 2013. Thank you also for letting me pursue this crazy project over the last few years – it was risky and maybe could have been disastrous, and you supported me endlessly in my quest to succeed. I am constantly amazed by your dedication to the work, your patience with students, your ability to multitask and remember our projects better than we remember them ourselves, and your ability to turn our failures into seemingly positive successes. Thank you also for teaching me that it's possible to succeed in work, while simultaneously being an all-around awesome, genuinely empathetic caring human. You've helped me transform from a young, naïve student into a scientist, and I am confident that everything you've taught me will be a major part of my success in my life and career moving forward.

Thank you to my committee members past and present, including Dr. Turlough Finan, Dr. Mike Surette, Dr. Joaquin Ortega, and Dr. J.P. Xu. Your guidance has been instrumental to this thesis. Thank you also to other students and professors in the IIDR. I think this institution puts every resource at our fingertips, and the collaborative environment within the institution has been one of my favourite parts of being a grad student at McMaster.

To all of my labmates past and present: thank you for making me look forward to coming into the Elliot lab every day. In particular, thank you to:

- Savannah – thank you for sharing my love of olives. You are by far the happiest-looking angry person I know. I continue to laugh over your claim: "I'm done". Thank you also for being a great bench-mate, and for supporting me whenever I suggested we go to Pancake House. I think you're awesome, and I look forward to seeing all the amazing things you do!

- Fei – you are by far the most dramatic person I've ever met. I thoroughly enjoyed your meltdown over 4-dash-H08. Thank you for continuing to amuse and perplex me with your hatred towards broccoli, your love of 1.7, and your stories about your brother. You're the senior grad student now, so I expect amazing things!

- Christine – the first student I was ever allowed to mentor! I truly feel so lucky to have been able to work with you. When I imagine the perfect student, it's you. You're so hard working, and I'm constantly amazed by how quickly you pick things up. Thank you for teaching me that I do enjoy mentoring students – it might seem like a small thing, but I think this is a lesson that will profoundly influence my career choices. Whether you go to grad school or not, I'm so excited to see what you do, and have no doubt you'll be amazing no matter what!

- Danielle – we started grad school at the same time, and it's been awesome to go through this journey with someone who can completely relate to everything I'm feeling. Thank you for venting with me, sharing similar feelings over the idea that 'maybe we should just try again tomorrow', and teaching me many things related to science and life in general.

- David – I remember when I walked into the lab on a Saturday morning and you were blasting Beyonce and Taylor Swift – that's when I knew we'd be friends. Your revelations to both Rachèle and to me will always be stuck in my mind – me standing on the freezer chair, demanding you quickly get on with your story (classic me). Thank you for many, many things. As has been said by others, thank you for delivering phrases to the world such as 'I feel like', and 'I wouldn't not' – these have all become a regular part of my dialect. Thank you also for our squash matches, which consisted of 80% chatting about our lives/judging other people walking by and our feelings, and 20% playing squash. These nights kept me sane throughout the latter half of my grad school experience. Thanks for putting my grad school social fun level on a new scale, ranging from 0.0-1.0 David. I do feel that our friendship was solidified that one fateful day in the bathroom at The Pheonix, and I will continue to use this scale throughout my life. You are truly a one of a kind human – I can say with confidence that I've never met someone who buys iced caramel macchiatos every day. On a more serious note, your friendship has brought me significant amusement and happiness throughout the past few years, and I am truly grateful we overlapped and got to develop this beautiful friendship… especially considering it's one that breaks all stereotypes about the types of people that are supposed to be friends. Now that I'm gone, you can wear sweatpants to the lab in completely and judgement-free freedom.

- Emma Sherwood – you were my benchmate and deskmate in the lab for three years, and my first true grad school mentor. I cannot thank you enough for your patience with me as I fumbled my way through trying to understand what I was doing. You once spent over an hour with me explaining what complementing a mutant means. You are an incredible teacher, and I feel so lucky to have been able to learn from you! I hope that you are continuing to wear waterproof trousers, and that you are continuing to be notty notty notty.

- Suzanne – although we only overlapped for a short time, I can say with confidence that you are one of the most brilliant, all-around A+ humans I've ever met. Thanks for courageously challenging and defeating Matt at all board games. You are going to be an amazing doctor!

- Renée – when I first met you, I was so excited because I thought there was someone else just like me in the lab! Although this didn't turn out to be the case, I'm so happy we overlapped.. Thank you for many chats over Taco Del Mar, Yogurtys and paint nights. I still don't know what many of the words you say mean – for example, 'flute'. Despite

this, you always amazed me in the lab, with your attention to detail and your technical expertise. Thank you for everything!

- Matt Moody – thank you for being an amazing human. When I first met you, I thought you were very strange because you ordered a caesar wrap with a side caesar salad. I then spent a year avoiding you because your topics of small talk included prompts such as 'plans for the weekend?' despite it being Monday, and much deeper topics such as 'do you think *Streptomyces* and Venezuelan poodle moths interact?'. Once we overcame these obstacles, I knew we were probably going to be great friends. You are the only person I know who also has a great taste in food, aka a love for Pancake House and a disdain for ketchup. Grad school can be hard, and even on the hardest days, I looked forward to coming in and seeing you. You were always so careful to not squish Goku, and you treated Rupert and Willy with the upmost respect. You also trained me in the lab… although I won't get into this because apparently we both blacked out that 6 month period of time. Thank you for teaching me that RNases are everywhere – I am afraid, very afraid. Thanks for letting me call you Mark, for being my knight in shining armour when it comes to invaders (insects) in my apartment, for making the worst dance parties my favourite nights, for teaching me to waterski, for changing my life through Avatar, for the legendary Grease karaoke performance, and for teaching me that the best ideas in science come from late night chats at PH3, not long-day library sessions. Some of the things you've done perplex me, and I want to thank you for these things because they provided me with great entertainment. For example, when you ate two jars of Nutella in one day, when you overdosed on children's gummy vitamins, and when you declared yourself 'caveman'. I think when I look back on grad school, I'll primarily remember the genius in our PH numbering system, and that I had an awesome friend who taught me many things, including how to think science and criticize science. I look forward to seeing all the amazing things you do, and to watching James blast off into space to colonize Mars in 2040.

Thank you also to my parents. You're now both able to explain my science to other people in sciencey terms, and I think this has to be a hallmark of a supportive science parent. Thank you for supporting me in all my endeavours, and celebrating my accomplishments large and small. Mom – you've expressed that research seems like so much fun, because it must be like a puzzle, where all we need to do is getting some pieces then try to understand how everything fits. On difficult days in the lab, this idea has kept me motivated. I feel so lucky to have a parent who I can talk to as a friend, and who has taught me that it's okay to speak up. I am constantly amazed by your energy and enthusiasm in the classroom. Your enjoyment of multiple careers has taught me that grad school, and whatever I do after is a labyrinth, not a ladder, where I can do whatever/whenever, as long as it feels challenging and fulfilling along the way. Dad – thank you for promoting my science by having a picture of exploring *Streptomyces* as your phone background for two years and showing it to everyone you know. Thank you for driving me to countless hours of hockey, supporting me through the challenges of April tryouts, helping me move from team to team, and generally, for just enduring the terror that is being a goalie parent. While I never would have predicted this would be the case, all those years playing

hockey translated directly into my last six years of grad school. Being a goalie is all about getting scored on, then somehow ignoring that failure, trying to maintain composure and stopping the next shot. Science is exactly the same – failure, perseverance, success. You have convinced me that I can be whatever I try to be, and more than anything, I want to thank you for being unconditionally supportive throughout my life and throughout my grad school experience.

To my brothers – thanks for showing interest in what I've been doing over the last few years. The process of grad school is much like Goku turning Super Saiyan to kill Frieza – progress is incremental and failures abound, then suddenly it's been a long time and something finally works. It's also like trying to catch 'em all, in that it's really slow and you might never fully succeed, but it's fun to try to try to make things evolve along the way. Mike, you've always been a role model to me. Your career advice has been invaluable to me as I've thought about what I want to do next. I think you're amazing, and thank you for being my favourite protective big brother. Matt, thank you for providing me with a safe space where I can act like I'm six or elleventy. I've never met a non-scientist who immediately grasps science as quickly as you do. I'm so proud of everything you're doing, and so happy to see you so passionate about your work. I have no doubt you'll crush it at whatever you do.

To Daisy – thank you for fueling much of my youth with sneaked-in Smore's flavoured Pop-Tarts, for taking interest in my work, and for inspiring me to print pages and pages of coloured photos of our favourite celebrities. Thank you also for helping train my science brain by playing hours of Tetris on Nintendo with me. You are genuinely the kindest, sweetest person I know, and I feel so lucky to know you!

Finally, thank you to my partner Rachèle – I've spent many long days in the lab talking to only bacteria, and as a result, I have often come home acting strangely or telling bizarre stories. Thank you for bringing me back down to earth. Of all the things I've done and experienced in grad school, I feel proudest and luckiest that I met you. I can't believe how well you're able to explain my project to other people – I think this is a testament to how much support you've given me over the past four years. Thank you for inspiring much of my work with the simple question: 'have you ever thought, how do *Streptomyces* just… go around?'. Thank you also for quietly listening to my rants, then laughing me back into reality. I think it's clear we bring out the best in each other, and I feel that we can accomplish anything together. I'm in love with your friends, your family and everything about our life together, and I can't wait for all the adventures ahead of us.

TABLE OF CONTENTS

LIST OF TABLES

LIST OF FIGURES

ABBREVIATIONS AND SYMBOLS

ABC	ATP-binding cassette
ACN	Acetonitrile
asRNA	Antisense ribonucleic acid
BAM	Binary alignment/map
BLAST	Basic local alignment search tool
bp	Base-pair
c-di-GMP	Cyclic-di-GMP
CAR	Carboxen
CDS	Coding sequence
CFU	Colony forming units
CHIP	Chromatin immunoprecipitation
cm	Centimeter
DMSO	Dimethylsulfoxide
DNA	Deoxyribonucleic acid
DTT	Dithiothreitol
DVB	Divinylbenzene
EMS	Ethyl methanesulfonate
FDAA	Fluorescent D-amino acid
Fe	Iron
g	Gram
G-	Absence of glucose
G+	Presence of glucose
GCxGC-TOFMS	Two-dimensional gas chromatography time-of-flight mass spectrometry
GEO	Gene expression omnibus
h	Hour
H_2O	Water
HADA	7-hydroxycoumarin-3-carboxylic acid–D-alanine
HCl	Hydrochloric acid
L	Litre
LB	Luria Bertani
LC-MS	Liquid chromatography-mass spectrometry
M	Molar
Mb	Mega base pairs
mg	Milligram
min	Minutes
mL	Milliliter
mRNA	Messenger ribonucleic acid
MS	Mass spectrometry
MSMEG	*Mycobacterium smegmatis*
MW	Molecular weight
MYM	Maltose-yeast extract-malt extract
ncRNA	Non-coding ribonucleic acid

NIST	National Institute of Standards and Technology
NRP	Non-ribosomal peptide
NSERC	National Sciences and Engineering Research Council of Canada
nt	Nucleotide
OD	Optical density
PCR	Polymerase chain reaction
PDMS	Polydimethylsiloxane
PG	Peptidoglycan
r-protein	Ribosomal protein
RBS	Ribosome binding site
RNA	Ribonucleic acid
RNA seq	RNA sequencing
RNase	Ribonuclease
rRNA	Ribosomal RNA
RT-PCR	Reverse transcription polymerase chain reaction
s	Second
S/N	Signal-to-noise
SAM	S-adenosyl methionine
SCO	*Streptomyces coelicolor*
SEM	Scanning electron microscopy
SNP	Single nucleotide polymorphism
SOB	Super optimal broth
SPME	Sold-phase microextraction
sRNA	Small ribonucleic acid
SVEN	*Streptomyces venezuelae*
TADA	TAMRA 3-amino-D-alanine/D-Lysine
TB	Tuberculosis
TCA	Tricarboxylic acid
TMA	Trimethylamine
TMAO	Trimethylamine *N*-oxide
UTR	Untranslated region
VOC	Volatile organic compound
WT	Wild type
wt/vol	Weight per volume
X-gluc	5-bromo-4-chloro-3-indolyl-beta-D-glucuronic acid
YP	Yeast extract-peptone
YPD	Yeast extract-peptone-glucose (dextrose)
λ	Lambda
µg	Microgram
µL	Microliter
σ	Sigma
β	Beta
˚C	Degrees Celsius
Δ	Delta or mutant

PREFACE

This ‘sandwich’ thesis was written following the guidelines provided by the McMaster University School of Graduate Studies. Chapter 1 provides a general introduction, Chapters 2-5 describe results, and Chapter 6 provides a general discussion and outline of future directions. Chapters 2 and 3 are each a reproduction of a manuscript previously published, and were modified to conform to the university guidelines: all figures that were supplementary in the manuscripts were renumbered as main figures. Chapter 4 represents a submitted manuscript, and Chapter 5 is unpublished work. All references were placed at the end of the thesis.

CHAPTER 1: GENERAL INTRODUCTION

1.1 Actinomycetes and the Genus *Streptomyces*

1.1.1 Actinomycetes

The actinomycetes were first observed in 1874, when Dutch physician Armauer Hansen identified the causal agent of leprosy. Three years later, the German botanist Carl Harz observed these microbes again, noting they grow as long filaments and form ray-like structures. He named these microbes *Actinomyces*, meaning "ray fungi". The classification of this group remained obscure for decades, with some believing these microbes represented an obscure group intermediate to bacteria and fungi. In 1943, the actinomycetes gained widespread attention when Selman Waksman – inspired by the discovery of penicillin and the idea that soil microbes might have evolved chemical agents to help them gain competitive advantages – found actinomycetes produce a wide array of antibiotics. In 1943, Waksman discovered actinomycetes produce streptomycin – the first effective antibiotic treatment for tuberculosis (TB). Around this time, Sir David A. Hopwood began studying a type of actinomycete called *Streptomyces*. It soon became clear that *Streptomyces* are not fungi, but are instead a unique class of filamentous, Gram-positive bacteria (Hopwood 2007).

The actinomycetes are ubiquitous in the soil, and can also be found in marine and freshwater environments. In the soil, these microbes are saprophytic, contributing to the decay and recycling of organic material (Chater, 2006). The actinomycetes are also members of the human skin and gut flora, and some are of relevance to human disease, causing tuberculosis (*Mycobacterium tuberculosis*), leprosy (*Mycobacterium leprae*), and diphtheria (*Corynebacterium diphtheriae*) (Könönen and Wade, 2015).

1.1.2 The genus *Streptomyces*

Streptomyces are a large genus within the actinomycetes. These bacteria are arguably the most medicinally important microbes, responsible for the production of ~two thirds of clinically used antibiotics, as well as a number of compounds with antifungal, anticancer, immunosuppressant, and herbicidal properties. These compounds are collectively termed 'specialized metabolites' (Hopwood, 2007). Humans have been mining *Streptomyces* for these products since the 1940's. Remarkably, it seems there is much left to be discovered: genomic analyses have revealed each *Streptomyces* species encodes 20-40 distinct specialized metabolites, far more than the number of compounds identified to date (Nett et al., 2009; Yoon and Nodwell, 2014). For example, the best-studied streptomycete species is *Streptomyces coelicolor* A3(2). Researchers initially identified four clusters involved in antibiotic production. In 2002, the complete genome was sequenced, and this revealed that *S. coelicolor* encodes 24 additional specialized metabolite clusters (Bentley et al., 2002). Unlike most other bacteria, *Streptomyces* have a large (~8 Mb), high GC (~72%) linear chromosome. The majority of genes involved in primary metabolism and viability are located in the chromosome core, while the majority of clusters encoding

specialized metabolites are located in the two flanking chromosome arms (Bentley et al., 2002; Ikeda et al., 2003). The activation of these 'cryptic' clusters represents a major focus for microbiology, and it is expected that the stimulation of these clusters could lead to the identification of novel products critical in combating the global emergence of antibiotic resistant pathogens.

1.2. *Streptomyces* growth and development

1.2.1 The *Streptomyces* life cycle: an overview

In addition to their massive antibiotic production potential, *Streptomyces* have a complex life cycle that is more similar to a fungus than a unicellular bacterium (Elliot et al., 2008) (**Fig. 1.1**). Specific stages of the *Streptomyces* life cycle are coordinated with the production of specialized metabolites. This life cycle has been studied since the 1950s, and key metabolic cues and regulators underlying the *Streptomyces* developmental programme have been identified. The *Streptomyces* life cycle initiates when germ tubes emerge from a single spore. These germ tubes extend by polar growth at the hyphal tips, and additional branches emerge from the lateral walls at random intervals. Continuous cycles of hyphal tip extension and branching result in the formation of a dense network of filamentous cells termed the vegetative mycelium, or the 'substrate hyphae'. This mycelial network anchors the colony in place, similar to the way a plant root system anchors a plant in the soil. As the vegetative colonies age, or in response to nutrient depletion, a second filamentous cell type is produced termed the 'aerial hyphae'. These non-branching hyphae are coated in a hydrophobic sheath, and rise into the air away from the vegetative mycelium. Aerial hyphae formation generally coincides with the production of specialized metabolites, and it is thought that these metabolites could serve as defenses against other microbes in nutrient-limited environments. Once aerial hyphal growth ceases, each multigenomic hyphal filament undergoes a round of septation that serves to divide them into 40-60 equally sized, unigenomic "prespore" compartments. Each compartment undergoes a series of maturation steps, eventually forming mature spores coated with coloured polyketide pigments. Finally, spores can be dispersed to begin the life cycle anew (Elliot et al., 2008; Flärdh and Buttner, 2009; McCormick and Flärdh, 2012).

Streptomyces developmental regulators fall into two major categories (**Fig. 1.1**). The transition from vegetative growth to aerial hyphae formation requires a group of regulators termed the '*bld*' genes – named because *bld* mutants have a 'bald' colony phenotype. The transition from aerial hyphal growth to sporulation requires regulators termed the '*whi*' genes, as *whi* mutants are often white and lack the pigment associated with mature spores. In the past few decades, significant progress has been made in unravelling how these regulators govern the transitions from vegetative hyphae to aerial hyphae, and from aerial hyphae to spores.

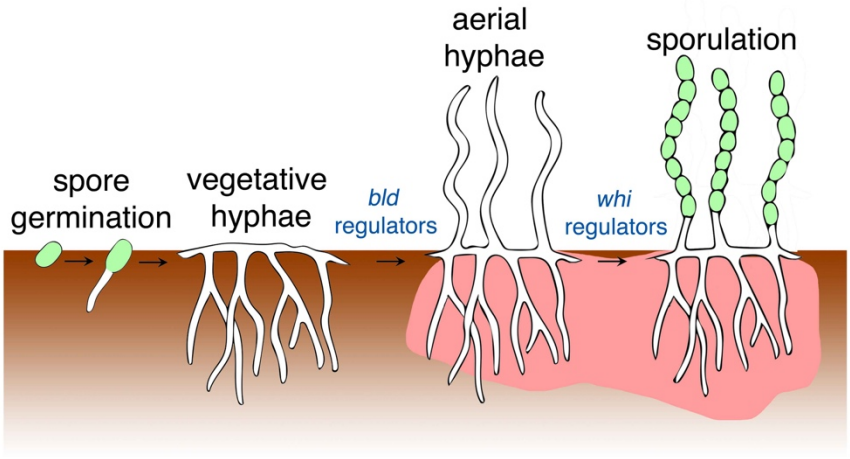

Fig. 1.1 The *Streptomyces* life cycle. Spores germinate, and germ tubes extend by hyphal growth at the hyphal tips. As the hyphae extend, branches emerge, forming a dense network of branching vegetative hyphae. When nutrients become depleted, aerial hyphae coated in a hydrophobic sheath rise into the air, away from the vegetative mycelium. Aerial hyphae continue growing by apical tip extension. The formation of aerial hyphae is associated with specialized metabolite production (pink). Once aerial hyphal growth ceases, the hyphae differentiate into long chains of spores coated in polyketide spore pigments. The *bld* gene products are required for the transition from vegetative hyphae to aerial hyphae, and the *whi* gene products are required for the differentiation of aerial hyphae into spores.

1.2.2 Vegetative growth

Streptomyces vegetative hyphae grow by tip extension and branching, and new cell wall material is incorporated exclusively at hyphal tips. This pronounced apical growth is strikingly different from growth mechanisms in the rod-shaped bacteria *Escherichia coli* and *Bacillus subtilis*. For these model organisms, cell elongation is coordinated by the bacterial actin homolog MreB (Cabeen and Jacobs-Wagner, 2005; Jones et al., 2001; Shi et al., 2018) (**Fig. 1.2**). Peptidoglycan (PG) synthesis machinery drives the rotation of curved MreB filaments along the long axis of cells (Domínguez-Escobar et al., 2011; Garner et al., 2011; van Teeffelen et al., 2011). In turn, MreB directs the insertion of new cell wall material along the lateral walls of cells. MreB is essential for the rod shape of microbes; MreB perturbations result in spherical cells (Kawai et al., 2014). Gram-negative bacteria typically possess one *mreB* gene, while Gram-positive bacteria usually encode three MreB-like proteins sharing >50% similarity (Shi et al., 2018). While most actinomycetes lack MreB homologs, *Streptomyces* are the exception. All streptomycetes sequenced to date contain at least two *mreB* genes. However, studies have shown these MreB homologs have no impact on vegetative growth or tip extension, and seem

to be primarily involved in the late stages of aerial hyphae development and in spore maturation (Heichlinger et al., 2011; Mazza et al., 2006).

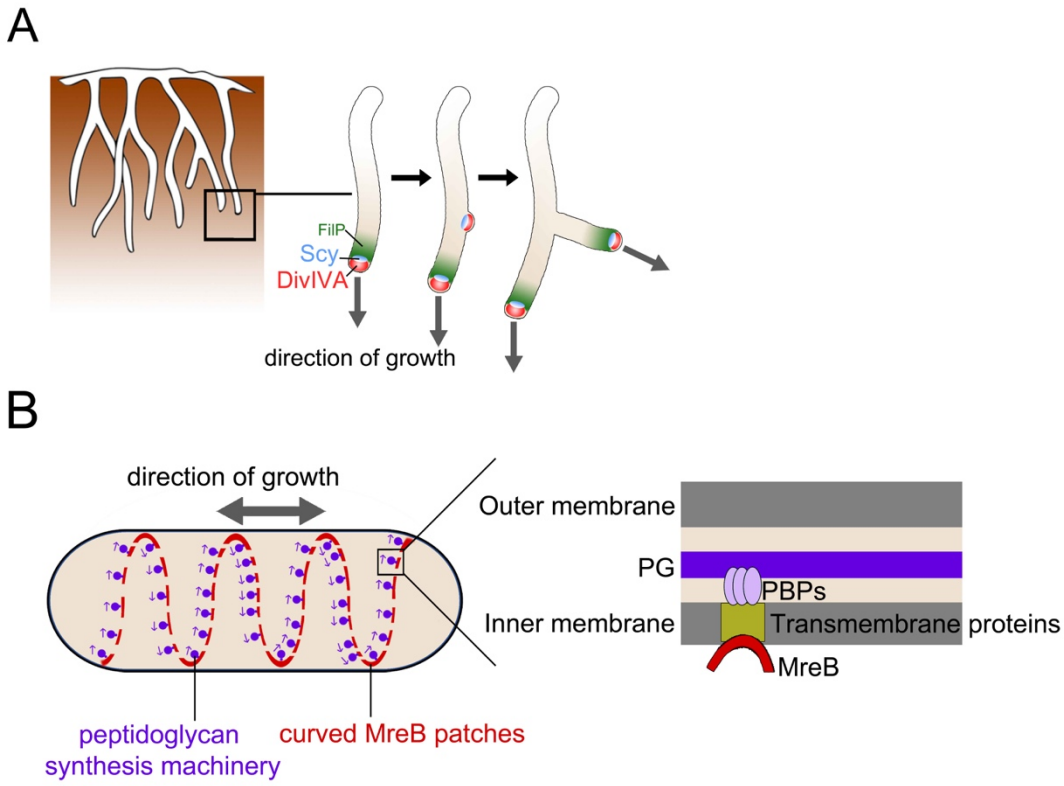

Fig. 1.2 Cell elongation strategies. A. *Streptomyces* vegetative hyphae grow by tip extension and branching. This polar mode of growth is directed by a complex termed the polarisome. DivIVA (red) recruits cell wall biosynthetic machinery, and directs peptidoglycan synthesis at the tips and at new branch points. Scy (blue) colocalizes with DivIVA, possibly assisting in polarisome assembly. FilP (green) localizes behind the polarisome, and may provide structural support for the polarisome. **B.** In contrast to *Streptomyces*, rod-shaped bacteria grow along the lateral walls using the actin-like filament MreB. Curved MreB filaments (red lines) move along the cell circumference, and MreB motion is guided by peptidoglycan synthesis machinery (purple circles). MreB filaments (red) bind the inner surface of the cytoplasmic/inner membrane through the transmembrane proteins RodA, RodZ, MreC, and MreD (yellow square). These transmembrane proteins are bound to penicillin-binding proteins (PBPs, purple circles), which are involved in peptidoglycan (PG) synthesis.

In contrast to *E. coli* and *B. subtilis*, MreB-independent apical growth in *Streptomyces* is directed by a complex called the polarisome (**Fig. 1.2**). This complex consists of the coiled-coil proteins DivIVA and Scy. DivIVA recruits cell wall machinery to hyphal tips and directs the insertion of PG (Flärdh, 2003; Hempel et al., 2008). Scy colocalizes with DivIVA, perhaps serving as a molecular

scaffold that facilitates polarisome assembly. The intermediate filament FilP localizes behind DivIVA, forming a network-like structure that may provide mechanical support for the polarisome (Holmes et al., 2013). To date, DivIVA is the only polarisome protein that is essential for *Streptomyces* viability. DivIVA depletion results in slowed growth, and DivIVA overexpression leads to hyperbranching (Flärdh, 2003). Polarisome dynamics are regulated by the Ser/Thr protein kinase AfsK, which localizes to hyphal tips, and phosphorylates DivIVA to initiate polarisome disassembly (Hempel et al., 2008) In addition to tip extension, DivIVA governs hyphal branching in vegetative hyphae. As apical tips grow, the polarisome splits to form a small daughter tip complex that is left behind at the membrane (Richards et al., 2012). This complex grows in size, ultimately driving the formation of a new branch point. Intriguingly, rod-shaped actinomycetes including *Corynebacterium* and *Mycobacterium* also grow using DivIVA-mediated mechanisms, indicating polar growth is an actinomycete-specific, rather than hyphae-specific, growth phenomenon (Surovtsev and Jacobs-Wagner, 2018).

While the factors regulating of the expression of MreB and the polarisome components are mostly unknown, other *Streptomyces* regulatory pathways are well established. The regulator BldD sits at the top of the *Streptomyces* developmental regulatory network, repressing ~170 genes during vegetative growth (Elliot et al., 2001; den Hengst et al., 2010). The second messenger cyclic-di-GMP (c-di-GMP) coordinates BldD dimerization, enabling BldD to bind its target genes (Tschowri et al., 2014). BldD targets include other *bld* regulators (σ^{bldN}*, bldM, bldH/adpA, bldA* and *bldC*), *whi* regulators (*whiA, whiB* and *whiG*), and other genes encoding components of the chromosome replication/segregation machineries involved in sporulation (Elliot et al., 2001; den Hengst et al., 2010). BldD essentially functions as a molecular 'brake', repressing genes whose products are required for the transition from vegetative to aerial hyphae. Also within the vegetative mycelium, the regulator BldM forms homodimers to activate expression of the sporulation regulator WhiB (Al-Bassam et al., 2014). When c-di-GMP levels fall and BldD-mediated repression is relieved, other Bld regulators activate genes required for *Streptomyces* to raise aerial hyphae. BldH and BldA mediate the production of the surfactant SapB, and BldN activates the expression of *bldM* and the *chp* and *rdl* genes.

1.2.3 Aerial hyphae growth

In response to nutrient depletion, *Streptomyces* enter their second stage of development. Non-branching aerial hyphae rise away from the vegetative mycelium and grow into their air. These hyphae are coated in a hydrophobic sheath consisting of three proteins: the 'chaplins', the 'rodlins' and SapB. In particular, the chaplins and SapB have surfactant properties that enable these non-branching hyphae to break the surface tension of the medium and grow into the air (Claessen et al., 2003; Elliot et al., 2003; Kodani et al., 2004; Tillotson et al., 1998). The chaplins contribute to aerial hyphae formation on both minimal and rich media, while SapB only functions during growth on rich medium (Capstick et al., 2007). Like vegetative hyphae, aerial hyphae grow by DivIVA-mediated tip extension (Ditkowski et al., 2013). Within the aerial hyphae, the regulator BldO represses the expression of *whiB*. When this repression is relieved (through an unknown mechanism), the heterodimer WhiB-WhiA and activates other genes necessary for the formation of prespore compartments (Bush et al., 2017). Aerial hyphae then

terminate extension and undergo synchronized septation, marking the entry into the final stage of *Streptomyces* development.

1.2.4 Sporulation

Once the aerial hyphae divide by a developmentally controlled form of cell division, pre-spore compartments are formed (Willemse et al., 2011; Zhou et al., 2016). A single hypha can contain up to 50 pre-spore compartments. Spore wall formation is associated with the thickening of the wall from 10-12 nm to 30-50 nm (McVittie, 1974). MreB plays a central role in spore wall assembly. In *S. coelicolor, mreB* mutants produce defective, heat-sensitive spores with abnormally thin spore walls (Heichlinger et al., 2011; Mazza et al., 2006). This MreB requirement for spore wall assembly may explain why other, non-sporulating actinomycetes lack this actin homolog. Mature spores are largely dormant, and can be dispersed by physical forces, like wind or other organisms. When individual dormant spores encounter favourable growth conditions, they can germinate, initiating a new round of the *Streptomyces* life cycle.

1.2.5 Chromosome segregation and cell division throughout the *Streptomyces* life cycle

Streptomyces chromosome segregation is coordinated by various factors throughout vegetative growth, aerial hyphae development, and sporulation. Chromosomes replicate throughout vegetative growth, and multinucleate hyphae are subdivided by occasional crosswalls (Kois-Ostrowska et al., 2016). The ATPase ParA localizes to the tips of aerial hyphae and forms helical filaments along the length of hyphae. ParA promotes the accumulation of nucleoprotein complexes by ParB (Donczew et al., 2016). Scy recruits ParA to the tips of aerial hyphae as sporulation is initiated, providing a potential link between the end of aerial hyphae extension and the segregation of chromosomes into spores (Ditkowski et al., 2013). Sporulation septation is coordinated by the bacterial tubulin homolog FtsZ. FtsZ polymerizes to form helical filaments along the length of the aerial hyphae, and these filaments are then remodeled into rings that are regularly distributed between chromosomes. Positioning of FtsZ is thought to depend on the sporulation proteins SsgA and SsgB (Traag and van Wezel, 2008; Willemse et al., 2011). As sporulation septa form, dividing aerial hyphae into unigenomic spores, the DNA translocase FtsK is targeted to division sites to clear DNA from the closing septa (Wang et al., 2007). The nucleoids then condense as the spores mature.

1.2.6 *Streptomyces venezuelae*: a new model species

Most of the foundational work on *Streptomyces* development was conducted using *S. coelicolor*, a species that fully differentiates on solid medium but not in liquid culture. *S. coelicolor* produces the pigmented antibiotics actinorhodin and undecylprodigiosin, facilitating the easy tracking of antibiotic outputs throughout the *Streptomyces* life cycle and in response to genetic perturbation (Hopwood, 2007). On solid medium, aerial hyphae constitute only ~10% of the colony mass, and these cells cannot be effectively separated from vegetative hyphae or spores. This colony organization has made the study of individual, differentiated *S. coelicolor* life cycle stages challenging (Chater, 2016). In recent years, studies on the growth and

development of streptomycetes have shifted to the species *Streptomyces venezuelae*. Like *S. coelicolor*, *S. venezuelae* undergoes its full life cycle on solid medium, but it also sporulates in liquid culture. For *S. venezuelae*, growth in liquid cultures commences with spore germination, and is followed by mycelial branching (vegetative growth), fragmentation of mycelial clumps, and conversion of these fragments into spore chains. The transitions from mycelial branching to fragmentation, and from fragmentation to sporulation are relatively synchronous, enabling researchers to more easily isolate individual cell types. For example, this isolation of cell types has facilitated the application of chromosome immunoprecipitation sequencing (ChIP-seq) experiments and RNA sequencing (RNA seq) experiments in identifying the factors underlying individual life cycle stages and the function of those regulators controlling the transitions between these stages (Al-Bassam et al., 2014; Bibb et al., 2012; Bush et al., 2013, 2017). This has led to significant progress in our understanding of the pathways governing *Streptomyces* development over the last 5-10 years.

In addition to sporulating in liquid cultures, *S. venezuelae* grows significantly faster (~48 hours to sporulation) than *S. coelicolor* (~5 days to sporulation). Although *S. venezuelae* does not produce coloured antibiotics, it produces the brown-pigmented specialized metabolite melanin throughout vegetative and aerial hyphae growth. *S. venezuelae* was first isolated from a mulched field in Venezuela in 1947, and researchers quickly discovered that *S. venezuelae* produces a broad-spectrum antibiotic (effective against Gram-positive and Gram-negative bacteria), which is now known to be chloramphenicol (Ehrlich et al., 1948). Chloramphenicol was the first antibiotic to be artificially synthesized on a large scale for clinical use. Although therapeutic use of chloramphenicol has declined due to its potentially adverse side effects, it remains on the World Health Organization's List of Essential Medicines. A recent study revealed that *S. venezuelae* produces chloramphenicol in the soil, although its production is not typically observed under laboratory conditions (Berendsen et al., 2013). In addition to chloramphenicol, *S. venezuelae* produces a group of angucycline natural products known as the jadomycins. These compounds have demonstrated antibacterial, antitumor, antifungal and anticancer activities. Jadomycin production takes place in nutrient-deprived, amino acid rich medium, and is induced by phage infection, ethanol shock or temperature shifts (Doull, 1993; Doull et al., 1994; Dupuis et al., 2011; Jakeman et al., 2006, 2009; S Brooks et al., 2012). In addition to chloramphenicol and jadomycin, *S. venezuelae* encodes 28 other specialized metabolite clusters across its 7.8 Mb linear chromosome. These clusters have a range of bioinformatically predicted products, including siderophores, terpenes, lantipeptides, butyrolactones, polyketides, and nonribosomal peptides (NRPs).

1.3 RNA metabolism

1.3.1 RNA metabolism in bacteria

Streptomyces development and specialized metabolism are subject to multiple layers of regulatory control, including DNA binding regulators (e.g. BldD), and post-translational modifications (e.g. DivIVA phosphorylation by AfsK). Post-transcriptional regulation likely also plays critical roles in the control of *Streptomyces* growth and metabolism. In bacteria, the

processing and decay of RNA transcripts allows cells to rapidly respond to changing environmental conditions, ensures they are able to produce appropriate levels of proteins, and enables energy conservation by helping to promote the recycling of ribonucleotides. RNA stability is controlled by proteins termed ribonucleases (RNases). There are two main classes of RNases: endoribonucleases, which cleave directly within RNA transcripts, and exoribonucleases, which attack the 5′ or 3′ ends of RNA transcripts. Different RNases cooperate to control RNA processing and degradation, and different bacteria employ distinct RNases (Durand and Condon, 2018; Mohanty and Kushner, 2016, 2018). RNA metabolism has been most extensively studied in *E. coli* and *B. subtilis*. In *E. coli*, the enzyme responsible for the majority of RNA metabolism is RNase E. This enzyme is the central component of a multiprotein complex termed the RNA degradosome (Mackie, 2013). *B. subtilis* lacks RNase E, and instead, the major enzyme responsible for RNA processing is the endonuclease RNase Y, which acts alongside the dual endo-/5′-3′ exonuclease RNase J1/J2 (Lehnik-Habrink et al., 2012; Shahbabian et al., 2009). All bacteria contain at least one of RNase E, RNase Y, or RNase J (Condon and Putzer, 2002). All of these enzymes are single strand-specific endonucleases with a preference for AU-rich sequences. These enzymes are, however, unrelated in primary sequence, and they therefore represent an impressive case of convergent evolution, and emphasize the importance of RNA processing in bacteria.

In addition to mRNA turnover, bacterial RNases also regulate the stability, processing and degradation of ribosomal RNA (rRNA) transcripts (Deana and Belasco, 2005; Hui et al., 2014) (**Fig. 1.3**). Precise rRNA processing is critical for the formation of fully functioning ribosomes. Assembled ribosomes contain 23S rRNA in the 50S subunit, and 16S and 5S rRNA in the 30S subunit. rRNA is initially transcribed as one long transcript, and individual 23S, 16S and 5S rRNA species must be liberated, processed and assembled with the appropriate ribosomal proteins (r-proteins). The double-strand-specific enzyme RNase III initially cleaves conserved stem-loop structures to release pre-16S (17S), pre-23S, and pre-5S rRNA transcripts. Combinations of other RNases, many of which remain to be identified, cleave the remaining 5′ and 3′ sequences flanking pre-rRNA species, producing mature 16S, 23S, and 5S rRNA transcripts.

1.3.2 RNA metabolism in *Streptomyces*

Streptomyces are unusual in that they contain both RNase E (known as RNase ES in *Streptomyces*) and RNase J, the key enzymes controlling RNA metabolism in *E. coli* and *B. subtilis*, respectively. This raises questions as to how these enzymes with similar substrate preferences cooperate throughout the *Streptomyces* life cycle in mRNA and rRNA metabolism. A number of studies have examined the roles of RNases in *Streptomyces* species. RNase III affects ~10% of transcripts during vegetative growth in *S. coelicolor* (Gatewood et al., 2012), and impacts antibiotic production and sporulation in *S. coelicolor*, *Streptomyces antibioticus*, and *Streptomyces lividans* (Lee et al., 2013; Price et al., 1999; Sello and Buttner, 2008). RNase J had dual endo/exonuclease activity in *S. coelicolor*, and is required for normal antibiotic production (Bralley et al., 2014). RNase ES interacts with the exonuclease PNPase, raising the possibility that these enzymes constitute part of the *Streptomyces* RNA degradosome (Hagège and Cohen, 1997; Lee and Cohen, 2003). The precise targets of RNase J and RNase E have not

been mapped, and the key players in rRNA processing remain largely unidentified. Given the complexity of the *Streptomyces* life cycle, it is expected that RNase activity, both in facilitating stable RNA processing and controlling mRNA metabolism, plays critical roles in development and specialized metabolite production.

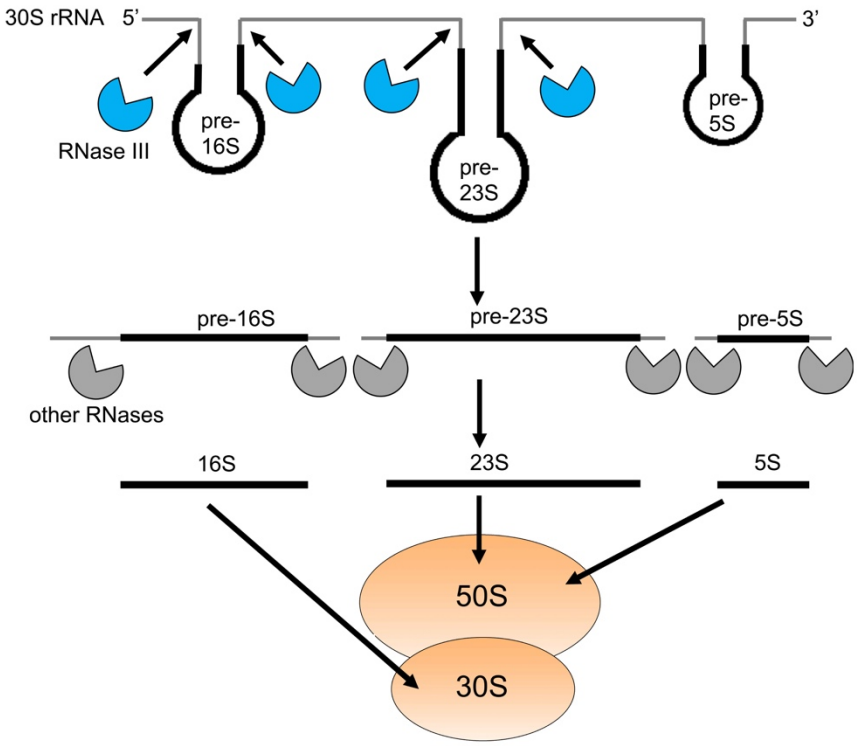

Fig. 1.3 rRNA processing in bacteria. rRNA is transcribed as one long 30S transcript containing pre-16S, pre-23S, and pre-5S rRNA species. rRNA is initially cleaved at the base of stem loops by the double-strand-specific enzyme RNase III. Pre-rRNA species are then further processed by other RNases. Mature 16S rRNA is part of the 30S ribosomal subunit, while mature 23S and 5S rRNA are part of the 50S ribosomal subunit. Note: rRNA forms complexes with ribosomal proteins throughout the rRNA processing steps.

1.4 Microbial interactions and communities

1.4.1 Interspecies interactions

The unusual life cycle, remarkable metabolic capabilities, and complex regulatory inputs of *Streptomyces* have likely evolved due to the selective pressures applied by the environment and competition with other organisms in the soil. Diverse communities of microbes exist in virtually every ecological niche, and microbial interactions can profoundly influence the behaviour and survival of bacteria and fungi. The soil plays host to a rich diversity of bacteria and fungi; a single gram of soil contains ~10^9 bacteria, 10^6 fungi, and millions of other eukaryotic organisms (Traxler and Kolter, 2015). It is hypothesized that interspecies interactions and responses to neighboring microbes are among the primary driving forces of microbial evolution, shaping the way microbes develop defense/survival mechanisms and competition strategies within their environments (Mitri and Foster, 2013). Bacteria and fungi have evolved both symbiotic and antagonistic interaction strategies, and the resulting interaction networks have been well studied from evolutionary perspectives. Interspecies interactions can be achieved through chemical warfare (*e.g.* via antibiotic and antifungal compounds), through the use of chemicals as signaling molecules, through direct contact (*e.g.* via protein secretion systems), and through localized nutrient depletion (Peleg et al., 2010; Wargo and Hogan, 2006). Several groups have studied the interactions of *Streptomyces* with other streptomycete species as well as other microbes, primarily with the goal of mimicking soil conditions to induce specialized metabolite production (Abrudan et al., 2015; Kolter, 2012; Traxler and Watrous, 2013). Outside of the soil, an increasing number of reports have described interkingdom interactions that influence the virulence of human pathogens. For example, both *Pseudomonas aeruginosa* and *Staphylococcus aureus* modulate the morphology and virulence of the human pathogen *Candida albicans* (Baena-Monroy et al., 2005; Morales et al., 2013). In addition to specific interaction responses, microbial interactions can also shape larger group behaviours. Interaction types – neutralism, commensalism, competition, and mutualism – determine bacterial spatial colony structures, and influence the spatial order of species within architecturally complex biofilms (Blanchard and Lu, 2015). We have only begun to appreciate the consequences of microbial interactions, and it is expected more research into microbial social environments will reveal novel bacterial and fungal behaviours.

1.4.2 Volatile organic compounds in microbial communities

Microbial modification of an environment can be achieved through the release of specialized metabolites or airborne volatile organic compounds (VOCs). The majority of studies on interspecies interactions to date have focused on the effects of specialized metabolites. However, these compounds have relatively short diffusion ranges. In contrast, VOCs are low-molecular-weight compounds capable of rapidly diffusing through air and water pockets, particularly within heterogeneous soil environments (Schmidt et al., 2016). Bacteria and fungi produce a plethora of VOCs having enormous chemical diversity. There is a growing appreciation for the roles of VOCs in microbial communities, and this topic has been the subject

of a number of recent reviews (Avalos et al., 2018; Bos et al., 2013; Farag et al., 2017; Insam and Seewald, 2010; Kai et al., 2009; Schmidt et al., 2015, 2016). VOCs can act as chemical weapons by directly acting as antibacterial or antifungal agents. Additionally, VOCs can mediate microbial competition by altering the sensitivity of bacteria to antibiotics. For example, biogenic ammonia produced by *E. coli* altered the resistance profiles of *P. aeruginosa*, *B. subtilis*, and *S. aureus* to tetracycline, ampicillin and various aminoglycosides through diverse mechanisms (Bernier et al., 2011). Other VOCs can act as infochemicals, mediating positive or neutral interspecies responses. VOCs have been reported as having roles in inducing broad responses in microbial gene expression, changing environmental conditions (*e.g.* pH and nutrient availability), triggering germination, and inducing various changes in microbial behaviour (*e.g.* altering morphology, motility, virulence) (Wheatley, 2002).

The best known *Streptomyces* VOC is geosmin, which is a compound that confers moist soils with a rich, earthy-odour (Gust et al., 2002; Hopwood, 2007). In addition to geosmin, *Streptomyces* produce a diverse array of VOCs. Schöller et al. (2002) screened 26 *Streptomyces* species and identified 120 VOCs. Included amongst these were alkanes, alkenes, esters, alcohols, ketones, sulfur compounds and isoprenoid compounds (Schöller et al., 2002). A 2015 study screened 12 *Streptomyces* species from various types of soil, and identified 536 additional VOCs (Cordovez et al., 2015). This work revealed some of these VOCs have potential antifungal and plant growth promoting properties. While the roles of the vast majority of microbial VOCs remain unidentified, it is clear that these compounds can influence microbial community dynamics. The roles of VOCs in mediating *Streptomyces* interspecies interactions – and perhaps in stimulating *Streptomyces* specialized metabolite production – will be interesting areas for future investigations.

1.4.3 Bacterial surface translocation

An interesting and effective bacterial response to competition with other organisms is movement away from these interactions, and/or towards more hospitable growth environments. Many bacteria have the ability to move in liquid and across surfaces using behaviours collectively known as motility. Within microbial communities, motility allows bacteria to scavenge for nutrients, migrate to optimal environments through chemotaxis or random tumbles, colonize new niches, and avoid toxic compounds (Harshey, 2003). Bacteria have developed diverse mechanisms of motility (**Fig. 1.4**). Broadly, motility can be divided into two categories: appendage-dependent (requiring flagella or pili) or appendage-independent. There are three known mechanisms of appendage-dependent motility. Swimming is the movement of individual bacterial cells in liquid, and is driven by rotating flagella. Swarming is the multicellular movement of bacteria across surfaces, also driven by rotating flagella. Twitching is the individual movement of bacterial cells across a surface, powered by the continuous extension and retraction of pili. In general, appendage-dependent motility has been well-studied, and the appendages driving these active forms of motility share high sequence similarity, even between distantly related bacteria (Jarrell and McBride, 2008; Kearns, 2010).

Appendage-independent motility includes gliding and sliding. In contrast to the conserved nature of the appendages shared by swimming, swarming and twitching bacteria, sliding and gliding bacteria share few traits beyond a common phenotype. Gliding motility is active surface movement. Recent work has shown diverse mechanisms underlie gliding motility in different bacteria. For example, *Flavobacterium* motility is driven by the proton motive force generated through ATP-binding transporters (Hoiczyk, 2000), while *Myxococcus xanthus* motility is powered by polysaccharide slime trails and propulsion by focal adhesion complexes (Faure et al., 2016; Fu et al., 2018; Mignot and Zusman, 2007), and *Mycoplasma* motility is drive by ATP-powered surface proteins that power inchworm-like movements across surfaces (Miyata and Hamaguchi, 2016). Sliding motility is phenotypically similar to gliding motility, but is defined as a passive form of multicellular surface translocation, powered by growth and facilitated by reduced friction between cells and surfaces. This reduced friction is achieved by unique surface properties of cells, such as glycopeptidolipids protruding from cell envelopes, or by secreted surfactant molecules. Sliding motility allows groups of cells to passively slide away from the colony centre, often resulting in the formation of elaborate colony wrinkles (Shroud, 2015). Like gliding motility, diverse mechanisms underlie sliding in different bacteria. Sliding has been described for *E. coli*, *Legionella pneumophila*, *Mycobacterium* species*, Pseudomonas* species, *Sinorhizobium meliloti*, *S. aureus*, *Vibrio* species, and *Bacillus* species. Genes contributing to sliding have been identified in each of these bacteria, but these are not homologous, and different environmental cues trigger sliding in each species (Shrout, 2015). These observations have raised questions as to whether sliding bacteria are all doing the same activity using different mechanisms, or whether various types of sliding should be classified.

Unlike many other bacteria, *Streptomyces* lack flagella and pili, and *Streptomyces* gliding motility has not been observed. Instead, *Streptomyces* exploit their environments using fungal-like hyphal filaments that extend into the surroundings to scavenge for nutrients. These mycelial networks are non-motile, and it has long been thought that spore formation is the sole means of dispersal or ‘movement’ to new environments.

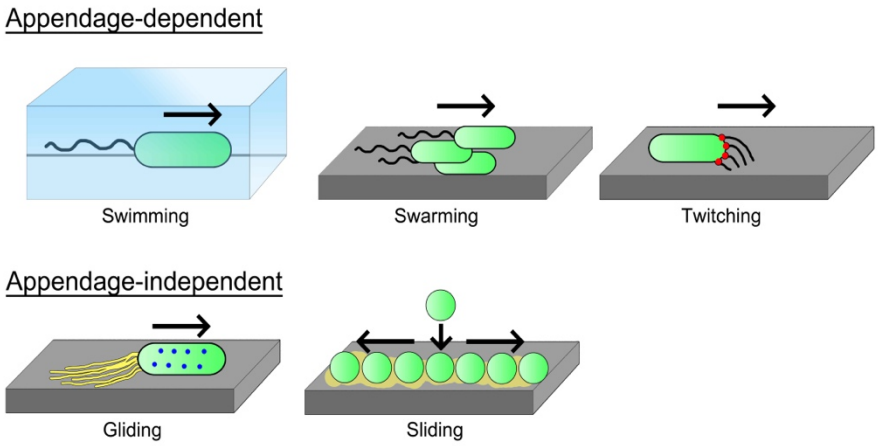

Fig. 1.4 Types of bacterial motility. The direction of cell movement is indicated by black arrows. Swimming is a unicellular movement through liquids, powered by flagella. Swarming is multicellular movement across a surface powered by flagella. Twitching is surface movement powered by continuous pili extension and retraction. Gliding is active surface movement powered by the rotation of focal adhesion complexes (blue dots), and facilitated by polysaccharide slime trails (yellow). Sliding motility is passive surface translocation, and is driven by growth from the centre and often facilitated by a surfactant (yellow).

1.5 Iron and microbes

1.5.1 Iron and bacteria

Motility is thought to have evolved as a means for bacteria to scavenge for essential nutrients, including iron. Iron is crucial for cellular processes including DNA replication, protein synthesis, and cellular respiration, and yet, the acquisition of iron poses major challenges. Although iron is the fourth most abundant element on Earth, the bioavailability of soluble ferrous iron (Fe^{2+}) in terrestrial environments is remarkably low. In most aerobic aqueous environments, iron exists in its insoluble ferric form (Fe^{3+}) (Lambert et al., 2014). To meet these challenges, bacteria have developed strategies to acquire poorly soluble Fe^{3+}. Most microbial genomes contain genes encoding specialized metabolites termed siderophores. Siderophores are among the strongest binders of Fe^{3+}, with some being used clinically to remedy iron overload in blood (Holden et al., 2015). Microbes secrete these high-affinity iron chelators into their surrounding environments, where they capture poorly soluble Fe^{3+}. Iron binding alters siderophore conformation, and this change in shape allows siderophores to be recognized and taken up by cells with appropriate siderophore membrane receptors. Once inside cells, siderophores reduce Fe^{3+} to biologically useful Fe^{2+}, and the reduced iron is released into the cytoplasm.

Siderophores can be divided into three major groups based on the chemical groups involved in iron binding: hydroxamates, catecholates, and carboxylates. Each group has distinct characteristics that affect iron binding affinity (Holden and Bachman, 2015). Most bacterial siderophores are catecholates, and these siderophores have the highest ferric iron affinity. Catecholates and hydroxamates are commonly produced by bacteria living in neutral to alkaline environments, whereas carboxylates are more common in bacteria living in acidic environments (McMillan et al., 2010). Bacteria typically encode multiple types of siderophores, and it is thought that this evolved as a means of adaptation to different environments. Intriguingly, some bacterial and fungal species are able to take up siderophores they do not produce. When this type of siderophore sharing occurs between cells of the same genotype, it is considered to represent microbial cooperation, or the sharing of public goods. However, it is also possible for strains to take up siderophores produced by another species. This strategy – where 'cheater' genotypes use siderophores without making them – is termed siderophore piracy (Traxler et al., 2012). Recent work has argued that siderophore production and uptake/piracy dynamics have critically influenced interspecies interactions in iron-limited environments (Niehus et al., 2017).

Iron acquisition influences bacterial and fungal growth in a wide range of environments. Many studies on iron acquisition have focused on the roles of siderophores in pathogens, both within the soil and the human body. For example, in the rhizosphere, *Pantoea stewartii* subsp. *Stewartii*, the causal agent of Stewart's wilt of sweet corn, produces siderophores under low iron conditions (Burbank et al., 2015). Siderophore production inhibits virulence, indicating active iron acquisition is essential for the pathogenic fitness of this plant pathogen. In the human body, for the pathogen *P. aeruginosa*, iron concentrations have the opposite effect: high iron concentrations promote biofilm formation, and low iron concentrations promote surface motility (Patriquin et al., 2008). The role of iron on various other human pathogens have been studied, including *Campylobacter jejuni*, *Helicobacter pylori*, *Shewanella* species, and *L. pneumophila* (Butcher and Stintzi, 2013; Chatfield and Cianciotto, 2007; Marsili et al., 2008; Miles et al., 2010). It appears that the ability to obtain iron has diverse effects on the morphology and survival of each pathogen, and it is clear that iron acquisition is a critical determinant of pathogen virulence.

In most bacteria, the iron starvation response is coordinated through DNA binding regulators. In high iron environments, these regulators bind and repress siderophore production/uptake genes. As intracellular iron concentrations fall, these regulators relieve repression of target genes, and siderophore production/uptake genes are expressed (Helmann, 2014). In Gram-negative bacteria and AT-rich Gram-positive bacteria, the ferric uptake regulatory (FUR) protein is the central regulator of iron homeostasis (Baichoo et al., 2002). In GC-rich Gram-positive bacteria including the actinomycetes, DtxR (diphtheria toxin repressor, named after the toxin produced by *Corynebacterium diphtheriae*) regulates responses to iron concentrations (Schmitt and Holmes, 1991).

1.5.2 Iron and *Streptomyces*

Streptomyces development and morphology are affected by iron availability and siderophore production. In environments where there is intense competition for iron, *S. coelicolor* vegetative colonies cannot raise aerial hyphae or form spores. For example, the actinomycete *Amycolatopsis sp.* AA4 inhibits aerial hyphae formation in *S. coelicolor* by secreting the siderophore amychelin, and by pirating siderophores produced by *S. coelicolor*, essentially imposing a severe iron deficiency on *S. coelicolor* (Traxler et al., 2012). Similarly, *Streptomyces* mutants unable to produce siderophores are unable to initiate aerial development (Lambert et al., 2014; Traxler et al., 2012). This phenotypic defect can, however, be rescued when *S. coelicolor* is grown near *Penicillium* species and *Engyodontium album* (Arias et al., 2015). Siderophores produced by these fungi could be taken up by *S. coelicolor* siderophore mutants. These studies suggest that *Streptomyces* can be both affected by and contribute to siderophore piracy, and suggest wide-ranging ramifications stemming from interkingdom siderophore piracy and bacterial development.

Desferrioxamines are the best-studied hydroxamate siderophores, and are produced by many actinomycetes, including *Streptomyces*, *Nocardia*, and *Micromonospora* (Gunter et al., 1993). These low-molecular-weight molecules are synthesized using the amino acids lysine and ornithine. The *Streptomyces* 11-gene desferrioxamine biosynthetic cluster has been well-studied, and the cluster is subject to control by the regulatory protein DmdR (a homolog of DtxR). (Tunca et al., 2007). In the presence of iron, DmdR1 represses the transcription of *desA*, the first gene in the desferrioxamine biosynthetic operon. Repression by Dmdr1 is relieved in low iron conditions, permitting the expression of *desA-D* and the corresponding production of desferrioxamines. Genes known to be involved in desferrioxamine uptake include *desE* and the alternative transporter *cdtB*. Additionally, it has been hypothesized the *bldK* operon (*bldKABCDE*) encoding an ABC transporter is involved in desferrioxamine uptake (Lambert et al., 2014). *S. venezuelae* encodes five predicted siderophore biosynthetic clusters, including one specific for desferrioxamine. The other four clusters are transcriptionally silent under laboratory conditions, and it is not known how these clusters are activated or regulated. Insights into these clusters, and into the roles played by siderophores in diverse environments should yield important insights into the nutritional cues influencing *Streptomyces* morphology and interspecies interactions.

1.6 Aims and Outline of this Thesis

RNA processing is a critical component of regulation in bacteria, and the roles of RNases in rRNA processing and ribosome biogenesis have not been examined in detail in *Streptomyces*. Chapter 2 describes our characterization of the roles of RNase III and RNase J in rRNA cleavage and ribosome assembly. This work was published in the *Journal of Bacteriology* in 2014 (Jones et al., 2014). In 2015, we made an unexpected discovery that ultimately shifted the focus of my work. We found that yeast triggers a new mode of *Streptomyces* growth termed 'exploration', and demonstrated that exploration represents a completely novel mode of *Streptomyces* development. Exploring cells rapidly grow and traverse solid surfaces, and can communicate or compete with other microbes using airborne VOCs. This work is described in chapter 3. We published this work in *eLife* in 2017 (Jones et al., 2017), and reviewed the topic in several

subsequent works (Jones and Elliot, 2017; Jones and Elliot, 2018). We next examined how VOCs produced by exploring cultures affect microbial community dynamics. We found VOCs reduce the survivability of other microbes by altering iron availability, and examined the roles of iron in *S. venezuelae* exploration. This work is described in Chapter 4, and this manuscript will be submitted in the coming weeks (June 2018). Finally, we investigated the cellular mechanisms underlying exploration. We found DivIVA and MreB cooperate to drive rapidly colony expansion, demonstrating a role for MreB in actinomycete vegetative development. This work is described in Chapter 5, and represents unpublished work.

CHAPTER 2: DEVELOPMENT, ANTIBIOTIC PRODUCTION, AND RIBOSOME ASSEMBLY IN *STREPTOMYCES VENEZUELAE* ARE IMPACTED BY RNASE J AND RNASE III DELETION

Stephanie E. Jones, Vivian Leong, Joaquin Ortega and Marie A. Elliot

Preface:

This chapter was published in the *Journal of Bacteriology* in 2014 (Jones 2014). Vivian Leong, a technician in Prof. Joaquin Ortega's lab (at the time at McMaster University), carried out the ribosome profiling and polysome profiling experiments. Joaquin performed the TEM experiments. I performed all other work.

2.1 Abstract (Chapter Summary)

RNA metabolism is a critical - but frequently overlooked - control element affecting virtually every cellular process in bacteria. RNA processing and degradation are mediated by a suite of ribonucleases having distinct cleavage and substrate specificity. Here, we probe the role of two ribonucleases (RNase III and RNase J) in the emerging model system *Streptomyces venezuelae*. We show that each enzyme makes a unique contribution to the growth and development of *S. venezuelae*, and further affects the secondary metabolism and antibiotic production of this bacterium. We demonstrate a connection between the action of these ribonucleases and translation, with both enzymes being required for the formation of functional ribosomes. RNase III mutants in particular fail to properly process 23S rRNA, form fewer 70S ribosomes and show reduced translational processivity. Loss of either RNase III or RNase J additionally led to the appearance of a new ribosomal species (the 100S ribosome dimer) during exponential growth, and dramatically sensitized these mutants to a range of antibiotics.

2.2 Introduction

Ribonucleases (RNases) are enzymes that process and degrade RNA molecules, and consequently are critical for RNA maturation, RNA stability and post-transcriptional regulation (Laalami et al., 2014). In bacterial cells, the finely tuned balance between RNA synthesis and RNA degradation allows for rapid adaption to changing environments, proper processing of non-coding RNAs, and efficient recycling of ribonucleotides (Arraiano et al., 2010).

Our understanding of RNA metabolism to date is based largely on studies of *Escherichia coli* and *Bacillus subtilis*, which employ distinct enzymes for RNA processing and degradation. In *E. coli,* RNase E is the central component of the 'RNA degradosome', and as such is responsible for much of the RNA decay in this organism. *B. subtilis* lacks this enzyme, and acting in its place are three other nucleases: RNase J1/J2 and RNase Y (Lehnik-Habrink et al., 2012; Shahbabian et al., 2009). Virtually all bacteria contain at least one of RNase E (or its paralog RNase G), RNase J or RNase Y (Kaberdin et al., 2011). These RNases are unrelated in primary sequence and mechanism of catalysis, but have similar substrate specificity: they all have single strand-specific endonuclease activity and preferentially cleave AU-rich regions (Callaghan et al., 2005; Even et al., 2005; Shahbabian et al., 2009). Unlike RNase E and Y, however, RNase J has the capacity to act both as an endonuclease and a 5' exonuclease (Li de la Sierra-Gallay et al., 2008; Mathy et al., 2007). Analysis of available genome sequences suggests that more than half of all bacteria, and over two-thirds of Archaea, possess an RNase J homolog (Even et al., 2005; Mathy et al., 2007). In addition to these diverse single strand-specific RNases, most bacteria also encode the double strand-specific RNase III (Nicholson, 2013). This enzyme is highly conserved in bacteria and eukaryotes, and has a critical role in post-transcriptional regulation, where it cleaves double-stranded substrates such as those resulting from the base-pairing of an mRNA and non-coding RNA (Viegas et al., 2011) or those associated with highly structured RNAs, such as ribosomal RNAs (rRNAs) (Nikolaev and Silengo, 1973; Westphal and Crouch, 1975). There can be considerable functional interplay between RNases, with a classic example being the

generation of mature 23S, 16S and 5S rRNAs from a single 30S transcript. RNase III typically functions initially to liberate 'pre-16S', 'pre-23S' and 'pre-5S' rRNAs from the full length primary transcript (Ginzburg, D, Steitz, 1975; Nikolaev and Silengo, 1973). These precursor rRNAs are processed further by a variety of RNases that may include (depending on the organism) RNase E, RNase G, RNase J, and other yet-to-be-identified ribonucleases (Britton et al., 2007; Li et al., 1999; Taverniti et al., 2011). Without the concerted and precisely coordinated activity of these RNases during ribosome assembly, complete rRNA processing cannot be achieved, and ribosome function is compromised.

As investigations into RNase activity begin to extend beyond the *E. coli* and *B. subtilis* model systems, it is becoming apparent that there is considerable diversity in the arsenal of RNases employed by any given bacterium (Condon and Putzer, 2002). The actinobacteria, a group of Gram-positive bacteria that include *Streptomyces* and *Mycobacterium,* encode a set of RNases that include not only RNase III, but also RNase E and RNase J (Taverniti et al., 2011). While the mycobacteria are best known for their pathogenic potential, the predominantly soil-dwelling *Streptomyces* are renowned for their ability to produce a vast array of useful secondary metabolites, including antibiotics, antifungals, and chemotherapeutic agents. The streptomycetes are also known for their multicellular life cycle that encompasses morphologically - and metabolically - distinct developmental stages. Their life cycle initiates with spore germination, and subsequent hyphal tip extension and branching leads to the formation of vegetative mycelial networks. Reproductive growth initiates with the emergence of aerial hyphae during solid culture growth (or hyphal fragmentation for those strains that differentiate in liquid culture), and culminates with the subdivision of the aerial cells/hyphal fragments into chains of uniformly sized exospores (Flärdh and Buttner, 2009).

Previous investigations into RNase III in *Streptomyces coelicolor* have revealed it to be essential for normal sporulation and the production of the antibiotics actinorhodin and undecylprodigiosin (Price et al., 1999; Sello and Buttner, 2008). Its fundamental importance to RNA metabolism in *Streptomyces* is further illustrated by the fact that up to 10% of all transcripts synthesized during vegetative growth are affected (directly or indirectly) by RNase III activity (Gatewood et al., 2012). More recently, studies have begun to explore the biochemical and biological role of RNase J in *Streptomyces.* The *S. coelicolor* enzyme - like its *B. subtilis* counterpart - has dual endo/exonuclease activity (Bralley et al., 2014; Mathy et al., 2007), and its deletion from the *S. coelicolor* chromosome results in altered antibiotic production (Bralley et al., 2014).

Here, we probe the roles of RNase III and RNase J in *Streptomyces venezuelae*. We provide evidence that both RNases are pleiotropic regulators, required for normal development and antibiotic production, with each enzyme making distinct contributions to these processes. While defects in mRNA turnover almost certainly contribute to these phenotypic abnormalities, we propose that defects in translation stemming from altered ribosome structure and activity may also play a role. We show that both RNase III and RNase J mutants have far greater numbers of translationally inactive ribosome dimers (100S ribosomes) than their wild type counterpart. RNase III mutants are further defective in rRNA processing, assemble fewer

mature 70S ribosomes than wild type and exhibit reduced ribosomal processivity (based on polysome profiles).

2.3 Results

2.3.1 Bioinformatic and expression analyses of RNase J and RNase III in *S. venezuelae*

To begin exploring the function of RNase J (SVEN_5394) and RNase III (SVEN_5265) in *S. venezuelae,* their sequence and genomic context were compared with other well-studied bacteria. They each shared >90% amino acid sequence identity with their *S. coelicolor* counterparts. RNase J also shared 41% full-length identity (59% similarity) with RNase J1 and 38% identity (60% similarity) with RNase J2 from *B. subtilis*. *S. venezuelae* appears representative of the streptomycetes in encoding a single RNase J protein, and in all species examined, its corresponding gene (*rnj*) is found immediately upstream of an rRNA operon and directly downstream of genes encoding a dihydropicolinate synthetase (*dapA*) and thymidylate synthase (*thyX*) (**Fig. 2.1A**). Analysis of data from previously published RNA-sequencing (RNA-seq) experiments (Moody et al., 2013) suggested that each of *rnj*, *dapA* and *thyX* was expressed from a distinct promoter, but also shared low-level read-through transcription, particularly between *dapA* and *rnj* (Fig 1A). The genetic connection between *rnj* and *dapA* is conserved in many bacteria, including *Mycobacterium* species and *B. subtilis* (in the case of *rnjB* encoding RNase J2), while the *rnj* association with rRNA operons seems limited to the streptomycetes.

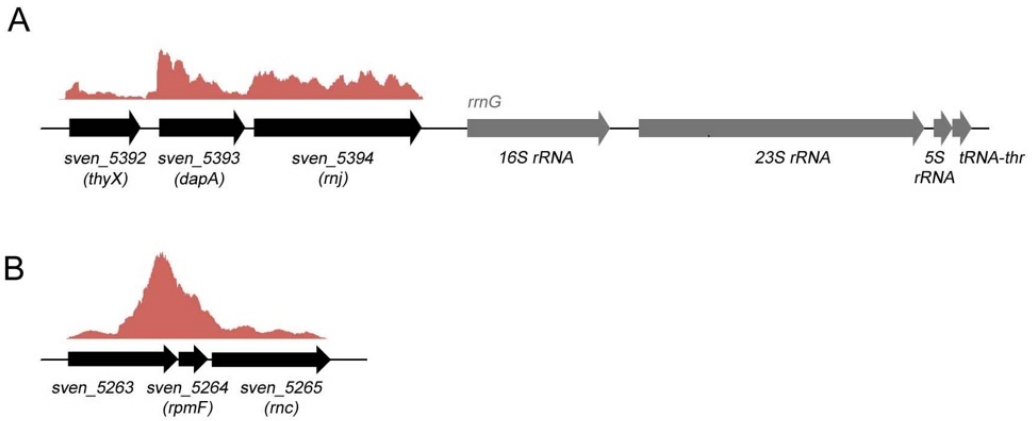

Fig. 2.1 Genetic organization and transcript profiles of *rnc* and *rnj*. A. Organization of the genes flanking the RNase J-encoding *rnj*. Above the three protein-encoding genes (*thyX, dapA* and *rnj*) is shown a graph of relative transcript levels throughout this region, as determined using RNA-seq data from RNA samples representing all stages of *S. venezuelae* growth (RNA was harvested at three distinct growth stages - vegetative, fragmentation and sporulation - and was combined prior to sequencing). **B.** Genetic organization of the RNase III-encoding *rnc* region. As described in **A.**, above these genes is depicted a graph of relative transcript levels for this region.

RNase III has been reasonably well-studied in *S. coelicolor* (Gatewood et al., 2012; Huang et al., 2005; Price et al., 1999; Sello and Buttner, 2008), and given the extensive sequence similarity shared with RNase III in *S. venezuelae*, these proteins are expected to function in a similar manner. For all *Streptomyces* species in the StrepDB database (http://strepdb.streptomyces.org.uk/), *rnc* appears to be the third gene in an operon that includes genes encoding a conserved, hypothetical protein, and the large ribosomal subunit protein L32 (*rpmF*) (**Fig. 2.1B**). Investigation of available RNA-seq data (Moody et al., 2013) suggested that while these three genes do indeed appear to be co-transcribed in *S. venezuelae*, there exists an additional strong promoter upstream of *rnc* (and *rpmF*), within the first gene in the operon (**Fig. 2.1B**). This observation is further supported by our complementation experiments described below.

2.3.2 RNase J and RNase III deletions affect growth and morphology in *S. venezuelae*

As a first step in investigating the biological role of RNase III and RNase J in *S. venezuelae*, we replaced their respective genes with an antibiotic-resistance cassette. Growth for 4 days on MYM agar revealed both mutant strains to be phenotypically distinct from their wild type parent (**Fig. 2.2A**). The Δ*rnj* strain had reduced melanin production and produced little of the green pigment associated with wild type *S. venezuelae* spores, suggesting a potential sporulation defect. In contrast, the Δ*rnc* mutant appeared to sporulate normally, although it did display unusual plate growth properties in that the edges of growth curled away from the growth medium, suggesting that the vegetative cells may be unusually hydrophobic (**Fig. 2.2A**). The morphological defects of both mutant strains could be restored upon complementation with wild type copies of their respective genes on the integrating plasmid vector pIJ82, when compared with wild type *S. venezuelae* carrying pIJ82 alone (**Fig. 2.2A**). We observed effective complementation of the *S. venezuelae rnc* mutant phenotype with the *rnc* coding sequence and ~300 nt of upstream sequence; this sequence encompassed the upstream *rpmF* gene and the C-terminal half of *SVEN_5263* and included the promoter region indicated in our RNA-seq data (**Fig. 2.1B**).

We next took advantage of the fact that *S. venezuelae* fully differentiates in liquid culture in a relatively synchronous and dispersed manner, and examined the effects of these two RNase deletions on *S. venezuelae* growth and development in liquid culture (**Fig. 2.2B**). We found that while the Δ*rnj* strain had similar growth kinetics as wild type, microscopic analyses revealed that it took longer to transition from mycelial growth to fragmentation, and that the onset of sporulation was significantly delayed (~6 h), consistent with the putative sporulation defects seen during growth on solid medium (lack of mature spore pigment) (**Fig. 2.2A**). The Δ*rnc* strain initially grew more slowly than either the wild type or *rnj* mutant, but by early stationary phase its growth kinetics matched that of the wild type. Despite this initial lag in growth, the Δ*rnc* strain exhibited only a modest delay in fragmentation and initiated sporulation at the same time as wild type (**Fig. 2.2B**).

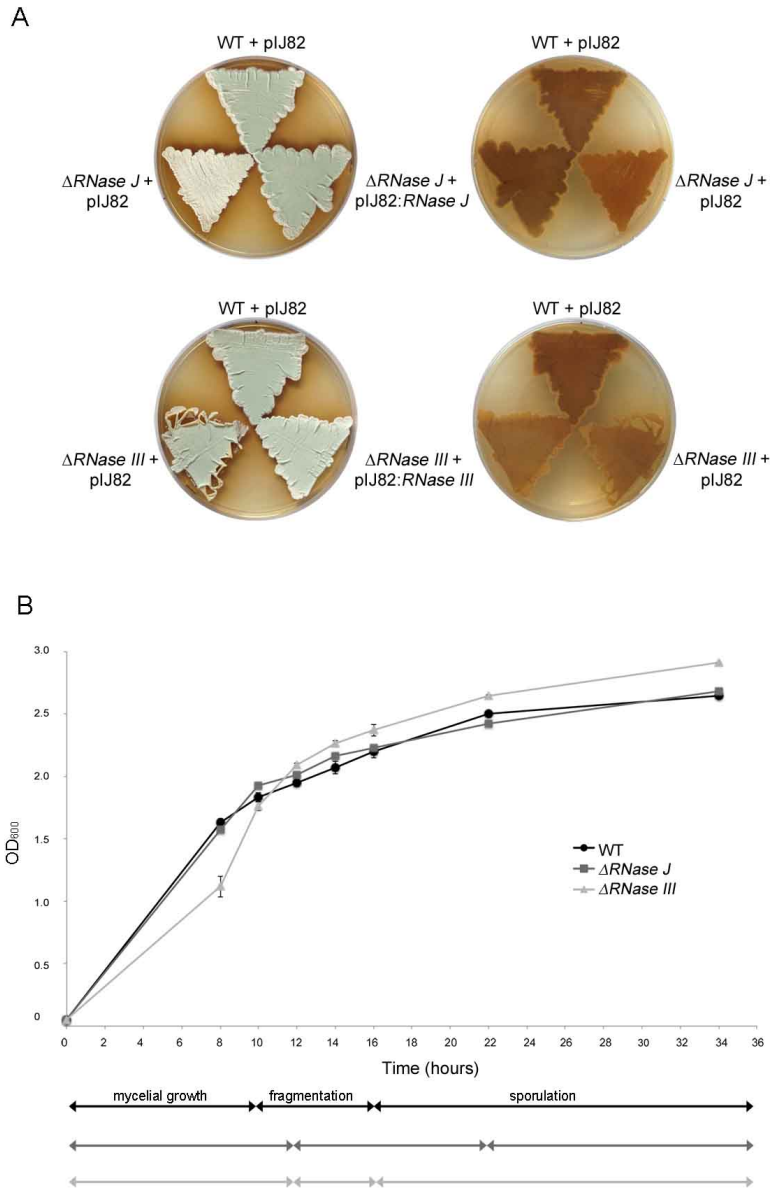

Fig. 2.2 Phenotypic comparison of wild type *S. venezuelae*, Δ*rnc* (*RNase III*) and Δ*rnj* (*RNase J*). **A.** Left: colony morphology of wild type *S. venezuelae* and RNase mutants (carrying the integrating plasmid vector pIJ82), and the corresponding complemented strains, grown on MYM agar medium for 4 days. Right: the undersides of the plates to the left, showing levels of the brown melanin pigment. **B.** Comparison of growth rates and transitions between life cycle stages of wild type, Δ*rnj* and Δ*rnc* strains. Cultures were inoculated to an OD_{600} of 0.05 and incubated shaking at 30°C for 34 hours. Optical density (OD_{600}) was measured at the indicated times, and life cycle stages (indicated below the graph) were assessed using light microscopy. Each OD_{600} value represents an average of three to four replicates; standard error for growth density was calculated at each time point.

2.3.4 RNase III and RNase J mutants form defective spores

The developmental defects of the Δ*rnj* strain, and the unusual growth of the Δ*rnc* strain on solid medium prompted us to investigate the morphology of these strains using scanning electron microscopy (SEM) (**Fig. 2.3**). After 6 days of growth, we observed few spore chains for the Δ*rnj* strain, suggesting that sporulation in this strain was an infrequent occurrence. For the Δ*rnc* mutant, spore chains were abundant, but the spores themselves were irregularly shaped when compared with the more uniformly sized spores of wild type *S. venezuelae*.

A rigorous assessment of spore size for mutant and wild type strains was then undertaken ($n \geq$ 1200 spores for each strain) using light microscopy images of spore chains adhering to glass coverslips. We found the Δ*rnj* strain had slightly shorter spores than wild type ($p < 0.001$), with the average spore length for the Δ*rnj* strain being 0.62 µm, compared with 0.7 µm for wild type (**Fig. 2.3**). While the average spore length for both Δ*rnc* and wild type strains was comparable (Δ*rnc*: 0.67 µm; wild type: 0.7 µm), the size range was far greater for the Δ*rnc* strain, with the standard deviation being 28% greater than that of the wild type ($p < 0.001$) (**Fig. 2.3**), further validating our SEM observations that this mutant formed irregular spores.

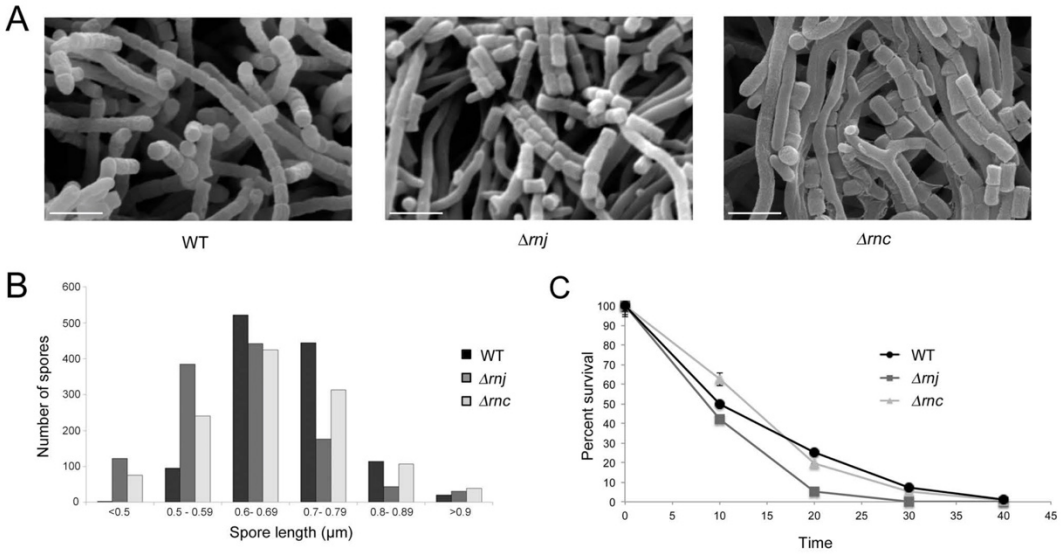

Fig. 2.3 Spore morphology and dormancy characteristics. A. Scanning electron micrographs comparing wild type strain (left), the Δ*rnj* strain (middle) and the Δ*rnc* strain (right) after growth for 6 days on MYM agar medium at 30°C. Bars = 2 µM. **B.** Distribution of spore lengths for wild type and mutant strains as determined using light microscopy images. Spore lengths were measured using ImageJ. For each strain, >1200 spores were measured, and calculated lengths were rounded to the nearest 0.01 µM. **C.** Heat sensitivity of wild type *S. venezeulae* and the RNase mutant strains. Spores were tested for the ability to survive heat shock at 50°C for the times indicated. Approximately 250 heat-shocked spores were spread on MYM agar plates and incubated for 30°C for 4 days. Their survival rates were then calculated as percentages. Each value is an average of three replicates, and the standard error was calculated for the percent survival at each time point.

Given that both RNase mutant strains appeared to form defective spores with shorter or variable spore lengths, we wanted to assess how these strains responded to heat stress, as heat sensitivity is suggestive of defects in spore maturation (Haiser et al., 2009; Mazza et al., 2006; Molle et al., 2000). We conducted heat shock assays using wild type and RNase mutant spores, and found the Δ*rnj* strain to be the most sensitive, displaying a ~five-fold increase in heat sensitivity after a 20 min heat shock, relative to wild type (**Fig. 2.3**). The Δ*rnc* strain was less impacted, appearing more heat resistant after 10 min, but showing a slight increase (~1.3 fold) in heat sensitivity after 20 min (**Fig. 2.3**).

2.3.5 RNase deletion abolishes/reduces jadomycin B production

RNase III is required for antibiotic production in several *Streptomyces* species (Adamidis and Champness, 1992; Lee et al., 2013; Price et al., 1999; Sello and Buttner, 2008), while RNase J was recently shown to have varied effects on antibiotic production in *S. coelicolor* (delayed actinorhodin, increased undecylprodigiosin, and reduced calcium dependent antibiotic) (Bralley et al., 2014). The melanin defect associated with the *rnj* mutant in *S. venezuelae* suggested that RNase J may impact secondary metabolite production in this species as well. To quantitatively probe the effect of losing either RNase III or RNase J on antibiotic production in *S. venezuelae*, we assayed production of the polyketide-derived anguacycline glycoside antibiotic jadomycin B – a secondary metabolite with antimicrobial, antifungal and antitumor activity (Zheng, 2005). While *S. venezuelae* is predicted to encode upwards of 30 secondary metabolic clusters [as determined using antiSMASH (Blin et al., 2013)], jadomycin B (whose biosynthetic cluster is shown in **Fig. 2.4A**), is the only antibiotic produced by this species for which a specific production assay has been developed. We grew wild type and mutant cultures in jadomycin B production medium, and found the jadomycin B levels of the Δ*rnj* mutant were typically 20-30% lower than that of the wild type strain, after controlling for growth. For the Δ*rnc* mutant, jadomycin B was never detected (**Fig. 2.4B**), confirming an essential role for this RNase in promoting antibiotic (or at least jadomycin B) production in *S. venezuelae*.

2.3.6 Transcriptional analysis of the jadomycin cluster.

The underlying basis for the jadomycin B production defects observed for RNase III and RNase J mutants, and the antibiotic production defects observed for equivalent mutants in other *Streptomyces* species, has yet to be clearly established. There is some evidence supporting a transcriptional mechanism in the case of RNase III, as reduced expression of several pathway-specific antibiotic regulators has been shown previously for *rnc* mutants (Hindra et al., 2010; Huang et al., 2005; Price et al., 1999). To determine whether the jadomycin B production defects seen here were due to transcriptional abnormalities, we isolated RNA from wild type and mutant strains induced to produce jadomycin B, and examined the expression of the jadomycin B pathway-specific regulator-encoding gene *jadJ* (Wang et al., 2009; Zhang et al., 2013), along with two biosynthetic genes (*jadA* and *jadM*) using semi-quantitative RT-PCR. These three genes appear to be part of a long operon and are likely expressed from the same

promoter (**Fig. 2.4A**) [note that the jadomycin B cluster organization in the sequenced *S. venezuelae* ATCC 10712 strain differs slightly from that reported in other studies (Wang, 2003; Zhang et al., 2013; Zheng et al., 2007)]. The Δ*rnj* strain had approximately wild type transcript levels for all three genes tested, while the Δ*rnc* strain had virtually undetectable expression of these same genes (**Fig. 2.4C**). This suggested that the failure of an RNase III mutant to produce jadomycin B may well be due to the lack of transcription of its biosynthetic genes (or dramatically reduced transcript stability); however, such an explanation does not hold for the RNase J mutant, which reproducibly yielded at least wild type levels of expression for the three genes tested, yet produced significantly less jadomycin B (**Fig. 2.4B,C**).

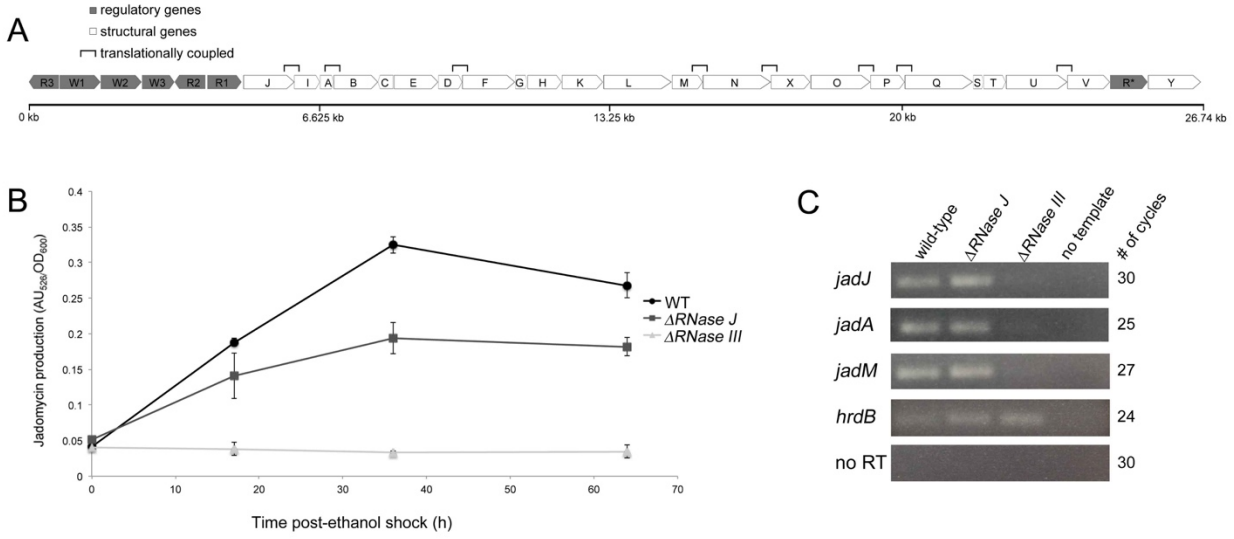

Fig 2.4 RNase J and RNase III are required for normal antibiotic production in *S. venezuelae*. A. Organization of the jadomycin B biosynthetic cluster. Regulatory genes are shown in grey and structural genes are shown in white. **B.** Wild type and RNase mutant strains were grown under jadomycin B-inducing conditions, and jadomycin B production at each time point was calculated by measuring the absorbance of the culture supernatant at 526 nm and normalizing to growth density (OD_{600}). These results reflect the average of three independent cultures, and error bars denote standard error for each time point. **C.** Semi-quantitative RT-PCR using RNA isolated from wild type and the RNase mutants during jadomycin B production (24 hours post-ethanol shock). The vegetative sigma factor-encoding gene *hrdB* served as a positive control for RNA loading and RNA integrity, while 'no RT' (template = RNA) and 'no template' reactions were included as negative controls with *hrdB*-specific primers to ensure a lack of DNA contamination in both RNA preparations and all PCR reagents.

2.3.7 RNase deletion strains are cold sensitive

Given that a transcriptional mechanism could not explain the reduced levels of jadomycin B observed for the RNase J mutant in particular, we wondered whether translation may play a role, given that RNase J - and RNase III - have been implicated in rRNA processing in different bacterial species (Britton et al., 2007; Madhugiri and Evguenieva-Hackenberg, 2009; Mathy et

al., 2007), and their respective genes are genetically linked to ribosomal components, where *rnc* is co-transcribed with a ribosomal protein and *rnj* is located upstream of an rRNA operon (**Fig. 2.1**) (Chang et al., 2005; Price et al., 1999; Xu et al., 2008). mRNA stability can also be influenced by ribosome activity and the associated protection that translating ribosomes provide.

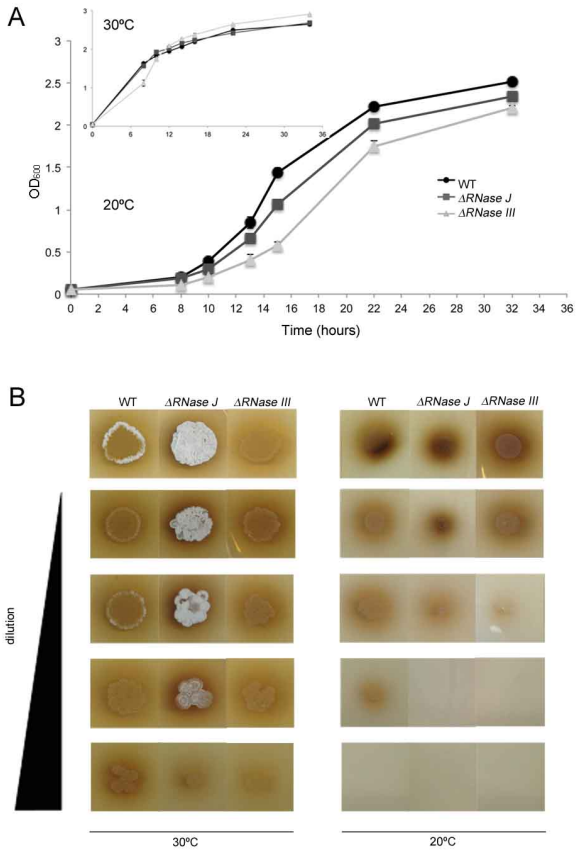

Fig. 2.5 Cold-sensitive phenotype of the RNase mutant strains. A. Growth profiles of wild type and RNase mutant strains in MYM liquid medium at 20°C and 30°C (inset). Cultures were inoculated to an OD_{600} of 0.05 and incubated shaking at 30°C for 34 hours. Each value is an average of three to four replicates, and standard error for growth density was calculated at each time point. **B.** Dilution plating of wild type and mutant strains. Cultures were grown shaking at 30°C to an OD_{600} of 0.4 before they were diluted in tenfold increments. Three microliters of each dilution were spotted onto MYM agar plates, and plates were incubated at either 20°C or 30°C for 4 days. The Δ*rnj* strain occasionally raised aerial hyphae more rapidly than either of the other strains when inoculated from liquid-grown culture (as seen here for the 30ºC-grown culture), but this phenotype was not reproducibly observed.

While heat sensitivity is indicative of sporulation defects, cold sensitivity is a hallmark of ribosome defects (Bylund et al., 1998; Connolly and Culver, 2009), and thus we tested the cold sensitivity of our mutant strains, comparing the growth of these strains to wild type at 30°C and 20°C. Both RNase deletion strains displayed greater cold sensitivity than wild type during growth at 20°C in liquid medium. The ratio between log phase growth rates of wild type and Δ*rnj* mutant strains was 1.0 at 30°C, and this diverged to 1.6 at 20°C (*i.e.* Δ*rnj* was ~30% more cold-sensitive than wild type), while the equivalent ratios for wild type and Δ*rnc* strain were 1.1 at 30°C and 1.4 at 20°C (*i.e.* Δ*rnc* was ~20% more cold-sensitive than wild type) (**Table 2.2; Fig. 2.5A**). The cold sensitivity of wild type and mutant strains was also analyzed during growth on solid medium, where dilution plating assays showed wild type and mutant strains grew equally robustly at 30°C, but that at 20°C, growth of the two RNase mutant strains was compromised (**Fig. 2.5B**).

2.3.8 RNase deletion strains are defective in ribosome assembly and form 100S ribosomes

The cold sensitive phenotypes of both RNase mutant strains suggested they may have defective ribosomes. To determine whether ribosome assembly was affected by mutations in *rnc* and *rnj*, we obtained ribosome profiles of wild type and mutant strains during early exponential growth using sucrose density gradient centrifugation, a technique that separates free 30S subunits, free 50S subunits and fully assembled 70S ribosomes. We found wild type and Δ*rnj* strains had similar profiles, with roughly equivalent proportions of free 30S and 50S subunits. In contrast, the Δ*rnc* strain had increased levels of free 30S (approximately two-fold) and 50S subunits (**Fig. 2.6A**).

Intriguingly, the sedimentation profiles of Δ*rnc* and Δ*rnj*, but not wild type, revealed an extra peak of ~100S beyond the expected 30S, 50S and 70S fractions (**Fig. 2.6A**), and this represented a significant proportion of the assembled ribosomes (**Fig. 2.6B**). Previous studies in *E. coli* showed that 70S ribosomes could dimerize to form translationally inactive 100S ribosomes during stationary phase (Wada et al., 1990). To determine whether the larger peak detected in the RNase mutants corresponded to 100S ribosomes, we examined the content of the 100S fraction using transmission electron microscopy, and compared these with the particles obtained from the 70S fraction. Even in the absence of crosslinking [100S particles are not stable complexes (Kato et al., 2010; Krokowski et al., 2011)], we observed abundant ribosome dimers in the 100S fraction (~10-15% of all ribosome particles) for both RNase mutants relative to the 70S fraction (3-4% dimers) (n >800 for each 100S and 70S fraction) (**Fig. 2.6C**).

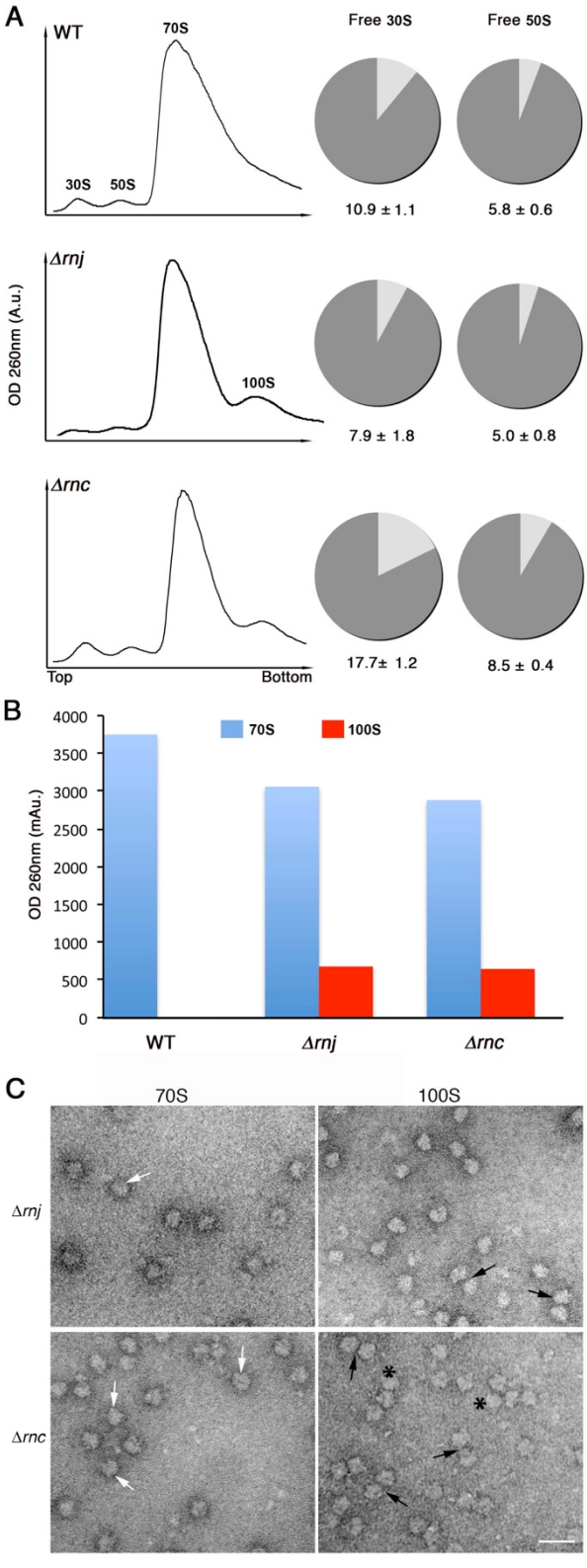

Fig. 2.6 Ribosome profiling of wild type and RNase mutant strains. A. Ribosomes from wild type (top), Δ*rnj* (middle) and Δ*rnc* (bottom) were fractionated on 10-30% sucrose gradients, and sedimentation profiles were plotted (left panels). Peaks corresponding to 30S and 50S ribosomal subunits, 70S ribosomes and 100S ribosome dimers are indicated. The pie graphs to the right depict the proportion of free and complexed subunits in wild type and RNase mutant strains, in the same order as the left panel. The proportion of free 30S to 'bound 30S' (*i.e.* 30S subunits in 70S and 100S ribosomes) and free 50S to 'bound 50S' (*i.e.* 50S subunits in 70S and 100S ribosomes) in the wild type and mutant strains was calculated using peak areas obtained from the sucrose gradient profiles (left). **B.** Plot representing the amount of 70S and 100S particles obtained from the profiles in **A.**. **C.** Electron micrographs of images corresponding to 70S peaks and the additional peaks from Δ*rnj* and Δ*rnc*. Peak fractions were pooled separately (*i.e.* 70S fraction and 100S fraction), purified and visualized using transmission electron microscopy. 70S and 100S ribosomal particles are indicated by white and black arrows, respectively. Polysomes are indicated by asterisks. Scale bars = 50 nm.

Given the sequestration of some of the 70S ribosomes into 100S particles in the Δ*rnj* and Δ*rnc* strains, there was a proportional decrease in the level of 70S ribosomes in these strains (**Fig. 2.6B**), with the number of 70S ribosomes further reduced in the Δ*rnc* strain, consistent with these cells having a larger proportion of free 30S and 50S particles (**Fig. 2.6A,B**).

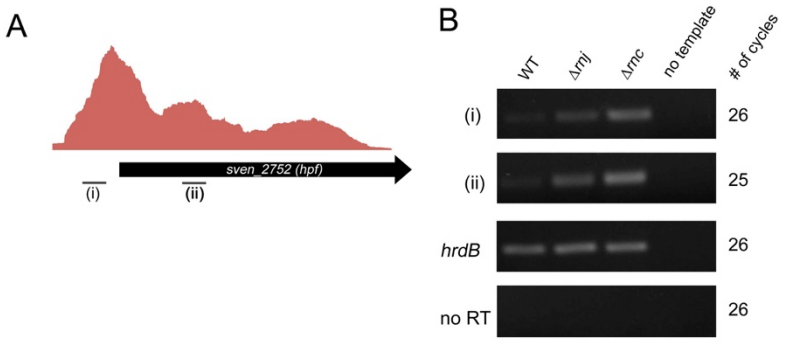

Fig. 2.7 Transcription of *hpf* - a ribosome dimer-promoting factor. A. Graph depicting the relative transcript levels of *hpf*, including what appears to be a long 5' untranslated region (5' UTR), as determined by analysis of RNA isolated from all growth stages, combined and subjected to RNA-seq. (i) and (ii) indicate the location of products analysed by RT-PCR. **B.** Semi-quantitative RT-PCR analysis of (i) the 5' UTR of *hpf* and (ii) the *hpf* coding sequence in wild type and RNase mutant strains using RNA isolated from early exponential phase cultures (OD_{600} of ~0.4). *hrdB* was used as a positive control for RNA abundance and RNA integrity, while 'no RT' (template = RNA) and 'no template' reactions with *hrdB*-specific primers served as negative controls, ensuring there was no DNA contamination of either RNA preparations or any PCR reagents.

In *E. coli*, ribosome dimer formation occurs in stationary phase and is promoted by the ribosome modulation factor Rmf, in conjunction with the so-called 'hibernation promoting factor' Hpf (Ueta et al., 2005; Wada et al., 1990). Rmf is confined to the gamma proteobacteria, and in most other bacteria, it is a longer form of Hpf that directs ribosome dimerization (Tagami et al., 2012; Ueta et al., 2010, 2013). The streptomycetes possess a gene encoding this longer Hpf form, and as such, we sought to determine whether the *rnc* and *rnj* mutant strains showed higher levels of expression of this gene (*SVEN_2752)* during exponential growth, compared with wild type. We have RNA-seq data suggesting that *hpf* was expressed from a promoter located considerably (~150-200 nt) upstream of the start codon (**Fig. 2.7A**), and so we investigated expression of both its 5' untranslated region and its coding sequence (to account for any transcriptional attenuation that may occur between the transcription and translation start sites), using RNA isolated from wild type and the two RNase mutant strains during exponential phase growth. We observed similar profiles for both coding sequence- and UTR-associated transcripts in all strains, and found that *hpf* transcripts were present at much higher levels in both *rnc* and *rnj* mutants than in the wild type (**Fig. 2.7B**), suggesting that increased expression of *hpf* in these strains may contribute to 100S dimer formation at a time when these are not present (or at least detected) in the wild type (**Fig. 2.6A,B**).

2.3.9 RNase deletion strains have reduced translation efficiency

The propensity of the two RNase mutants to form translationally inactive 100S ribosomes, and the cold sensitivity phenotype of the Δ*rnc* strain, collectively suggested that RNase III and RNase J may be required to produce ribosomes capable of efficient translation. To probe how these RNases affected global translation in *S. venezuelae*, we conducted polysome profiling for wild type and mutant strains using sucrose density gradient ultracentrifugation. Polysome profiles provide a snapshot of translation activity and reveal the density of actively translating ribosomes on mRNA transcripts (Qin and Fredrick, 2013). Wild type profiles revealed three clear polysome peaks, similar to that of the Δ*rnj* strain. However, the Δ*rnc* strain profile revealed only two small polysome peaks, indicating that translation activity and ribosome density on mRNA transcripts were severely reduced in this mutant strain (**Fig. 2.8**).

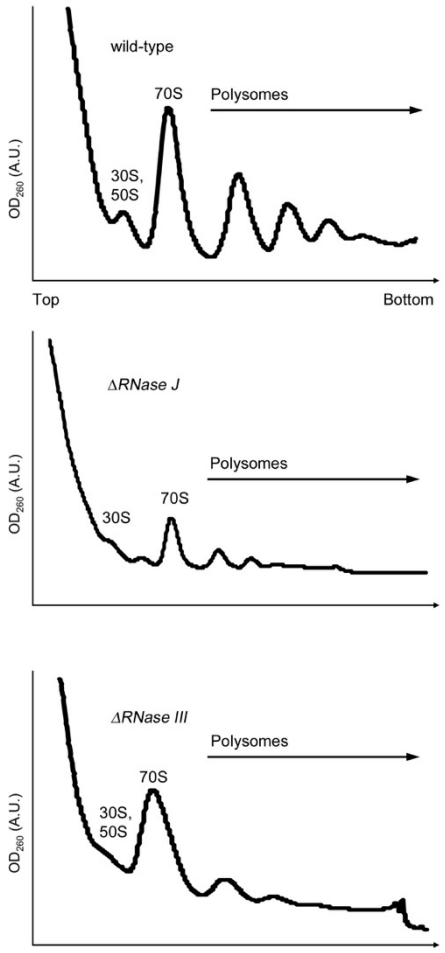

Fig. 2.8 Polysome profiles of wild type and RNase mutant strains. Polysome profiles for each of the three strains were generated following fractionation on a 10-40% sucrose gradient. Peaks corresponding to 30S subunits, 50S subunits and 70S ribosomes are labeled, and the locations of polysomes are indicated.

2.3.10 RNase III but not RNase J is involved in rRNA processing at the 5' end.

Having established that *rnc* and *rnj* mutants formed abnormal ribosomes with reduced processivity, we considered the possibility that these defects stemmed from altered rRNA processing. RNase J1 is involved in 16S rRNA processing in *B. subtilis* (Britton et al., 2007) and in 16S and 23S rRNA maturation in *Mycobacterium smegmatis*, while RNase III has a conserved role in rRNA processing in nearly all bacteria, cleaving the stem-loop structures flanking mature 16S and 23S species [reviewed in (Deutscher, 2009)]. rRNA processing in *Streptomyces* has not been studied in any detail, although there is some data suggesting that 30S rRNA (full length) transcripts accumulate in *rnc* null mutants in *S. coelicolor* (Price et al., 1999); the role of RNase J in rRNA processing has not been examined.

S. venezuelae has seven rRNA operons dispersed throughout its linear genome, and of these, only two (*rrnC* and *rrnF*) have been fully sequenced. The two sequenced operons differ only in the spacer regions between 16S and 23S (the *rrnC* spacer is 10 nt longer than that of *rrnF*) and between 23S and 5S (the *rrnF* spacer is 1 nt longer than that of *rrnC*) (**Fig. 2.9**).

We set out to map rRNA processing sites using primer extension analyses on total RNA isolated from wild type and RNase mutant strains during exponential growth, and radiolabeled oligonucleotides complementary to regions near the 5' end of the mature 16S and 23S transcripts (p16 and p23, respectively, in **Fig. 2.9**). Extension of primer p16 revealed the primary processing site to be +105/106 in all three strains, relative to the transcription start site of the rRNA operon (**Fig. 2.9**). This suggested that neither RNase III nor RNase J was involved in processing the 5' end of pre-16S rRNA. Extension of primer p23 revealed the primary 5' pre-23S processing site to be located at +1896 (relative to the start site for transcription of the rRNA operon). The Δ*rnc* strain lacked this processing site, while processing appeared wild type in the Δ*rnj* strain, indicating that RNase III, but not RNase J was needed for cleavage of 5' pre-23S rRNA (Fig. **2.9**).

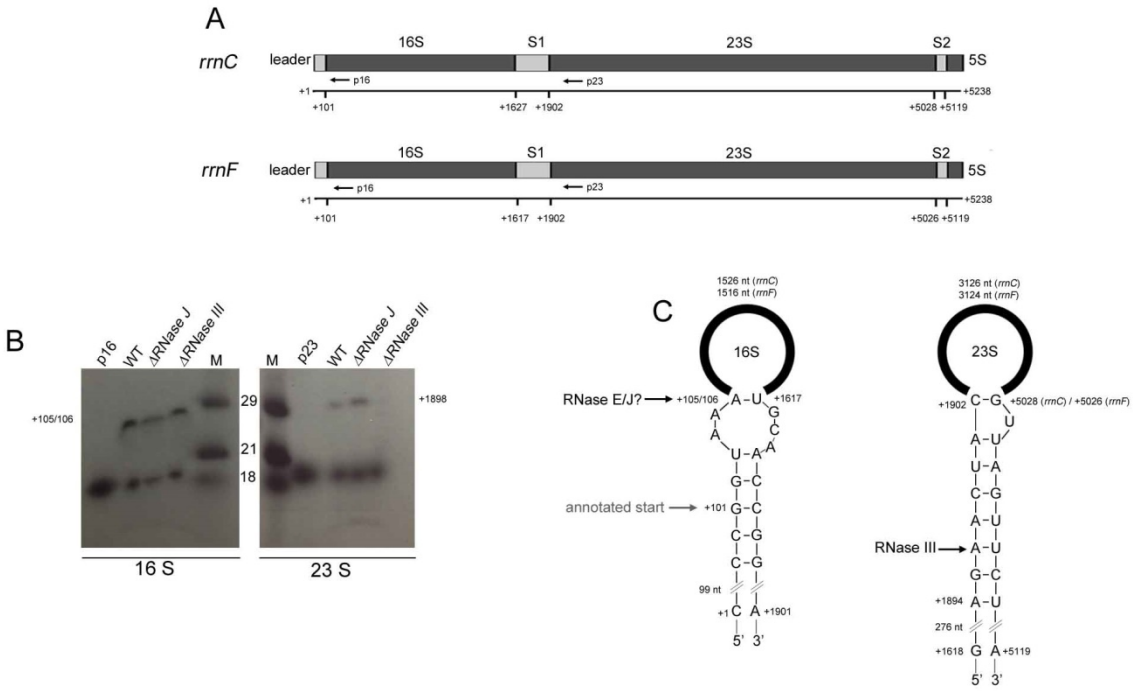

Fig. 2.9 Analysis of the 5' end maturation of pre-16S rRNA and pre-23S rRNA. A. Schematic representation of the *rrnC* and *rrnF* operons in *S. venezuelae*. The mature 16S, 23S and 5S rRNA sequences are indicated in dark grey, while the light grey are shown the leader, spacer 1 (S1) and spacer 2 (S2) sequences. The figure is to scale with respect to the length of each component of the rRNA operon. The scale bar below the rRNA operon shows the predicted start and stop coordinates of each mature rRNA species. The relative locations of oligonucleotides used for primer extension are shown (p16 for 16S and p23 for 23S). **B.** Primer extension analysis of 16S and 23S processing. Primer p16 was extended to detect 16S 5' processing sites, while primer p23 was extended to detect 23S 5' processing sites. The extension products were serparated on a 6% (w/v) denaturing polyacrylamide gel and radiolabelled oligonucleotides were used to create a ladder (M) with the expected sizes of 18 nt, 21 nt and 29 nt. The location of the primary 16S and 23S processing sites are indicated on the left (16S) and right (23S) of the gels, relative to the promoter (+1) of the *rrnF* operon. **C.** Secondary structure models of *S. venezuelae* pre-16S and pre-23S rRNA. Structure are based on M-fold analyses with modifications. Nucleotide numbers are as per the scale bar in **A.**. Predicted and experimentally determined processing sites are indicated with arrows, along with the RNase(s) responsible for cleavage. Black circles at the top of the 16S and 23S chematics represent the mature rRNA sequences. For the 16S structure, the sequence at the 5' corresponds to the operon leader sequence, while the region at the 3' end corresponds to spacer 1 (S1). Similarly for the 23S structure, the 5' end sequence corresponds to spacer 1 (S1), and that at the 3' end corresponds to spacer 2 (S2), as indicated in A..

2.3.11 RNase deletion strains display differential sensitivities to antibiotics that target the ribosome.

Collectively, our results showed that both RNase mutant strains had proportionally greater numbers of translationally inactive 100S ribosome dimers, and exhibited varying defects in ribosome assembly and translational efficiency. For Δ*rnc*, this may be explained in part by the abnormal processing of the 23S rRNA, but no such processing defect was observed for Δ*rnj*. In an attempt to gain further insight into the ribosome defects of the two RNase mutants, we took advantage of recent structural studies that have revealed the molecular basis by which diverse antibiotics target the bacterial ribosome [reviewed in (Lambert, 2012; Wilson, 2014)].

We analyzed the sensitivities of wild type and RNase mutant strains to antibiotics that specifically target different sites in the ribosome: tetracycline, which binds the 30S subunit and inhibits delivery of aminoacylated-tRNAs to the A-site; the aminoglycosides viomycin (Modolell and Vázquez, 1977), spectinomycin (Thom and Prescott, 1997), and hygromycin B (Brodersen et al., 2000), which bind the 30S subunit and inhibit translocation of tRNAs from the A-site to the P-site; the macrolide erythromycin, which binds the 50S subunit and inhibits elongation of the peptide chain (Tenson et al., 2003); and the lincosamide clindamycin, which binds the 50S subunit and inhibits peptide bond formation between the tRNA-bound amino acid at the P-site of the ribosome and the growing tRNA-anchored polypeptide chain in the A site (Tenson et al., 2003). For all antibiotics, we used antibiotic concentrations that inhibited growth of the wild type by ~50-85%.

We determined that both RNase mutants were hypersensitive to the majority of ribosome-targeting antibiotics tested (**Fig. 2.10**), but that the *rnj* mutant was generally more sensitive than the *rnc* mutant to antibiotics targeting the 30S subunit (tetracycline and the aminoglycosides hygromycin, spectinomycin and viomycin). Unexpectedly, the Δ*rnj* strain exhibited increased resistance to clindamycin: ~35% of wild type cells survived clindamycin treatment, while 65% of Δ*rnj* cells survived exposure to this antibiotic (**Fig. 2.10**).

To probe the effect of antibiotics targeting other cellular systems, we assessed the sensitivities of all strains to rifampicin (inhibits RNA polymerase activity) (Hartmann, Guido, Honikel, Kari Otto, Knusel, Fritz, Nuesch, 1967) and vancomycin (inhibits cell wall synthesis) (Hammes and Neuhaus, 1974). Interestingly, both strains exhibited increased sensitivity to rifampicin, with the Δ*rnj* strain in particular being 2.7-fold more sensitive than wild type (**Fig. 2.10**). Wild type and Δ*rnj* strains were equally sensitive to vancomycin, while the Δ*rnc* strain had heightened sensitivity.

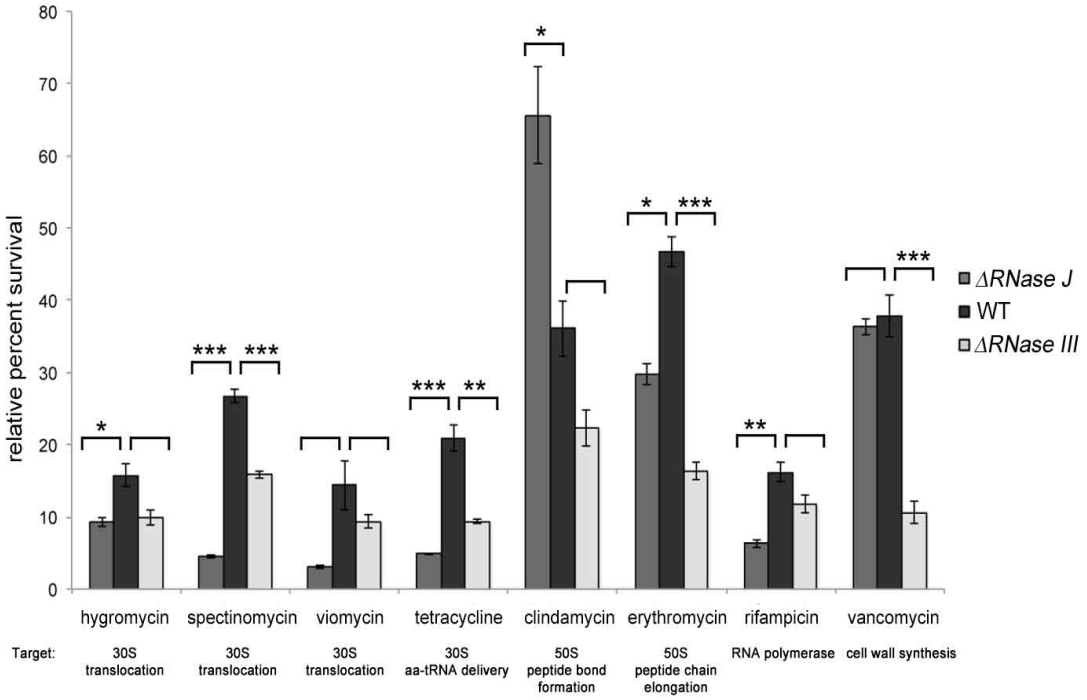

Fig. 2.10 RNase mutant sensitivity to ribosome-targeting antibiotics. Wild type, *rnj* and *rnc* mutant strains were tested for their resistance to a variety of antibiotics, including: 2.5 µg/mL hygromycin B, 2.5 µg/mL spectinomycin, 0.5 µg/mL viomycin, 0.5 µg/mL tetracycline, 0.1 µg/mL clindamycin, 0.5 µg/mL erythromycin, 0.025 µg/mL rifampicin and 0.5 µg/mL vancomycin. Relative survival rates were calculating by dividing optical density (OD_{600}) after growth in the presence of antibiotics by the optical density (OD_{600}) of cultures without antibiotics and are shown as percentages. Each value is an average of three replicates, and the standard error was calculated for the percent survival at each time point. Asterisks indicate statistically significant differences (* = *p*-value 0.05 to 0.01; ** = *p*-value 0.01 to 0.005; *** = *p*-value below 0.005), as determined by a student's T-Test.

2.4 Discussion

2.4.1 Developmental defects associated with RNase deletion

We observed striking but distinct developmental defects for each of the *rnc* and *rnj* mutant strains in *S. venezuelae*. The heterogenous spore sizes observed for the RNase III mutant are consistent with those seen for an equivalent mutant in *S. coelicolor* (Sello and Buttner, 2008); however, the unusual 'peeling' phenotype observed here has not been noted before. These morphological defects may stem from misregulation of the important developmental regulator AdpA. Previous work in *S. coelicolor* has shown that loss of RNase III function (due to an *rnc* point mutation) results in increased expression of AdpA (Xu et al., 2010). AdpA controls the expression of the RamR-encoding gene, and RamR in turn promotes the synthesis of SapB, an

aerial hyphae-promoting, amphipathic peptide (Wolanski et al., 2011; Xu et al., 2010). Enhanced SapB production may contribute to the peeling phenotype of the *rnc* mutant. This phenotype may be further exacerbated by the lack of agarase produced by *S. venezuelae;* in *S. coelicolor*, agarase production leads to vegetative hyphal growth into the agar substrate, and this would likely prevent the colony peeling seen here for *S. venezuelae*. AdpA was first identified in *Streptomyces griseus,* and in this system it also controls the expression of *ssgA* (Higo et al., 2012; Yamazaki et al., 2003), which encodes a key determinant of spore septum placement (Willemse et al., 2011). It will be interesting to see whether *ssgA* levels are altered in an *rnc* mutant strain, and if this contributes to the irregular placement of sporulation septa seen for this mutant in *S. venezuelae*.

Unlike the *rnc* mutant, *rnj* mutants failed to achieve robust sporulation, and those spores that did form were generally smaller and less heat resistant than wild type, suggesting defects in spore formation and spore maturation. In *Bacillus*, where RNase J has been best-studied, mutation and/or depletion of one or both *rnj* genes results in profound sporulation defects (Figaro et al., 2013; Mäder et al., 2008). Transcriptional and proteomic analyses in *Bacillus* have revealed dramatic alterations in the expression of at least two sporulation genes in an *rnj* mutant: higher *spo0E* transcript levels were observed by Durand and colleagues (Durand et al., 2012), where Spo0E is a phosphatase responsible for dephosphorylating the sporulation checkpoint protein Spo0A (Ohlsen et al., 1994), alongside increased levels of *spoVG* transcripts and its corresponding protein (Durand et al., 2012; Mäder et al., 2008), where SpoVG inhibits asymmetric septation (Matsuno and Sonenshein, 1999). While homologs of these gene products are not found in *Streptomyces* species, these results support the idea that RNase J is important for promoting sporulation and adoption of a dormant state in evolutionarily divergent bacteria.

2.4.2 Metabolic defects associated with RNase deletion

RNase III has long been associated with antibiotic production defects in *S. coelicolor* (Gravenbeek and Jones, 2008; Price et al., 1999; Sello and Buttner, 2008), and more recent work has revealed a role for RNase III in promoting actinomycin production in *Streptomyces antibioticus* (Lee et al., 2013). Here, we show that *S. venezuelae* also requires RNase III for jadomycin B production. In *S. coelicolor,* and now *S. venezuelae*, these antibiotic production defects are due at least in part to aberrant transcription (or dramatically reduced transcript stability) of the corresponding biosynthetic genes and cognate pathway-specific regulators (Aceti and Champness, 1998; Huang et al., 2005). While this cannot be a direct effect, how it is mediated remains to be determined.

RNase J has not been as well studied in the streptomycetes as RNase III, but its effects on antibiotic production extend to both *S. coelicolor* (Bralley et al., 2014) and *S. venezuelae*. In *S. venezuelae*, loss of RNase J resulted in reduced jadomycin B production, but unlike the situation for RNase III, the biosynthetic cluster (or at least the three genes tested here) was transcribed at near wild type levels. This suggested the jadomycin B production defect was not due to transcriptional mis-regulation, although we cannot exclude the possibility that biosynthetic

genes outside of this operon were not expressed at wild type levels. Our observation that there were increased numbers of presumably translationally inactive 100S ribosomes in this strain during exponential growth, coupled with phenotypic characteristics consistent with ribosome defects (cold sensitivity and a notable response to ribosome-targeting antibiotics), instead suggested a possible role for translational regulation of jadomycin B production. Given that ribosomal defects were also seen for the RNase III mutant, it is not unreasonable to presume that translational defects (in conjunction with RNA metabolism defects) may also contribute to reduced antibiotic production in this strain. Antibiotic biosynthetic genes are typically organized in large operons, with many genes being translationally coupled. Studies in *Saccharomyces cerevisiae* (Ciandrini et al., 2013) and *E. coli* (Valleriani et al., 2011) have revealed strong negative correlations between translation ratios (the amount of protein produced per mRNA) and mRNA lengths, with longer mRNAs having slower rates of translation initiation and correspondingly decreased ribosome densities. As translational efficiency would be adversely affected by the long mRNAs associated with many antibiotic biosynthetic clusters, and RNase mutation could further compromise ribosome activity, these transcripts may be translated less effectively than in a wild type strain.

Interestingly, ribosome alterations have been broadly linked with changes in antibiotic levels in a multitude of streptomycetes, although in different ways than shown here. Specifically, mutations in *rpsL* (encoding ribosomal protein S12) and *rsmG* (encoding a 16S rRNA methyltransferase) significantly enhance antibiotic production (Hosaka et al., 2009; Nishimura et al., 2007; Tanaka et al., 2009); mutations in these genes are also associated with increased antibiotic (specifically streptomycin) resistance. A consistent effect stemming from the *rsmG* mutation is enhanced S-adenosyl methionine (SAM) production, due to increased transcription of the SAM synthetase-encoding gene *metK*. In the streptomycetes, overexpression or exogenous application of SAM has found broad-spectrum utility in stimulating antibiotic production (Okamoto et al., 2003). In *B. subtilis*, RNase J mutations have been associated with reduced levels of *metK* (Mäder et al., 2008). Whether an analogous expression defect for *metK* exists in the streptomycetes remains to be seen, but reduced levels of *metK* in either RNase mutant could further contribute to the antibiotic defects observed for these strains.

2.4.3 Role of RNase III and RNase J in the assembly of functional ribosomes in the streptomycetes

The ribosomal defects associated with the loss of RNase III include abnormal 5' end processing of 23S rRNA, a reduced ability to assemble 70S ribosomes and a propensity to form 100S ribosome dimers. Collectively, these characteristics would indicate this strain has serious translational defects, a prediction borne out by the dramatic reduction in polysome peaks observed for the *rnc* mutant relative to wild type. The final 23S rRNA processing step occurs in polysomes (Srivastava and Schlessinger, 1988), suggesting that only when the ribosomes are associated with mRNAs, do they adopt a conformation conducive to the final stages of maturation. As fewer polysomes were detected in the *rnc* mutant than the wild type (and *rnj* mutant), this could contribute to a further reduction in the number of fully mature ribosomes present in this strain, excluding those sequestered as 100S dimers. The situation is less clear-cut

for RNase J, where its loss led to cold sensitivity and accumulated 100S ribosome dimers, but no enrichment in ribosome subunits or any obvious rRNA processing defects, at least at the 5' ends of the 16S and 23S rRNAs. In *M. smegmatis,* RNase E acts alongside RNase J to process all three rRNA molecules (Taverniti et al., 2011), and it is conceivable that RNase E has an equivalent role in *S. venezuelae*.

The accumulation of 100S ribosome dimers for both *rnc* and *rnj* mutants was unexpected, as such a phenomenon has not been observed for equivalent mutants in other bacteria. All evidence to date suggests that 100S ribosomes are translationally inactive: their peptidyl transferase centres and peptide exit tunnels are inaccessible, and they are not associated with tRNAs or mRNAs (Kato et al., 2010; Wada et al., 1995; Yoshida et al., 2002). These inactive dimers typically form during stationary phase and their formation has been tied to the stringent response (Izutsu et al., 2001; Tagami et al., 2012), although it is worth noting that not all bacteria adopt such ribosome configurations. In *Mycobacterium*, for example, the essential dormancy regulator DosR promotes the formation of translationally inactive 'stabilized' 70S ribosomes during conditions of stress, and in *M. smegmatis,* this is mediated by a protein termed RafH (MSMEG_3935) (Trauner et al., 2012). The Hpf homolog (MSMEG_1878) was found associated with ribosomes in stationary phase, but its presence was not sufficient to promote dimerization. Our observations here suggest that the streptomycetes differ from their mycobacterial relatives in forming 100S ribosome dimers, and this may be mediated - at least in part - by Hpf proteins. It is conceivable that losing either RNase J or RNase III in *S. venezuelae* results in a cellular stress response analogous to that occurring during stationary phase, leading to a down-regulation of translation.

2.4.4 RNase activity and antibiotic sensitivity

One of the most profound phenotypic changes observed for the *rnc* and *rnj* mutants was significantly increased sensitivity to a range of antibiotics targeting not only the ribosome, but also RNA polymerase (particularly for Δ*rnj)* and the cell wall (for Δ*rnc*). The response to ribosome-specific antibiotics may stem from the fact that ribosomes in these strains are already defective, and consequently are hypersensitive to antibiotic effects. It is also possible that the inability of these strains to effectively turn over aberrant ribosome precursors formed during antibiotic treatment contributes to the observed increase in antibiotic sensitivity (Maguire, 2009). An exception to this sensitization comes with clindamycin, where we observed increased resistance for an *rnj* mutant. This antibiotic binds to the base of the peptide tunnel, in part through extensive hydrogen bonding with the 23S rRNA in this region (Tu et al., 2005) - a region not expected to be modified or processed by RNase J given its central position within the 23S rRNA. Hence it is currently unclear why this strain exhibits increased clindamycin resistance.

Our work suggests that RNase III and RNase J contribute to the formation of fully functional ribosomes. In addition to directing translation, ribosomes also contribute directly to RNA polymerase processivity through the close coupling of transcription and translation in bacteria (Proshkin et al., 2010). As *rnc* and *rnj* appear to have reduced ribosomal processivity, this may

in turn lead to less effective transcription elongation, and an exacerbated effect of any antibiotic targeting RNA polymerase, such as was observed following rifampicin treatment here.

While an *rnj* mutant had an essentially wild type response to vancomycin, the *rnc* mutant was again more sensitive. The mechanism underlying this observation is not immediately obvious, but previous RNA-seq and chromatin immunoprecipitation analyses in *S. coelicolor* revealed a number of membrane proteins, lipoproteins and other secreted protein-encoding genes to be affected by the loss of RNase III (Gatewood et al., 2012), and it is conceivable that one or more of these may contribute to increased vancomycin sensitivity, or indeed general antibiotic sensitivity through enhanced uptake/reduced efflux.

It is clear from this work, and from that of others, that RNase III and RNase J play important but distinct roles in morphological development, secondary metabolism and ribosome assembly and function in the streptomycetes. Further investigations into the cellular targets of these RNases, and the accompanying downstream effects of their activities, will allow us to better understand the role that these enzymes play in the regulatory and metabolic networks governing these processes, and others in the cell.

2.5 Materials and Methods

2.5.1 Bacterial strains and culture conditions

Streptomyces strains, *E. coli* strains, and all plasmids/cosmids used in this study are summarized in **Table 2.1**. *S. venezuelae* ATCC 10712 was typically grown on the surface of maltose-yeast extract-malt extract (MYM) agar medium (Yang et al., 2001) or in shaken flasks containing liquid MYM at 20°C or 30°C. During conjugation with *E. coli*, *S. venezuelae* was grown on soy flour-mannitol agar medium (Kieser et al., 2000), whilst Difco nutrient agar medium was used in screening for double cross-over recombinants when creating RNase mutant strains. Finally, when assessing antibiotic production - specifically jadomycin B - by *S. venezuelae*, strains were grown in jadomycin B production medium (Brooks et al., 2012), as detailed below. *E. coli* strains were grown in or on LB (Luria Bertani) medium or in SOB (super optimal broth) medium, with DH5α and ET12567/pUZ8002 strains grown at 37°C and BW25113/pIJ790 grown at 30°C or 37°C.

Dilution plating experiments involved the overnight growth of *S. venezuelae* in MYM liquid medium, and subsequent use of these cultures to inoculate 10 mL fresh liquid MYM to an OD_{600} of ~0.1. Cultures were grown shaking at 30°C until they reached an OD_{600} of 0.4, at which point serial dilutions were made in 10-fold increments. Three microlitres of each dilution were immediately spotted onto MYM agar plates and incubated at either 20°C or 30°C for 3-4 days.

2.5.2 Construction of *rnc* (RNase III) and *rnj* (RNase J) deletion strains

In frame deletions of *rnc/SVEN_5265* (RNase III) and *rnj/SVEN_5394* (RNase J) were generated using ReDirect technology (Gust et al., 2003). For each of *rnc* and *rnj*, the coding sequence (from start codon to stop codon) was replaced with an *oriT*-containing apramycin resistance cassette. RNase gene deletions were verified by polymerase chain reactions (PCRs) performed using combinations of primers located upstream, downstream and internal to the deleted genes (see **Table 2.3**).

The *rnc* mutant phenotype was complemented using a DNA fragment encompassing the wild type *rnc* gene and associated upstream (278 bp) and downstream (212 bp) sequences (see **Table 2.3** for primer information), cloned into the integrating plasmid vector pIJ82. The same complementation strategy was used for the *rnj* mutant, only the complementing DNA fragment contained the wild type *rnj* gene, along with 280 bp upstream and 153 bp downstream flanking sequences (**Table 2.3**). In each case, the complementing fragment was expected to include the native *rnc/rnj* promoter region, and all associated upstream and downstream regulatory elements. To control for any phenotypic effects stemming from plasmid integration, pIJ82 alone was introduced into wild type and *rnc/rnj* mutant strains, and these strains served as the basis for phenotypic comparisons during complementation experiments.

2.5.3 Light microscopy and scanning electron microscopy

Samples for light microscopy were obtained by growing strains on MYM agar for 3 days, and pressing sterile coverslips against the growing colonies, or by applying a 20 µL aliquot of liquid MYM-grown cultures to a slide and overlaying with a cover slip. Images were obtained using a Nikon Eclipse TE2000-S inverted microscope, and where appropriate, spore lengths were determined using ImageJ software (Abràmoff et al., 2004). For each strain, a minimum of 400 spores were measured for each of three replicates ($\geq$1200 spores in total).

Scanning electron microscopy (SEM) was used to examine strains grown for 6 days on MYM agar. Samples were prepared and visualized using a TEMSCAM LSU scanning electron microscope, as described previously (Haiser et al., 2009).

2.5.4 Heat shock assay

Heat shock assays were performed as described previously (Haiser et al., 2009), with minor modifications. Briefly, spore suspensions were diluted in distilled water to a final concentration of ~250 spores/100 µL. One hundred microlitre aliquots were heated at 50°C for 10 to 40 min before being spread on MYM agar plates and incubated at 30°C for 4 days. Survival rates were calculated by dividing the number of colonies on plates after heat treatment, by the number of colonies on plates without heat treatment; the resulting values were converted to percentages.

2.5.5 Jadomycin B production assay

Jadomycin B production was assayed as described previously (Jakeman et al., 2006), with minor alterations to the published protocol. *S. venezuelae* was streaked for single colonies on MYM agar and plates were grown for a minimum of 3 days. A single colony was then used to inoculate 125 mL of liquid MYM and the culture was grown with shaking at 30°C for 22 hours. Four to six millilitres of culture were then used to inoculate 100 mL glucose/isoleucine-based jadomycin production medium (S Brooks et al., 2012) to an OD_{600} of 0.3. Cultures were shaken at 30°C until an OD_{600} of 0.6 was reached (~5 hours), at which point 95% ethanol was added to the flasks (3% v/v) to induce jadomycin B production. Samples for jadomycin B analyses were taken immediately after ethanol shock, and after 16, 36 and 64 hours. Jadomycin B was quantified by measuring the absorbance of culture supernatant at 526 nm, and normalizing to culture growth (OD_{600}) at that time point.

2.5.6 RNA isolation

S. venezuelae was grown at 30°C in shaken flasks containing liquid MYM. Cells were harvested either at time points corresponding to vegetative growth (6-8 hours) for rRNA analysis and *hpf* expression analysis, or 23 hours after ethanol shock for analysis of jadomycin B biosynthetic cluster transcripts. RNA was extracted as described previously (Chomczynski, 1987), using a modified guanidium thiocyanate protocol (Moody et al., 2013). Cells were lysed by vortexing for 2 min with glass beads in a solution containing 4 M guanidium thiocyanate, 25 mM trisodium citrate dihydrate, 0.5% w/v sodium N-lauroylsarcosinate, and 0.8% β-mercaptoethanol. The resulting suspension was subjected to two phenol-chloroform extractions, followed by an acid phenol-chloroform extraction. Total nucleic acids were precipitated overnight using 3 M sodium acetate and an equal volume of isopropanol. Samples were then pelleted, washed in 70% ethanol, and resuspended in nuclease-free water. Contaminating DNA was removed using Turbo DNase (Life Technologies), and RNA quantity and purity were determined using a Nanodrop spectrophotometer. RNA quality was analyzed by agarose gel electrophoresis prior to RT-PCR and primer extension analyses.

2.5.7 Primer extension

Gene-specific primers (**Table 2.3**) internal to the mature sequence of rRNA genes were radiolabelled with γ-(^{32}P) ATP using T4 polynucleotide kinase (New England Biolabs). Two micrograms of total RNA were heated at 80°C for 3 min before being added to an annealing mix containing 1 µL of a 10 mM deoxynucleoside triphosphate mixture and 2 pmol radiolabelled primer. The mixture was then incubated at 65°C for 8 min before being chilled on ice for 5 min. Reverse transcription (RT) was performed using SuperScript III reverse transcriptase (Invitrogen) according to the manufacturer's instructions, with minor modifications. Briefly, 4 µL 5× First-Strand buffer, 1 µL 0.1 M dithiothreitol (DTT), 1 µL RNaseOUT™ and 1 µL (200 units) SuperScript III were mixed and incubated at 55°C for 1 hour, followed by incubation at 70°C for 15 min to inactivate the enzyme. Reaction products were mixed with 2× loading dye, heated to 95°C for 5 min, and 2-12 µL were loaded and separated on a 6% denaturing polyacrylamide gel.

The primer ladder was generated by radiolabelling 2 pmol of each of five differently sized primers (**Table 2.3**) as described above.

2.5.8 Reverse transcription-PCR (RT-PCR)

RT-PCR was conducted as described by Hindra *et al.* (Hindra et al., 2010). Specifically, RT was performed as outlined above for the primer extension experiment, with the only change being the use of 0.9 µg total RNA as template. The resulting cDNA in turn served as template for PCR amplification using Taq DNA polymerase and gene-specific primers (**Table 2.3**). The number of cycles was optimized to ensure products were detected in the linear range of amplification. Negative controls containing nuclease-free water instead of reverse transcriptase were included to ensure RNA samples - and reverse transcription/amplification reagents - did not contain residual or contaminating genomic DNA. cDNA corresponding to the vegetative sigma factor-encoding gene *hrdB* was amplified as a positive control for RNA levels and RNA integrity. Ten microlitres of each PCR mixture were separated on a 2% agarose gel and visualized by staining with ethidium bromide. All reactions were conducted in triplicate, using at least two independently isolated RNA samples.

2.5.9 Ribosome profiles

Overnight cultures of *S. venezuelae* were used to inoculate 300 mL MYM in 2 L flasks to an OD_{600} of 0.05, and these cultures were grown until they reached an OD_{600} of ~0.4. All subsequent steps were carried out at 4°C. Cultures were harvested by centrifugation at 7,798 ×*g* for 10 min. Cell pellets were washed and resuspended in 20 mL of 10 mM Tris-HCl pH 7.5, 10 mM $MgCl_2$ and 60 mM KCl. The cell resuspension was then centrifuged again at 3,400 ×*g* for 15 min. The resulting cell pellet was resuspended in 7 mL lysis buffer containing 10 mM Tris-HCl pH 7.5, 10 mM $MgCl_2$, 60 mM KCl, 1 mM DTT, together with 35 µL of Tween 20, a Roche cOmplete Mini Protease Inhibitor Cocktail Tablet and 20 µL DNase I (1 mg/mL). Resuspended cells were lysed by three times passage through a French press at 20,000 lbs/in^2. The cell lysate was clarified by centrifugation at 16,000 ×*g* for 10 min, and the resulting supernatant was further spun at 135,000 ×*g* for 2 hours and 25 min. Resuspension of the pelleted ribosomes was allowed to proceed for 30 min on ice, in buffer containing 20 mM Tris-HCl pH 7.5, 6 mM $MgCl_2$, 30 mM NH_4Cl and 1 mM DTT. An equal amount of 20 mM Tris-HCl pH 7.5, 6 mM $MgCl_2$, 800 mM NH_4Cl and 1 mM DTT was then added and incubation on ice was continued for another hour. The mixture was clarified by centrifugation at 22,000 ×*g* for 20 min, and the crude ribosomes were pelleted by centrifuging the supernatant at 135,000 ×*g*, again for 2 hours and 25 min. The resulting ribosome pellet was resuspended on ice for 1 hour in 20 mM Tris-HCl pH 7.5, 10 mM $MgCl_2$, 30 mM NH_4Cl and 1 mM DTT. After another clarifying spin, 10-15 A_{260} units of resuspended crude ribosomes were applied to 10.5 mL 10%–30% (w/v) sucrose gradients prepared with 'buffer B' (20 mM Tris-HCl pH 7.5, 10 mM $MgCl_2$, 50 mM NH_4Cl, 1 mM DTT). The gradients were spun for 16 h at 40,000 ×*g* in a Beckman SW41 Ti rotor. Gradients were fractionated using a Brandel fractionator apparatus and an AKTA Prime FPLC system (GE Healthcare). Elution profiles were monitored by UV absorbance at 260 nm and fractions

corresponding to 70S and 100S subunit peaks were individually pooled and collected for negative staining electron microscopy. The subunits were removed from the sucrose buffer by centrifugation at 135,000 ×*g* for 2 hours and 25 min, after which the pellet was rinsed and resuspended in buffer B, prior to storage at -80^{0}C.

The proportion of free 30S to 'bound 30S' (30S subunits contained within 70S and 100S ribosomes) and free 50S to 'bound 50S' (50S subunits contained within 70S and 100S ribosomes) in the wild type and mutant strains was calculated using peak areas obtained from the sucrose gradient profiles. The area of the 30S peak was divided by the area corresponding to the total number of 30S subunits (30S peak plus one-third the area of the 70S peak and 100S peak when observed) to obtain the percentage of free 30S subunits. To obtain the percentage of free 50S subunits, the area of the 50S peak was divided by the area corresponding to the total number of 50S subunits (50S peak plus two-thirds the area of the 70S peak and 100S peak when observed). Prior to obtaining these percentages, we normalized all ribosomes profiles by making the entire area under the 30S, 50S, 70S and 100S (when present) peaks constant; this allowed for direct comparison of the peaks representing the 70S and 100S particles between strains. These experiments were conducted using two (mutant) or three (wild type) independently grown cultures, with a minimum of three technical replicates conducted for each biological sample.

2.5.10 Polysome profiles

Polysome profiles were generated as described in Leong et al. (2013), with minor adjustments. Overnight cultures of *S. venezuelae* were used to inoculate 300 mL MYM in 2 L flasks to an OD_{600} of 0.05, and cultures were grown by shaking at 30°C until reaching an OD_{600} of ~0.4. Polysomes are typically stabilized by adding chloramphenicol (Brow, David A. and Noller, 1983), but *S. venezuelae* can produce chloramphenicol and consequently is resistant to the effects of this antibiotic. We therefore attempted to use clindamycin to stabilize polysomes (this targets the same site/process as chloramphenicol and is not reported to cause ribosome distortion); however, we found that *S. venezuelae* polysomes were most stable without antibiotic addition. Cells were harvested by centrifugation at 7,798 ×*g* for 10 min, and each pellet was resuspended in 0.5 mL cold resuspension buffer (20 mM Tris-HCl pH 7.5, 15 mM $MgCl_2$), with lysozyme added to a final concentration of 1 mg/mL. Tubes were incubated on ice for 15 min, and the suspensions were subjected to three cycles of freezing in liquid nitrogen/thawing at 30°C. Cell lysis was completed by adding 15 µL 10% sodium deoxycholate and 10 µL DNase I (1 mg/mL). The mixtures were centrifuged at 5,000 ×*g* for 15 min, after which the supernatants were transferred to new tubes. Sample concentrations were measured by absorbance at 260 nm, and 10 A_{260} units of resuspended crude ribosome particles were added to buffer containing 10 mM Tris-HCl pH 7.5, 50 mM KCl, 10 mM $MgCl_2$, and 6 mM β-mercaptoethanol before being loaded onto a 10 mL 10-40% (w/v) sucrose gradient prepared in the same buffer. The gradients were spun for 16 hours at 40,000 ×*g* in a Beckman SW41 Ti rotor at 4°C. Gradients were fractionated using a Brandel fractionator apparatus and a syringe pump, and the elution profiles were monitored by UV absorbance at A_{260}. All polysome profiles were conducted using

at least two independent cell cultures and three technical replicates per strain. The obtained profiles were normalized before plotting them by making the area under each profile constant.

2.5.11 Electron Microscopy

Fractions corresponding to 70S and 100S subunit peaks were diluted to 18 µg/mL in buffer B. Electron microscopy grids freshly coated with a continuous layer of carbon were floated in 5 µL drops of sample immediately following glow discharge application to the grid (5 mA for 15 sec). Grids were then blotted and floated for 1 min in a 5 µL drop of 1% uranyl acetate for staining. Excess stain was removed by blotting and the grids were air-dried. Specimens were visualized in a JEOL1200EX electron microscope operated at 80 kV at a magnification of 200,000×. Images were acquired with an AMT 4-megapixel digital camera (Advanced Microscopy Techniques, Woburn, MA). Between 800 and 1000 particles per sample were counted and each particle was assigned to one of the following three categories: 70S (monomer), 100S (dimer) or polysome (3 or more 70S ribosomes in a row).

2.5.12 Antibiotic sensitivity assays

Overnight cultures of *S. venezuelae* were used to inoculate 10 mL liquid MYM in 25 mL flasks to an OD_{600} of 0.04. Antibiotics were added to each flask to allow for between 15% and 50% growth relative to that of the wild type strain in the absence of antibiotic. The final antibiotic concentrations used were: 2.5 µg/mL hygromycin B, 2.5 µg/mL spectinomycin, 0.5 µg/mL viomycin, 0.5 µg/mL tetracycline, 0.1 µg/mL clindamycin, 0.5 µg/mL erythromycin, 0.025 µg/mL rifampicin and 0.5 µg/mL vancomycin. Following antibiotic addition, cultures were grown with shaking at 30°C for 6 h, and relative survival rates were calculating by dividing OD_{600} values after growth in the presence of antibiotics, by OD_{600} values of cultures without antibiotics, with results being presented as percentages.

Table 2.1 Bacterial strains and plasmids

Streptomyces venezuelae	Genotype, description, or use	Reference or source
ATTC10712		
E325	ATC10712 Δ*SVEN_5265(rnc)::[aac(3)IV-oriT]*	This work
E326	ATC10712 Δ*SVEN_5394(rnj)::[aac(3)IV-oriT]*	This work
E. coli		
DH5α	Plasmid construction and general subcloning	Invitrogen
ET12567/pUZ8002	Generation of methylation-free plasmid DNA and conjugation into *Streptomyces*	(MacNeil et al., 1992; Paget et al., 1999)

BW25113/pIJ790	Construction of cosmid-based knockouts	(Gust et al., 2003)
Plasmids or cosmids		
pIJ790	Temperature-sensitive plasmid carrying λ-RED genes	(Gust et al., 2003)
pIJ82	Integrating plasmid vector; complementation of mutant strains	Gift from H. Kieser
pIJ773	Plasmid carrying the apramycin knockout cassette	(Gust et al., 2003)
3B03	*S. venezuelae* cosmid carrying *SVEN_5265* (*rnc*)	Gift from M. Bibb and M. Buttner
3J08	*S. venezuelae* cosmid carrying *SVEN_5394 (rnj*)	Gift from M. Bibb and M. Buttner
pMC110	pIJ82 + *rnc*; *rnc* complementation plasmid	This work
pMC111	pIJ82 + *rnj*; *rnj* complementation plasmid	This work

Table 2.2 Doubling time and growth rates of *S. venezuelae* strains in MYM liquid media

* Standard deviations were calculated from 3-4 replicates per strain.

	Doubling time (DT) (h)*		Growth rate, k = ln2/DT (h^{-1})*	
	30°C	20°C	30°C	20°C
WT	1.59 ± 0.01	2.43 ± 0.09	0.436 ± 0.002	0.286 ± 0.010
rnj	1.61 ± 0.01	3.93 ± 0.1	0.431 ± 0.002	0.177 ± 0.005
rnc	1.79 ± 0.04	3.42 ± 0.08	0.387 ± 0.009	0.203 ± 0.005

Table 2.3 Oligonucleotides used in this study

Name	Sequence (5’ to 3’)	Use
Sven5265 Fwd	GGTCCTCTCGGTCTGATTGGGCTGGTGAGAGGCGCA ATGATTCCGGGGATCCGTCGACC	Creation of Δ*rnc* strain; confirmation of Δ*rnc* mutation
Sven5265 Rev	TGGGGCGGGGTTCTCGGGAAGCGTGGGGGACGGCC GTCATGTAGGCTGGAGCTGCTTC	Creation of Δ*rnc* strain; confirmation of Δ*rnc* mutation
Sven5265 up	GGGAACCGATGAGAAGGAC	Cloning of *rnc* for mutant complementation;

		confirmation of Δ*rnc* mutation
Sven5265 in	CGGTACAGCGTGTCCGTGAC	Confirmation of Δ*rnc* mutation
Sven5265 dwn	CTGGGGTGCAGGACCTCG	Cloning of *rnc* for mutant complementation
Sven5394 Fwd	CAAGGGGTACGTGGCGTGCGTGGTGAGGAGAGTCTTTTGAATTCCGGGGATCCGTCGACC	Creation of Δ*rnj* strain; confirmation of Δ*rnj* mutation
Sven5394 Rev	CGCTCCGGTGCTGCGCTGGTCAGACCGTCAGGCCCGTCATGTAGGCTGGAGCTGCTTC	Creation of Δ*rnj* strain; confirmation of Δ*rnj* mutation
Sven5394 up	CCAGAAGCTGCTCCCGGTC	Cloning of Δ*rnj* for mutant complementation; confirmation of Δ*rnj* mutation
Sven5394 in	GTTCCGGCCGATCTCACCG	Confirmation of Δ*rnj* mutation
Sven5394 dwn	GTCGGATTTCCCGCCTCCC	Cloning of *rnj* for mutant complementation; confirmation of Δ*rnj* mutation
M13 FWD	GTAAAACGACGGCCAGT	Cloning and sequencing
16S rRNA	CGGAGAGTTTGATCCTGGC	Reverse transcription for primer extension
23S rRNA	GGACGCGAGCATCTGTGGC	Reverse transcription for primer extension
ladder1	TCAGGTGGGCGACGGCGTCGGCGAGGCTCATGCGGACACTGTAGGCTGGAGCTGCTTC	Primer extension ladder
ladder2	GTGGTGGTGCTCAAGCGGCTCATCGCTACGACTTAGGTGAGCC	Primer extension ladder
ladder3	ATATCATATGTCGATCGACGTCAACAACG	Primer extension ladder
ladder4	CACTGACCAGGAGACTTTCGC	Primer extension ladder
ladder5	ATCGCCTCCGCGTCCACG	Primer extension ladder
HrdBF	CCGTTTCCATCGTTCCGAGA	Semi-quantitative RT-PCR
HrdBR	ATCTGCCCATCAGCCTTTCC	Semi-quantitative RT-PCR

JadAF	AATTCGACGCCTCCGAGATG	Semi-quantitative RT-PCR
JadAR	TCGAAGTCCTGGAGGTGGAA	Semi-quantitative RT-PCR
JadMF	GGGCACCCTCAACTACATCC	Semi-quantitative RT-PCR
JadMR	TCTTGAGCAGCTTCACGGAG	Semi-quantitative RT-PCR
JadJF	CGAAATCGCTGTCCGTGTG	Semi-quantitative RT-PCR
JadJR	GATAACTGGTCGCCGGAGTG	Semi-quantitative RT-PCR
Hpf UTRF	GACAGGAGTTCAGGGCGAAT	Semi-quantitative RT-PCR
Hpf UTRR	ATTACCGGAGCTCGGACTTG	Semi-quantitative RT-PCR
Hpf codingF	GAAAGCCTGCCGTTCCCA	Semi-quantitative RT-PCR
Hpf codingR	GACCTCGCCAGCGACAAG	Semi-quantitative RT-PCR

CHAPTER 3: *STREPTOMYCES* EXPLORATION IS TRIGGERED BY FUNGAL INTERACTIONS AND VOLATILE SIGNALS

Stephanie E. Jones, Louis Ho, Christiaan A. Rees, Jane E. Hill, Justin R. Nodwell, Marie A. Elliot

Preface:
This chapter was published in *eLife* in 2017 (Jones et al., 2017). Louis Ho, a Ph.D. student in Justin Nodwell's lab at the University of Toronto, carried out the *S. cerevisiae* haploid deletion library screens, setup the *C. albicans* – *S. venezuelae* interactions, and took the *S. venezuelae* time lapse video. Christiaan Rees, an M.D.-Ph.D. student in Jane Hill's lab at Dartmouth College, carried out the GC-MS profiling experiments. I performed all other work.

3.1 Abstract (Chapter Summary)

It has long been thought that the life cycle of *Streptomyces* bacteria encompasses three developmental stages: vegetative hyphae, aerial hyphae and spores. Here, we show interactions between *Streptomyces* and fungi trigger a previously unobserved mode of *Streptomyces* development. We term these *Streptomyces* cells 'explorers', for their ability to adopt a non-branching vegetative hyphal conformation and rapidly transverse solid surfaces. Fungi trigger *Streptomyces* exploratory growth in part by altering the composition of the growth medium, and *Streptomyces* explorer cells can communicate this exploratory behaviour to other physically separated streptomycetes using an airborne volatile organic compound (VOC). These results reveal that interkingdom interactions can trigger novel developmental behaviours in bacteria, here, causing *Streptomyces* to deviate from its classically-defined life cycle. Furthermore, this work provides evidence that VOCs can act as long-range communication signals capable of propagating microbial morphological switches.

3.2 Introduction

Our current understanding of microbial growth and development stems largely from investigations conducted using single-species cultures. It is becoming clear, however, that most bacteria and fungi exist as part of larger polymicrobial communities in their natural settings (Scherlach et al., 2013; Traxler and Kolter, 2015). Microbial behavior is now known to be modulated by neighbouring organisms, where interspecies interactions can have profound and diverse consequences, including modifying virulence of human pathogens (Peleg et al., 2010), altering antibiotic resistance profiles of mixed-species biofilms (Oliveria et al., 2015), enhancing bacterial growth (Romano and Kolter, 2005), and increasing production of specialized metabolites by fungi and bacteria (Schroeckh et al., 2009; Stubbendieck and Straight, 2016). Consequently, an important next step in advancing our developmental understanding of microbes will be to expand our investigations to include multi-species cultures, and in doing so, unveil new and unexpected microbial growth strategies.

The soil is a heterogeneous environment that is densely populated with bacteria and fungi, and as such, represents an outstanding system in which to study the effects of bacterial-fungal interactions. Within the polymicrobial communities occupying the soil, *Streptomyces* represent the largest genus of the ubiquitous actinomycetes group. These Gram-positive bacteria are renowned for both their complex developmental life cycle (Elliot et al., 2008) and their ability to produce an extraordinary range of specialized metabolites having antibiotic, antifungal, antiparasitic, and anticancer properties (Hopwood, 2007).

The *Streptomyces* life cycle encompasses three developmental stages (**Fig. 3.1A**). First, a spore germinates to generate one or two germ tubes. These grow by apical tip extension and hyphal branching, ultimately forming a dense vegetative mycelial network that scavenges for nutrients. Second, in response to signals that may be linked to nutrient depletion, non-branching aerial hyphae extend into the air away from the vegetative cells. These aerial hyphae are coated in a hydrophobic sheath that enables escape from the aqueous environment of the vegetative

mycelium (Claessen et al., 2003; Elliot et al., 2003), and their emergence coincides with the onset of specialized metabolism within the vegetative cells (Kelemen and Buttner, 1998). Aerial development requires the activity of the '*bld*' gene products, where mutations in these genes result in colonies lacking the fuzzy/hydrophobic characteristics of wild type. The final developmental stage involves the differentiation of aerial hyphae into spores through a synchronous cell division and cell maturation event. This process is governed by the *whi* (for 'white') gene products, whose mutants fail to form mature, pigmented spores (McCormick and Flärdh, 2012). In addition to being highly stress-resistant, spores also provide a means of dispersing *Streptomyces* to new environments, as all characterized *Streptomyces* cell types are non-motile.

In this work, we identify a novel interaction between *Streptomyces venezuelae* and fungal microbes that induces a previously unknown mode of bacterial growth. We refer to this as 'exploratory growth', whereby cells adopt a non-branching vegetative hyphal conformation that can rapidly traverse surfaces. We show that part of the mechanism by which fungi induce exploratory growth involves glucose depletion of the growth medium. Remarkably, this novel mode of growth can be communicated to other – physically separated – streptomycetes through a volatile compound. Volatile signalling further alters cell propagation and survival of other bacteria.

3.3 Results

3.3.1 Physical association with yeast stimulates *Streptomyces* exploratory behaviour

To explore interactions between *Streptomyces* and fungi, we cultured *Streptomyces venezuelae* alone or beside the yeast *Saccharomyces cerevisiae* on solid agar (**Fig. 3.1B**), and incubated these cultures for 14 days. As expected, during this time *S. venezuelae* on its own formed a colony of normal size. In contrast, when *S. venezuelae* was grown beside *S. cerevisiae*, its growth was radically different. During the first 5 days, the cells appeared to consume *S. cerevisiae*, before initiating a rapid outgrowth that led to *S. venezuelae* colonizing the entire surface of a 10 cm agar plate after 14 days. Remarkably, growth did not cease when physical obstructions were encountered: *S. venezuelae* cells were able to spread over rocks and polystyrene barriers (**Fig. 3.1C**).

To gain insight into this phenomenon, we visualized the leading edge of the rapidly migrating *S. venezuelae* cells (**Video 3.1**: https://www.youtube.com/watch?v=Iq6iIIT1fTU). We found it initially progressed at a rate of ~1.5 µm/min. This is an order of magnitude faster than would be explained by growth alone, given that hyphal tip extension has been calculated to occur at a rate of 0.13 µm/min (Richards et al., 2012). We refer to this rapid movement as "exploratory growth", and these spreading cells as "explorers", based on their ability to effectively traverse surfaces. To further investigate the morphology of these explorer cells, we used scanning electron microscopy (SEM) to visualize *S. venezuelae* grown alone, *S. venezuelae* at the yeast interface, and *S. venezuelae* explorer cells, after 14 days of growth (**Fig. 3.1B**). We found *S.*

venezuelae alone grew vegetatively, albeit without any obvious branches (branching vegetative cells were observed during growth on other media types, as expected), whereas *S. venezuelae* growing on *S. cerevisiae* raised aerial hyphae and sporulated. Microscopic analysis of explorer cells revealed that they failed to branch and were reminiscent of aerial hyphae. Unlike aerial hyphae, however, these filaments were hydrophilic, based on their inability to repel aqueous solutions (**Fig. 3.2**).

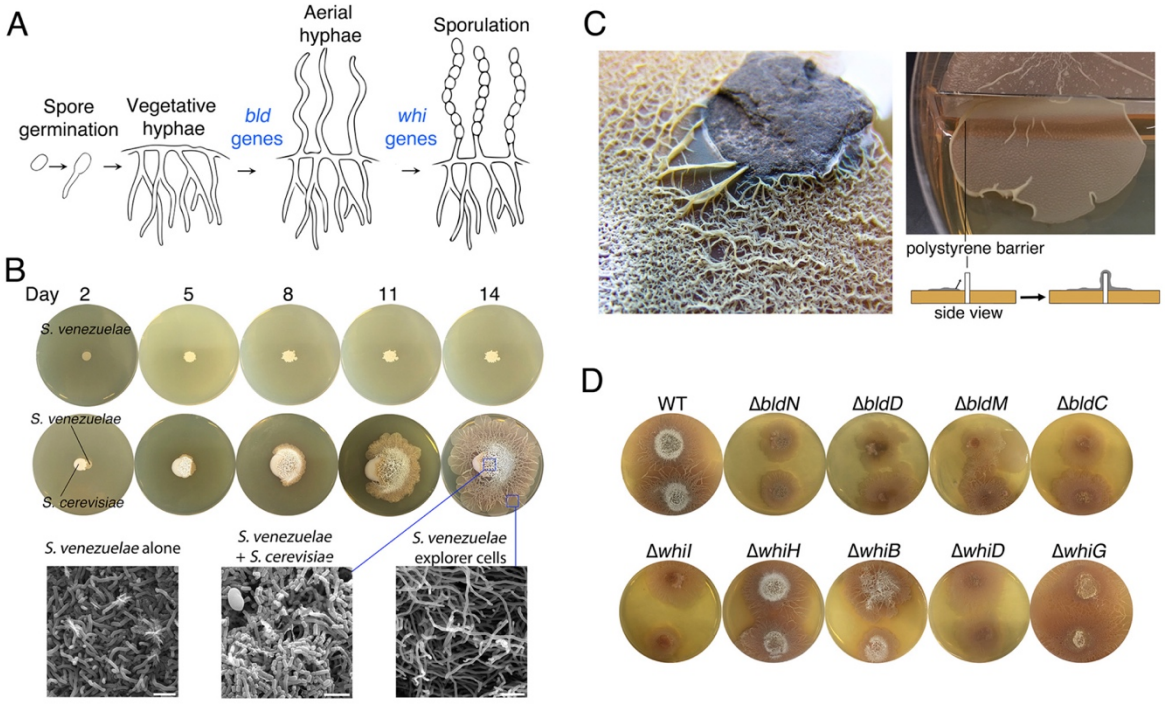

Fig. 3.1 Physical association with yeast triggers *Streptomyces* exploratory behaviour. A. Developmental life cycle of *Streptomyces*. Germ tubes emerge from a single spore, and grow by apical tip extension and hyphal branching, forming a dense network of branching vegetative hyphae. In response to unknown signals, non-branching aerial hyphae coated in a hydrophobic sheath, escape into the air. Aerial hyphae differentiate into chains of dormant, stress-resistant non-motile spores. The *bld* gene products are required for the transition from vegetative growth to aerial hyphae formation, while the *whi* gene products are required for the differentiation of aerial hyphae into spore chains. **B.** *S. venezuelae* grown alone (top row) and beside *S. cerevisiae* (middle row) on YPD (yeast extract-peptone-dextrose) medium over 14 days. Bottom panels: scanning electron micrographs of *S. venezuelae* grown alone (left), *S. venezuelae* on *S. cerevisiae* (middle), and *S. venezuelae* beside *S. cerevisiae* (right) for 14 days on YPD agar medium. White bars: 5 µm. **C.** *S. venezuelae* explorer cells growing up a rock embedded in agar (left), and over a polystyrene barrier within a divided petri dish (right, and schematic below). **D.** *S. venezuelae* wild type and developmental mutants grown beside *S. cerevisiae* on YPD agar medium for 14 days. Top: *S. cerevisiae*, together with wild type and Δ*bld* mutant strains (*bld* mutants cannot raise aerial hyphae). Bottom: *S. cerevisiae* grown next to Δ*whi* mutant strains (*whi* mutants can raise aerial hyphae but fail to sporulate).

To determine whether exploratory growth required classic developmental regulators (the *bld* and *whi* gene products), we grew a suite of *S. venezuelae* developmental mutants beside *S. cerevisiae* to evaluate whether these mutations impacted colony spreading (**Fig. 3.1D**). Four *S. venezuelae bld* mutants (*bldC,D,M,N*) and five *S. venezuelae whi* mutants (*whiB,D,G,H,I*) were inoculated beside *S. cerevisiae*. Unexpectedly, all developmental mutant strains displayed a similar exploratory behaviour as wild type after 14 days, although the *bldN* mutant exhibited slower exploration than the other strains. The mutant strains did, however, differ in their growth on yeast, with the *bld* mutants failing to raise aerial hyphae, and the *whi* mutants failing to sporulate. This demonstrated that exploratory growth was distinct from the canonical *Streptomyces* life cycle, and represented a new form of growth for these bacteria.

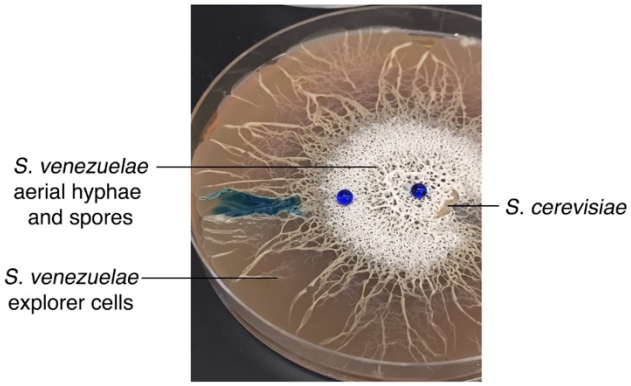

Fig. 3.2 Explorer cells are hydrophilic. *S. venezuelae* growing on top of *S. cerevisiae* cells raise hydrophobic aerial hyphae and spores. These structures effectively repel aqueous droplets (bromophenol blue dye dissolved in water). In contrast, explorer cells are hydrophilic, and application of aqueous droplets (as above) results in liquid dispersion.

To determine whether this exploratory behaviour was unique to *S. venezuelae*, we inoculated other commonly studied streptomycetes beside *S. cerevisiae*. We found that well-studied *Streptomyces* species, including *S. coelicolor, S. avermitilis, S. griseus,* and *S. lividans,* failed to exhibit an analogous spreading behaviour when plated next to *S. cerevisiae*. We next tested 200 wild *Streptomyces* isolates, growing each beside *S. cerevisiae*. Of these, 19 strains (~10%) exhibited exploratory growth similar to *S. venezuelae*. To determine whether this behaviour was confined to a particular *Streptomyces* lineage, we performed a phylogenetic analysis of these explorer-competent strains using *rpoB* sequences, and included non-exploratory model *Streptomyces* species as outgroups (**Fig. 3.3**). We found *S. venezuelae* and these wild *Streptomyces* did not form a monophyletic group, suggesting that exploratory growth is wide-spread in the streptomycetes.

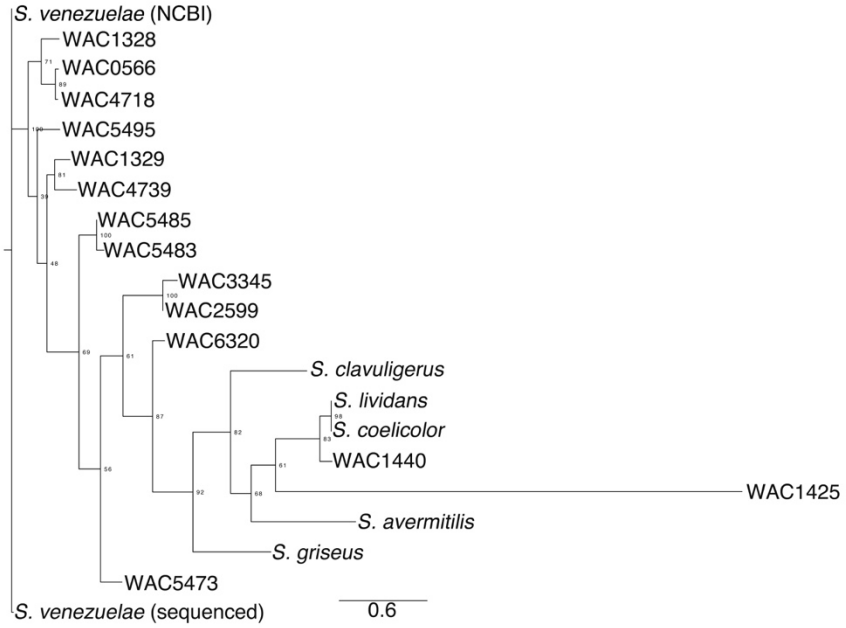

Fig. 3.3 Phylogeny of exploratory streptomycetes. The phylogeny was created using aligned *rpoB* sequences from wild *Streptomyces* isolates (WAC strains) that exhibited exploratory growth. For comparison, we included the non-spreading *S. coelicolor, S. lividans, S. avermitilis, S. griseus* and *S. clavuligerus*. A maximum likelihood tree was built using RaxML with a GTRGAMMA model of nucleotide substitution, with 500 bootstrap replicates to infer support values of nodes. Output was created using FigTree.

We next sought to determine whether *Streptomyces* exploratory behaviour could be triggered by other fungi. *S. venezuelae* was inoculated beside laboratory strains of *Candida albicans*, *Candida parapsilosis,* and *Crypotococcus neoformans*, and beside wild soil isolates of *S. cerevisiae, Zygosaccharomyces florentinus*, *Saccharomyces castellii*, *Pichia fermentans* and *Debaryomyces hansenii* (**Fig. 3.4**). We observed that all species, apart from *C. neoformans* and *P. fermentans*, induced *S. venezuelae* exploratory behaviour. This indicated that a broad range of microbial fungi could trigger exploratory growth.

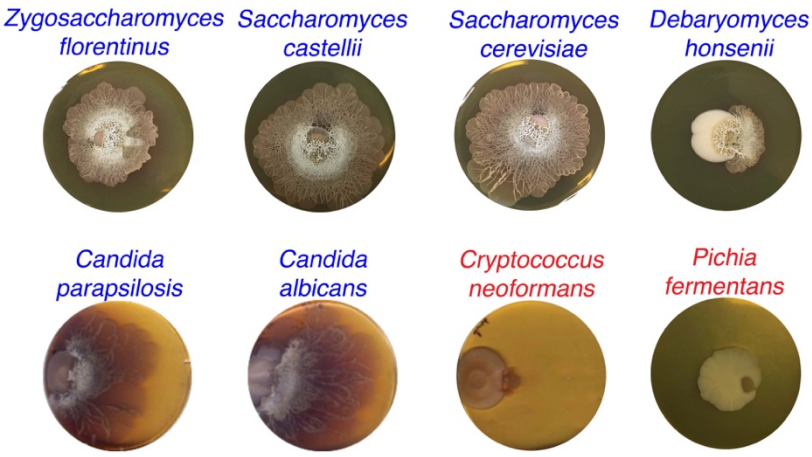

Fig. 3.4 *S. venezuelae* grown beside diverse yeast strains. *S. venezuelae* was grown beside the indicated yeast strains on YPD agar medium for 14 days. *Z. florentinus, S. castellii, S. cerevisiae, D. honsenii,* and *P. fermentas* are soil isolates, while *C. parapsilosis, C. albicans* and *C. neoformans* are laboratory strains. Yeast strains able to induce *S. venezuelae* exploratory growth are labelled in blue text, and yeast strains unable to induce *S. venezuelae* exploratory growth are shown in red.

3.3.2 The yeast TCA cycle must be intact to stimulate *S. venezuelae* exploratory behaviour

To understand how fungi could stimulate exploration, we took advantage of an *S. cerevisiae* haploid knockout collection containing 4,309 individual knockout strains. Each *S. cerevisiae* mutant was pinned adjacent to *S. venezuelae* and after 10 days, *S. venezuelae* exploratory growth was assessed. We identified 16 mutants that were unable to promote *S. venezuelae* exploration (**Fig. 3.5A**). Of these, 13 had mutations affecting mitochondrial function, including eight in genes coding for enzymes in the tricarboxylic acid (TCA) cycle (**Fig. 3.5A**), three in genes whose products contribute to the mitochondrial retrograde signalling pathway, as well as two whose products are involved in mitochondrial metabolism.

We confirmed these mutant effects using *Candida albicans* strains carrying tetracycline-repressible haploid mutations (**Fig. 3.6**). We grew four mutant strains adjacent to *S. venezuelae*, and found that two of them, Δ*LPD1* and Δ*KGD2,* also failed to stimulate *S. venezuelae* exploratory behaviour. As the products of these two genes act in the TCA cycle (**Fig. 3.5A**), these data collectively suggest that fungal respiration, and in particular TCA cycle function, influences exploratory growth in *S. venezuelae*.

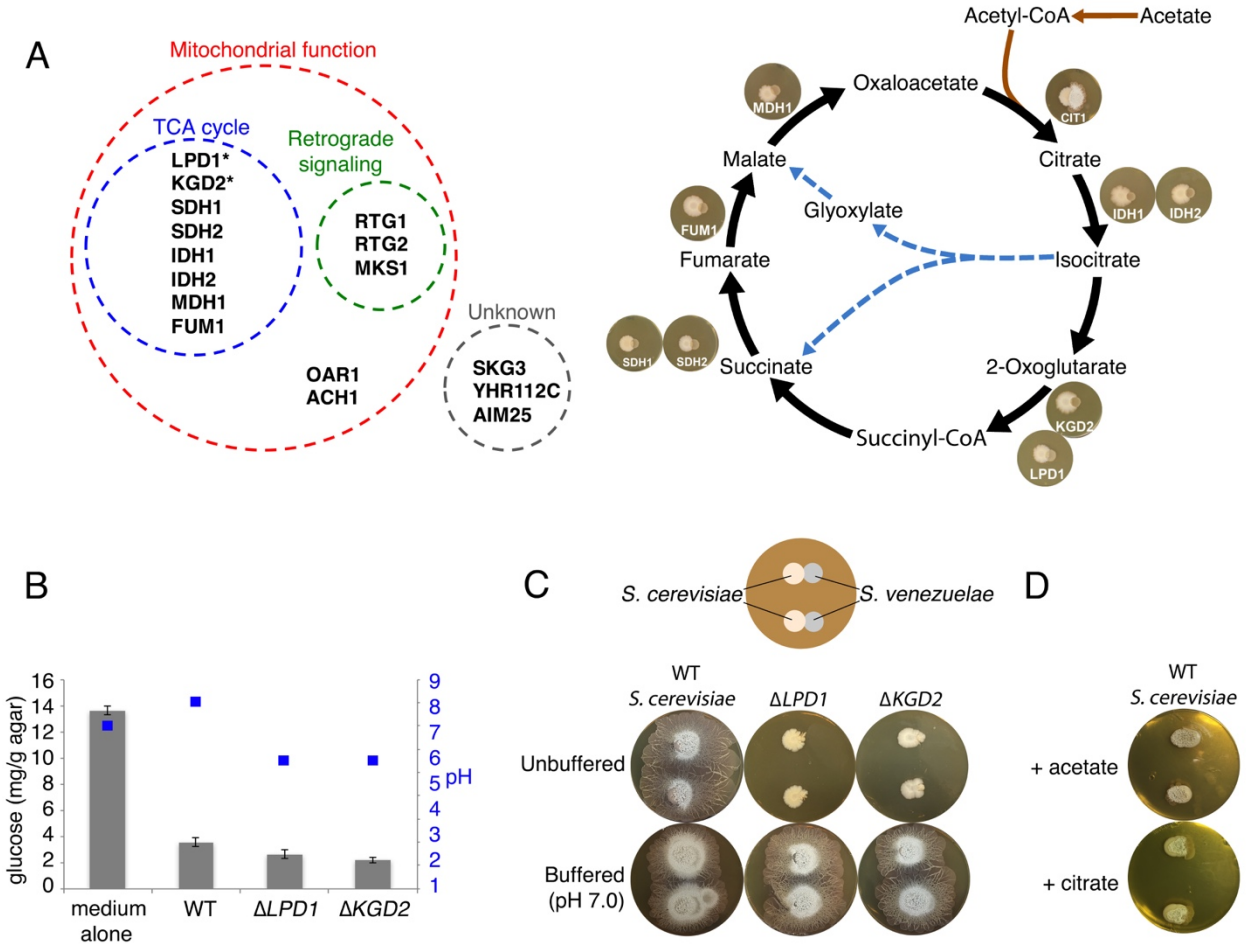

Fig. 3.5 Yeast stimulates *S. venezuelae* exploratory growth by consuming glucose and inhibits it by acidifying the medium. A. *S. cerevisiae* mutants that fail to stimulate *S. venezuelae* exploratory growth. Left: functional grouping of the exploration-deficient *S. cerevisiae* mutations. Asterisks indicate genes also identified in *C. albicans* as affecting *S. venezuelae* exploratory growth. Right: Mutations in *S. cerevisiae* TCA cycle-associated genes affect exploration after citrate production. For each interaction, the indicated *S. cerevisiae* mutant was grown beside wild type *S. venezuelae* for 7 days on YPD agar medium. **B.** Glucose concentration and pH associated with wild type and mutant *S. cerevisiae* strains grown on YPD agar medium. Glucose concentrations (grey bars) and pH (blue squares) were measured from medium alone, and beneath wild type, Δ*LPD1* or Δ*KGD2 S. cerevisiae* strains grown on YPD medium for 7 days. All values represent the mean ± standard error for four replicates. **C.** Top: schematic of the experimental set up, with *S. cerevisiae* grown to the left of *S. venezuelae* on YPD medium. Two replicates are grown on each agar plate. Bottom: wild type, Δ*LPD1*, and Δ*KGD2 S. cerevisiae* strains grown for 14 days beside wild type *S. venezuelae* on unbuffered YPD agar and YPD agar buffered to pH 7.0 with MOPS. **D.** Wild type *S. cerevisiae* spotted beside wild type *S. venezuelae* and grown for 14 days on YPD agar medium plates supplemented with acetate or citrate, each buffered to pH 5.5.

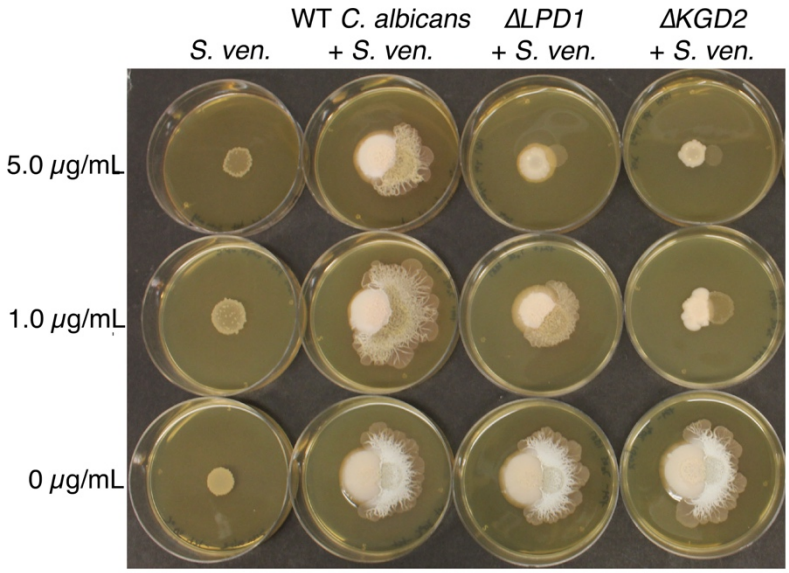

Fig. 3.6 *C. albicans* gene mutations that affect *S. venezuelae* exploratory growth. *S. venezuelae* (*S. ven.*) was inoculated alone or beside wild type (WT), Δ*LPD1*, or Δ*KGD2 C. albicans* strains on YPD agar for 10 days. *C. albicans* mutant strains were from the GRACE collection of tetracycline repressible deletion mutants. The indicated amount of tetracycline was added to YPD medium to induce the *C. albicans* gene deletion phenotype.

3.3.3 Exploration is glucose-repressible and pH-dependent

In considering how TCA cycle defects could influence *S. venezuelae* behaviour, we hypothesized that glucose uptake and/or consumption might play a role. We measured glucose levels of a YPD agar control, and compared this with YPD agar underneath *S. cerevisiae*. Uninoculated medium had 3.8 times as much glucose as *S. cerevisiae*-associated agar (**Fig. 3.5B**), confirming that *S. cerevisiae* consumed glucose during growth on YPD agar. This suggested that either glucose depletion by yeast, or some product of glucose metabolism, may trigger *S. venezuelae* exploratory growth.

To test these possibilities, we first asked whether exploratory growth could be triggered by lowering glucose concentrations. We plated *S. venezuelae* on YP (yeast extract-peptone) in the presence (G+) and absence (G-) of glucose (**Fig. 3.7**). After 10 days, we found growth on G- medium permitted *S. venezuelae* exploration, irrespective of whether yeast was present. This implied that glucose repressed exploratory growth.

We also tested glucose consumption by the *S. cerevisiae LPD1* and *KGD2* mutants. The products of these genes, along with that of *KGD1,* comprise the 2-oxoglutarate dehydrogenase complex responsible for converting 2-oxoglutarate into succinyl-CoA in the TCA cycle (Przybyla-Zawislak et al., 1999) (**Fig. 3.5A**). We found wild type, Δ*LPD1* and Δ*KGD2 S. cerevisiae* strains consumed

similar levels of glucose (**Fig. 3.5B**), suggesting that other factors must be inhibiting *S. venezuelae* exploration when grown adjacent to these TCA cycle mutants.

All TCA cycle-associated *S. cerevisiae* mutants that failed to stimulate *S. venezuelae* exploratory behaviour were blocked after the production of citrate in the TCA cycle (**Fig. 3.5A**). We hypothesized that this disruption might result in an accumulation of organic acids, and that *S. cerevisiae* mutants secreted these acids to maintain a neutral intracellular pH. We measured the pH of wild type, Δ*LPD1* and Δ*KGD2* strains when grown on YPD (G+) agar, and found wild type *S. cerevisiae* raised the agar pH from 7.0 to 7.5, whereas both TCA cycle mutants lowered the agar pH to 5.5 (**Fig. 3.5B**).

To test whether acid secretion by the *S. cerevisiae LPD1* and *KGD2* mutants prevented *S. venezuelae* exploratory growth, the two mutants were grown beside *S. venezuelae* on non-buffered YPD agar, and equivalent medium buffered to pH 7.0 (**Fig. 3.5C**). After 14 days growth on non-buffered plates, the *S. cerevisiae* mutants failed to stimulate *S. venezuelae* exploratory behaviour, whereas the same strains on buffered agar – which would counter the pH-lowering effects of the secreted acids – could now promote *S. venezuelae* exploration. To further verify this pH-dependent effect, we grew wild type *S. cerevisiae* beside *S. venezuelae* on YPD agar supplemented with citrate or acetate (**Fig. 3.5D**). We found that after 14 days, *S. venezuelae* spreading was inhibited, confirming that secreted acids inhibited *S. venezuelae* exploration.

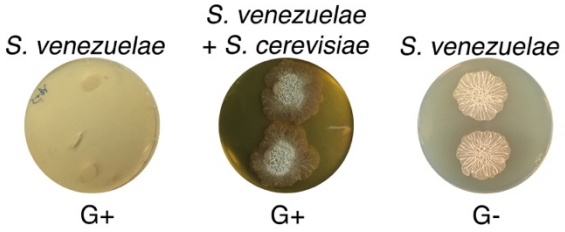

Fig. 3.7 *S. venezuelae* grown alone on glucose-deficient medium exhibits similar exploratory growth to *S. venezuelae* growing next to yeast on glucose medium. *S. venezuelae* was grown either alone or beside *S. cerevisiae* on G+ (glucose-containing) agar medium, and alone on G- (no glucose). Two replicates were spotted per plate, and plates were incubated for 10 days.

Collectively, these results suggested that *S. venezuelae* exploratory growth is a glucose- and acid-repressible phenomenon. Consistent with these observations, we also determined that *S. venezuelae* exploration was associated with a significant rise in pH: as *S. venezuelae* consumed the yeast, the medium pH rose from 7.0 to 8.0, and once *S. venezuelae* exploratory growth initiated (day 5), the pH rose further to 9.5 (**Fig. 3.8**). This increase in pH was also observed for *S. venezuelae* grown on G- medium (in the absence of yeast) (**Fig. 3.9**), suggesting that the rise in pH was mediated by the *Streptomyces* cells. To determine whether high pH was sufficient to promote exploration, we inoculated *S. venezuelae* cells on YPD agar medium buffered to pH 9.0. Exploration was not induced under these growth conditions (**Fig. 3.10**). These data

indicated that alkaline conditions were important but not sufficient for exploration, and further suggested that an adaptation phase was required during the transition to exploratory growth.

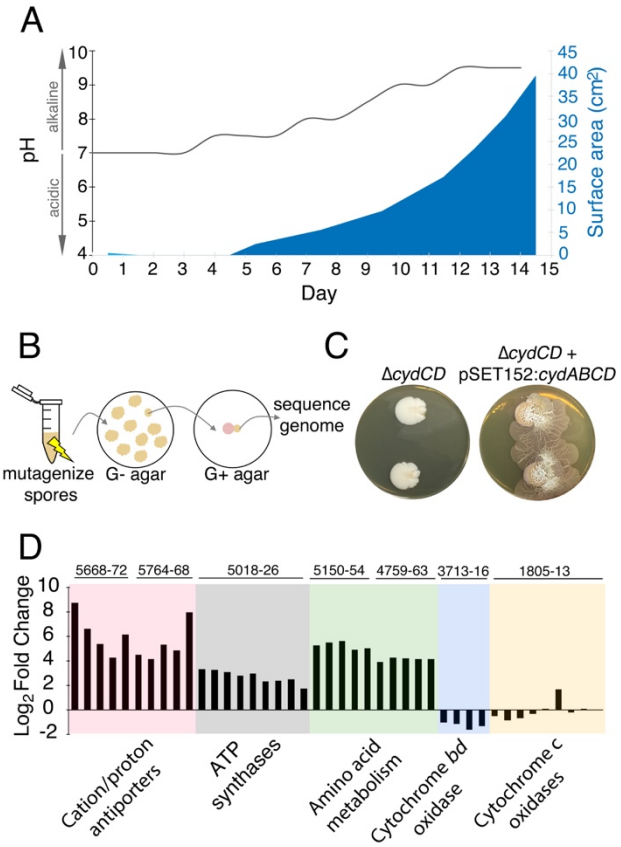

Fig. 3.8 The alkaline stress response is associated with *S. venezuelae* exploratory behaviour. A. The surface area and medium pH associated with *S. venezuelae* explorer cells beside *S. cerevisiae* on YPD agar were measured and plotted every day for 14 days. **B.** Schematic of the method used to identify genes required for *S. venezuelae* exploratory growth. *S. venezuelae* spores were subject to chemical mutagenesis, then screened on G- agar (no glucose, exploration-permissive without *S. cerevisiae*) for a lack of exploratory growth. Static colonies (beige) were grown beside *S. cerevisiae* (pink) on YPD medium to confirm a lack of exploratory growth. Genomic DNA was isolated from strains unable to initiate exploratory growth on G- agar, and when inoculated beside *S. cerevisiae* on YPD medium. Whole genome sequencing was performed to identify mutations responsible for the lack of exploratory growth. **C.** Morphology of a mutant cytochrome *bd* oxidase *S. venezuelae* strain (Δ*cydCD*) and the corresponding complemented strain grown on YPD agar for 14 days. **D.** Transcript levels for alkaline stress-responsive genes in *S. venezuelae* explorer cells (grown beside *S. cerevisiae* on YPD medium), divided by levels for non-exploratory *S. venezuelae* cells (grown alone on YPD medium). Transcript levels were normalized and differential expression was log2-transformed. The associated *sven* gene numbers are shown above the bar graphs.

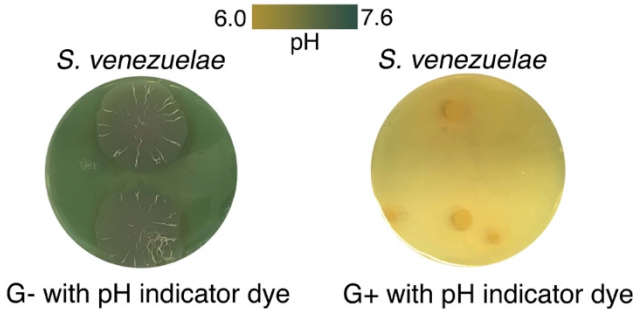

Fig. 3.9 *S. venezuelae* grown alone raises the pH of glucose-deficient medium. *S. venezuelae* was grown alone on G- (no glucose) or G+ (glucose-containing) agar medium containing the pH indicator bromothymol blue. Two replicates were inoculated on each plate, and these were grown for 14 days.

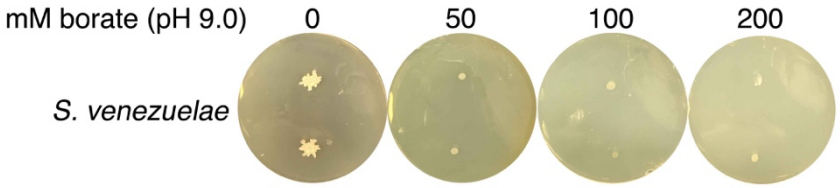

Fig. 3.10 High pH alone does not stimulate *S. venezuelae* exploration. *S. venezuelae* was grown alone on YPD agar medium buffered to pH 9.0 using 50, 100 or 200 mM borate. Two replicates were inoculated on each plate, and these were grown for 14 days.

3.3.4 *S. venezuelae* exploration requires an alkaline stress response

To investigate the genetic basis for this phenomenon we employed chemical mutagenesis, and screened for *S. venezuelae* mutants that failed to display exploratory behaviour when grown on G- medium (where yeast is not required) (**Fig. 3.8B**). Candidate non-spreading mutant colonies were identified, and were tested in association with *S. cerevisiae* on YPD (G+) medium to confirm their inability to spread. Of the 48 exploration-defective mutants identified on G- medium, only three were also unable to spread when grown on YPD medium beside *S. cerevisiae*. This indicated that exploratory growth on G- agar may have distinct genetic requirements from exploratory growth on YPD (G+) medium.

We sequenced the genomes of wild type *S. venezuelae* and the three non-spreading mutants of interest (those unable to spread on both G- medium alone and YPD (G+) medium beside *S.*

cerevisiae). Each mutant harbored point mutations in the *sven_3713-3716* operon. This operon is predicted to encode subunits of the cytochrome *bd* oxidase complex (*cydA/sven_3713* and *cydB/sven_3714*), along with an ABC transporter required for cytochrome assembly (*cydCD/sven_3715*) (Brekasis and Paget, 2003). One strain had a mutation in *sven_3715* (H673Y), while the other two strains had mutations in *sven_3713* (Q186stop) and were likely clonal. To ensure that these mutations were responsible for the exploration-defective phenotype, we complemented the exploratory growth defect in each mutant with a cosmid carrying an intact *cydABCD* operon, and confirmed that exploration was restored (**Fig. 3.11**). We also deleted *cydCD* in a wild type *S. venezuelae* background, and confirmed that this strain was unable to initiate exploration when grown beside *S. cerevisiae*. As before, spreading could be restored to the mutant after introducing *cydABCD* on an integrating plasmid vector (**Fig. 3.8C**). These data indicated that the cytochrome *bd* oxidase complex was essential for *S. venezuelae* exploration.

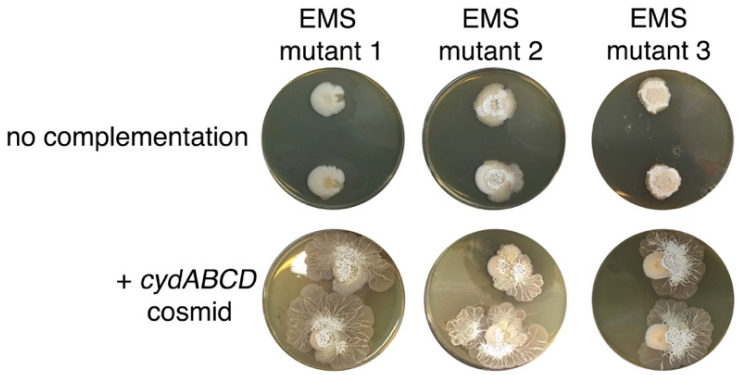

Fig. 3.11 Complementation of explorer mutant phenotypes. Top row: EMS (ethyl methanesulfonate) mutagenesis-derived *S. venezuelae* explorer mutants containing point mutations in the *cydABCD* operon, grown beside *S. cerevisiae*. Bottom row: Explorer mutants complemented with a cosmid carrying the wild type *cydABCD* operon. Two replicates were inoculated on each plate.

S. venezuelae, like many other bacteria, encodes two cytochrome oxidase complexes. The cytochrome *bd* oxidase catalyzes terminal electron transfer without a concomitant pumping of protons across the membrane, while the cytochrome bc_1-aa_3 complex requires proton transfer from the cytoplasm. The cytochrome *bd* oxidase functions as part of the alkaline stress response in other bacteria (Krulwich et al., 2011). As we had established that alkaline conditions were a pre-requisite for *S. venezuelae* exploration, we questioned whether other alkaline stress-responsive genes might be associated with exploratory growth. Using RNA-sequencing (RNA-seq), we examined the transcription profiles of *S. venezuelae* alone, compared with *S. venezuelae* exploratory cells grown beside *S. cerevisiae* on YPD medium (**Fig. 3.8D**). The five gene clusters mostly highly upregulated in *S. venezuelae* explorer cells encoded the ATP synthase complex (*sven_5*018-26; 7.6-fold increase relative to non-spreading), two predicted cation/proton antiporter complexes (95.9- and 85.3-fold increase relative to non-spreading for *sven_5668-72* and *sven_5764-68*, respectively), and two peptide transporters (17.4- and 38.3-

fold increase relative to non-spreading for *sven_4759-63* and *sven_5150-54*, respectively) (**Fig. 3.8D**).

Higher expression of the cation/proton antiporters, alongside increased ATP synthesis, would be expected to enhance proton uptake into the cell; equivalent genes are upregulated as part of the alkaline stress response in other bacteria (Krulwich et al., 2011). Amino acid catabolism is also upregulated under alkaline growth conditions in other bacteria (Padan et al., 2005). Given the dramatically increased expression of the peptide transporters, we confirmed that exploratory growth required an amino acid source (**Table 3.1**). Collectively, these results suggest that exploration is coupled with a metabolic reprogramming that permits robust growth under highly alkaline conditions.

3.3.5 *S. venezuelae* explorer cells alkalinize the medium using an airborne volatile organic compound

S. venezuelae exploration is associated with high pH conditions, and our data suggested this rise in pH was promoted by *S. venezuelae* itself. We hypothesized that this pH effect could be mediated either through the secretion of diffusible basic compounds, or through the release of volatile organic compounds (VOCs). To differentiate between these possibilities, we set up a two-compartment Petri plate assay, where *S. venezuelae* was grown beside *S. cerevisiae* on YPD agar in one compartment, while the adjacent compartment contained uninoculated YPD agar (**Fig. 3.12A**). As a negative control, we set up an equivalent set of plates, only with *S. venezuelae* alone (no yeast) on YPD agar in the first compartment. In each case, the two compartments were separated by a polystyrene barrier. After 10 days, we measured the pH of the uninoculated YPD compartment, and found the compartment adjacent to *S. venezuelae* alone remained at pH 7.0, whereas the one adjacent to *S. venezuelae* explorer cells had risen from pH 7.0 to 9.5, indicating the explorer cells produced a basic VOC (**Fig. 3.12A**).

To verify that the VOC was produced by *S. venezuelae* explorers and not by *S. cerevisiae*, we repeated the two-compartment assay with *S. venezuelae* grown alone on G- agar, a condition that also induced exploratory behaviour. We found that *S. venezuelae* growing alone on G- agar could alkalinize the adjacent YPD compartment. This confirmed that a basic VOC was produced by *S. venezuelae* explorer cells (**Fig. 3.12B**).

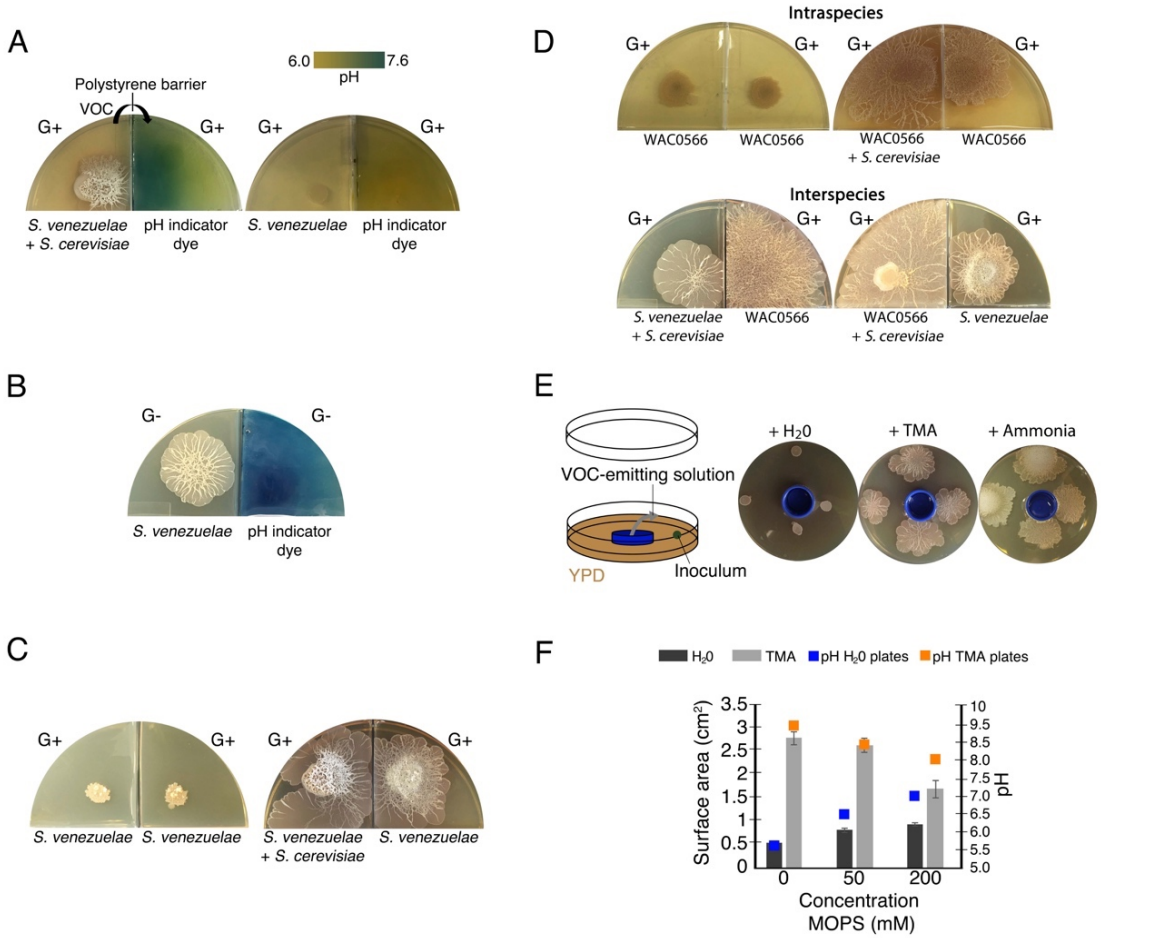

Fig. 3.12 Volatile organic compounds released by *S. venezuelae* raise the medium pH and induce exploratory growth in physically separated *Streptomyces*. A. Effect of *S. venezuelae* explorer cells on pH of physically separated medium. Each compartment is separated by a polystyrene barrier. *S. venezuelae* and *S. cerevisiae* were grown in the left compartment of one plate (left), while *S. venezuelae* alone was grown in the left compartment of the other plate (right). After 10 days, bromothymol blue pH indicator dye was spread on the agar in the right compartment of each plate. Blue indicates VOC-induced alkalinity. **B.** *S. venezuelae* was grown alone on YP (G- agar) in the left compartment, while the right compartment contained uninoculated YP (G-) agar. After 7 days, the same pH indicator dye as in Fig. 3.12A was spread over the agar in the right compartment. Blue represents a rise in pH above 7.6. **C.** Left: *S. venezuelae* alone was inoculated in each compartment. Right: *S. venezuelae* was grown beside *S. cerevisiae* in the left compartment, and *S. venezuelae* alone was grown in the right compartment. All strains were grown on YPD (G+) agar medium for 10 days. **D.** Top left: Wild *Streptomyces* isolate WAC0566 was grown alone in each compartment. Top right: WAC0566 was grown beside *S. cerevisiae* in the left compartment, and grown alone in the right compartment. Bottom left: *S. venezuelae* was grown beside *S. cerevisiae* in the left compartment, and WAC0566 was grown alone in the right compartment. Bottom right: WAC0566 was grown beside *S. cerevisiae* in the left compartment, while *S. venezuelae* was grown alone in the right compartment. All strains were cultured on YPD (G+) agar medium for 10 days. **E.** Schematic of the plate-based assay used to assess the effects of volatile-emitting solutions (and controls) on nearby *Streptomyces* colonies. H_20, TMA, or ammonia solutions were placed in a blue plastic dish, and *S. venezuelae* was spotted around each dish on YPD medium. Plates were incubated at room temperature for 7 days. **F.** Surface area and pH of *S. venezuelae* colonies grown on YPD medium around small dishes containing H_20 or TMA solutions, as shown in Figure 4E. *S. venezuelae* was grown at room temperature for 7 days on either unbuffered YPD medium or YPD medium buffered to pH 7.0 using MOPS. All values represent the mean ± standard error for four replicates.

3.3.6 *S. venezuelae* exploratory cells use VOCs to induce exploration in other streptomycetes at a distance

Bacterial VOCs can influence a wide range of cellular behaviours. To determine whether the VOC produced by explorer cells represented an exploration-promoting signal for physically separated *Streptomyces* colonies, we leveraged our two-compartment assay, inoculating one with *S. venezuelae* beside *S. cerevisiae* on YPD agar, and the adjacent compartment with *S. venezuelae* on the same medium (a condition where exploration by *S. venezuelae* otherwise requires yeast association). As expected, after 10 days the *S. cerevisiae*-associated cells were actively spreading. Remarkably, the adjacent *S. venezuelae* cells (in the absence of yeast) had also initiated exploratory growth (**Fig. 3.12C**). As a negative control, *S. venezuelae* alone was grown in both compartments on YPD agar; spreading was not observed for cells grown in either compartment after 10 days (**Fig. 3.12C**). These data implied that *S. venezuelae* explorer cells released a VOC that effectively promoted exploratory growth in distantly located *S. venezuelae* cells. We tested whether our exploration-deficient *cydCD* mutant was able to respond to this VOC, and observed that despite its inability to explore when grown next to yeast, this mutant was capable of exploration when stimulated by neighbouring explorer cells (**Fig. 3.13**).

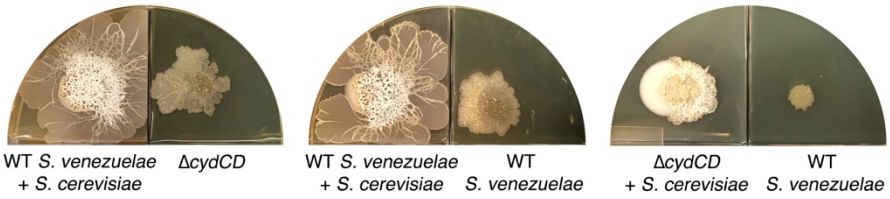

Fig. 3.13 The *S. venezuelae cydCD* mutant strain can explore in response to volatile signals produced by neighbouring explorer cells. Left: Wild type *S. venezuelae* was grown beside *S. cerevisiae* in the left compartment, and wild type *S. venezuelae* was grown alone in the right compartment. Right: Wild type *S. venezuelae* was grown beside *S. cerevisiae* in the left compartment, and the *S. venezuelae cydCD* mutant strain was grown alone in the right compartment. All strains were grown on YPD (G+) agar medium for 10 days.

To determine whether *S. venezuelae* explorers used VOCs to potentiate exploration in other species, we again used our two-compartment assay. We cultured *S. venezuelae* with *S. cerevisiae* in one compartment, and tested whether these cells could stimulate exploratory growth of the wild *Streptomyces* isolate WAC0566 in the adjacent compartment (**Fig. 3.12D**) (WAC0566 initiates exploratory growth when cultured next to yeast, but fails to spread on its own; **Fig. 3.12D**). Negative control plates were set up in the same way as before, with WAC0566 alone in both compartments. After 10 days, WAC0566 grown adjacent to *S. venezuelae* explorers initiated exploratory growth, and this was not seen for the negative control (**Fig. 3.12D**). This indicated that exploratory growth could be communicated to unrelated streptomycetes.

We tested the volatile-mediated communication between these strains in a reciprocal experiment, and found that *S. venezuelae* exploration could also be stimulated by a VOC produced by yeast-associated WAC0566 (**Fig. 3.12D**). This inter-species promotion of *S. venezuelae* exploration was observed for at least 13 other wild *Streptomyces* strains (**Fig. 3.14**). Importantly, VOC communication of exploratory growth was confined to those species with exploratory capabilities (*S. coelicolor* failed to respond to the VOC elicitor).

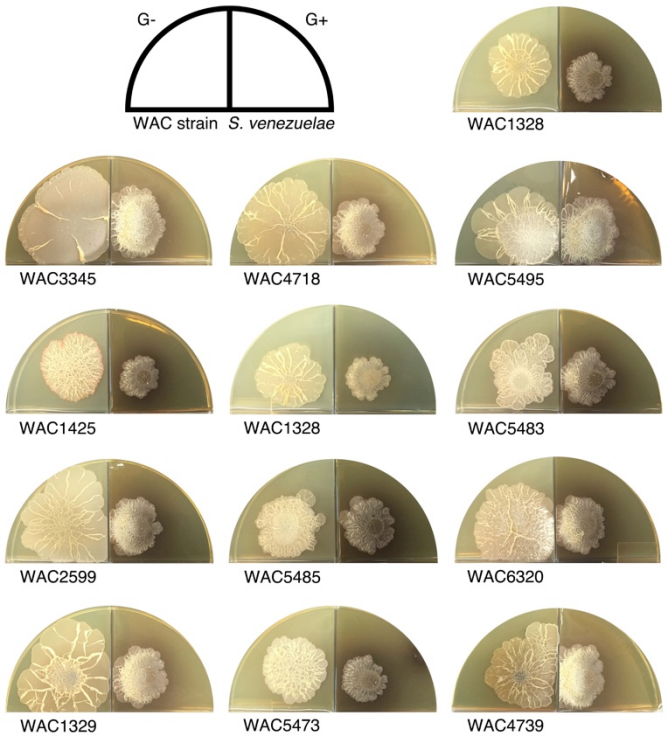

Fig. 3.14 Wild explorer *Streptomyces* species promote exploration in *S. venezuelae* using volatile signals. Using our two-quadrant assay, 13 independent wild *Streptomyces* isolates (WAC strains) were inoculated on G- agar, adjacent to *S. venezuelae* inoculated on G+ agar medium (where no exploration was observed on its own). Each WAC strain was able to promote *S. venezuelae* exploration through the release of a volatile compound.

3.3.7 The VOC trimethylamine stimulates *Streptomyces* exploratory behaviour

We determined that the exploration-promoting VOC could be produced by liquid-grown (G-) cultures, and that it stimulated exploratory growth by both *S. venezuelae* and WAC0566 (**Fig. 3.15**). To rule out the possibility that any liquid-grown culture could promote exploration, we also grew *S. venezuelae* and WAC0566 in YPD (G+) liquid medium, and found these cultures were unable to stimulate exploration. This suggested that VOC production was glucose-repressible, and its production correlated with growth conditions that promoted exploration.

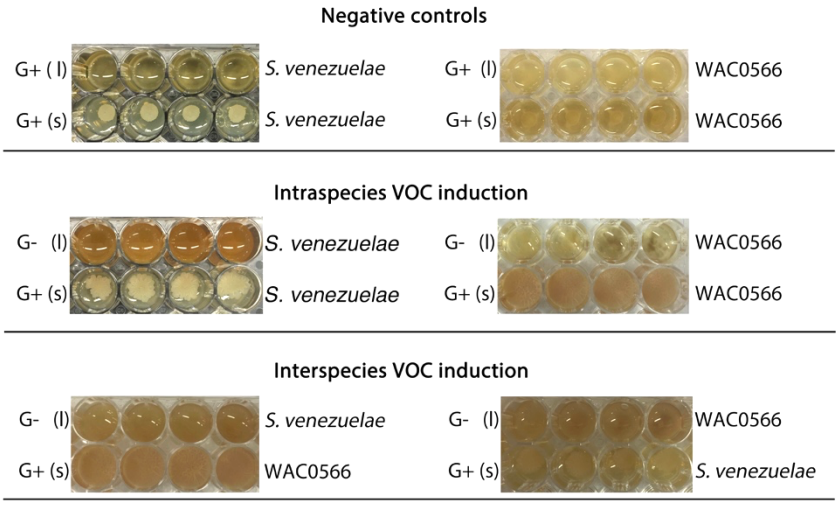

Fig. 3.15 The VOC produced by *S. venezuelae* explorer cells can be produced by liquid-grown (G-) *S. venezuelae* and WAC0566 cultures. All strains were grown in 48-well plates, with (l) indicating liquid cultures (top rows), and (s) indicating solid YPD agar (bottom rows). Liquid cultures were either G+ (glucose-containing) or G- (no glucose), while all solid medium was G+ (exploration repressive condition). Plates were grown shaking for 3 days. For all plates, we monitored exploration by strains growing on G+ agar (bottom rows), in response to VOCs produced by the liquid-grown cultures. The top panel shows *S. venezuelae* (left) and the wild *Streptomyces* strain WAC0566 (right) grown in G+ liquid (a condition where the VOC of interest is not expected to be produced). The middle panel shows the same strains, only grown in G- liquid (where the VOC was predicted to be produced). The bottom panel shows the test for interspecies VOC production/response, with *S. venezuelae* and WAC0566 grown in G- liquid, opposite WAC0566 and *S. venezuelae*, respectively.

To determine the identity of the VOC, we grew *S. venezuelae* and WAC0566 in G+ and G- liquid culture for three days. We collected the supernatants of each culture, and assayed them using two-dimensional gas chromatography time-of-flight mass spectrometry (GC×GC-TOFMS). From this, 1400 unique compounds were identified. To determine which compound(s) were responsible for promoting exploration, we applied a stringent filter, requiring the compound(s) to be: i) present in at least 50% of *S. venezuelae* and WAC0566 exploration-inducing (G-) cultures; ii) present in at least 10-fold greater abundance in exploration-inducing (G-) cultures versus static (G+) cultures; and iii) have at least a 60% similarity score to known compounds in the 2011 National Institute of Standards and Technology (NIST) Mass Spectral Library. We arrived at a list of 21 candidate compounds (**Table 3.2**). Of these, 12 were not detected in the negative controls (G+ cultures). Within this group of 12, only four were detected in 100% of *S. venezuelae* and WAC0566 exploration-promoting cultures: trimethylamine (TMA), thiocyanic acid, 6-methyl-5-hepten-2-one, and 2-acetylthiazole. Notably, TMA was >10 fold more abundant than the other three compounds, and thus we focussed our initial investigations on this molecule.

TMA is a volatile nitrogen-containing metabolite with a high pKa (9.81). As we knew *S. venezuelae* produced a basic VOC, we hypothesized that TMA was responsible for promoting exploration. To test this possibility, we placed commercially-available TMA in a small plastic container at the centre of a YPD (G+) agar plate, and then inoculated *S. venezuelae* at defined positions around this container (**Fig. 3.12E**). After 7 days, *S. venezuelae* cultured adjacent to the TMA-emitting solutions had initiated exploratory growth, while those grown next to a water-containing control failed to spread. This implied that TMA was the VOC used by *S. venezuelae* and WAC0566 to elicit exploratory growth.

TMA production is not well understood, although recent work has revealed two mechanisms by which it can be generated from quaternary amines. *Acinetobacter* sp. employ a carnitine oxygenase (product of the *cntAB* gene cluster) in converting L-carnitine into TMA (Zhu et al., 2014), while *Desulfovibrio desulfuricans* converts choline into TMA using a choline-trimethylamine lyase (encoded by the *cutCD* genes) (Craciun and Balskus, 2012). *S. venezuelae* lacks any gene with similarity to *cntA*, and thus does not use an equivalent pathway to generate TMA. It does possess homologs of *cutCD*; however, these genes were more highly expressed (~5-fold) in static *S. venezuelae* cultures (where no TMA was ever detected), than in spreading cultures. This suggested that these gene products may not direct TMA production in *S. venezuelae*, and that TMA may be synthesized via a novel pathway in this system. TMA can also be produced upon biogenic reduction of trimethylamine *N*-oxide (TMAO) by TMAO reductases. Bacteria known to carry out this reaction typically encode one or more TMAO reductase operons, including some combination of *torSTRCAD* (or *torSTRCADE*), *torYZ, dmsABC,* and *ynfEFGH* (Dunn and Stabb, 2008; McCrindle et al., 2005). *S. venezuelae* encodes homologs to some of these genes [specifically *torA* (top hit: *sven_1326), dmsAB* (top hit: *sven_3040-3039),* and *ynfEFG* (top hit: *sven_3040, 3040 and 3039)*]. In our RNA seq data, however, all of these genes (along with more divergent homologs) were expressed at extremely low levels, with equivalent levels for each gene being observed in both static and exploratory cultures. This suggested these gene products were unlikely to be involved in converting TMAO to TMA in *S. venezuelae*.

3.3.7 TMA induces exploratory growth by raising the pH of the growth medium

To confirm that TMA could raise the pH of the growth medium in the same way as explorer cells, we measured the pH of non-inoculated YPD agar around dishes containing TMA, and found the pH rose from 7.0 to 9.5. To test whether TMA induced exploratory growth by raising the pH, we repeated our plate assays described in Figure 3.12E, and buffered the agar to 7.0 using 50 or 200 mM MOPS (**Fig. 3.12F**). The pH of these plates rose to 8.0 (as opposed to 9.5 on non-buffered plates), and TMA failed to induce *S. venezuelae* exploration to the same extent as on non-buffered plates. To further validate the pH-mediated effect of TMA, we tested whether ammonia (another basic VOC) had the same effect (**Fig. 3.12E**). After 7 days, ammonia induced *S. venezuelae* exploratory growth, suggesting that VOC-mediated alkalinity stimulated *Streptomyces* exploration.

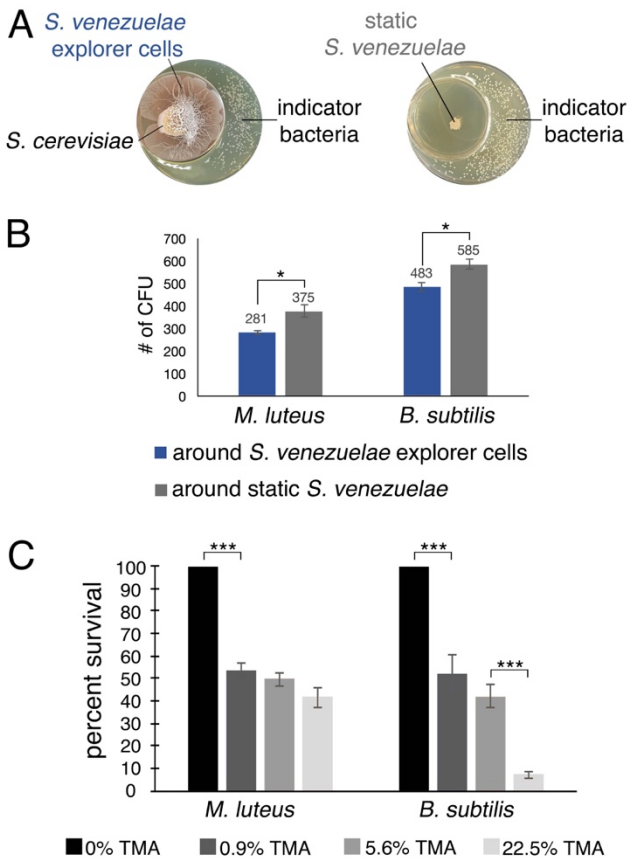

Fig. 3.16. *S. venezuelae* VOCs inhibit the growth of other bacteria. A. *S. venezuelae* was grown beside *S. cerevisiae* (left) or alone (right) on YPD agar in a small dish placed within a larger dish containing YPD medium. After 10 days, an indicator strain (*B. subtilis* or *M. luteus*) was spread around the dish. **B.** Quantification of *B. subtilis* and *M. luteus* colonies following growth adjacent to static or explorer *S. venezuelae* cultures. Values represent the mean ± standard error for three replicates. The asterisk (*) indicates p <0.05, as determined by a student's t-test. **C.** Quantification of *B. subtilis* and *M. luteus* survival following incubation around small dishes containing TMA solutions at concentrations ranging from 0-22.5%. Plates were incubated at room temperature for 2 days. Percent survival indicates the OD_{600} of strains around wells containing 0.9%, 5.6%, or 22.5% TMA solutions compared to the OD_{600} of strains around wells containing H_20 (100% survival). Values represent the mean ± standard error for three biological replicates, and each biological replicate is the average of four technical replicates. The asterisks (***) indicate p <0.005, as determined by a student's t-test.

3.3.8 TMA can reduce the survival of other bacteria

TMA can alter the developmental program of streptomycetes, and is known to modify the antibiotic resistance profiles of bacteria (Létoffé et al., 2014). Given the antibiotic production capabilities of *Streptomyces* bacteria, we wondered whether the release of TMA might also inhibit the growth of other bacteria. To explore this possibility, we set up a small petri dish of

YPD agar inside a larger dish of YPD agar (**Fig. 3.16**). *S venezuelae* and *S. cerevisiae* (exploratory cultures) or *S. venezuelae* alone (static cultures) were inoculated on the smaller dish, and plates were incubated for 10 days. The soil-dwelling bacteria *Bacillus subtilis* or *Micrococcus luteus* were then spread on the larger petri dish. Growth of *B. subtilis* and *M. luteus* in association with exploratory or static *S. venezuelae* cultures, was then assessed after overnight incubation. *B. subtilis* and *M. luteus* colony numbers were reduced by an average of 17.4% and 25.1%, respectively, on plates exposed to VOCs produced by exploratory *S. venezuelae*, relative to those grown adjacent to static cultures. We determined that the pH of medium adjacent to exploratory *S. venezuelae* had risen to 9.5, suggesting that TMA and its pH-modulatory effects could be responsible for the growth-inhibition of these bacteria.

To directly test the inhibitory potential of TMA, we set up an equivalent assay, where the TMA-producing *S. venezuelae-S. cerevisiae* combination was substituted with aqueous TMA solutions of varying concentrations. We spread *B. subtilis*, and *M. luteus* around the TMA-containing receptacles, and after 2 days, quantified growth (**Fig. 3.16C**). We observed an approximately 50% drop in viable cells when exposed to 0.9% TMA, and in the case of *B. subtilis,* a further drop in viability was observed as TMA concentrations increased. This confirmed that TMA adversely affected the growth and survival of other soil bacteria.

3.4 Discussion

The canonical multicellular lifecycle of *Streptomyces* bacteria begins with fungus-like hyphal growth, and ends with sporulation (**Fig. 3.1A**). In this system, spore dispersal is the sole means by which these bacteria can establish themselves in new environments. Here, we demonstrate a new developmental behavior for *Streptomyces* that provides them with an alternative means of colonizing new habitats. In response to fungal neighbours and nutrient (glucose) depletion, *Streptomyces* can escape the confines of their classically defined lifecycle, and initiate exploratory growth. Exploratory growth is remarkably relentless: explorer cells are not limited by inanimate barriers, and can grow over abiotic surfaces. Explorer cells alter their local environment through the release of the alkaline, volatile compound TMA. Emitting TMA not only promotes exploratory behaviour by the producing cells, it also functions as an airborne signal that elicits an exploratory response in physically distant streptomycetes, and provides further fitness benefits by inhibiting the growth of other bacteria.

3.4.1 Metabolic cues trigger a developmental switch

S. venezuelae exploration is triggered by two key metabolic cues: glucose depletion and a rise in pH. We observed exploratory growth under low glucose conditions. In low-glucose areas of the soil, *Streptomyces* may initiate exploratory growth in an attempt to colonize environments with more readily available nutrients, whereas in high-glucose areas (*e.g.* near plant roots, or in association with fruit) (Kliewer, 1965; Lugtenberg et al., 1999; Romano and Kolter, 2005), exploration may be less advantageous, initiating only after nearby fungi – or other microbes - consume the existing glucose supply. Microbial alteration of nutrient profiles is likely to be

common in the soil environment (*e.g.* Romano and Kolter, 2005), and we expect that the exploratory growth away from glucose-depleted areas would provide a benefit analogous to that of motility systems in other bacteria. Although the mechanism underlying exploration remains to be elucidated, it may be linked to sliding motility given its apparently passive nature (no appendages involved), and the fact that *Streptomyces* are known surfactant producers.

S. venezuelae exploration is also promoted by a self-induced rise in extracellular pH. Alkaline growth conditions trigger morphological switches in a range of fungi, including the human pathogens *C. albicans*, *C. neoformans,* and *Aspergillus fumigatus* (Bertuzzi et al., 2014; Davis et al., 2000; O'Meara et al., 2014). This is this first time this phenomenon has been observed in bacteria.

3.4.2 Volatile compounds promote communication and enhance competition

Exploratory growth by *Streptomyces* cells is coordinated by the airborne compound TMA. TMA can further induce exploration in physically distant streptomycetes. Importantly, this volatile signal is not limited to *S. venezuelae,* and can be both transmitted and sensed by other *Streptomyces* species. Consequently, it is possible for *Streptomyces* to respond to TMA produced by other bacteria and initiate exploratory growth under conditions where glucose concentrations are high and/or glucose-titrating organisms are absent. Developmental switching in response to VOC eavesdropping has not been previously reported, but exploiting community goods in this way is not unprecedented. For example, quorum signals and siderophores produced by one organism can be taken up or used by others (Lyons and Kolter, 2015; Traxler et al., 2012). The VOC repertoire of microorganisms appears to be vast (Chuankun et al., 2004; Insam and Seewald, 2010; Kai et al., 2009; Schöller et al., 2002; Schulz and Dickschat, 2007; Wilkins and Schöller, 2009). Volatile compounds have historically been implicated in the "avoidance responses" of fungi, promoting their growth away from inanimate objects (Cohen et al., 1975; Gamow and Böttger, 1982). Increasingly, these compounds are now being found to have important roles in communication between physically separated microbes (Audrain et al., 2015; Bernier et al., 2011; Briard et al., 2016; Kim et al., 2013; Létoffé et al., 2014; Schmidt et al., 2015, 2016; Tyc et al., 2015; Wang et al., 2013; Wheatley, 2002). A range of fungi use the volatile alkaline compound ammonia to induce morphological switches in other fungi, and to mediate inhibition of neighbouring colonies (Palková et al., 1997). Our observations suggest that VOCs may also be key bacterial morphological determinants, communicating developmental switches both within and between different microbial species.

In addition to serving as communication signals, VOCs may also provide their producing organisms with a competitive advantage in the soil. Volatile molecules can modulate the antibiotic resistance profiles of bacteria (Létoffé et al., 2014), and can themselves have antifungal or antibacterial activity (Schmidt et al., 2015). TMA is a particularly potent example. Here, we show that exposure of other bacteria to TMA inhibits their growth, while previous work has revealed that TMA exposure increases bacterial sensitivity to aminoglycoside antibiotics. Notably, *Streptomyces* synthesize an extraordinary range of antibiotics, including many aminoglycosides. Thus in the soil, *Streptomyces*-produced TMA may have direct

antibacterial activity, in addition to sensitizing bacteria to the effect of *Streptomyces*-produced antibiotics. The ability of *Streptomyces* to modulate the growth of other soil-dwelling bacteria during exploratory growth would maximize their ability to colonize new environments, and exploit whatever nutrients are present.

3.4.3 Ecological implications for exploratory growth within microbial communities

Exploratory growth represents a powerful new addition to the *Streptomyces* developmental repertoire, and one that appears to be well-integrated into the existing life cycle. When grown next to yeast, explorer cells emerge from a mass of sporulating cells (**Figure 3.17**). This functional differentiation represents an effective bet-hedging strategy, whereby spreading explorer cells scavenge nutrients for the group, while the sporulating cells provide a highly resistant genetic repository, ensuring colony survival in the event of failed exploration. Explorer cells resemble vegetative hyphae, in that their surface is hydrophilic; however, unlike traditional vegetative hyphae, explorer cells do not appear to branch. We presume that explorer cells dispense with frequent branching as a trade-off for the ability to rapidly spread to new environments. Exploratory growth also occurs independently of the typical *bld*- and *whi*-developmental determinants, supporting the notion that this is a unique growth strategy. It is possible, however, given the slower exploration observed for *bldN* mutants (where *bldN* encodes a sigma factor), that BldN regulon members help to facilitate the exploration process.

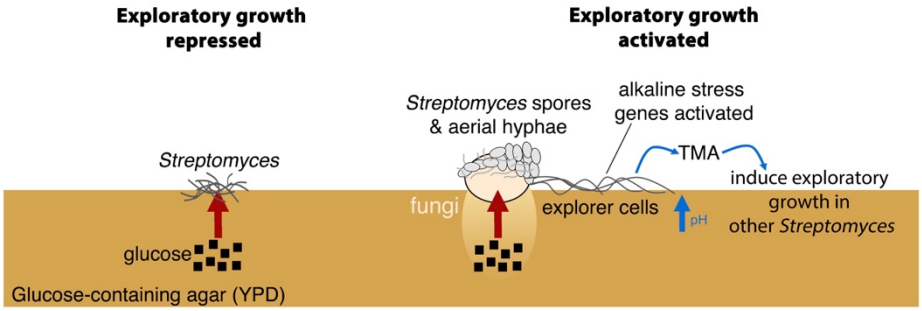

Fig. 3.17 New model for *Streptomyces* development. When *S. venezuelae* is grown alone on glucose-rich medium *S. venezuelae* exploratory growth is repressed (left). When *S. venezuelae* is grown beside *S. cerevisiae* or other yeast on glucose-rich medium (right), the yeast metabolizes glucose, relieving the repression of *S. venezuelae* exploration. *S. venezuelae* explorer cells produce the volatile pheromone TMA, which raises the pH of the medium from 7.0 to 9.5. Explorer cells activate alkaline stress genes to withstand the alkaline pH. TMA, and its associated medium alkalinisation, can induce exploratory growth in physically separated *Streptomyces*.

While we observed exploratory growth in a subset of *Streptomyces* species, it is possible that this capability is more broadly conserved and is stimulated by different conditions than those investigated here. Indeed, microbes are abundant in the soil, and interactions between

different organisms within these communities are likely to be more the norm than the exception. Our work illustrates the importance of inter-species interactions in bacterial development, as a key to revealing novel growth strategies. It also emphasises the need to consider long-range communication strategies, in the form of volatile compounds, which may play widespread roles in regulating development and metabolic activities in microbial communities.

3.5 Materials and Methods

3.5.1 Strains, plasmids, media and culture conditions

Strains and plasmids used in this study are listed in Table 3.4. *S. venezuelae* ATCC 10712 was grown on MYM (maltose-yeast extract-malt extract) agar medium for spore stock generation. Spreading was investigated during growth on the surface of YPD (yeast extract-peptone-dextrose/glucose) agar, glucose-deficient YP (G-) agar, yeast extract agar supplemented with different amino acid sources (tryptone or 2% casamino acids) or YPD/G- agar medium supplemented with citrate, acetate, borate or MOPS buffer. All strains were grown at 30°C, apart from the TMA experiments which were conducted at room temperature in a fume hood. *S. cerevisiae* strain BY4741 (*MATa; his3Δ1; leu2Δ0 ura3Δ0 met15Δ0*) was grown on the same spreading-investigative media at 30°C or room temperature. Prior to plating *S. venezuelae* and *S. cerevisiae* together, *S. venezuelae* was cultured in liquid MYM at 30°C, while *S. cerevisiae* was grown in liquid YPD at 30°C overnight. Three microliters of *S. venezuelae* cultures were applied to the right of 3 µL *S. cerevisiae* on the surface of YPD agar medium, and plates were then incubated at 30°C or room temperature for up to 14 days.

3.5.2 Scanning electron microscopy (SEM) and light microscopy

SEM was used to examine strains grown on YPD or MYM agar for up to 14 days. Samples were prepared and visualized using a TEMSCAN LSU scanning electron microscopy as described previously (Haiser et al., 2009). To monitor the rate of exploratory growth (**Video 3.1**: https://www.youtube.com/watch?v=Iq6iIIT1fTU), an Olympus SZX12 Sterioscope and CoolSNAP HQ photometric camera were used to capture 70 frames of growth over the course of 17 hours.

3.5.3 Phylogenetic analyses

rpoB (Guo et al., 2008) was amplified from each of the 19 exploration-competent wild isolates using primers RpoBPF and RpoBPR (**Table 3.3**), before being sequenced using RpoBF1 and RpoBR1 (**Table 3.3**). Trimmed *rpoB* sequences were aligned using Mafft version 7.2.6.6. A maximum likelihood tree was built using RAxML version 8.2.4 (Stamatakis, 2006), using a GTRGAMMA model of nucleotide substitution, with 500 bootstrap replicates to infer support values of nodes. Outputs were visualized using FigTree.

3.5.4 Yeast library screening

Overnight cultures of *S. venezuelae* were spotted onto rectangular plates containing YPD agar (OmniTray: Nunc International) using a 384-pin replicator. Each strain of a *S. cerevisiae* BY4741 haploid deletion library was inoculated beside an individual *S. venezuelae* colony using a 384-pin replicator. Plates were grown for 5 days at 30°C and screened for an absence of *S. venezuelae* exploratory growth. Yeast mutants unable to stimulate *S. venezuelae* exploratory growth were re-tested on individual YPD agar plates. For *C. albicans* deletion screens, *C. albicans* GRACE collection tetracycline repressible deletion mutants (Roemer et al., 2003) were inoculated beside *S. venezuelae* on YPD agar plates. Mutants were induced using 1 or 5 µg/mL tetracycline, which is below the minimum inhibitory concentration of tetracycline for *S. venezuelae*.

3.5.5 Glucose assays and measurement of pH

Measurements of glucose levels beneath *S. cerevisiae* colonies and in YPD alone were performed using a Glucose (GO) Assay Kit (Sigma). For all experiments, pH levels of solid agar were measured using one or a combination of pH sticks and the pH indicator dye bromothymol blue (Sigma).

3.5.6 Chemical mutagenesis and whole-genome sequencing

Approximately 10^8 *S. venezuelae* spores were added to 1.5 mL 0.01 M KPO_4 at pH 7.0. Spores were centrifuged and resuspended in 1.5 mL 0.01 M KPO_4 at pH 7.0. The spores were then divided into two 750 µL aliquots in screw-cap tubes. As a control, 25 µL H_20 was added to one aliquot, while 25 µL ethyl methanesulfonate (EMS, Sigma, M0880) was added to the other aliquot. Tubes were vortexed for 30 seconds, and incubated shaking at 30°C for 1 hour, with an additional inversion being performed every 10 min. Spores were centrifuged at 3381 ×*g* for 3 min at room temperature, prior to being resuspended in 1 mL freshly made and filter-sterilized 5% w/v sodium thiosulfate solution. Spores were washed twice in 1 mL H_20, after which they were resuspended in 1 mL H_20. For each tube, a dilution series ranging from 10^{-4} to 10^{-8} was made using H_20, and 100 µL of each dilution was then spread onto MYM agar plates and incubated for 3 days at 30°C. Individual colonies were counted to ensure that survival of the EMS-treated spores was, at most, 50% that of the untreated (H_20) control. Colonies were collected from plates inoculated with EMS-treated spores, and were screened for loss of spreading capabilities on G- agar plates. Select mutants were then tested for their inability to spread when plated next to yeast; those mutants that also failed to initiate spreading in the presence of *S. cerevisiae* were grown in liquid MYM, and chromosomal DNA was extracted using the Norgen Biotek Bacterial Genomic DNA Isolation kit for downstream sequencing.

Using the Illumina Nextera XT DNA sample preparation kit, DNA libraries were prepared for three non-exploratory *S. venezuelae* mutants, alongside their wild type *S. venezuelae* parent. Whole genome-sequencing was performed on an Illumina MiSeq instrument (Illumina, San

Diego, CA, USA) using 150 bp paired-ends reads. Reads were aligned to the *S. venezuelae* reference genome using Bowtie 2 (Langmead and Salzberg, 2012) and were converted to BAM files using SAMtools (Li et al., 2009). Single nucleotide polymorphisms (SNPs) were called using SAMtools mpileup and bcftools, and SNP locations, read depth, and identities were generated using VCFtools (Danecek et al., 2011).

3.5.7 Construction of *cydCD* (cytochrome *bd* oxidase) deletion strain and mutant complementation

An in-frame deletion of *sven_3715-3716* was generated using ReDirect technology (Gust et al., 2003). The coding sequence was replaced by an *oriT*-containing apramycin resistance cassette. The gene deletion was verified by PCR, using combinations of primers located upstream, downstream and internal to the deleted genes (see **Table 3.3**). The *cydCD* mutant phenotype was complemented using a DNA fragment encompassing the WT genes, *sven_3713-3714*, and associated upstream and downstream sequences (see **Table 3.3**), cloned into the integrating plasmid vector pSET152. To control for any phenotypic effects caused by plasmid integration, pSET152 alone was introduced into wild type and the *cydCD* mutant strains, and these strains were used for phenotypic comparison with the complemented mutant strain.

3.5.8 RNA isolation, library preparation and cDNA sequencing

RNA was isolated as described previously from two replicates of *S. venezuelae* explorer cells growing beside *S. cerevisiae* for 14 days, and two replicates of *S. venezuelae* alone grown for 24 hours on YPD agar plates (we were unable to isolate high quality RNA from *S. venezuelae* alone at later time points). For all four replicates, ribosomal RNA (rRNA) was depleted using a Ribo-zero rRNA depletion kit. cDNA and Illumina library preparation were performed using a NEBnext Ultra Directional Library Kit, followed by sequencing using unpaired-end 80 base-pair reads using the HiSeq platform. Reads were aligned to the *S. venezuelae* genome using Bowtie 2 (Langmead and Salzberg, 2012), then sorted, indexed, and converted to BAM format using SAMtools (Li et al., 2009). BAM files were visualized using Integrated Genomics Viewer (Robinson, 2012), and normalization of transcript levels and analyses of differential transcript levels were conducted using Rockhopper (McClure et al., 2013). RNA-seq data has been deposited in NCBI's Gene Expression Omnibus and are accessible through GEO Series accession number GSE86378 (http://www.ncbi.nlm.nih.gov/geo/query/acc.cgi?token=idmrgcmexranpun&acc=GSE86378).

3.5.9 Analysis of volatile metabolites via GC×GC-TOFMS

S. venezuelae and WAC0566 were grown in liquid YPD (G+) or YP (G-) for 3 days. For each strain and condition, six biological replicates were grown, and for each, three technical replicates were analyzed. Four milliliters of each culture supernatant was transferred to 20 mL air-tight headspace vials, which were stored at -20°C prior to volatile analysis. Headspace volatiles were concentrated on a 2 cm triphasic Divinylbenzene/Carboxen/Polydimethylsiloxane

(DVB/CAR/PDMS) solid-phase microextraction (SPME) fiber (Supelco, Bellenfonte, PA) (30 min, 50°C, 250 rpm shaking). Volatile molecules were separated, identified, and relatively quantified using two-dimensional gas chromatography time-of-flight mass spectrometry (GC×GC-TOFMS), as described previously (Bean et al., 2012; Rees et al., 2016). The GC×GC-TOFMS (Pegasus 4D, LECO Corporation, St. Joseph, MI) was equipped with a rail autosampler (MPS, Gerstel, Linthicum Heights, MD) and fitted with a two-dimensional column set consisting of an Rxi®-624Sil (60 m × 250 µm × 1.4 µm (length × internal diameter × film thickness); Restek, Bellefonte, PA) first column followed by a Stabilwax (Crossbond Carbowax polyethylene glycol; 1 m × 250 µm × 0.5 µm; Restek, Bellefonte, PA) second column. The main oven containing column 1 was held at 35°C for 0.5 min, and then ramped at 3.5°C/min from 35°C to 230°C. The secondary oven containing column 2, and the quad-jet modulator (2 s modulation period, 0.5 s alternating hot and cold pulses), were heated in step with the primary oven with +5°C and +25°C offset relative to the primary oven, respectively. The helium carrier gas flow rate was 2 mL/min. Mass spectra were acquired over the range of 30 to 500 a.m.u., with an acquisition rate of 200 spectra/s. Data acquisition and analysis was performed using ChromaTOF software, version 4.50 (LECO Corp.).

3.5.10 Identification of candidate volatile signals

Chromatographic data were processed and aligned using ChromaTOF. For peak identification, a signal-to-noise (S/N) cutoff was set at 100, and resulting peaks were identified by a forward search of the NIST 2011 Mass Spectral Library. For the alignment of peaks across chromatograms, maximum first and second-dimension retention time deviations were set at 6 s and 0.15 s, respectively, and the inter-chromatogram spectral match threshold was set at 600. Analytes that were detected in greater than half of exploration-promoting *Streptomyces* cultures (grown in G- medium) and not detected in media controls or *S. venezuelae* grown in G+ medium (failed to promote exploration), were considered candidate molecules associated with the phenotype of interest.

3.5.11 Assays for volatile-mediated phenotypes

Aqueous solutions (1.5 mL) of commercially available TMA solutions (Sigma), ammonia solutions (Sigma) or water (negative control) were added to small, sterile plastic containers and placed in a petri dish containing 50 mL YPD agar. TMA solutions were typically diluted to 11.5% w/v, although concentrations as low as 0.9% were able to promote spreading and inhibit the growth of other bacteria. Ammonia solutions of 0.1 – 1 M were used, and all were able to induce spreading. *S. venezuelae* was inoculated around the small vessels, after which the large petri dish was closed and incubated in the fume hood at room temperature for up to 10 days. For buffering experiments, YPD plates were supplemented with 50 or 200 mM MOPS buffer (pH 7.0). Medium pH was measured as above, while colony surface areas were measured using ImageJ (Abràmoff et al., 2004). For bacterial survival assays around TMA-containing vessels, *B. subtilis* and *M. luteus* strains were grown overnight in LB medium, before being subcultured to an OD_{600} of 0.8. One hundred microliters of each culture were then spread on YPD agar plates,

adjacent to water or TMA-containing vessels. For assays to measure how *S. venezuelae* explorer VOCs affect the survival of other bacteria, *S. venezuelae* was grown alone or beside *S. cerevisiae* in a small petri dish containing YPD agar. This small dish was placed inside a larger dish containing YPD agar. Plates were grown for 10 days, before *B. subtilis* and *M. luteus* were subcultured to an OD_{600} of 0.8, and diluted 1/10 000. Fifty microliters of each culture were then spread on the larger plate containing YPD agar, and colonies were quantified after overnight growth. To test the effect of TMA on *B. subtilis* and *M. luteus* growth, these indicator strains were grown overnight in LB medium, before being subcultured to an OD_{600} of 0.8. One hundred microlitres were spread around wells containing 1.5 mL solutions of TMA at different concentrations on YPD (water control, 0.9%, 5.6% and 22.5%). Plates were incubated for 2 days at room temperature in the fume hood, before cells were scraped into 2 mL YPD and vigorously mixed. Dilution series were used to measure the OD_{600} of the resulting cell suspensions. Error bars indicate standard error of three biological replicates, and four technical replicates of each.

3.6 Acknowledgements

We would like to extend our thanks to Dr. Leah Cowen and Teresa O'Meara for access to the *S. cerevisiae* and GRACE yeast library collections, Dr. J.P. Xu and Aaron Vogen for access to environmental yeast strains, Dr. Gerry Wright for access to his wild *Streptomyces* library, Dr. Mark Buttner and Maureen Bibb for the *S. venezuelae* developmental mutants, Ben Furman for assistance with the *Streptomyces* phylogeny, David Crisante for artistic assistance, and Dr. Heather Bean, Dr. Mark Buttner, Dr. Erin Carlson, Andy Johnson and Matt Moody for helpful discussions.

3.7 Tables

Table 3.1 Effects of media composition on *S. venezuelae* exploration when grown in the absence of yeast. *p = peptone, c = casaminoacids, t = tryptone, ✓=component present

	Glucose represses exploratory behaviour					A peptide source is required to induce exploratory behaviour						Various peptide sources induce exploratory behaviour	
Maltose							✓	✓	✓				
Yeast extract		✓	✓		✓	✓	✓	✓	✓	✓		✓	✓
Malt extract								✓	✓				
Amino acid source		✓ (p)		✓ (p)	✓ (p)		✓ (p)		✓ (p)		✓ (p)	✓ (c)	✓ (t)
Glucose	✓	✓	✓	✓	✓								
pH	6	5	5	5	5	9	9.5	6.5	9.5	8	8	9.5	9.5
Spreading						✓	✓		✓			✓	✓

Table 3.2. VOCs identified using GC×GC-TOFMS.

Compound	G- TIC* average	G+ TIC* average	% of G- samples	% of G+ samples
1,5-Heptadiene, 2,5-dimethyl-3-methylene-	157486	909	69.00	83.3333333
2,5-Cyclohexadien-1-one, 4-ethyl-3,4-dimethyl-	58829	0	53.85	0
2-Acetylthiazole	27658	0	100.00	0
2-Methylisoborneol	3963625	76398	100.00	100
3-Caren-10-al	111806	354	53.85	33.3333333
4-Hydroxy-3-hexanone	10995	0	53.85	0
5-Hepten-2-one, 6-methyl-	13963	0	100.00	0
Acetamide, N-(2-methylpropyl)-	59056	0	61.54	0
Acetonitrile, (dimethylamino)-	4501	0	76.92	0
Aniline, N-methyl-	1084056	43298	100.00	100
Butanoic acid, 3-methyl-	64178	1273	69.23	16.6666667
Dimethyl trisulfide	4289376	43303	100.00	100
Disulfide, dimethyl	15430045	460968	100.00	100
Disulfide, methyl (methylthio)methyl	5610	0	53.85	0
Furan, 2-methyl-	33530	1608	100.00	100
Hexanenitrile	5956	0	84.62	0
N-(3-Methylbutyl)acetamide	37841	0	92.31	0
Propane, 1-bromo-2-methyl-	4981	218	53.85	16.6666667
Tetrasulfide, dimethyl	24737	0	76.92	0
Thiocyanic acid, methyl ester	43203	0	100.00	0
Trimethylamine	453549	0	100.00	0

*TIC = Total Ion Chromatogram (GC peak area, = measure of abundance)

Table 3.3 Oligonucleotides used in this study

Name	Sequence (5′ to 3′)	Use
Sven3715 Up	TCAAGATCATGACCTGGTGC	Confirmation of Δ*cydCD* mutation
Sven3715 Down	CAGGAGCTGGGGCACTCGG	Confirmation of Δ*cydCD* mutation
Sven3715 in	CTTCTGGAAGGACCCCACC	Confirmation of Δ*cydCD* mutation
Sven3715 Fwd	CGCCGAGACCCACTAGCCGGTCCTGTCCAGG GAGCAATGATTCCGGGGATCCGTCGACC	Creation of Δ*cydCD* strain; Confirmation of Δ*cydCD* mutation
Sven3715 Rev	GACGCGGCGGCGGTCATGGCTTGAGCCTAGT	Creation of Δ*cydCD* strain;

	AAGTCCTATGTAGGCTGGAGCTGCTTC	Confirmation of Δ*cydCD* mutation
rpoBPF	GAGCGCATGACCACCCAGGACGTCGAGGC	Amplification of *rpoB* from WAC strains and *S. venezuelae*
rpoBPR	CCTCGTAGTTGTGACCCTCCCACGGCATGA	Amplification of *rpoB* from WAC strains and *S. venezuelae*
rpoBF1	TTCATGGACCAGAACAACC	Sequencing of *rpoB* from WAC strains and *S. venezuelae*
rpoBR1	CGTAGTTGTGACCCTCCC	Sequencing of *rpoB* from WAC strains and *S. venezuelae*

Table 3.4 Strains and plasmids used in this study

Streptomyces	Genotype, description, or use	Reference or source
Streptomyces venezuelae ATTC 10712		Gift from M. Buttner
	Δ*SVEN_1089(bldD)::[aac(3)IV-oriT]*	Gift from M. Buttner
	Δ*SVEN_4453(bldM)::[aac(3)IV-oriT]*	Gift from M. Buttner
	Δ*SVEN_3185(bldN)::[aac(3)IV-oriT]*	Gift from M. Buttner
	Δ*SVEN_3846(bldC)::[aac(3)IV-oriT]*	Gift from M. Buttner
	Δ*SVEN_5827(whiI)::[aac(3)IV-oriT]*	Gift from M. Buttner
	Δ*SVEN_5498(whiH)::[aac(3)IV-oriT]*	Gift from M. Buttner
	Δ*SVEN_2776(whiB)::[aac(3)IV-oriT]*	Gift from M. Buttner
	Δ*SVEN_4452(whiD)::[aac(3)IV-oriT]*	Gift from M. Buttner
	Δ*SVEN_5300(whiG)::[aac(3)IV-oriT]*	Gift from M. Buttner
All WAC strains	From Wright Actinomycete Collection	Gift from G. Wright
Fungi		
S. cerevisiae BY4741	*MATa; his3Δ1; leu2Δ0 ura3Δ0 met15Δ0*	Gift from L. Cowen; (Brachmann et al., 1998)
	Haploid deletion library strains	Gift from L. Cowen
C. albicans	GRACE collection tetracycline repressible deletion mutants	Gift from L. Cowen; (Roemer et al., 2003)
Other wild fungal strains		Gift from J. P. Xu
E. coli		
DH5α	Plasmid construction and general subcloning	Invitrogen
ET12567/pUZ8002	Generation of methylation-free plasmid DNA and conjugation into *Streptomyces*	(MacNeil et al., 1992; Paget et al., 1999)

BW25113/pIJ790	Construction of cosmid-based knockouts	(Gust et al., 2003)
Plasmids or cosmids		
pIJ790	Temperature-sensitive plasmid carrying λ-RED genes	(Gust et al., 2003)
pIJ773	Plasmid carrying the apramycin knockout cassette	(Gust et al., 2003)
pIJ82	Integrating plasmid vector; complementation of mutant strains	Gift from H. Kieser
3E07	*S. venezuelae* cosmid carrying *SVEN_3713-16* (*cydABCD*)	Gift from M. Bibb and M. Buttner

CHAPTER 4: *STREPTOMYCES* EXPLORER CELLS USE VOLATILE SIGNALS TO CONTROL NUTRIENT AVAILABILITY AND MODULATE MICROBIAL COMMUNITY DYNAMICS

Stephanie E. Jones, Christine A. Pham, Joe McKillip, Erin Carlson, Marie A. Elliot

Preface:

This manuscript will be submitted in June 2018. Christine Pham was a co-op student in the Elliot Lab, and she created and complemented the double mutant *bldK* strain, and performed the phenotypic assays comparing the surface area of wild type and some mutant strains. Joe McKillip, a Ph.D. student in Erin Carlson's lab at the University of Minnesota, carried out the mass spectrometry experiments. I performed all other work.

4.1 Abstract (Chapter Summary)

Bacteria and fungi produce a wide array of volatile organic compounds (VOCs), and these VOCs can act as infochemicals or competitive tools. Compared to specialized metabolites, VOCs can rapidly diffuse through soils, allowing them to play important roles in influencing microbial community structures. Recent work demonstrated *Streptomyces* explorer cells can rapidly spread over surfaces, and communicate and compete with other microbes using the VOC trimethylamine (TMA). Here, we examined how TMA impacts microbial community dynamics. We found TMA dramatically alters environmental pH. As a result, environmental iron availability is reduced, and iron-starved microbes cannot survive. *Streptomyces* thrive in these iron-depleted niches by secreting unique siderophores, and by upregulating genes associated with siderophore uptake. Our work reveals VOCs released by explorer cells mediate nutrient availability in the environment, and suggest VOCs play critical roles in influencing the makeup of microbial communities.

4.2 Introduction

Bacteria and fungi frequently live in densely populated multispecies communities. These microbes modulate community dynamics by emitting a vast array of products, including specialized metabolites and volatile organic compounds (VOCs) (Westhoff et al., 2017). Soil environments are particularly complex: not only are they home to multitudes of microbes, but they are also highly heterogeneous systems, containing solid microenvironments and environmental gradients connected by networks of water- and air-filled pores (Bauer et al., 2017). To date, the majority of studies on interspecies competition in microbial communities have focused on the effects of specialized metabolites. These compounds effectively mediate microbial communication and competition, but only in close proximity due to their limited diffusion capabilities. In contrast, VOCs are low-molecular-weight compounds capable of rapidly diffusing across water channels and air pockets, and consequently they can act as longer-range signals (Schmidt et al., 2016). The biological roles of VOCs are only now starting to be dissected, and can have broad effects on both producing organisms and their neighbours. Indeed, VOCs can alter the antibiotic resistance profiles of bacteria, act as antifungal or antibiotic compounds, induce group behaviours such as motility and biofilm formation, stimulate various types of microbial growth, and induce widespread changes in the gene expression of nearby microbes (Avalos et al., 2018).

One group of prolific volatile producers are the *Streptomyces* bacteria (Jones and Elliot, 2017; Schmidt et al., 2015; Schöller et al., 2002). In the soil, the ubiquitous *Streptomyces* are better known for their ability to produce a vast array of specialized metabolites, and for their complex, morphologically differentiated, filamentous life cycle (Elliot et al., 2008; Hopwood, 2007). Recent work has, however, revealed that *Streptomyces* species also use volatile compounds to promote novel growth strategies (Jones and Elliot, 2018; Jones et al., 2017). These species, including the model *Streptomyces venezuelae,* can escape their classically defined life cycle using a new mode of growth termed ‘exploration’. Exploration is initiated in response to the

production of the VOC trimethylamine (TMA), with explorer cells then rapidly spreading across surfaces. TMA production also profoundly alters the surrounding environment, raising the pH to levels approaching pH 9.5. TMA further serves as a *Streptomyces* communication signal, inducing exploration in physically separated streptomycete colonies. TMA-mediated induction of exploration appears to be a function of its alkalinity, as ammonia, another alkaline VOC, can induce exploration in a similar manner. Finally, TMA serves as a weapon against non-streptomycetes: both exploring *Streptomyces* colonies and TMA solutions reduce the survival of other soil bacteria, including *Bacillus subtilis* and *Micrococcus luteus* (Jones et al., 2017).

The effects of TMA on environmental alkalinisation, *Streptomyces* exploration, and the growth of other microbes suggest far-reaching effects for this simple VOC. How TMA affects microbial community dynamics and impacts the growth of other microbes is, however, not clear. Here, we demonstrate that TMA emitted by *Streptomyces* explorer cells reduces the survival of other soil bacteria and fungi by starving them of iron – a micronutrient essential for microbial growth and viability. Within these self-induced iron-depleted environments, *Streptomyces* thrives and explores by secreting unique siderophores and rewiring gene expression to maximize siderophore uptake. We show that iron depletion by other microbes can enhance *Streptomyces* exploration, suggesting that low iron may be a driver of exploration. Taken together, our results show that lowering the available environmental iron levels, either by VOC-mediated alkalinisation or by iron sequestration/piracy, profoundly impacts the viability of a wide range of microbes and enhances *Streptomyces* exploration.

4.3 Results

4.3.1 Environmental iron availability impacts the survival of bacteria and fungi

Iron is an essential nutrient for most organisms; however, its acquisition is a major challenge. Cells use ferrous iron (Fe^{2+}) however, iron in the environment exists predominantly in its poorly soluble ferric form (Fe^{3+}). To access this essential element, bacteria release iron-chelating siderophores (Ahmed and Holmström, 2014). These compounds solubilize iron, and siderophore-iron complexes are taken back into cells through dedicated membrane transporters. In alkaline environments, ferric iron forms stable complexes with hydroxide ions, further reducing iron solubility and preventing the formation of siderophore-iron complexes. Indeed, iron solubility drops by ~1000 fold with each unit rise in pH (McMillan et al., 2010; Serrano et al., 2004; Shaddox et al., 2016).

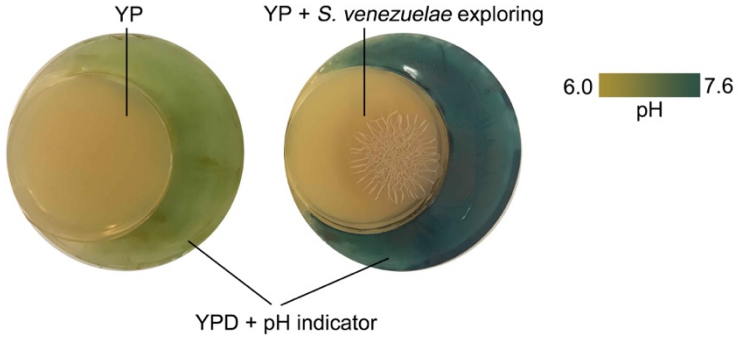

Fig. 4.1 Exploring *S. venezuelae* creates an alkaline environment through the release of TMA. A smaller dish containing YP (left) or YP with exploring *S. venezuelae* was incubated within a larger dish containing LB medium. After 10 days, bromothymol blue pH indicator dye was spread on the larger agar compartment. Blue indicates VOC-induced alkalinity.

S. venezuelae exploration requires an alkaline environment, which they create by releasing the volatile compound TMA (**Fig. 4.1**). TMA emission also results in dramatically decreased survival of other soil-dwelling bacteria (Jones et al., 2017). Accordingly, we wondered whether low iron availability could explain the decreased survival of other microbes exposed to exploration VOCs and the corresponding alkaline environment. To address this possibility, we tested the extent to which low iron affected the growth of *B. subtilis*, *M. luteus*, and the fungus *Saccharomyces cerevisiae* (**Fig. 4.2**). For each strain, we first compared their growth on solid medium, relative to that on media supplemented with two concentrations (160 µM and 320 µM) of the iron-specific chelator 2,2′-dipyridyl. For *M. luteus*, growth was equivalent on LB and LB with 160 µM 2,2′-dipyridyl. On 320 µM 2,2′-dipyridyl however, colonies were smaller, suggesting that low iron slowed the growth of these organisms. In contrast, for *B. subtilis*, we observed a linear growth decrease on LB medium containing 2,2′-dipyridyl compared with LB medium alone: on 160 µM 2,2′-dipyridyl, growth was reduced by ~30%, while on 320 µM 2,2′-dipyridyl, it dropped further to ~60%. Finally, in the case of *S. cerevisiae*, growth decreased by an average of ~40% on YPD with 160 µM 2,2′-dipyridyl. Colonies failed to grow on 320 µM 2,2′-dipyridyl.

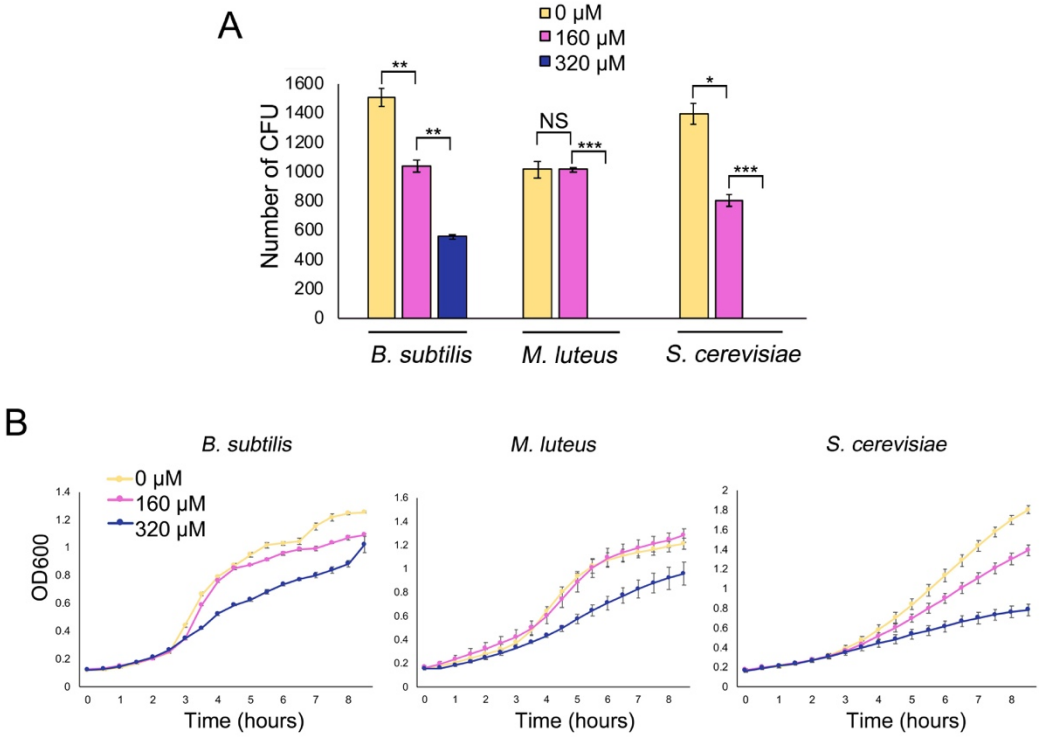

Fig. 4.2 Iron availability impacts the survival of bacteria and fungi. A. Quantification of colony forming units (CFU) for *B. subtilis* and *M. luteus* on LB agar medium and *S. cerevisiae* on YPD agar medium, supplemented with 0, 160 or 320 µM 2,2′-dipyridyl. Plates were incubated for 48 hours. All values represent the mean ± standard error for three or four replicates. Asterisks indicate statistically significant differences (* = *p*-value 0.05 to 0.01; ** = *p*-value 0.01 to 0.005; *** = *p*-value below 0.005, NS = no significant difference) as determined by a student's t-test. Note *M. luteus* and *S. cerevisiae* did not grow at 320 µM 2,2′-dipyridyl. **B.** Growth curves of *B. subtilis* and *M. luteus* in liquid LB medium and *S. cerevisiae* in liquid YPD medium, supplemented with in 0, 160 or 320 µM 2,2′-dipyridyl and grown for 8 hours. Values represent the mean ± standard error for three replicates.

We also tested the effect of 2,2′-dipyridyl on the liquid culture growth of each of these organisms. Each microbe was grown in liquid medium (LB for *B. subtilis* and *M. luteus*, and YPD for *S. cerevisiae*), and its growth was compared with that in media supplemented with 160 µM or 320 µM 2,2′-dipyridyl. In each case, we found growth rate decreased as 2,2′-dipyridyl concentration increased (**Fig. 4.2**). These experiments confirmed that iron is important for the survival and growth of these microorganisms.

4.3.2 Iron supplementation rescues microbial growth in the presence of explorer cells

Having demonstrated that sufficient iron was essential for robust growth by *B. subtilis*, *M. luteus* and *S. cerevisiae*, we sought to test our hypothesis that the volatile compounds produced

by exploring *S. venezuelae* reduced the survival of other microbes by creating an alkaline, iron-deficient environment (**Fig. 4.3A,B**). To test this, we set up a small petri dish of YPD agar (non-exploring medium) or YP agar (exploring medium) inside a larger dish of solid media, either alone or supplemented with 1 mM $FeCl_3$. The small petri plates were inoculated with *S. venezuelae* and incubated for 10 days, after which *B. subtilis*, *M. luteus* or *S. cerevisiae* were spread on the larger, surrounding agar plates. Growth of each microbe was assessed after 2 days. When grown adjacent to YP plates without inoculum or non-exploring *S. venezuelae* cultures on YPD medium, colony numbers for each microbe were similar on all plates, irrespective of whether iron had been added. This suggested that under these growth conditions, iron was unlikely to be limiting for these organisms. In contrast, when grown next to exploring *S. venezuelae* on YP medium, colony numbers on the surrounding agar plates differed drastically depending on the iron supplementation status. For *B. subtilis*, *M. luteus* and *S. cerevisiae*, when grown without iron supplementation adjacent to exploring *S. venezuelae,* colony numbers were reduced by an average of 32%, 63%, and 100%, respectively, relative to controls (those grown on plates adjacent to blank YP or non-exploring *S. venezuelae* on YPD). In contrast, supplementing with iron at least partially restored the survival of each species. When *B. subtilis* was exposed to exploring VOCs, colony numbers on LB medium supplemented with iron were restored to the same level as controls. For *M. luteus* and *S. cerevisiae*, supplementation with iron when exposed to exploring VOCs restored survival by an average of 70% and 64%, respectively, relative to controls. These data suggest that alkaline environments produced by exploring *S. venezuelae* reduce the growth and viability of other soil microbes by effectively starving them of iron.

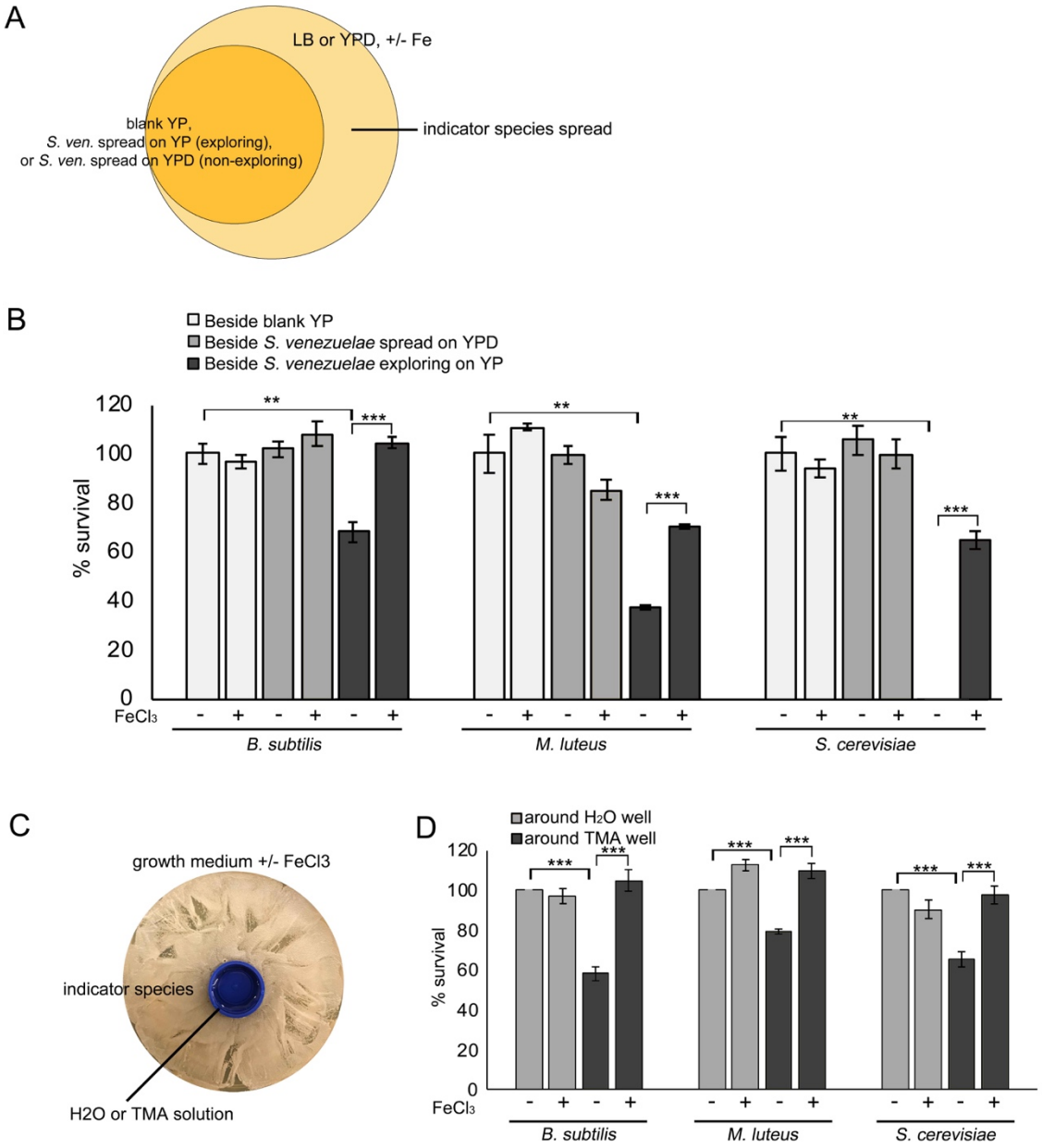

Fig. 4.3 Iron supplementation rescues microbes exposed to VOCs. A. Schematic of the experiment performed in **B**: *S. venezuelae* exploring on YP, blank YP, or non-exploring *S. venezuelae* spread on YPD was incubated in smaller dishes for 10 days. After 10 days, an indicator strain (*B. subtilis, M. luteus*, or *S. cerevisiae*) was spread around the dish on medium with or without 1 mM $FeCl_3$ supplementation. **B.** Quantification of *B. subtilis, M. luteus*, or *S. cerevisiae* colonies on medium with or without $FeCl_3$ supplementation following growth adjacent to exploring *S. venezuelae*, non-exploring *S. venezuelae*, or uninoculated medium **C.** H_2O or TMA solutions were placed in a small blue plastic dish, and indicator strains (*B. subtilis, M. luteus*, or *S. cerevisiae*) were spread around the dish on growth medium with or without 1 mM $FeCl_3$ supplementation. Plates were incubated at room temperature for 2 days. **D.** Quantification of *B. subtilis, M. luteus*, or *S. cerevisiae* colonies on medium with or without $FeCl_3$ supplementation following growth adjacent to H_2O or TMA solutions. For **B and D:** Values represent the mean ± standard error for three or four replicates, and statistical significance was determined using one-way analysis of variance (ANOVA), followed by Tukey's multiple comparison test: **, *P* 0.01 to 0.005; ***, *P* below 0.005.

To determine whether this was a TMA-dependent phenomenon, or whether it was due to other volatiles produced by exploring *Streptomyces,* we set up equivalent assays where *S. venezuelae* colonies were replaced with water or TMA solutions (**Fig. 4.3C,D**). We spread *B. subtilis*, *M. luteus* and *S. cerevisiae* around the water or TMA-containing wells on agar medium, with or without iron supplementation. We then quantified growth after 2 days. For each microbe, the addition of iron had no impact on cell survival when cultures were grown next to water-containing wells. In contrast, growth and survival of *B. subtilis*, *M. luteus* and *S. cerevisiae* decreased by an average of 42%, 21%, and 35%, respectively, on plates exposed to TMA, compared with those grown on plates adjacent to water wells. Again, iron supplementation restored the TMA-adjacent growth to levels equivalent to those around the water wells. This indicated that the growth inhibition observed for bacteria plated next to exploring *S. venezuelae* was most likely due to TMA emission, and that this inhibited the survival of bacteria and fungi by reducing iron availability.

4.3.3 Explorer cells upregulate genes associated with polypeptide transport

The adverse effects of TMA on iron availability led us to question how exploring *Streptomyces* dealt with these low iron conditions. To begin to address this issue, we took advantage of transcriptomic data previously acquired for exploring versus non-exploring *S. venezuelae* (Jones et al., 2017).

In the actinobacteria, iron homeostasis is primarily controlled by the DesR/IdeR/DtxR family of repressors, which share low level sequence similarity with the well-characterized *Escherichia coli* Fur regulator (Tunca et al., 2007; Ventura et al., 2007). These proteins all act to repress the expression of iron acquisition systems when iron is abundant, and this repression is relieved when iron becomes scarce. In *Corynebacteria,* transcription of the *dtxR* gene is unaffected by growth in iron-depleted versus iron-rich conditions, and instead, its product senses and responds to intracellular iron levels (Gunter et al., 1993). Nothing is known about the transcriptional control of the *dtxR* homolog in *Streptomyces* (known as *desR* or *dmdR*), and so as a first step, we examined the transcript levels of this gene in *S. venezuelae* cultures. Unexpectedly, given that DesR homologs are active in iron-replete states where they repress the expression of iron acquisition systems, we found that *desR/sven_4209* was expressed more highly in exploring cultures than in static cultures. We also assessed the expression of different Fur homologs, where Fur proteins function as repressors of iron-starvation genes in iron-rich conditions in Gram negative bacteria (Bagg and Neilands, 1987). *S. venezuelae* encodes five Fur-like regulators, and like for the *desR* gene, we found the genes for all of these were either upregulated in explorer cultures (*sven2299* (*zur*); *sven4859* (*per*); *sven4414* and *sven7338*), or unchanged relative to static cultures [*sven3930* (*nur*)]. This suggested that the response of *S. venezuelae* explorer cells to alkaline, low iron conditions must be mediated by means other than the transcriptional control of iron regulatory genes.

We next examined the products of the most significantly differentially expressed genes in *S. venezuelae* exploring colonies. Two of the most highly upregulated gene clusters encoded ATP-binding cassette (ABC) transporter systems (38.3- and 17.4-fold increase relative to non-spreading for *sven_5150-54* and *sven_4759-63,* respectively) (**Fig. 4.4A**). We searched for homologs of these genes in the model *Streptomyces coelicolor*, and found the closest characterized match for each was to the *bldK* locus (*sco5112-16*). Recent work has suggested that BldK transporters function in siderophore uptake, where siderophores are high affinity iron chelators secreted from cells to capture lowly soluble iron from the environment (Lambert et al., 2014). Specifically, products of the *bldK* locus are thought to be involved in the uptake of ferrioxamine siderophores. The upregulation of two *bldK*-like transporter gene clusters in *S. venezuelae* suggested that exploring cultures may adapt to alkaline, low-iron environments by enhancing ferrioxamine uptake. We searched for other genes in *S. venezuelae* that were homologous to the *S. coelicolor bldK* locus, and found *S. venezuelae* encoded seven additional *bldK*-like clusters (**Fig. 4.4B**). Of these, three were not expressed in exploring cultures or static cultures (*sven_7198-02*, *sven_7135-39*, *sven_7154-58*); three were expressed at low levels in both exploring cultures and static cultures, but were not significantly differentially expressed based on *q*-values (*sven_4765-69*, *sven_4820-23*, *sven_5369-73*); and one was expressed at intermediate levels in exploring cultures, but was only 1.7 fold upregulated in exploring versus static cultures and is predicted to function in nickel transport (*sven_6981-85*). Thus, we focused on the roles of the *sven_5150-53* and *sven_4759*-63 clusters.

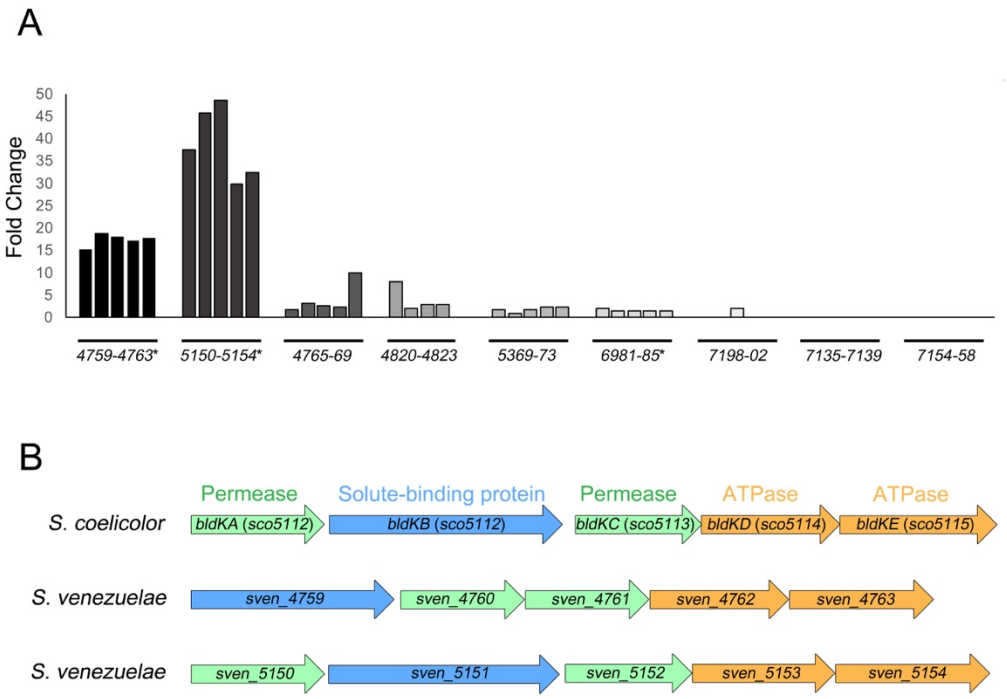

Fig. 4.4 Upregulation of two gene clusters associated with siderophore transport in explorer cells. A. Normalized transcript levels for *S. venezuelae* clusters with homology to the *S. coelicolor bldKABCDE* locus, where normalized transcript levels in *S. venezuelae* explorer cells were divided by those in non-exploring cells. The associated *sven* gene numbers are shown below each cluster, and asterisks beside gene numbers indicate genes in that cluster are significantly differentially expressed in exploring versus non-exploring cultures, based on calculated *q*-values. **B.** Organization of the *S. coelicolor bldK* locus and the two *S. venezuelae bldK*-like clusters that are significantly and highly differentially expressed in exploring versus non-exploring cultures.

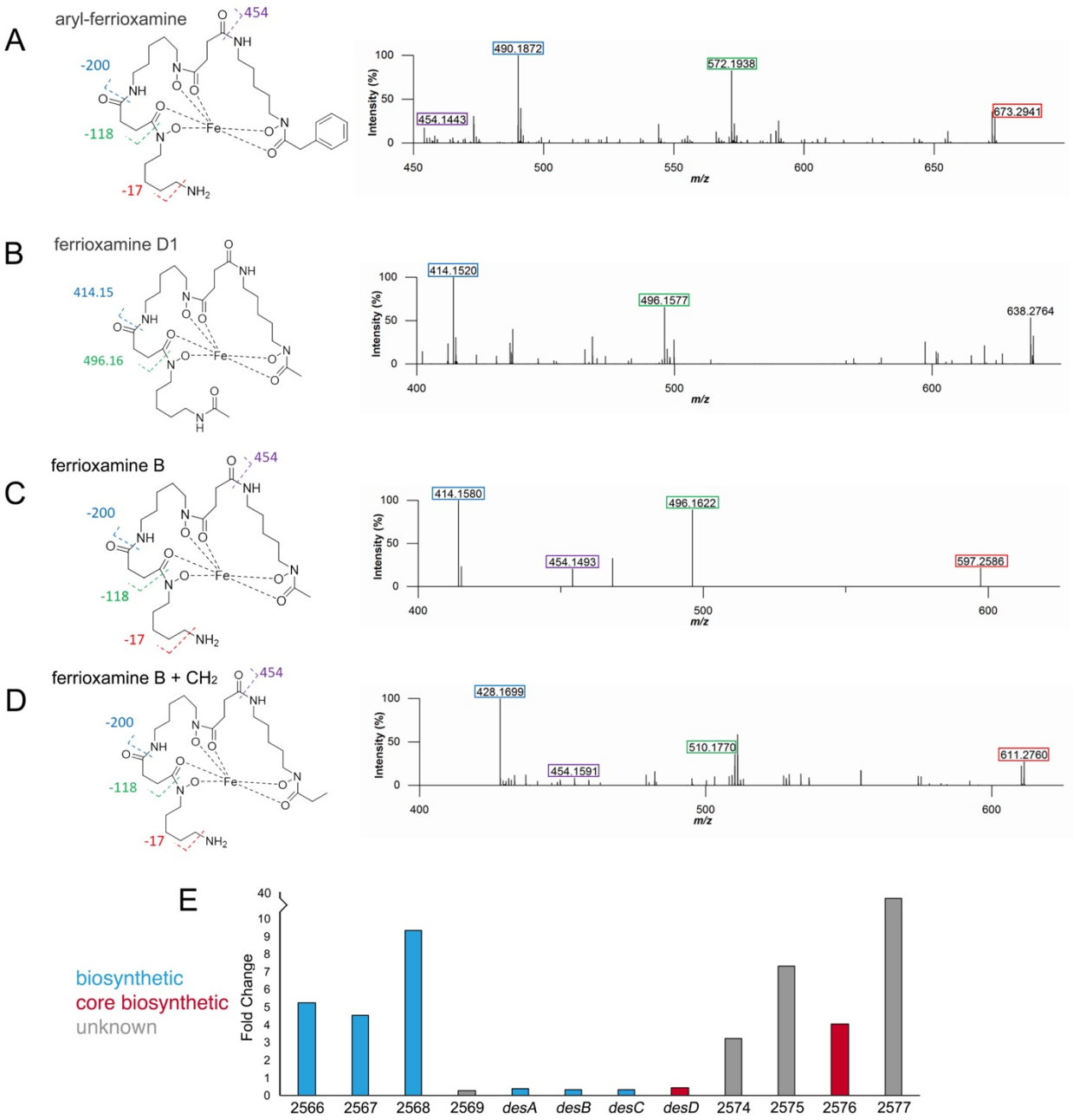

Fig. 4.5 Explorer cells produce desferrioxamines. A-D represent mass spectra of metabolite peaks and molecular structures of associated desferrioxamine or ferrioxamine (iron-complexed desferrioxamine) compounds. All desferrioxamines were absent from non-exploring cultures (*S. venezuelae* spread on YPD). **A.** Aryl-ferrioxamine, from *S. venezuelae* exploring on YP and *S. venezuelae* exploring beside *S. cerevisiae* on YPD. **B.** Ferrioxamine D1, from *S. venezuelae* exploring on YP and *S. venezuelae* exploring beside *S. cerevisiae* on YPD. **C.** Ferrioxamine B, from *S. venezuelae* exploring on YP and *S. venezuelae* exploring beside *S. cerevisiae* on YPD. **D.** Ferrioxamine B + CH_2, from *S. venezuelae* exploring beside *S. cerevisiae* on YPD. **E.** Normalized transcript levels for genes in the *S. venezuelae* desferrioxamine biosynthetic clusters in explorer cells divided by those for non-exploring cells. The associated gene names or *sven* gene numbers are shown below each gene, and bar colours indicate putative gene function (as predicted by antiSMASH).

4.3.4 Desferrioxamines are produced during exploration

Given the upregulation of putative ferrioxamine transport clusters, we wanted to determine whether siderophore production was also enhanced in exploring *S. venezuelae* cultures. We performed liquid chromatography coupled with mass spectrometry (LC-MS) to analyze the metabolic output of exploring colonies (*S. venezuelae* grown alone on YP medium or beside *S. cerevisiae* on YPD medium) versus non-exploring colonies (*S. venezuelae* grown alone on YPD medium or alone on MYM medium) (**Fig. 4.5**). We found that all exploring colonies produced analogs of the siderophore desferrioxamine or ferrioxamine (iron-complexed desferrioxamine), including ferrioxamine B, D, and aryl-ferrioxamine. Colonies exploring beside *S. cerevisiae* on YPD also produced ferrioxamine B+CH_2, a novel ferrioxamine analog. Ferrioxamines were not detected in non-exploring cultures. Unexpectedly, transcript levels associated with the core desferrioxamine biosynthetic genes (*desABCD, sven_2570-73*) (Tunca et al., 2007) were not significantly upregulated in exploring cultures, relative to static cultures (**Fig. 4.5E**). This suggested that there must be some as yet unknown post-transcriptional regulatory mechanism(s) functioning to enhance desferrioxamine levels. It is worth noting that transcript levels for the genes flanking this operon were increased (**Fig. 4.5E**), although whether these gene products contribute to desferrioxamine production remains to be determined.

4.3.4 Iron uptake capabilities impact exploration

Our observations that exploring colonies secrete a suite of desferrioxamines and upregulate predicted ferrioxamine transport clusters suggested that iron acquisition was important for exploring *Streptomyces*. To examine how iron uptake capabilities affected exploration, we constructed mutations in the two upregulated *bldK*-like gene clusters. We focused on key genes within these clusters that were upregulated in exploring colonies, and generated mutations within these (Δ*sven_4759* and Δ*sven_5151*). To account for the possibility of functional redundancy shared by these two clusters, we also created a double (*sven_4759* and *sven_5151*) deletion strain. We found that the single deletion strains each behaved like wild type on YP medium with and without 2,2′-dipyridyl (**Fig. 4.6**). However, the surface area of the double mutant was significantly larger (~3 times greater) compared with wild type (**Fig. 4.7A,C**). This suggested that *sven_4759* and *sven_5151* have redundant functions during exploration, and that their collective function impacted exploration. The enhanced exploration capabilities observed for the double mutant could be restored to wild type upon introducing a cosmid carrying an intact *sven_4759-63* operon (**Fig. 4.8**).

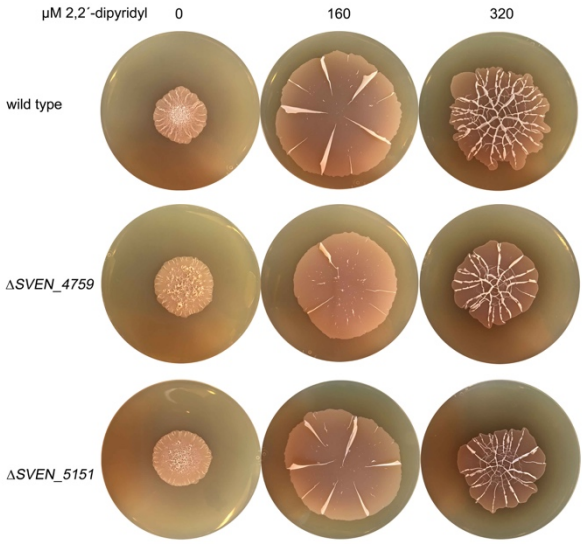

Fig. 4.6 *bldK* single deletion strains do not impact exploration. Wild type *S. venezuelae*, Δ*sven_4759* and Δ*sven_5151* grown on YP medium with 0, 160 or 320 μM 2,2′-dipyridyl. Plates were incubated for 10 days. Images are representative of three replicates per strain per condition.

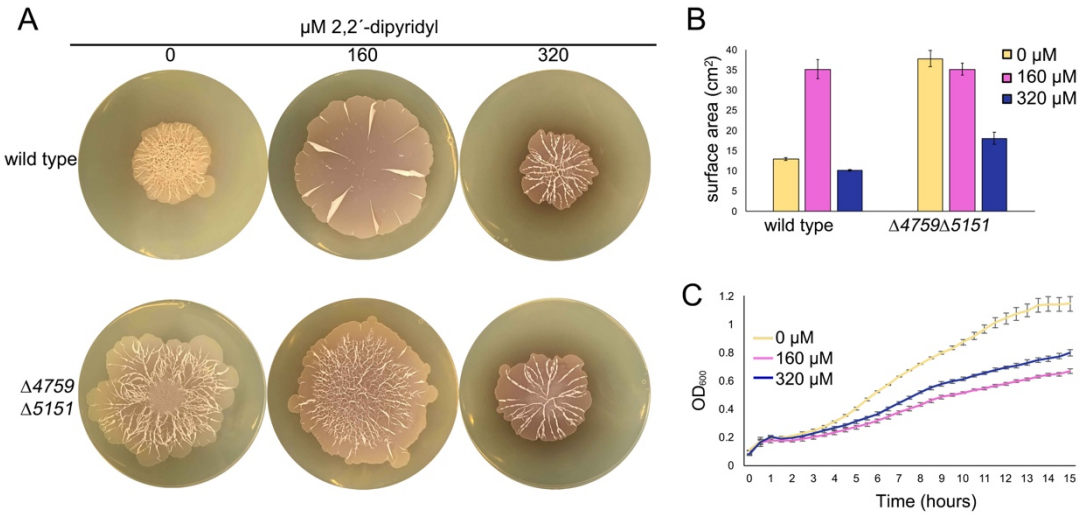

Fig. 4.7 Iron uptake capabilities impact exploration. A. Wild type *S. venezuelae* and the Δ*sven_4759*Δ*sven_5151* double mutant exploring on YP with 0, 160 or 320 μM 2,2′-dipyridyl. Plates were incubated for 10 days. Images are representative of three replicates per strain, per 2,2′-dipyridyl concentration. **B.** Quantification of colony expansion by wild type *S. venezuelae* and the Δ*sven_4759*Δ*sven_5151* double mutant on YP with 0-320 μM 2,2′-dipyridyl. Values represent the mean ± standard error for three replicates. **C.** Growth curves of wild type *S. venezuelae* grown in liquid YP medium with 0-320 μM 2,2′-dipyridyl over 15 hours. Values represent the mean ± standard error for three or four replicates.

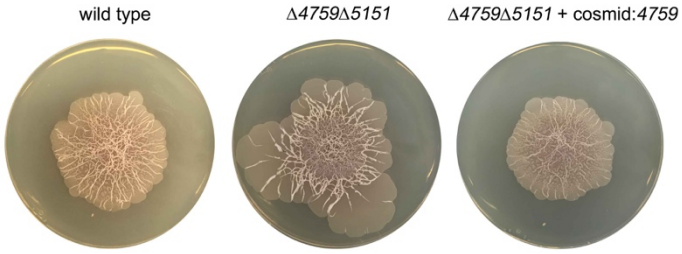

Fig. 4.8 Complementation of the double *bldK* mutant. Wild type *S. venezuelae*, the double *bldK* mutant, and the double *bldK* mutant complemented with a cosmid carrying the wild type sequence of *sven_4759* were grown on YP medium for 10 days.

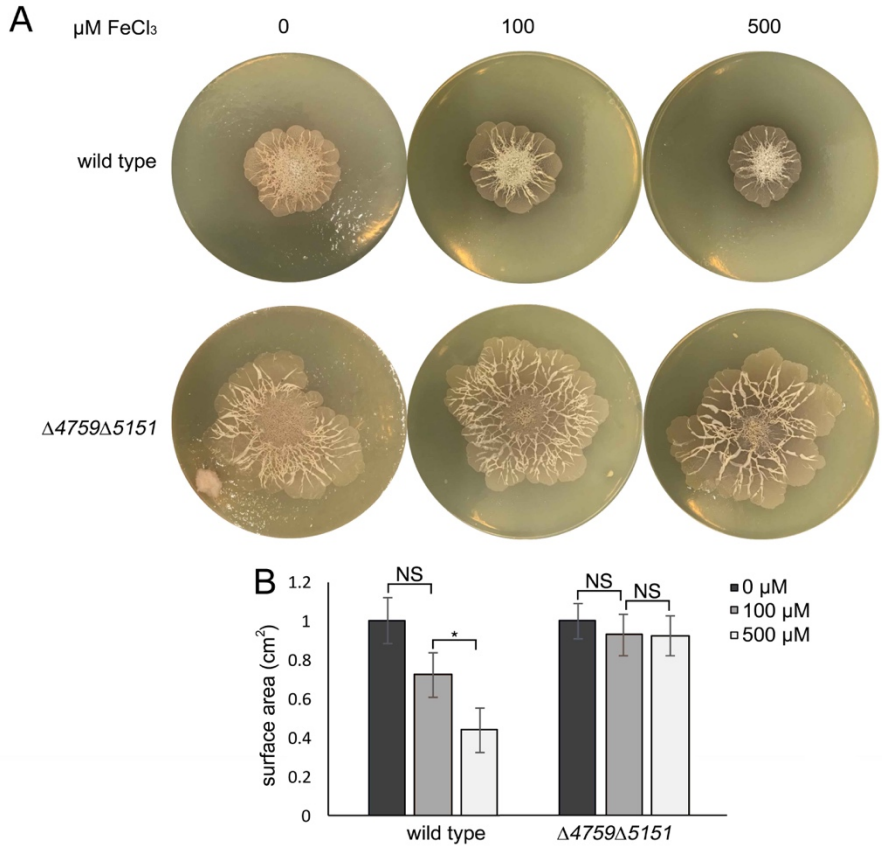

Fig. 4.9 The double *bldK* mutant does not respond to iron supplementation. A. Wild type *S. venezuelae* and Δ*sven_5759*Δ*sven_5151* grown on YP supplemented 0-500 μM $FeCl_3$. Plates were incubated for 10 days, and are representative of three replicates per strain per iron concentration. **B.** Quantification of the surface area of wild type *S. venezuelae* and Δ*sven_5759*Δ*sven_5151* grown on YP supplemented 0-500 μM $FeCl_3$. All values represent the mean ± standard error for three replicates. The asterisk indicates significant differential expression (p <0.05), and NS indicates no statistically significant difference.

The double mutant phenotype suggested that iron starvation – or the inability to transport iron-complexed siderophores – prompts colonies to increase surface area, presumably to scavenge for iron. To test how low iron affected exploration, we first grew wild type *S. venezuelae* on YP medium supplemented with a range of concentrations of the iron-chelator 2,2′-dipyridyl. When grown on medium containing 160 μM 2,2′-dipyridyl, *S. venezuelae* had surface areas averaging 2.7 times larger than colonies grown without chelator (**Fig. 4.7A,B**). Doubling the chelator concentration, however, led to explorer colony sizes slightly smaller than seen in the absence of chelator, suggesting that there is a minimum threshold of iron required to promote exploration. The larger surface area associated with moderately low-iron conditions could be due to enhanced exploration, or it could be a result of increased growth. To differentiate between these two possibilities, we grew *S. venezuelae* for 15 hours in liquid YP medium, with or without 2,2′-dipyridyl (**Fig. 4.7C**). We found that chelator supplementation led to reduced *S. venezuelae* growth, although the addition of 320 μM 2,2′-dipyridyl was less deleterious than 160 μM 2,2′-dipyridyl. This suggested that the enhanced exploration observed when grown on YP medium containing 160 μM 2,2′-dipyridyl was the result of increased colony expansion, instead of more rapid *S. venezuelae* growth. We cannot, however, formally exclude the possibility that there is something specific about YP agar medium that promotes *S. venezuelae* growth under low iron conditions.

The enhanced exploration observed for the wild type strain growing on YP with 160 μM 2,2′-dipyridyl was reminiscent of that observed for the double transporter mutant growing on YP medium. This suggested that the mutant strain was growing as if it were iron starved, even when in iron-replete conditions. To further examine the possibility that the double mutant was unable to effectively sense environmental iron levels, we grew the mutant on YP medium plus 160 μM 2,2′-dipyridyl. The presence of this chelator did not alter the surface area of the mutant strain. Notably, the double mutant also failed to respond to iron supplementation, further supporting the idea that this mutant is unable to sense and respond to external iron concentrations (**Fig. 4.9**).

Given the iron-starved response observed for the double transporter mutant, we were interested in understanding how this strain overcame the apparent iron deficit associated with exploration and an associated high pH environment. We isolated RNA from wild type and double transporter mutant strains after 8 days of exploration, and analyzed the expression profiles of genes involved in siderophore production and uptake in these strains using semi-quantitative RT-PCR (**Fig. 4.10**). *S. venezuelae* encodes five predicted siderophore clusters (as predicted by antiSMASH, see **Table 4.1**) (Blin et al., 2013). Transcript levels associated with the genes in the desferrioxamine biosynthetic cluster were higher in the double transporter mutant compared to wild type, while genes in the other four siderophore biosynthetic clusters were unaltered in wild type versus mutant strains (**Fig. 4.10**). *S. venezuelae* encodes three potential siderophore uptake systems and one ferrous iron uptake system in addition to the *bldK* clusters (**Table 4.1**), and none of these were differentially expressed in wild type compared with the uptake mutant strain. Our finding that the double *bldK* mutant has enhanced exploration even

on high-iron medium suggested it always behaves as if it is iron-starved. Supporting this idea, our RT-PCR data indicated the double mutant likely overproduces desferrioxamines.

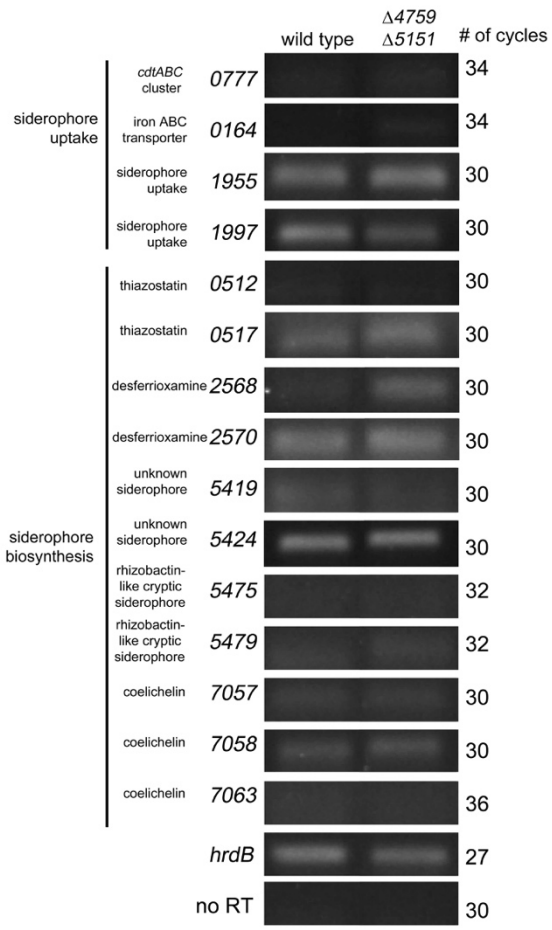

Fig. 4.10. Expression profiles of genes involved in iron uptake in siderophore synthesis. Semiquantitative RT-PCR using RNA isolated from the wild-type strain and Δ*sven_5759*Δ*sven_5151* grown for 8 days on YP medium. The vegetative sigma factor *hrdB* served as a positive control for RNA loading and RNA integrity, and no-RT reactions (using RNA as template with *hrdB*-specific primers) were included as negative controls to ensure a lack of DNA contamination on RNA samples and all PCR reagents.

4.3.5 Low iron environments can be created by interspecies interactions

Soil bacteria live in densely populated microbial communities, where there is intense competition for key nutrients including iron. Given our findings that low iron reduced the survival of other microbes and enhanced exploration, we wondered whether interactions with other bacteria – conditions in which organisms would be competing for iron – would affect *S. venezuelae* exploration. *Streptomyces* and *Amycolatopsis* bacteria have been isolated from the

same soil samples, indicating that interactions between these bacteria could be common in the environment. It has been demonstrated that *Amycolatopsis sp.* AA4 can pirate desferrioxamine E from *S. coelicolor* in low iron environments (Traxler and Watrous, 2013; Traxler et al., 2012).

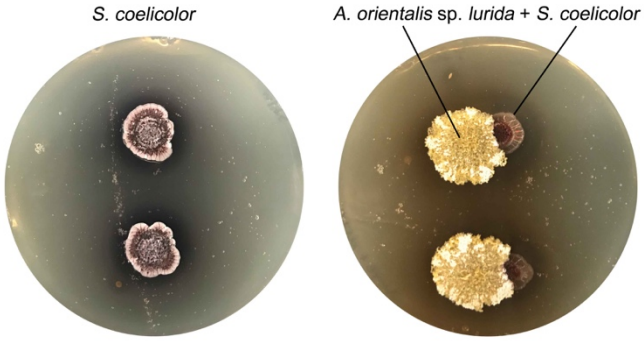

Fig. 4.11 *Amycolatopsis* prevents *S. coelicolor* aerial hyphae growth. Left: *S. coelicolor* grown alone, and right: *S. coelicolor* grown beside *Amycolatopsis orientalis* sp. *lurida.* There are two replicates per plate, and both plates were incubated for 14 days.

As a result, *S. coelicolor* is unable to raise aerial hyphae. We were able to recapitulate this phenotype using another *Amycolatopsis* strain: we grew *S. coelicolor* beside *Amycolatopsis orientalis* sp. *lurida*, and found *S. coelicolor* was unable to raise aerial hyphae (**Fig. 4.11**). This indicated siderophore piracy by *Amycolatopsis* may be a widespread phenomenon.

To examine whether naturally occurring microbial interactions can affect exploration by altering iron availability, we examined the growth of *S. venezuelae* beside the soil-dwelling actinomycete *Amycolatopsis orientalis* sp. *lurida* (**Fig. 4.12**). *S. venezuelae* was spotted alone or beside *A. orientalis* on YP or YP plus 2,2′-dipyridyl, and plates were incubated for 7 days. On YP plates without 2,2′-dipyridyl, the surface area of *S. venezuelae* increased by >100% when grown beside *A. orientalis*. This was analogous to growth of *S. venezuelae* alone on YP medium supplemented with moderate concentrations (160 µM) of 2,2′-dipyridyl (**Fig. 4.12**). However, the combination of proximal *A. orientalis* and further iron sequestration (through the addition of 160 or 320 µM 2,2′-dipyridyl) led to a decrease in the surface area of exploring *S. venezuelae* by 14% and 76%, suggesting that iron levels under these conditions were below the threshold required for optimal exploration.

Our results suggested that *A. orientalis* promoted increased exploration by *S. venezuelae* in the same way as low iron. To test whether the effect of *A. orientalis* on *S. venezuelae* exploration was mediated by depleting iron and/or pirating siderophores produced by *S. venezuelae*, we grew *S. venezuelae* beside *A. orientalis* on YP medium supplemented with $FeCl_3$ for 7 days (**Fig. 4.12**). For both $FeCl_3$ concentrations tested, the surface area of *S. venezuelae* was nearly identical when grown alone or beside *A. orientalis*, indicating the exploration-promoting effects of *A. orientalis* could be suppressed by the presence of excess iron. These findings indicated that iron sequestration by *A. orientalis* enhanced *S. venezuelae* exploration by depleting iron, and suggested that microbial interactions native to the soil can modulate exploration by altering nutrient profiles.

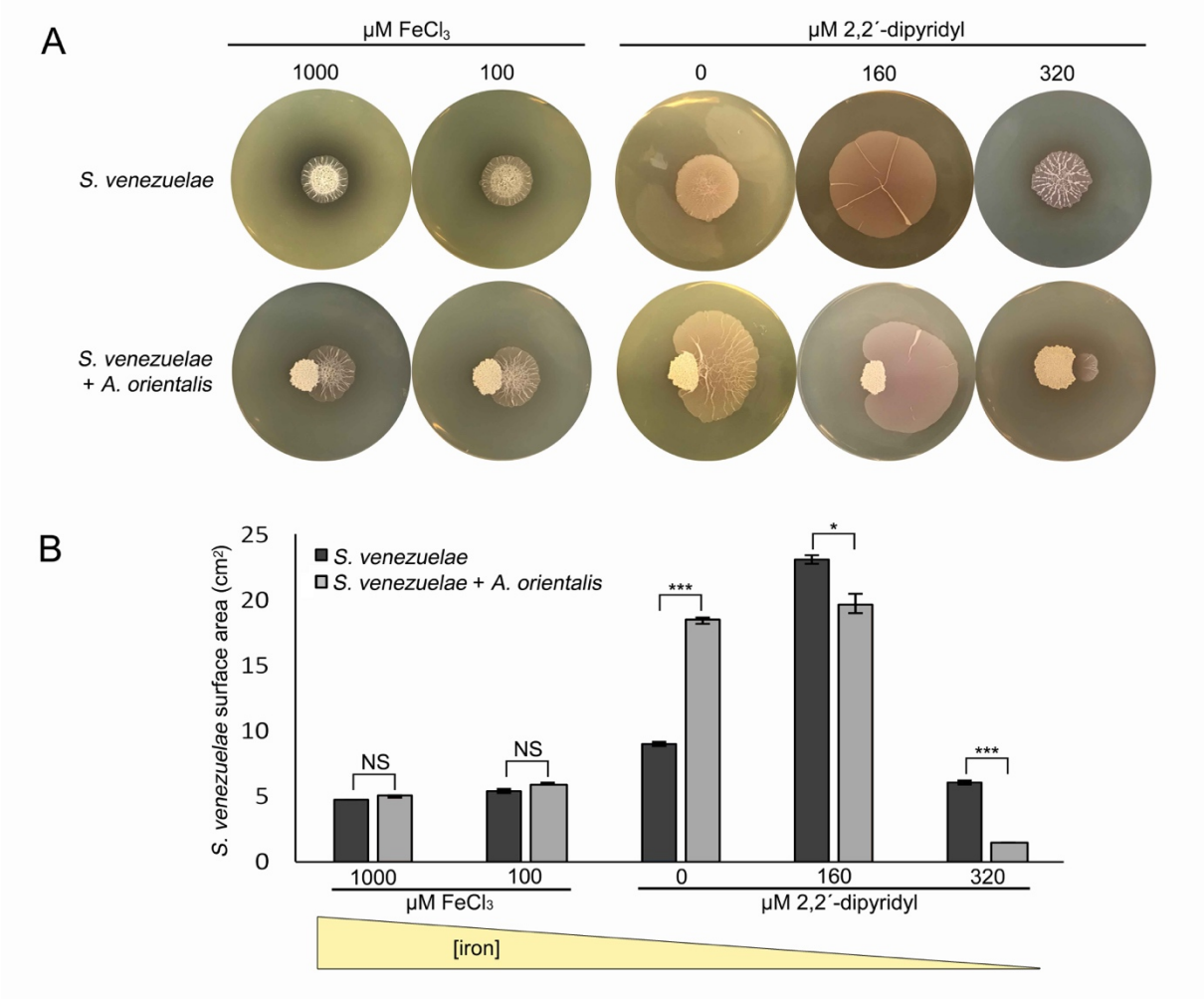

Fig. 4.12 Interspecies interactions alter exploration by creating low iron environments. A. *S. venezuelae* grown alone (top row) or beside *A. orientalis lurida* on YP supplemented with $FeCl_3$ or 2,2′-dipyridyl. Plates were incubated for 7 days, and all images are representative of three replicates per condition. **B.** Quantification of *S. venezuelae* grown alone or beside *A. orientalis* on YP with decreasing levels of available iron (left to right). Values represent the mean ± standard error for three replicates. All values represent the mean ± standard error for three or four replicates. Asterisks indicate statistically significant differences (* = *p*-value 0.05 to 0.01; ** = *p*-value 0.01 to 0.005; *** = *p*-value below 0.005, NS = no significant difference) as determined by a student's t-test.

4.3.6 Glucose trumps iron in the hierarchy of nutrients affecting exploration

The profound effect of iron levels on *S. venezuelae* exploration (through decreased iron solubility, microbial competition or siderophore piracy), led us to question whether low iron could overcome the exploration inhibitory effects of other nutrients. Previous work revealed that exploration was glucose-repressible (Jones et al., 2017), and thus we were interested in determining whether low iron conditions could alleviate the need for a low-glucose

environment. We grew *S. venezuelae* and the Δ*sven_4759*Δ*sven_5151* double mutant strain on YP plus glucose (YPD) plates supplemented with 160 µM or 320 µM 2,2′-dipyridyl for 10 days. We found that *S. venezuelae* failed to explore under these conditions (**Fig. 4.13**), indicating that the glucose effects were able to override the effects of iron deficiency, with respect to

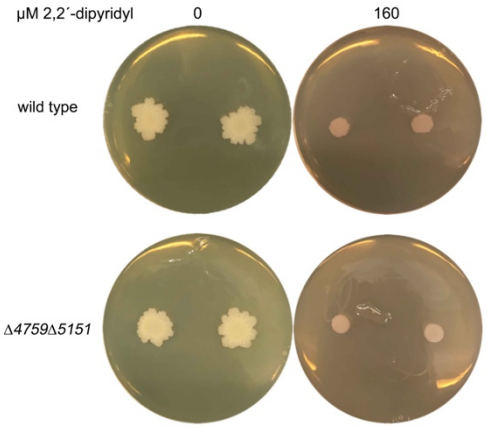

Fig. 4.13 Glucose represses exploration, even in the presence of low iron. Wild type *S. venezuelae* and the Δ*sven_5759*Δ*sven_5151* strain grown on 0 or 160 µM 2,2′-dipyridyl. Two replicates of each strain were spotted on each plate, and strains were incubated for 10 days.

exploration promotion.

We also tested whether additional iron could inhibit exploration. We grew wild type *S. venezuelae* on YP medium (exploration-promoting medium) and MYM medium (classic development-promoting medium) with increasing concentrations of iron (**Fig. 4.14**). *S. venezuelae* explored on YP with iron levels ranging from 0-10 mM, although the surface area was slightly reduced at the highest iron levels, relative to conditions without iron supplementation. A pigmented metabolite was also newly detectable during growth on high levels of iron. Interestingly, *S. venezuelae* did not survive on MYM when iron levels exceeded 2.5 mM. This suggested that exploration could also protect *S. venezuelae* from otherwise toxic levels of iron in their environment, presumably by reducing the amount of bioavailable iron through environmental alkalinization.

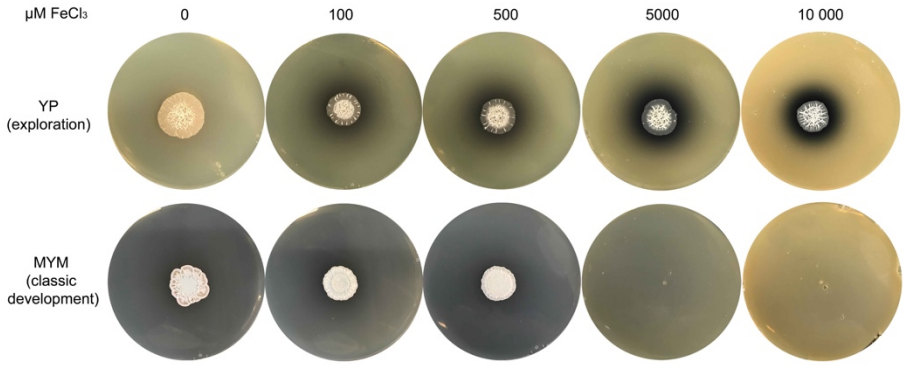

Fig. 4.14 *S. venezuelae* survival on growth medium supplemented with iron. Wild type *S. venezuelae* grown on YP medium (top row) or MYM medium (bottom row) supplemented with 0-10,000 µM $FeCl_3$. Images are representative of three replicates per media type, per iron concentration.

4.4 Discussion

Our work here reveals a new role for bacterial VOCs in modulating nutrient availability. The release of TMA by *Streptomyces* explorer cells dramatically alters the pH of their surrounding environment, and in doing so, reduces the survival of nearby soil microbes by starving them of iron. Within these iron-depleted niches, *Streptomyces* ensure maximal iron uptake by secreting unique siderophores, and upregulating genes encoding desferrioxamine transport systems. Exploration is enhanced in low iron environments, whether that be due to the presence of iron chelators, or the activity of siderophore cheaters/pirates. Collectively, our results reveal exploration to be not only an effective mechanism for dealing with both iron starvation and iron toxicity, but also a potent mediator of nutrient availability in the environment.

4.4.1 Volatile compounds impact microbial community dynamics by controlling nutrient availability

Streptomyces exploration is coordinated by the volatile molecule TMA, whose release raises the pH of the environment from 7.0 to 9.5 (Jones et al., 2017). Remarkably, TMA functions as both a communication signal, inducing other *Streptomyces* to explore, and as a competitive weapon, reducing the survival of other microbes. The antibacterial and antifungal properties of TMA appear to be related to its nutrient modulatory effects. Alkaline conditions, such as those resulting from TMA release, create an inhospitable environment for many microbes by reducing the levels of bioavailable iron (McMillan et al., 2010; Ratzke and Gore, 2018; Serrano et al., 2004). We show here that iron supplementation can restore the growth of otherwise susceptible bacteria and fungi in the presence of TMA, suggesting that iron starvation is at the heart of the TMA antimicrobial effects.

Microbial interactions are often mediated through changes in their immediate environment: microbes modify the environment by taking up nutrients or excreting metabolites, and in doing so, impact the growth of themselves and others (Andrade-Domínguez et al., 2014; Ratzke and Gore, 2018; Shirtliff et al., 2009). Changes in pH represent an environmental modification with significant consequences for microbial survival. For example, in the human gut, the bacterium *Corynebacterium ammoniagenes* raises the pH by excreting ammonia, and its own growth improves as pH rises (Collins, 1987). Not surprisingly, pH values also have a considerable influence on microbial community structure and availability of nutrients in the soil (Nicol et al., 2008; Rousk et al., 2010). Here, we show that exploring *Streptomyces* not only change their local environment, but raise pH at a distance, having profound effects on the environmental microbial community dynamics by altering iron availability. The VOC repertoire of many microorganisms appears to be vast (Jones et al., 2017), and our work indicates that VOC-mediated pH changes could have far-reaching effects on microbial community structures, and unlike many specialized metabolites, has the ability to influence community dynamics at a distance.

4.4.2 Promoting exploration in iron-depleted environments

Streptomyces exploration is enhanced during growth in low iron environments, although below a certain level, exploration stimulation ceases. Iron is limited in the soil (Niehus et al., 2017; Traxler et al., 2012), and rapid exploratory growth in iron-limited environments could allow *Streptomyces* to rapidly access nutrients in more distant locations. We have determined that exploration is rapid and remarkably processive; explorer cells spread over surfaces at a rate ~12 times faster than has previously been seen for *Streptomyces* colonies (Jones et al., 2017), and it is not known how (or whether) exploration can be stopped. Our data suggest the relentless nature of exploration could be explained by a positive feedback loop, with iron acting as a central player: explorer cells produce TMA, TMA emission leads to increased pH and reduced iron availability, explorer cells spread more to get more iron, TMA continues to be produced, and the cycle continues (**Fig. 4.15**). Indeed, a recent study modeling the effects of pH on bacterial growth demonstrated that when environmental modification is beneficial for a bacterium, there is a positive feedback on their growth: the more they change the environmental pH, the more cells grow, and the more they can continue to alter pH (Ratzke and Gore, 2018). Within the exploration feedback cycle, several additional factors could account for the increase in exploration surface area in low iron environments. The classic *Streptomyces* life cycle involves a transition from vegetative hyphal growth to raising reproductive aerial structures. For *S. coelicolor*, 2,2′-dipyridyl prevents colonies from raising aerial hyphae or sporulating, and instead locks cells in the vegetative growth phase (Traxler et al., 2012). Explorer cells share many properties with vegetative hyphae (Jones et al., 2017), and it is possible that low iron serves to inhibit aerial development, and thereby enhance the rate of exploration by preventing entry into the classical reproductive differentiation phase. In support of this proposal, we found that supplementing YP plates with iron led to slower exploring cultures that appeared to raise aerial hyphae in the centre.

We also noted that colonies growing on YP with 2,2′-dipyridyl, or in association with *A. orientalis* were much flatter and less structured than colonies growing alone on YP. Other bacteria (*e.g. Pseudomonas aeruginosa*), require iron for normal biofilm structure, and low iron, like the conditions tested here, triggers increased surfactant production and motility, reducing colony structure (Banin et al., 2005; Glick et al., 2010). Similar connections between iron availability and motility have been made in other microbes (Burbank et al., 2015; Helmann, 2014; Ojha and Hatfull, 2007; Pelchovich et al., 2013). *Streptomyces* exploration is phenotypically similar to sliding motility – a form of passive motility driven by growth and facilitated by a surfactant. It is possible that low iron leads to enhanced surfactant production by explorer cells, altering the colony structure and enhancing motility, along with the ability to scavenge for iron.

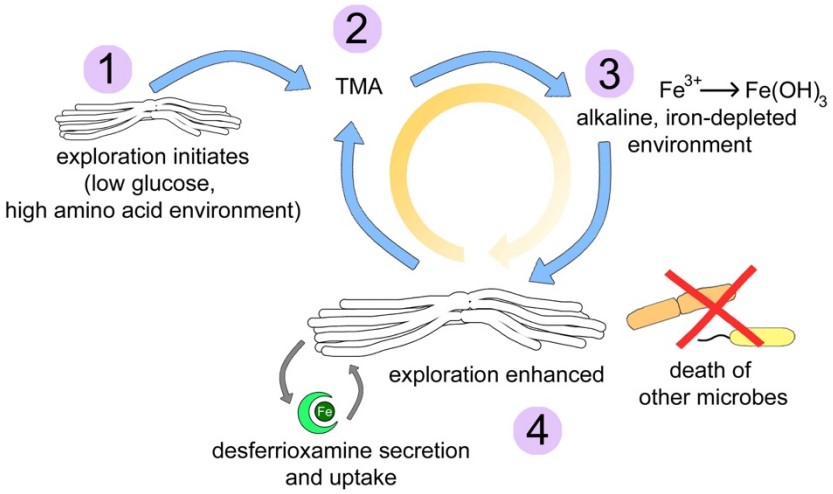

Fig. 4.15 *S. venezuelae* explorer cells thrive and reduce the survival of other microbes in alkaline, low-iron environments. 1. *S. venezuelae* exploration is triggered by a combination of low glucose and high amino acid concentrations. 2. Explorer cells release the VOC TMA into the surrounding environment. 3. TMA raises the pH of the environment from ~7.0 to 9.5, significantly reducing the solubility and bioavailability of iron. 4. To cope with low iron conditions, *S. venezuelae* explorer cells release desferrioxamines. These siderophores return solubilized iron to cells. At the same time, *S. venezuelae* exploration is enhanced, perhaps as a mechanism to reach more iron-rich environments. This enhancement of exploration leads to increased TMA production, creating a positive feedback loop (orange arrow): TMA depletes iron, explorer cells spread more to get more iron, TMA production continues, and the cycle repeats. Within these alkaline, iron-depleted environments, the survival of other bacteria and fungi is reduced.

4.4.3 Competition for iron mediates interspecies interactions

While specialized metabolites have received attention for their roles in mediating microbial competition, it is being increasingly found that competition for iron drives the outcomes of interspecies interactions (Holden and Bachman, 2015; Niehus et al., 2017; Patin et al., 2015; Traxler et al., 2012). Iron is critical for classic *Streptomyces* differentiation. When other microbes use desferrioxamines produced by *Streptomyces* – a strategy known as siderophore piracy – *Streptomyces* development is arrested (Traxler et al., 2012). *Streptomyces* are capable of producing several siderophores, and of these, only the desferrioxamines seem to be conserved throughout the streptomycetes and closely related genera (Yamanaka et al., 2005). Exploring colonies produce a suite of ferrioxamines, providing evidence these iron-chelating molecules play important roles in all aspects of *Streptomyces* development. We have not identified antibiotic or antifungal compounds produced by *S. venezuelae* exploring cells. Here, we show that a major competitive mechanism employed by exploring *Streptomyces* is the

modulation of iron availability. TMA creates alkaline, iron-starved environments unfavourable for other microbes, and *S. venezuelae* explorers capitalize on remaining iron stocks using desferrioxamines, further depleting iron resources. *Amycolatopsis* iron acquisition enhances *S. venezuelae* exploration – perhaps by pirating desferrioxamines from *S. venezuelae*. Thus, even when microbes are primed for iron acquisition, *S. venezuelae* is driven to explore to more iron-rich environments.

4.5. Materials and Methods

4.5.1 Strains, plasmids, media and culture conditions

Strains, plasmids and primers used in this study are listed in **Table 4.2**. *S. venezuelae* ATCC 10112 was grown on MYM (maltose, yeast extract, malt extract) agar for spore stock generation, and for examining the behavior of classically developing cultures. Exploration was investigated on YP (yeast extract, peptone) agar, and non-exploring controls were grown on YP agar supplemented with dextrose/glucose (YPD). For iron experiments, plates were supplemented with the indicated concentration of 2,2′-dipyridyl (0-360 µM) or $FeCl_3$ (0-10 mM). All strains were grown at 30˚C, except those experiments involving TMA which were conducted at room temperature in a fume hood. Prior to growing on plates, *S. venezuelae* was grown in liquid MYM at 30˚C, and 5 µL were spotted to agar plates. *A. orientalis* subsp. *lurida* was also grown in liquid MYM at 30˚C, and spotted alone or directly beside *S. venezuelae* on agar plates. All plates were incubated for up to 14 days. Colony surface areas were measured using ImageJ (Abràmoff et al., 2004). *E. coli* strains were grown in or on LB (Luria Bertani) medium or in SOB (super optimal broth) medium. DH5α and ET12567/pUZ8002 strains were grown at 37°C, and BW25113/pIJ790 was grown at 30°C or 37°C. *Amycolatopsis* strains were cultured in LB liquid medium at 30°C overnight. Five microliters of culture were spotted beside *S. venezuelae* on the surface of MYM agar medium, or *S. coelicolor* M145 on the surface of R2YE agar medium. *S. coelicolor* was spotted directly from a spore stock. Plates were incubated at 30°C for up to 14 days.

For iron growth assays, *B. subtilis* and *M. luteus* were grown in LB medium, while *S. cerevisiae* was grown in YPD medium. Each strain was grown in 10 mL liquid medium shaking overnight at 30˚C. To quantify strain survival in response to iron chelation on solid medium, each strain was subcultured and grown to an OD_{600} of 0.8, before being diluted 1/5000, with 100 µL being spread on agar medium containing 2,2′-dipyridyl (0-360 µM). Colony numbers were quantified after 2 days. To quantify the survival of each strain in response to iron chelation in liquid medium, varying amounts of overnight cultures of each strain were added to 1.5 mL fresh media to give an OD_{600} of 0.1 in 48-well plates. Plates were shaken at 30˚C in a plate reader and OD_{600} readings were taken every 30 min for 8 hours.

4.5.2 Identification and analysis of desferrioxamines

To analyze metabolite production by explorer cultures, agar from each culture plate was diced, placed in a 50 mL falcon tube, and frozen at -80°C. The cultures were then dried by lyophilization. Extraction of metabolites was performed by adding 45 mL of 50:50 n-butanol/ethyl acetate to each falcon tube and rotating overnight at room temperature. The extracts were filtered, and the solvent removed under vacuum at room temperature (Genevac EZ-2 Series Personal Evaporator, method low + medium BP, lamp off).

All mass spectrometry experiments were conducted using UPLC-ESI-QTOF MS instrumentation (Agilent, 6540). Each extract was dissolved in 400 µL of 50:50 H_2O/acetonitrile (Fisher, LC-MS grade), of which 2 µL were injected onto a C18 column (Agilent, Zorbax, 2.1 x 50 mm, 1.8 µm). Compounds were separated using a constant flow of 0.4 mL/min and the following gradient: 0-3 min at 0% B (A, 95:5:0.1%, H_2O/acetonitrile(ACN)/formic acid and B, 95:5:0.1% ACN/H_2O/formic acid), 3-17 min at 0-100% B, and 17-20 min at 100% B. Accurate mass data were acquired in triplicate in both profile and centroid mode with source/fragmentor voltage of 100 V, positive mode ion detection between 100–1,700 *m/z*, gas temperature of 325°C, and capillary voltage of 3,500 V. Fragmentation data were acquired with a fixed collision energy of 35 V with positive mode product ion detection between 50-1,650 *m/z*. Data were processed using Agilent Masshunter Qualitative Analysis and Origin.

4.5.3 Construction of deletion strains and mutant complementation

An in-frame deletion of *sven_4759* (*bldK* homolog) was generated using ReDirect technology (Gust et al., 2003). The coding sequence (excluding the start and stop codon) was replaced with an *oriT*-containing apramycin resistance cassette. For mutation of *sven_5151* (a second *bldK* homolog), the gene was disrupted in the chromosome. A 1,406-bp region of the gene was amplified and cloned into the TOPO vector (Invitrogen). Mutant cosmids/disruption plasmids were introduced into the non-methylating *E. coli* strain ET12567/pUZ8002 prior to conjugation into wild type *S. venezuelae*. For creating the Δ*sven_4759*Δ*sven_5151* double mutant strain, the ET12567/pUZ8002 strain carrying the *sven_5151* TOPO construct was introduced into the Δ*sven_4759*:apramycin strain. Resulting exconjugants were screened for double-crossover recombinants (in the case *sven_4759 bldK*) or single-crossover integration (in the case of *sven_5151* and Δ*sven_4759*Δ*sven_5151*). Correct replacement of *sven_4759* and disruption of the *sven_5151* coding sequence was confirmed using diagnostic PCR combinations (see **Table 4.3**). The Δ*sven*_4759Δ*sven_5151* double mutant phenotype was complemented using a cosmid carrying the wild type *sven_4759* sequence, along with the downstream cluster, to account for any polar effects. The ampicillin resistance gene on the cosmid backbone was replaced with an *oriT*-containing viomycin resistance cassette using the ReDirect protocol.

4.5.4 RNA isolation and RT-PCR analysis

RNA was isolated as described previously from two replicates from each of wild type and Δ*sven_4759*Δ*sven_5151 S. venezuelae* exploring colonies grown for 8 days on YP agar plates (we were unable to isolate high quality RNA from exploring *S. venezuelae* at later time points).

For all replicates, contaminating DNA was removed using Turbo DNase (Life Technologies), and RNA quality and purity were assessed using a Nanodrop spectrophotometer. RNA quality was analyzed by agarose gel electrophoresis prior to reverse transcription-PCR (RT-PCR) analysis. One microgram of RNA was used as template for reverse transcription using gene-specific primers (see **Table 4.3**) and Superscript III polymerase (Invitrogen), according to the manufacturer's instructions. The resulting cDNA then served as template for PCR amplification using Taq DNA polymerase and the gene-specific primers listed in **Table 4.3**. The number of cycles was optimized to ensure products were detected in the linear range of amplification. Negative controls containing nuclease-free water instead of reverse transcriptase were included to ensure RNA samples and other reagents did not contain residual contaminating DNA ('no RT'). cDNA corresponding the gene encoding the vegetative sigma factor *hrdB* was amplified as a positive control for RNA levels and RNA integrity. Ten microliters of each PCR were separated on a 1.5% agarose gel and visualized by staining with ethidium bromide. All reactions were conducted in triplicate, using two independently isolated RNA samples.

4.5.5 Assays for volatile-mediated phenotypes

To quantify how *S. venezuelae* VOCs affected the survival of other bacteria or fungi, *S. venezuelae* was grown in a small petri dish containing YP or YPD agar. The small dish was placed inside a larger dish containing agar or agar supplemented with 1 mM $FeCl_3$. LB agar was used for the growth of *B. subtilis* and *M. luteus*, while YPD agar was used for *S. cerevisiae*. *S. venezuelae*-inoculated plates were grown for 10 days, after which the indicator organisms were spread on the surrounding plates. *B. subtilis*, *M. luteus*, or *S. cerevisiae* were subcultured and grown to OD_{600} of 0.8 in liquid LB/YPD, after which the cultures were diluted 1/10 000 and 50 µL was then spread on the agar. Colony numbers on the outer plate were then quantified after 48 hours.

Measuring how iron supplementation affected the responses of microbes to TMA involved adding either 1.5 mL of commercially available TMA solutions (Sigma) diluted to 0.9% w/v, or water (negative control) to sterile plastic containers. These were then placed in a petri dish containing 50 mL LB or YPD agar, with or without 1 mM $FeCl_3$ supplementation. *B. subtilis*, *M. luteus*, or *S. cerevisiae* were subcultured and grown to an OD_{600} of 0.8 in liquid LB/YPD, before 100 µL of the subculture were spread on each plate. Plates were incubated at room temperature for 48 hours, before cells were scraped into tubes containing 2 mL liquid LB or YPD and vigorously mixed. Dilution series were used to measure the OD_{600} of the resulting cell suspensions. A minimum of four biological replicates were assessed, with two technical replicates tested per biological replicate.

4.6 Tables

Table 4.1 *S. venezuelae* siderophore production and uptake genes

Genes	

Synthesis clusters	**Predicted siderophore**
sven_0503-17	Thiazostatin
sven_2566-77	Desferrioxamine
sven_5413-26	Unknown siderophore
sven_5472-82	Rhizobactin-like cyptic siderophore
sven_7032-80	Coelichelin
Uptake systems	**Annotation**
sven_0776-78	Salmycin transporter CdtABC
sven_0164-66	Putative siderophore transporter system
sven_1997	Putative iron-siderophore uptake system
sven_1954-57	Ferrous iron transport system EfeUOB

Table 4.2 Bacterial strains and plasmids

Strain	Genotype, description, or use	Reference or source
Streptomyces		
Streptomyces venezuelae ATTC 10712		Gift from M. Buttner
	ATTC 10712 Δ*SVEN_4759::[aac(3)IV-oriT]*	This work
	ATTC 10712 Δ*SVEN_5151::*TOPO 2.1	This work
	ATTC 10712 Δ*SVEN_4759::[aac(3)IV-oriT]* + Δ*SVEN_5151::*TOPO 2.1	This work
Streptomyces coelicolor M145		(Kieser et al., 2000)
Amycolatopsis		
Amycolatopsis orientalis sp. *lurida*		Gift from G. Wright
E. coli		
DH5α	Plasmid construction and general subcloning	Invitrogen
ET12567/pUZ8002	Generation of methylation-free plasmid DNA and conjugation into *Streptomyces*	(MacNeil et al., 1992; Paget et al., 1999)
BW25113/pIJ790	Construction of cosmid-based knockouts	(Gust et al., 2003)
Plasmids or cosmids		
3D02	*S. venezuelae* cosmid carrying *SVEN_4759*	Gift from M. Bibb and M. Buttner
TOPO 2.1	Plasmid used for disruption of *SVEN_5151*	Invitrogen
pIJ790	Temperature-sensitive plasmid carrying λ-	

	RED genes	
pIJ773	Plasmid carrying the apramycin knockout cassette	
pIJ10701	Plasmid carrying the *hyg-oriT* cassette	
pIJ780	Plasmid carrying the *vio-oriT* cassette	

Table 4.3 Oligonucleotides used in this study

Name	Sequence (5′ to 3′)	Use
SVEN4759 Fwd	CTTGTAGTGACAAAGTGGACTCATGAGGAG GAACCCATGATTCCGGGGATCCGTCGACC	Creation of Δ*4759* strain; Confirmation of Δ*4759* mutation
SVEN4759 Rev	TCAGCCCCGCATCGCAGGCGGACTACGCTTG GGTGATTATGTAGGCTGGAGCTGCTTC	Creation of Δ*4759* strain; Confirmation of Δ*4759* mutation
SVEN4759 Up	TCCGGTACGTGTGTTAACGG	Confirmation of Δ*4759* mutation
SVEN4759 Down	TCAGCCCCGCATCGCAGGCGGACTACGCTTG GGTGATTATGTAGGCTGGAGCTGCTTC	Confirmation of Δ*4759* mutation
SVEN4759 In	CGGCGTTGATCATCTCCAGC	Confirmation of Δ*4759* mutation
SVEN5151 Up	ATATGGTACCACTTCGCCCGCTACTACACG	Creation of Δ*5151* strain; Confirmation of Δ*5151* mutation
SVEN 5151 Down	ATATTCTAGAGGTGAAGGGCAGGTAGACCG	Creation of Δ*5151* strain; Confirmation of Δ*5151* mutation
SVEN5151 CheckF	CAACGCCTCCGACAAGAAGG	Confirmation of Δ*5151* mutation
SVEN5151 CheckR	CTGCTTGCCGACGAACATCG	Confirmation of Δ*5151* mutation
blaF	CCCTGATAAATGCTTCAATAATATTGAAAAA GGAAGAGTA	Amplification of *hyg-oriT* and *vio-oriT* cassette; cosmid-based complementation of Δ*4759*Δ*5151* mutant strain
blaR	AATCAATCTAAAGTATATATGAGTAAACTTG GTCTGACAG	Amplification of *hyg-oriT* and *vio-oriT* cassette; cosmid-based complementation of Δ*4759*Δ*5151* mutant strain
HrdBF	CCGTTTCCATCGTTCCGAGA	Semiquantitative RT-PCR
HrdBR	ATCTGCCCATCAGCCTTTCC	Semiquantitative RT-PCR
0164F	GTGTCGTTCTCCTGGCCGG	Semiquantitative RT-PCR
0164R	GTTGTCCGCGACGACGGTG	Semiquantitative RT-PCR
0512F	TGATGACCCTCGTCAATCGG	Semiquantitative RT-PCR
0512R	CAACAATGCCTCCCAGGACC	Semiquantitative RT-PCR

0517F	CTGCACGCGGAGGAGTACG	Semiquantitative RT-PCR
0517R	GAGCAGATAGGCCGCCTGC	Semiquantitative RT-PCR
0777F	GTCGTCGAGCACCTCATCG	Semiquantitative RT-PCR
0777R	CCTTGGGCTCGTTCTTCAGC	Semiquantitative RT-PCR
1955F	TGCACCGAGAAGAGCGACG	Semiquantitative RT-PCR
1955R	CGGCGAGGTTCACGTGACC	Semiquantitative RT-PCR
1997F	GAGGAGGCGACGGAGGATCC	Semiquantitative RT-PCR
1997R	GCGTCGCCGAAGTCCTTGC	Semiquantitative RT-PCR
2568F	GAGATCGTCCGCGAGATGG	Semiquantitative RT-PCR
2568R	GAGATCGTCCGCGAGATGG	Semiquantitative RT-PCR
2570F	CCGTTCACCGGTGTGACCC	Semiquantitative RT-PCR
2570R	GGAGGTAGACGCTCTCCAGC	Semiquantitative RT-PCR
5419F	ACCGAGTCCCGACGGATCC	Semiquantitative RT-PCR
5419R	CCTCCCGTCCACAGCTCGG	Semiquantitative RT-PCR
5424F	AGGTGATCTCCACCGGATCG	Semiquantitative RT-PCR
5424R	CGTCAGGGTCGTCTTACCG	Semiquantitative RT-PCR
0164F	GTGTCGTTCTCCTGGCCGG	Semiquantitative RT-PCR
0164R	GTTGTCCGCGACGACGGTG	Semiquantitative RT-PCR
5475F	CAGCCGGGTACCACCGTCC	Semiquantitative RT-PCR
5475R	GTACTGCGGGCCGGATAGG	Semiquantitative RT-PCR
5479F	CGCCATGAATGACGCAAGC	Semiquantitative RT-PCR
5479R	GGTGAGACCGGAGCTGTCG	Semiquantitative RT-PCR
7057F	GTCACCGCCCACTTCTTCG	Semiquantitative RT-PCR
7057R	CCTTGAGGAAGGACACCTGC	Semiquantitative RT-PCR
7058F	CGGCGGGACCGAGAAGTCC	Semiquantitative RT-PCR
7058R	CCGTACTTGTGCTCGACGG	Semiquantitative RT-PCR
7063F	TCGTTGTCCGTCGAATCCCG	Semiquantitative RT-PCR
7063R	CAGGCCTAAGCCCCGGTACG	Semiquantitative RT-PCR

CHAPTER 5: DIVIVA AND MREB COOPERATE TO DRIVE *STREPTOMYCES* EXPLORATION

Stephanie E. Jones, Yen-Pang Hsu, Yves Brun, Sara Mitri, Marie Elliot

Preface:
This chapter represents as yet unpublished work. Yen-Pang Hsu, a postdoc in Prof. Yves Brun's lab (at the time at Indiana University Bloomington), carried out the fluorescent D-amino acid uptake experiments. Dr. Sara Mitri, a professor at Université de Lausanne in Switzerland, quantified colony wrinkling patterns. I performed all of the other work.

5.1 Abstract (Chapter Summary)

Streptomyces are filamentous bacteria best known for producing a multitude of medicinally useful metabolites, and for having a complex life cycle. For decades it had been thought that these bacteria grew as static colonies, rooted in place by a dense network of filaments. We recently demonstrated a new mode of *Streptomyces* growth termed exploration, whereby cells are no longer rooted, and instead grow and traverse surfaces at unprecedented rates. How this rapid rate of colony progression is achieved is unknown, and we sought to investigate the mechanisms underlying exploration. Classical *Streptomyces* growth is driven by the protein DivIVA, which recruits cell wall machinery to hyphal tips. In contrast, rod-shaped bacteria like *Escherichia coli* and *Bacillus subtilis* grow using the actin-like protein MreB, which drives cell wall synthesis along the lateral walls cells. Surprisingly, we found DivIVA is required for the initial stages of exploration, but is dispensable for subsequent phases. Instead, MreB-mediated lateral growth drives rapid colony expansion during this later phase. This work represents a novel example of cooperation by two canonical cell growth proteins to drive microbial growth.

5.2 Introduction

Bacteria display diverse cell shapes, ranging from spherical and rod-shaped, to curved and filamentous (Caccamo and Brun, 2017). Cell shape is primarily dictated by the peptidoglycan (PG), which consists of layers of glycan strands cross-linked together by short peptides. The PG layer surrounds the cytoplasmic membrane, and provides protection against cytoplasmic turgor pressure (Surovtsev and Jacobs-Wagner, 2018). Cell growth, and the corresponding insertion of new PG is directed by diverse cytoskeletal elements (*e.g.* FtsZ). In many rod-shaped bacteria (*e.g. E. coli* and *B. subtilis*), PG insertion occurs along the lateral walls of cells. This process is controlled by the actin homolog MreB (Jones et al., 2001; Salje et al., 2011). MreB filaments associate with the inner face of the cytoplasmic membrane, and are connected to the PG layer through transmembrane proteins (*e.g.* MreC, MreD, and RodZ) (Dempwolff et al., 2011; Salje et al., 2011). PG synthesis promotes the movement of MreB filaments around the circumference of cells, while the curved nature of MreB filaments is thought to influence the site of new PG insertion (Domínguez-Escobar et al., 2011; Garner et al., 2011; van Teeffelen et al., 2011). Gram-negative bacteria typically possess a single *mreB* gene in an operon with *mreC* and *mreD*. Gram-positive bacteria encode one *mreB* gene in an operon with *mreC* and *mreD*, and two additional MreB-like proteins (Carballido-Lopez, 2006).

In contrast to *E. coli* and *B. subtilis*, some rod-shaped bacteria lack MreB and instead grow at their poles using MreB-independent mechanisms. In rod-shaped actinomycetes (*e.g. Mycobacterium* and *Corynebacterium*), polar growth is driven by the coiled-coil protein DivIVA (Joyce et al., 2012; Kang et al., 2008; Meniche et al., 2014). Non-rod-shaped actinomycetes also employ polar growth mechanisms. The streptomycetes are a large genus of filamentous actinomycetes, and hyphal growth is driven by DivIVA positioned at the filament tips.

Streptomyces bacteria are best known for their ability to produce a wide range of medicinally useful compounds (*e.g.* antibiotics and antifungals) and for their complex, morphologically

differentiated life cycle (Elliot et al., 2008; Hopwood, 2007). The *Streptomyces* life cycle encompasses three stages, beginning with spore germination and the growth of branching vegetative hyphae. The reproductive phase of growth initiates when non-branching hydrophobic aerial hyphae rise into the air. The life cycle culminates when these aerial hyphae are sub-divided into chains of unigenomic pre-spore compartments, which go on to develop into mature spore chains. *Streptomyces* hyphal tip extension (for both vegetative and aerial cells) is directed by a complex of proteins termed the polarisome (Flärdh et al., 2012). This complex recruits cell wall biosynthetic machinery to the hyphal tips. The core component of the polarisome is the essential protein DivIVA. DivIVA co-localizes with Scy, which is thought to act as a molecular scaffold for other polarisome components. The intermediate filament protein FilP localizes behind the DivIVA-Scy complex, and plays a structural role in supporting tip growth. Unlike DivIVA, neither Scy nor FilP are essential for *Streptomyces* viability. New hyphal branches emerge following the breaking off of DivIVA-containing daughter foci from the main tip complex; these daughter complexes localize to regions adjacent to the growing tip. Notably, when tip extension is arrested in aerial hyphae, the polarisome complex disappears (Ditkowski et al., 2013; Flärdh, 2003).

Actinomycetes lack genes encoding MreB, with the exception of *Streptomyces*. Given that *Streptomyces* grow by DivIVA-mediated tip extension, while MreB drives lateral wall growth in rod-shaped bacteria, the conservation of MreB in streptomycete genomes has been puzzling. Like *B. subtilis, S. coelicolor* encodes three MreB homologs, referred to as MreB (encoded by *sco2611*), MreB-like (encoded by *sco6166*), and Mbl (encoded by *sco2451*). MreB and Mbl are expressed during aerial hyphae development and sporulation, and contribute to sporulation septa formation and spore wall thickening (Heichlinger et al., 2011; Mazza et al., 2006). MreB-like is expressed during vegetative growth and the early stages of aerial hyphae growth, but deletion of its associated gene does not affect the phenotype of vegetative hyphae. Instead, the protein appears to co-localize with MreB in driving spore wall maturation (Heichlinger et al., 2011).

While the classical *Streptomyces* life cycle encompasses branching vegetative hyphae, aerial hyphae and spores, recent work has shown some *Streptomyces* species can escape this classically defined life cycle, instead growing as 'explorer cells' capable of rapidly traversing surfaces (Jones et al., 2017). Exploring hyphae do not employ the 'Bld' regulators required for aerial hyphae development and are hydrophilic, indicating that explorer cells may grow as vegetative hyphae. Unlike vegetative hyphae in the classic life cycle; however, exploring vegetative hyphae are non-branching. A remarkable aspect of exploration is the rate at which colonies expand. Exploring colonies spread over surfaces at a rate ~12 times faster than has previously been seen for *Streptomyces* growth. This rapid spreading led us to investigate the cellular mechanisms underlying exploration. While previous work in *S. coelicolor* has shown DivIVA is essential for viability and MreB homologs are dispensable for vegetative growth, here, we reveal that the mechanisms driving growth in explorer cells are different that those defined for the traditional *Streptomyces* life cycle. In the exploring species *S. venezuelae*, DivIVA is essential for the initial phase of exploration. Once exploration is established, DivIVA is no longer

required, and growth instead depends on MreB. Thus, exploration involves coordinating the activities of DivIVA and MreB to promote rapid cell growth and pervasive colony expansion.

5.3 Results

5.3.1 DivIVA is required for the initial stages of exploration, but is dispensable once exploration has initiated

Streptomyces growth is well-established as being driven by DivIVA at the hyphal tips. Given the different growth and physical properties associated with exploring cells, we wondered whether DivIVA was required for exploration. DivIVA is essential for viability in *S. venezuelae*, and thus to address this question, we created a DivIVA depletable strain. We cloned *divIVA* downstream of the thiostrepton-inducible promoter *tipAp* (Murakami et al., 1989) on an integrating plasmid, and introduced this construct into wild type *S. venezuelae*. We successfully deleted *divIVA* from its native chromosomal locus when the second copy of *divIVA* was induced using thiostrepton. On medium supporting classic growth (MYM), the DivIVA depletion strain grew well (albeit with an atypical colony shape) with thiostrepton induction (**Fig. 5.1A**). On MYM without thiostrepton induction, the strain grew minimally. The *tipA* promoter has low level activity in the absence of inducer (Ali et al., 2002; Flärdh, 2003), and thus we hypothesized that *divIVA* was expressed at a low level that was sufficient to maintain minimal cell growth. A similar observation had been made previously for *S. coelicolor* (Flärdh, 2003).

Having established that the *S. venezuelae* DivIVA depletion strain grew well with thiostrepton and grew minimally without thiostrepton on MYM medium, we next examined how the strain behaved on exploration-promoting growth medium (YP) (**Fig. 5.1A**). We grew the depletion strain on YP medium with or without thiostrepton, and after 5 days in the absence of thiostrepton, colonies were very small. In contrast, when the DivIVA depletion strain colonies were grown on YP with thiostrepton, the resulting colonies were the same size as wild type grown on YP. However, by 8 days, the phenotypes of the different colonies had drastically changed: colonies grown without DivIVA induction were nearly the same size as those grown with thiostrepton and as wild type colonies. These observations suggested that DivIVA was important for growth when the explorer colonies were getting established, but was dispensable during the rapid out-growth phase of exploration.

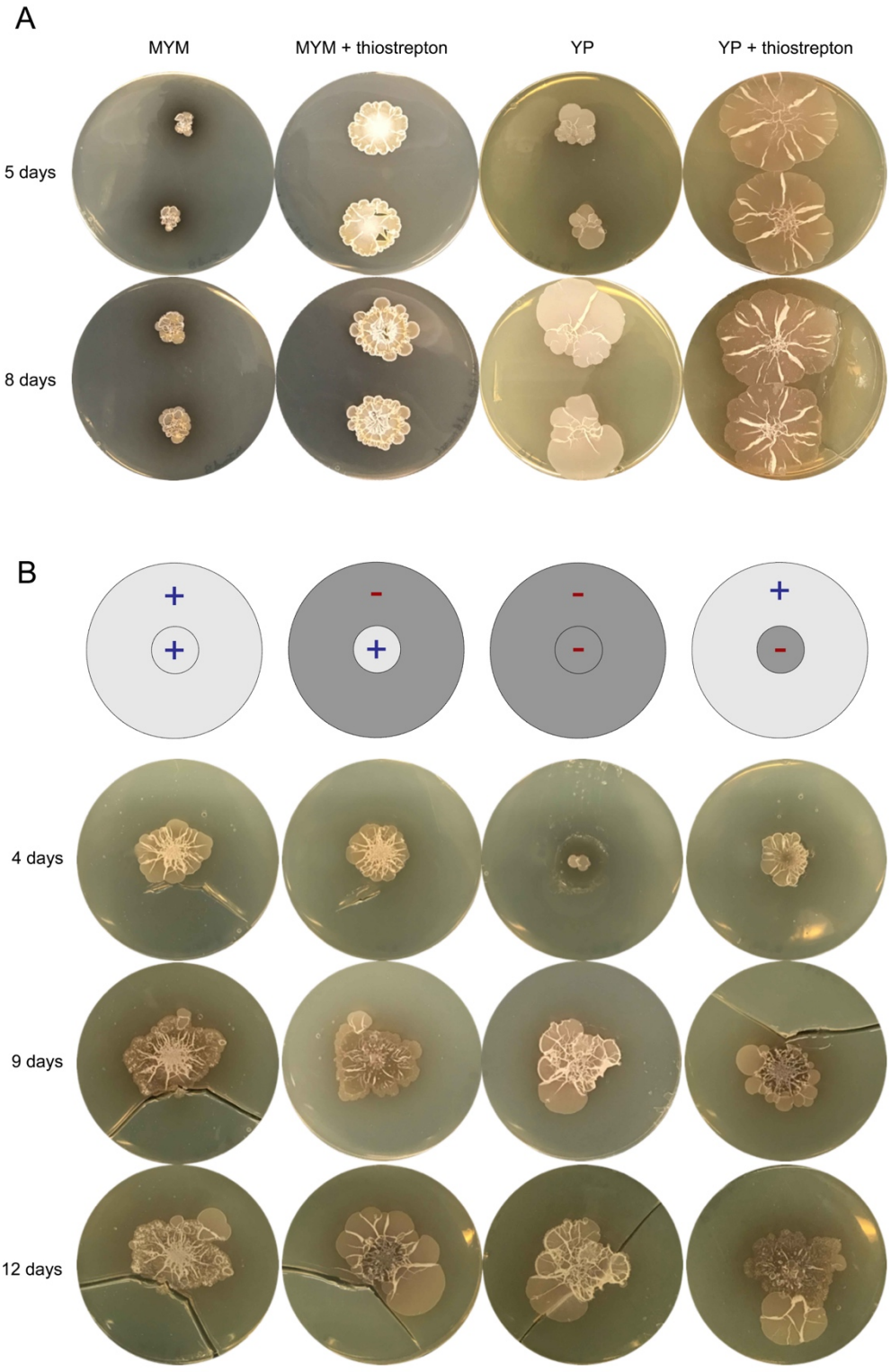

Fig. 5.1 DivIVA induction and exploration phenotypes. A. *S. venezuelae* Δ*divIVA* carrying an integrated plasmid with *divIVA* under the control of the thiostrepton-inducible promoter *tipAp*, was grown on different media types with or without 50 µg/mL thiostrepton. Two replicates per plate are shown. **B.** Top: schematic of plate setups for each column. All plates are subdivided into two areas: (i) a centre YP medium plug, with (+) or without (-) thiostrepton and (ii) the surrounding YP medium, again, with or without thiostrepton.

To further examine the role of DivIVA in the initial versus later stages of exploration, we set up YP plates with a centre medium plug, surrounded by a second medium type. These two regions were supplemented with either nothing, or with thiostrepton (**Fig. 5.1B**). The DivIVA depletion strain was spotted on the centre medium plug of each plate, and growth was assessed over 12 days. By 4 days, the strain had grown to the edge of the centre plug when supplemented with thiostrepton. The strain also grew well on a centre plug without thiostrepton, when the surrounding medium contained thiostrepton. Here, we cannot exclude the possibility that thiostrepton from the outer medium region diffused into the medium in the centre plug. Importantly however, the strain did not grow well on a centre plug without thiostrepton when the surrounding medium also lacked thiostrepton, supporting our previous findings that a lack of thiostrepton/DivIVA induction slows the initial phase of exploration. By 9 days, the strain had spread past the plugs, and onto the surrounding media compartments. For all plates, strains were exploring to the same extent, regardless of the presence of thiostrepton. These data supported our earlier findings that DivIVA activity was important for the initial phase of exploration, but that DivIVA was not required once colonies had progressed into the later, active stages of exploration.

5.3.2 DivIVA does not localize to the majority of tips in exploring cells

Our data thus far could be explained by several models. First, it is possible that DivIVA is involved in the initial phase of exploration, and is dispensable (or only required at low levels) for the later stages of exploration. The DivIVA depletion strain grown without thiostrepton initially grew slowly, leading us to assume that DivIVA is required for the initial phase of exploration, and that the leaky *tipA* promoter ultimately yielded sufficient DivIVA (and colony growth) to transition to later stages of exploration. Secondly, it is possible that DivIVA is required for both the initial and later phase of exploration. In the depletion strain grown without thiostrepton, the leaky promoter could allow for a threshold level of DivIVA to be reached, allowing exploration to rapidly proceed. Finally, DivIVA may be essential for exploration, and suppressor mutations arise in days 1-5, allowing exploration to rapidly proceed. In considering this final possibility, it seems unlikely that another protein could substitute for DivIVA in driving tip growth. A more likely possibility is that a suppressor mutation arose in the integrated plasmid carrying the inducible *divIVA* gene, resulting in higher DivIVA levels. To investigate the possibility of mutations within the *tipA* promoter that led to enhanced DivIVA expression, we amplified and sequenced this DNA from robustly exploring colonies grown in the absence of thiostrepton inducer, and found the sequence to be wild type. However, when we restreaked the depletion strain from MYM or YP without thiostrepton to MYM without thiostrepton, the depletion strain grew well. Therefore, we are considering the possibility that mutations elsewhere in the chromosome are responsible for increased *tipAp* activity and we are currently testing this proposal.

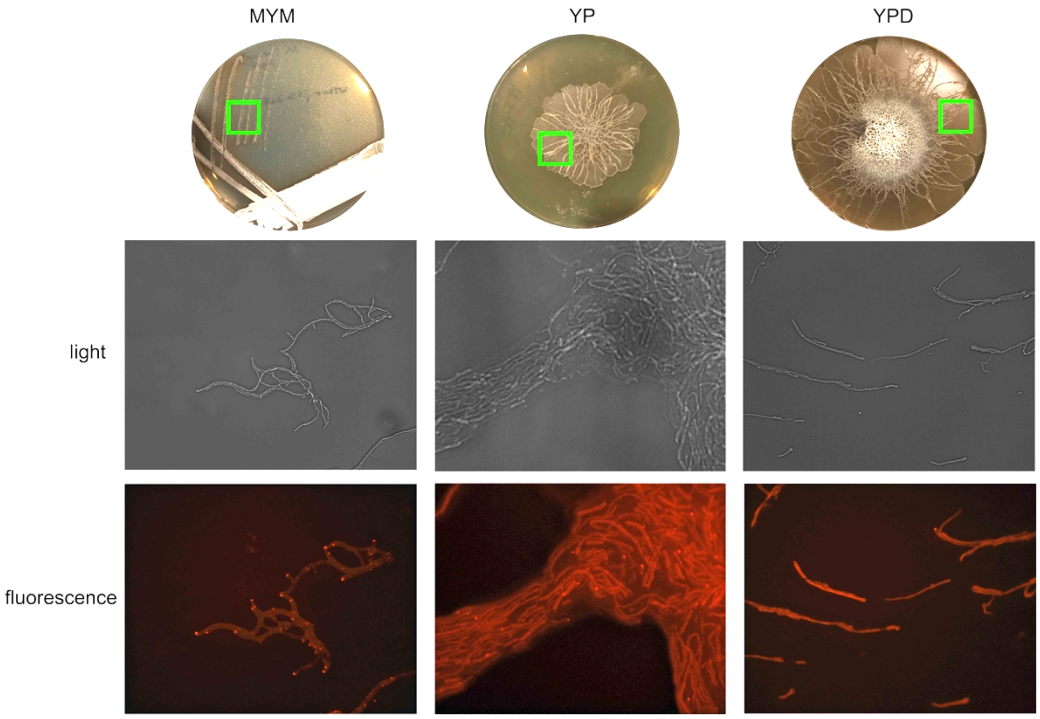

Fig. 5.2 DivIVA localization in explorer cells. Top: *S. venezuelae* containing a DivIVA-mCherry translational fusion grown on MYM (16 hours), YP (10 days), or with *S. cerevisiae* on YPD (14 days). Green boxes show the approximate regions from which the images were taken.

To address the first two models, we examined the localization of a translational DivIVA-mCherry fusion in *S. venezuelae* exploring colonies (**Fig. 5.2**). We examined over ~1000 hyphal tips from various areas of exploring colonies, and found DivIVA was only localized to hyphal tips in 10% of hyphae. In contrast, DivIVA localized to the tips of >90% of classically growing vegetative cells on MYM medium. To further differentiate between the possible models described above, we pulse-labeled *S. venezuelae* growing on MYM and YP with fluorescent D-amino acids (FDAA's) (**Fig. 5.3A**). FDAA's are incorporated into new sites of PG by the D,D-transpeptidation activity of penicillin-binding proteins, permitting the visualization of new sites of cell wall growth (Hsu et al., 2017; Kuru et al., 2012). FDAA's have been developed to have different fluorophores, permitting the visualization of FDAA's at a range of emission wavelengths on the visible spectrum. We tried three different types of FDAA's in our experiments: Rotor (RF470), TADA (TAMRA 3-amino-D-alanine/D-Lysine), and HADA (7-hydroxycoumarin-3-carboxylic acid–D-alanine) (Hsu 2017). Rotor-FDAA's (unpublished) fluoresce only upon incorporation into PG in the cell wall. TADA is a yellow-orange emitting FDAA, and has been shown to be effective in Gram-positive bacteria. HADA is a blue emitting FDAA, and is the most sensitive to prolonged light exposure and has been shown to be effective in Gram-positive and Gram-negative bacteria (Kuru et al., 2017). We visualized cells from the colony edge of *S. venezuelae* growing

vegetatively on MYM (classic growth medium) for 16 hours. As expected, we saw fluorescence at the tips of all hyphae, representing FDAA incorporation and likely sites of new PG synthesis. In contrast, for cells at colony edge of *S. venezuelae* exploring on YP for 12 days, we did not see any FDAA incorporation. We wondered whether colony growth was instead being driven from the colony centre. We flooded a 15-day-old exploring colony with a solution containing FDAA's. Although we saw strong fluorescence in the colony centre, we also saw fluorescence after flooding with a solution containing wheat germ agglutinin (fluorescently binds PG), and with a solution containing L-isomer versions of the fluorescent amino acids. This suggested that the fluorescence observed with FDAA's in the colony centre was likely to be either non-discriminately binding PG in the colony centre, or an artifact stemming from dye accumulation in the colony centre (**Fig. 5.3B**).

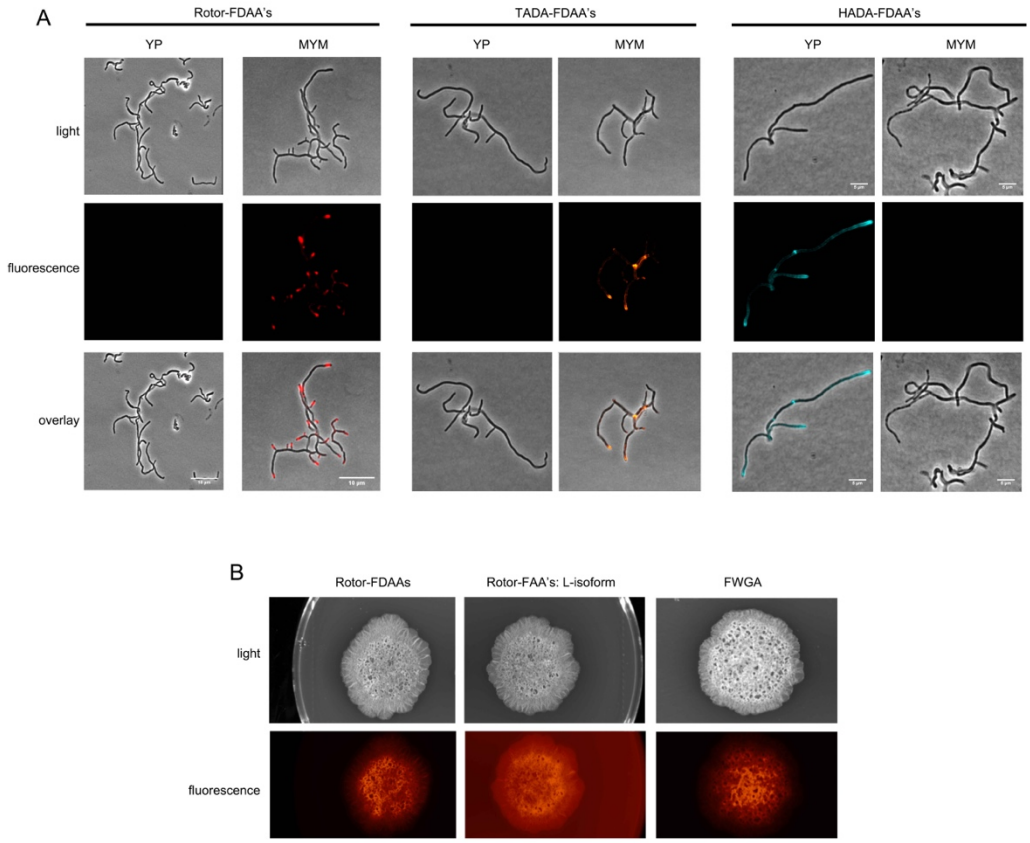

Fig. 5.3 New sites of PG synthesis are not visible at the tips of explorer cells. A. FDAA's fluoresce at sites of new PG synthesis. Three types of FDAA's (Rotor, TADA and HADA) were tested. Colonies were grown on MYM agar for 16 hours or YP agar for 12-15 days. For each type of FDAA, images show the same field of view, visualized with light, fluorescence, or both light and fluorescence images overlaid. **B.** Exploring colonies flooded with solutions indicated at the top. Solutions contained either Rotor-FDAA's, an L-isoform of Rotor-FDAA's, or FWGA (Fluorescent Wheat Germ Agglutinin).

Our translational fusion microscopy experiments revealed that DivIVA did not localize to the tips in the majority of hyphae in exploring colonies. In parallel, our FDAA uptake experiments demonstrated that the majority of hyphae in exploring colonies were not growing by tip extension. Collectively, these data best support the first model described above, where DivIVA was required for the initial phase of exploration, and was dispensable (or only required at low levels) for later stages of exploration.

Growth is not occurring at the colony periphery, and does not appear to be DivIVA-dependent. Where and how are cells growing? A wild type *S. venezuelae* strain constitutively expressing sfGFP or mCherry fluoresced much more brightly in the colony centre than the periphery, suggesting that the colony centre was either more densely populated than the outer regions, or that cells here were more transcriptionally active (**Fig. 5.4A**). Visually, the colony centre appeared very wrinkled and dense, with the number of wrinkles decreasing towards the colony periphery (**Fig. 5.4B**). We hypothesized that DivIVA was required for exploration during this initial phase of colony growth. Once a biomass threshold was achieved, exploration initiated, with the colony edges expanding rapidly outward. In principle, this is similar to sliding motility, where passive surface translocation is powered by growth from the colony centre and is facilitated by the release of compounds that reduce the friction between cells and their surface. To investigate whether sliding motility driven by growth from the centre might contribute to exploration, we compared the growth of colonies with the core excised to normal colonies. We found that removing the colony centre from exploring colonies led to a reduction in colony surface area of ~30% relative to those that retained the core region (**Fig. 5.4C**).

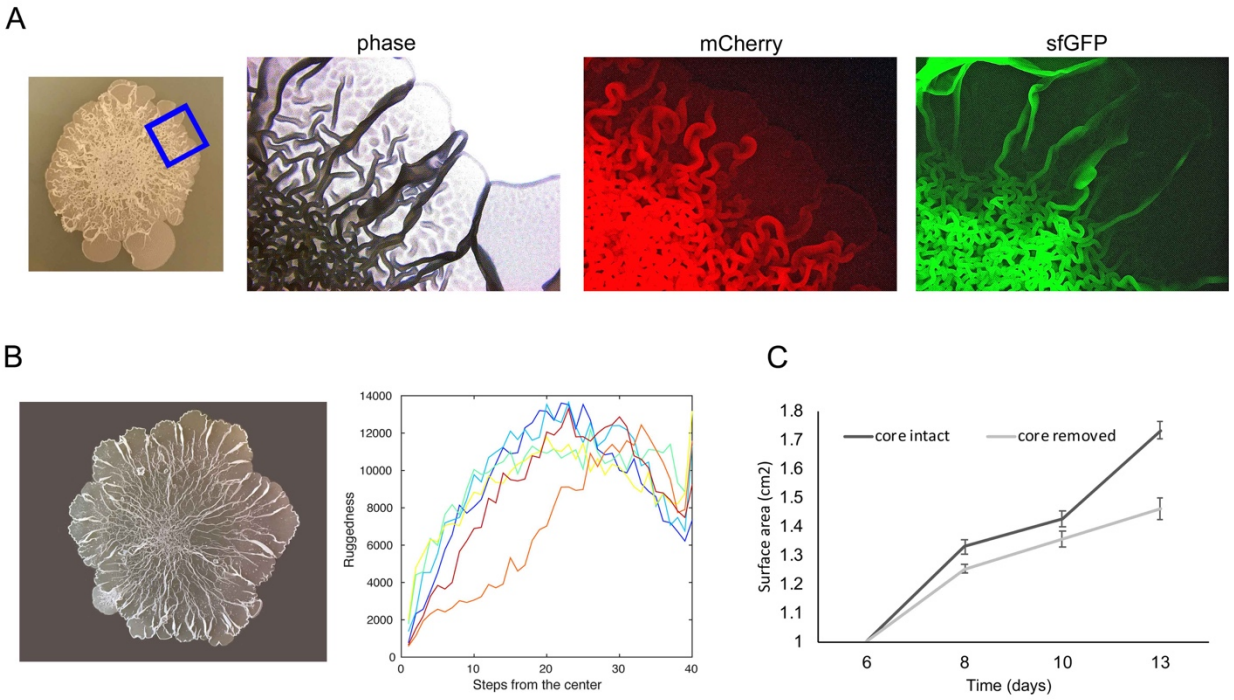

Fig. 5.4 Expression levels and wrinkling patterns throughout exploring colonies. A. Top: representative colony showing approximate region where images to the right were taken from. Strains were grown on YP agar medium for 10 days. Middle eft: a phase contrast image. Middle and right: *S. venezuelae* containing an integrating plasmid carrying the strong constitutive promoter *ermE** driving the expression of *mCherry* (middle) or *sfGFP* (right). **B.** Left: a representative image of a colony used to quantify colony wrinkling. Right: a graph quantifying colony wrinkles. The X axis depicts the distance from the centre of the colony, and the Y axis depicts the degree of wrinkling at each position in the colony. **C.** Two sets of *S. venezuelae* colonies exploring on YP agar medium were grown for 6 days, after which the core was removed from one set. Changes in surface area between the two sets are shown. Values represent the mean ± standard error for four replicates.

5.3.3 *S. venezuelae* encodes four MreB homologs

Our data suggested that after the initiation of exploration, exploration proceeded without DivIVA-mediated tip extension. This raised the question of how colonies rapidly spread over surfaces. While it is possible sliding motility plays a role – as exploration is phenotypically similar to sliding motility reported for other microbes – we wondered whether other growth mechanisms might contribute to exploration. MreB drives lateral wall growth in many rod-shaped bacteria. *Streptomyces* hyphae are up to ~50 times longer than some rod-shaped bacteria, and MreB-mediated lateral wall growth along the length of the hyphae could explain the rapid rate at which exploration proceeds. To probe whether MreB contributed to exploration, we first searched for *S. venezuelae* homologs of the *S. coelicolor mreB*-like genes

(**Fig. 5.5A**). We found *S. venezuelae* possessed equivalent genes to those encoded by *S. coelicolor*: *sven_2228* (homologous to *sco2451/mbl*), *sven_2389* (homologous to *sco2611/mreB*), and *sven_7281* (homologous to *sco6166/mreb-like*). Surprisingly, *S. venezuelae* also encoded a fourth *mreB* homolog: *sven_2393* (also homologous to *sco2611/mreB*, and here called *mreB2*). Of the four *S. venezuelae mreB* homologs, *sven_2393* and *sven_2389* shared the greatest sequence similarity with key MreB homologs in other model species (MreB and MreBH in *B. subtilis*, and MreB in *E. coli*), while *sven_2228* and *sven_7281* appeared to encode more distant MreB homologs.

5.3.4 *mreB* genes are expressed in exploring colonies

We previously performed RNA sequencing (RNA-seq) experiments on exploring cultures (grown beside *S. cerevisiae* on YPD) and static cultures (grown alone on YPD). We analyzed the normalized expression profiles of the four *mreB* homologs in our RNA-seq data (**Fig. 5.5B**). *sven_2228/mbl* was not expressed in exploring or static cultures, while both the *sven_2389-87/mreBCD* operon and *sven_2389/mreB2* were expressed in both cultures, but not significantly differentially expressed. Of the four genes, only *sven_7281/mreb-like* was significantly differentially expressed (~3× higher in exploring cultures versus static cultures).

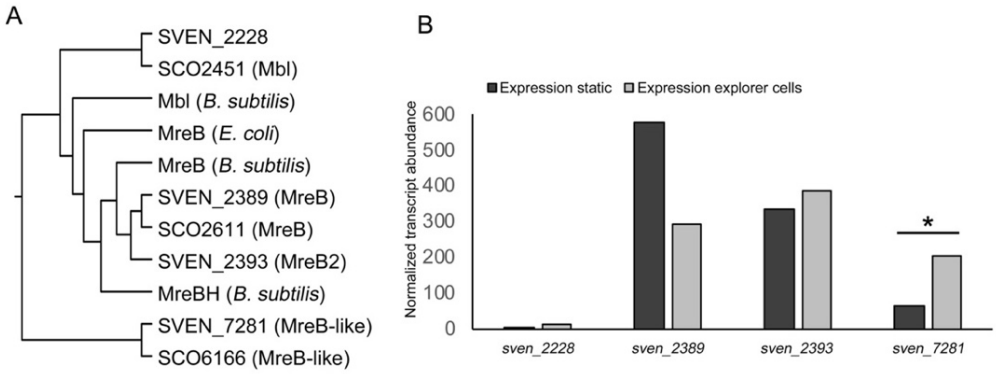

Fig. 5.5 *mreB* homologs and expression levels in *S. venezuelae*. A. Phylogeny of MreB protein sequences from *S. venezuelae* (SVEN), *S. coelicolor* (SCO), *B. subtilis* and *E. coli*. *S. venezuelae* encodes an additional MreB homolog (here called MreB2). **B.** Normalized transcript abundance levels of the four *S. venezuelae mreB* homologs in static (*S. venezuelae* alone on YPD medium) and exploring (*S. venezuelae* beside *S. cerevisiae* on YPD medium) cultures. Data show the average of two replicates per condition. The asterisk indicates significant differential expression (p <0.05). Note: for *sven_2389,* despite the different in transcript abundance levels shown here, there were drastic differences between replicates, and the difference between static and exploring cultures was not statistically significant.

5.3.5 MreB perturbation affects exploration

To examine whether any of the MreB proteins was involved in exploratory growth, tested the effects of the small molecule A22 (S-(3,4-dichlorobenzyl) isothiourea), which is a potent MreB inhibitor (Bean et al., 2009). We grew *S. venezuelae* on MYM or YP agar medium supplemented with increasing concentrations of A22, and found *S. venezuelae* survived better on MYM than YP with high A22 concentrations (**Fig. 5.6A**). This suggested that the MreB-inhibitory effects of A22 were YP- and/or exploration-specific. We also grew *S. venezuelae* on MYM or YP agar medium with and without an intermediate concentration of A22, and compared the surface areas of colonies (**Fig. 5.6B**). On MYM, A22 reduced the surface area of colonies by ~5% on average. In contrast, on YP, A22 reduced the surface area of colonies by nearly 50%, further supporting the conclusion that MreB inhibition is profoundly detrimental to cells exploring on YP medium.

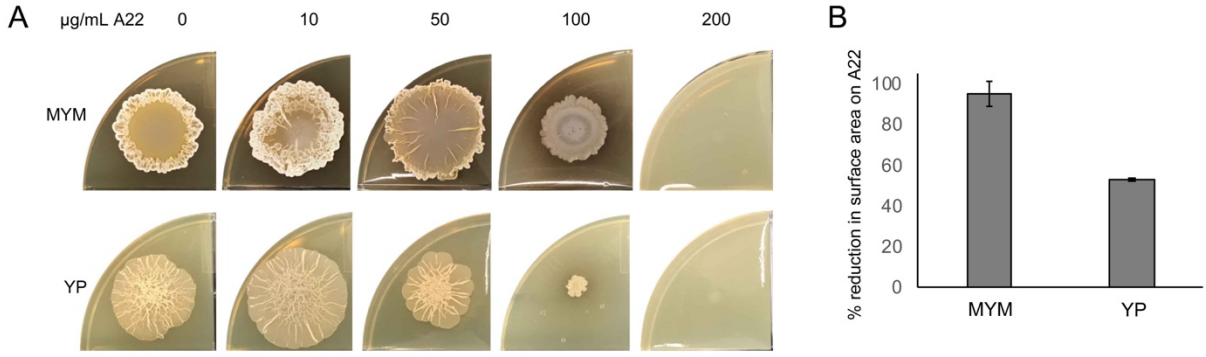

Fig. 5.6 A22 perturbation impacts exploration more than classic development. A. *S. venezuelae* grown on classic growth medium (MYM, top) or exploration medium (YP, bottom) with the indicated concentration of the MreB inhibitor A22. Plates were grown for 6 days. B. Colonies were grown on MYM or YP agar medium with an intermediate concentration of A22 (50 µg/mL) for 9 days. For each media type, the percent reduction in surface area on 50 µg/mL A22 compared to 0 µg/mL A22 is shown. At this concentration of A22, colonies on MYM were unaffected by A22, whereas colonies on YP were dramatically impacted. Values shown are the average of three replicates, and bars denote the standard error.

5.3.6 MreB is required for exploration

In *S. coelicolor*, *mreB-like* is only expressed in vegetative hyphae, although its deletion does not impact vegetative growth. In contrast, *mreB* and *mbl* are lowly expressed in *S. coelicolor* vegetative hyphae, and are highly expressed in aerial hyphae and spores where they are required for spore maturation (Heichlinger et al., 2011). As *S. venezuelae* exploring cells appeared to be vegetative-type cells, and *sven_7281* (*mreB-like*) was significantly upregulated

in exploring versus static cultures, we first investigated the role of this gene in exploration. We replaced *sven_7281* with an apramycin resistance cassette, and examined the growth of the resulting mutant strain on classic growth medium (MYM) and exploration medium (YP, and YPD with *S. cerevisiae*), compared with wild type (**Fig. 5.7**). We found the Δ*sven_7281* deletion strain was indistinguishable from wild type on all media types.

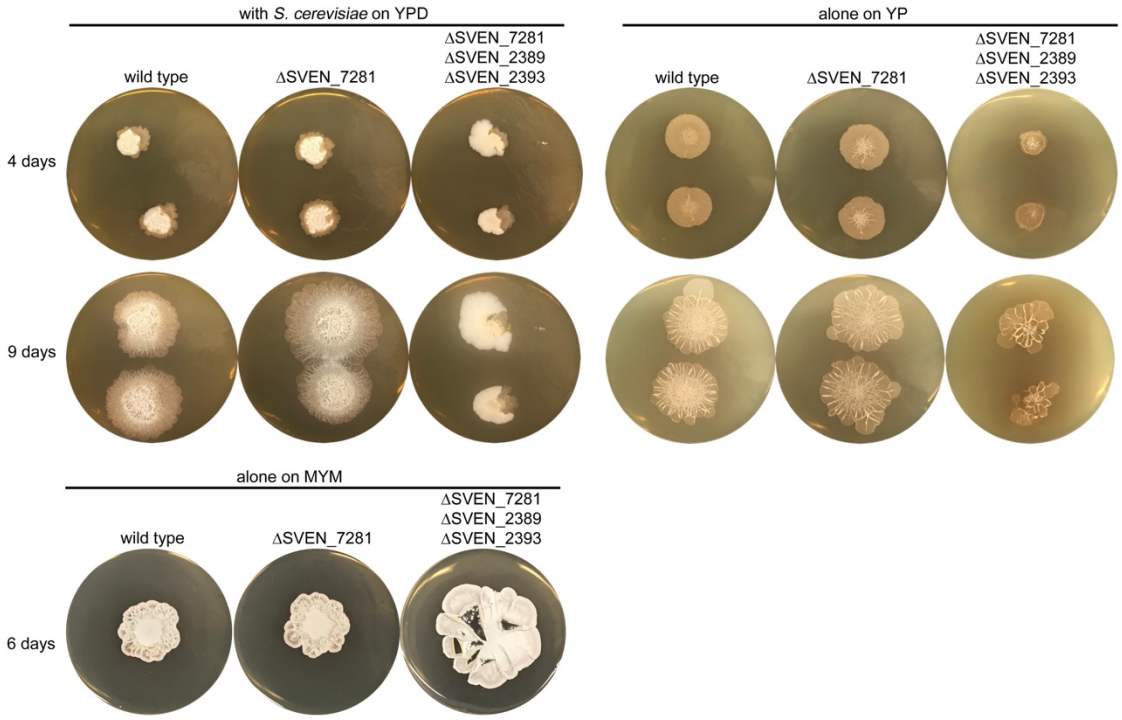

Fig. 5.7 MreB deletion phenotypes. Wild type, Δ*SVEN_7281* and a triple *mreB* mutant strain were grown under exploration-permissive conditions, either beside *S. cerevisiae* on YPD (left) or alone on YP (right), or on MYM medium supporting classic growth (bottom).

While Gram-negative rod-shaped bacteria require a single MreB homolog for growth, many Gram-positive bacteria encode three MreB homologs that have some functional redundancy. In *B. subtilis*, these three MreB isoforms display partial functional redundancy under different stress conditions (Kawai et al., 2009). Strains lacking one of *mreB*, *mbl* or *mreBH* maintain their rod-shape, while strains lacking all three homologs grow as bulging spheres (Strahl et al., 2014). Given that our Δ*sven_7281* strain grew in the same way as wild type, we were interested in testing whether *S. venezuelae* MreB homologs shared similar functional redundancy. Of the remaining three *mreB* homologs encoded by *S. venezuelae*, only *sven_2389* (*mreB*) and *sven_2393* (*mreB2*) were expressed by exploring cells in our RNA-seq data. We created a triple *mreB* mutant by replacing *sven_2389* with a viomycin resistance cassette and replacing *sven_2393* with an 81 bp "scar" sequence in the Δ*sven_7281* mutant background. We grew the resulting Δ*sven_2389*Δ*sven_2393*Δ*sven_7281* triple mutant strain on MYM, YPD with *S. cerevisiae*, and YP agar media (**Fig. 5.7**). On MYM, the triple mutant colony sporulated in the same way as wild type, but appeared to be partially peeling off the agar. Given *S. coelicolor* homologs have known roles in spore wall thickening, we assumed the *S. venezuelae* mutant

phenotype on MYM might stem from defective sporulation. On YPD with *S. cerevisiae*, the triple mutant strain was unable to form aerial hyphae or sporulate over *S. cerevisiae*, and was unable to explore. On YP, the surface area of the triple mutant was similar to wild type after 4 days of growth. However, upon further incubation, the triple mutant did not continue to explore: by 9 days, the surface area of the triple mutant was significantly reduced compared to wild type. This indicated MreB homologs were essential for normal *S. venezuelae* exploration.

5.3.6 MreB and DivIVA have different transcription profiles

Our data suggested that DivIVA was important in the early stages of exploration, while MreB homologs appears to be more critical at later phases. To assess the timing of expression for each of these genes, we created transcriptional reporters by cloning the promoter region of each gene upstream of a β-glucuronidase-encoding reporter gene (Myronovskyi et al., 2011). With this system, promoter activity drives β-glucuronidase expression, and the resulting enzyme cleaves a colourimetric substrate (here called "X-gluc"), leading to blue colouration. Although the substrate is typically incorporated directly into growth medium, we have found exploring *S. venezuelae* is unable to take up X-gluc from the medium (unpublished). To get around this issue, we instead flooded colonies with an X-gluc-containing solution at specific time points, and then captured colony images 5 hours after flooding (**Fig. 5.8**). As a positive control, we used the constitutively expressed, strong *ermE** promoter, and found it was turned on within 24 hours of growth, with expression levels remaining high throughout the experiment. As expected, the negative control (promoterless reporter)-containing strain showed no expression throughout the assay. The four *mreB* reporters (bearing the promoters of *sven_2228, sven_2389, sven_2393* and *sven_7281*) were all active after 48 hours of growth, with expression peaking at day 6 before declining. While the timing of promoter activity for each gene appeared to be coordinated, the levels to which they were expressed differed: *sven_2389* and *sven_2393* were expressed more highly than *sven_2228* and *sven_7281*. In comparison, the *divIVA* reporter was turned on earlier than the *mreB* reporters, with expression intiating after 24 hours. After 9 days, the *divIVA* expression levels were equivalent to those of *sven_2389, sven_2393* and *sven_7281*. Combined with our earlier findings that *divIVA* depletion has the biggest impact on the early stages of exploration, while *mreB* deletions more severely impacted the later stages of exploration, these data supported the hypothesis that *divIVA* and *mreB* collectively drive *Streptomyces* exploratory growth, where each are required, but alone are not sufficient to promote effective exploration.

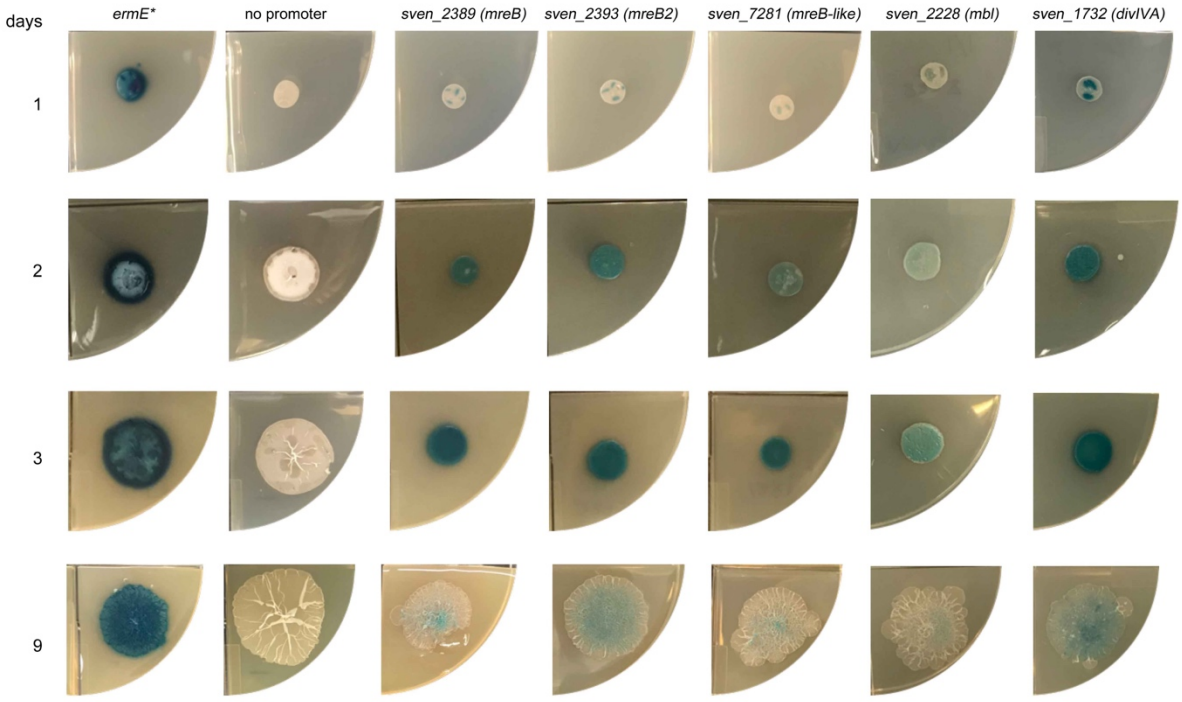

Fig. 5.8 Transcription reporter assays for *mreB* homologs and *divIVA* under exploration conditions. Wild type *S. venezuelae* containing a construct with a β-glucuronidase enzyme driven by the indicated promoter. Plates were grown for the indicated number of days before being flooded with X-gluc, which turns blue upon cleavage by β-glucuronidase. Following overlay, plates were incubated for an additional 5 hours before imaging. The two left columns show controls: the constitutively expressed, strong *ermE** promoter, and a promoter-less construct.

5.4 Discussion

A number of elegant studies have shown that *Streptomyces* grows exclusively by tip extension, through a process governed by DivIVA and other members of the polarisome complex (McCormick and Flärdh, 2012). Our work here reveals that *Streptomyces* exploration requires not only canonical growth mechanisms mediated by DivIVA, but also a novel mode of growth directed by MreB proteins. In the initial phase of exploration, when the colony is growing as a dense, wrinkled group of cells, DivIVA depletion dramatically slowed colony growth. Deleting the three *mreB* homologs expressed in explorer cells did not impact growth initially. In the later stages of exploration, when the colony starts flattening and rapidly expanding outwards, the DivIVA and MreB requirements were reversed. DivIVA depletion had little effect on exploration, and DivIVA localization or new PG synthesis at the hyphal tips was rarely detected. In contrast, the triple *mreB* deletion strain was unable to explore. Collectively, our findings suggest that

Streptomyces exploration may proceed using an unprecedented growth-switching mechanism, whereby DivIVA and MreB drive distinct phases of exploration.

5.4.1 MreB conservation in the streptomycetes

Within the actinomycetes, MreB homologs have only been identified in *Streptomyces* – the genus that produces aerial hyphae and spores. BLASTp searches confirmed other actinomycetes lack MreB. Previous work identified a role for MreB homologs in *Streptomyces* spore wall thickening, which led to the assumption that this ancestral protein was conserved in the streptomycetes for the purpose of spore maturation. However, other sporulating actinomycetes, including *Micromonospora* and *Actinoplanes*, lack MreB, raising the possibility that MreB has been maintained in the streptomycetes for other reasons. Our work here suggests MreB may also have been maintained in the *Streptomyces* genome to facilitate exploration – a form of growth that allows cells to rapidly traverse surfaces and scavenge for nutrients. Ten percent of tested *Streptomyces* species have demonstrated exploration capabilities, and these species do not form a monophyletic group, indicating that exploration is a widespread phenomenon. *S. venezuelae* encodes an additional MreB homolog (*sven_2393*), and of the other streptomycete genomes available on the *Streptomyces* database StrepDB, it appears only one of 15 other species encode this additional homolog. It will be interesting to determine whether this additional homolog is unique to exploring *Streptomyces* species.

5.4.2 The duality of DivIVA and MreB in cell wall expansion and exploration

Our findings have suggested that DivIVA is required for the initiation of exploration, while MreB is needed for the rapid growth/expansion of exploring colonies. How are these two growth mechanisms coordinated? It is possible the activity of these systems are controlled at the transcriptional level, whereby *divIVA* is expressed first, after which some signal leads to the concomitant activation of *mreB* expression and repression of *divIVA* expression. Our transcriptional reporter assays provide some support for this idea, in that *divIVA* expression was turned on before that of the *mreB* homologs; however, expression levels of *divIVA* and several of the *mreB* genes does not differ dramatically after the first day. Our phenotypic assays suggested that DivIVA was required in the initial 4-5 days, with MreB homologs not being required until day 5, despite them being transcribed much earlier. Whether the MreB proteins have a yet-to-be determined role earlier in exploration, or whether there is some post-transcriptional level of regulation governing the translation or activity of the MreB proteins remains to be seen. Future investigations aimed at understanding the post-transcriptional/post-translational regulation of these genes/proteins, and any associated regulatory partners (*e.g.* AfsK for DivIVA) will be needed to fully understand the regulatory controls governing their expression and activity.

Other bacteria encode both DivIVA and MreB, and perhaps the mechanisms of cooperation between these two proteins in other species could guide our understanding of how they cooperate in *S. venezuelae* explorer cells. In the rod-shaped bacterium *B. subtilis,* DivIVA localizes to cell poles and recruits effectors involved in regulating division, sporulation and

chromosome anchoring to the poles (Edwards and Errington, 1997; Edwards et al., 2000; Lenarcic et al., 2009; Ramamurthi et al., 2009), while the three MreB proteins drive lateral cell wall synthesis. It is thought that the polar localization of DivIVA is achieved by recognition of negatively curved membranes at the polar caps. Consistent with this hypothesis, heterologously expressed DivIVA in the Gram-negative rod-shaped bacterium *E. coli* localizes to the poles of cells, even though this bacterium does not encode DivIVA (Bergé and Viollier, 2017). Thus, it appears that DivIVA localizes to the poles of *B. subtilis*, while MreB drives lateral wall growth. It is possible that in explorer cells, DivIVA still weakly localizes to the poles, while MreB drives cell wall growth along the length of filaments.

It is also possible that DivIVA in explorer cells takes on a function entirely separate from its role in the canonical *Streptomyces* life cycle. The rod-shaped actinomycete *Corynebacterium glutamicum* grows by DivIVA-mediated polar growth, and depleting DivIVA leads to a coccoid morphology. Rod-shaped morphology could be restored upon introducing DivIVA from other Actinobacteria, but interestingly not when introducing DivIVA from Firmicutes (e.g. *B. subtilis* or *Streptococcus pneumoniae*) (Letek et al., 2008). Additionally, DivIVA from the Firmicutes accumulated at septation sites and interfered with cell division, while DivIVA from the Actinobacteria localized to the poles and drove polar growth in the same way as DivIVA from *C. glutamicum*. These results suggested DivIVA functions differently in these two phyla of Gram-positive bacteria (Letek et al., 2008). It is possible that in exploring colonies, DivIVA functions more similarly to DivIVA from the Firmicutes, by organizing chromosome dynamics. Indeed, there are links between chromosome segregation and tip-associated proteins in *Streptomyces*. The proteins ParA and ParB direct chromosome segregation, and ParA interacts with Scy in the polarisome (Ditkowski et al., 2013; Holmes et al., 2013). Perhaps DivIVA is required to facilitate chromosome replicate and partitioning throughout the long vegetatative hyphae in exploring colonies.

5.4.3 Analysis of our experiments and future directions

Further experimentation is required to address our hypotheses and explain some of our data. In the FDAA uptake experiments, we do not see FDAA incorporation at the majority of hyphal tips. While we take this to mean hyphal tip extension does not drive exploration, if MreB drives exploration, we would expect to see FDAA incorporation along the lateral walls of cells. In FDAA experiments using other rod-shaped microbes, there is typically visible fluorescence along the lateral walls. One explanation is that these microbes are typically 1-3 µM in length, while a *Streptomyces* hyphal filament can be up to 50 µM in length. We used the same concentration of FDAA as is typically used for other microbes, and it is possible the FDAA concentration was simply too low to see appreciable fluorescence in the lateral walls. Additionally, exploring colonies significantly raise the pH of growth medium (from pH. 7.0 to 9.5), and it is not currently known whether FDAA's are destabilized or otherwise impacted by alkaline conditions.

From the DivIVA depletion experiments, we raised several possibilities to explain why the depletion strain was initially very slow growing, before expanding to explore in the same way as wild type. One possible explanation was that suppressor mutations either permitted DivIVA

activity or circumvented the need for DivVIA in facilitating rapid exploratory growth. Although subsequent experiments have ultimately supported our model that DivIVA is only critical during the initial stages of exploration, it will be important to more definitely exclude the possibility of suppressors. We have performed preliminary western blots using antibiotics specific for DivIVA, to determine the levels of DivIVA in the depletion strain. Conditions for these immunoblots are still being optimized at this time. We expect that if we grow the depletion strain without induction and suppressors allow for DivIVA expression by day 4-5, we will see high protein levels after this time. If there are no suppressors of DivIVA expression levels, then we would expect to see low level DivIVA throughout all stages of exploration. Additionally, we may need to sequence the genomes of strains with potential suppressors mutations to determing whether another protein is functioning in place of DivIVA. For the DivIVA fluorescence microscopy experiments, we saw tip-associated fluorescence for the majority of cells growing on MYM, but only for a minority of those cells exploring on YP. An important control will be to test DivIVA localization during growth in liquid MYM and YP, as this will allow us to determine whether these differences in localization are media-specific, or exploration versus classical growth-specific.

After elucidating the roles of DivIVA, it will be important to establish a mechanistic understanding of how MreB contributes to exploration. At the cellular level, we are working to create MreB-fluorescent protein translational fusions. Previous studies in *S. coelicolor* employed C-terminal MreB translational fusions; however, work in other species has since shown MreB terminal fusions can impact MreB localization, and are not fully functional (Salje et al., 2011). In the hopes of circumventing these issues, we will create a 'sandwich' fusion, in which a fluorescent protein-encoding gene is cloned within a poorly conserved region in the *mreB* genes. Additionally, it will be important to gain more information about the relative transcriptional activity of the *mreB* homologs and *divIVA*. We note that our pGUS transcriptional reporters showed blue specks throughout all colonies. We are not sure whether these are biologically meaningful, but it is possible there is localized, stochastic expression in some colony regions. Another option would be to create transcriptional promoter reporters with a fluorescent protein, and follow fluorescence throughout colony growth; this would provide additional spatial (three dimensional) information on the transcription of these genes. Finally, we are working to determine which MreB homologs contribute to exploration by complementing the triple MreB mutant with the individual genes.

5.5 Materials and Methods

5.5.1 Strains, plasmids, media and culture conditions

Strains, plasmids and primers used in this study are listed in **Table 5.1** and **Table 5.2.** *S. venezuelae* ATCC 10712 was grown on MYM (maltose, yeast extract, malt extract) agar for examining the behavior of classically developing colonies. Exploration was investigated by growing *S. venezuelae* alone on YP (yeast extract, peptone) agar or with *S. cerevisiae* on YPD (YP plus dextrose/glucose) agar. For experiments with the small molecule A22, plates were supplemented with the indicated concentration of A22 (0-200 μg/mL) purchased from Sigma

(SML0471). All strains were grown at 30˚C. Prior to inoculation on plates, *S. venezuelae* was grown overnight in liquid MYM at 30˚C, after which 5 µL were spotted to agar plates. Agar plates were incubated for up to 14 days. Colony surface areas were measured using ImageJ (Abràmoff et al., 2004). For experiments with the *divIVA* depletion strain, the strain was grown overnight in MYM liquid medium supplemented with 50 µg/mL thiostrepton, after which 5 µL were spotted onto agar medium. For *divIVA* induction, the strain was grown on agar medium with 0, 12.5, or 50 µg/mL thiostrepton. For *S. venezuelae* strains constitutively expressing sfGFP and mCherry, the fluorescent proteins were cloned into the hygromycin-resistant, integrating *Streptomyces* vector pIJ82 downstream of the constitute *ermE** promoter. For transcriptional reporter assays of the four *mreB* homologs and *divIVA*, the promoter region of each gene was cloned into the pGUS plasmid (Myronovskyi et al., 2011). using the restriction sites KpnI and XbaI. The *ermE** promoter was also cloned into the pGUS plasmid using XbaI sites.

5.5.2 Construction of depletion and deletion strains

To create a *divIVA*-inducible construct, the thiostrepton resistance gene *tsr* and the *tipAp* promoter were cloned into were cloned into the integrating hygromycin-resistant *Streptomyces* vector pIJ6902 (Huang et al., 2005), along with a gene encoding the activator of *tipAp*, *tipA*. The *divIVA* gene and its downstream terminator were then cloned into the vector. This construct was then introduced into wild type *S. venezuelae*. In-frame deletions of *sven_1732* (*divIVA)* sven*_7281* (*mreB-like*), *sven_2389* (*mreB*), and *sven_2393* (*mreB2*) were generated using ReDirect technology (Gust et al., 2003). For *sven_1732* and *sven_7281*, the coding sequences (from start to stop codon) were replaced with an *ori*T-containing apramycin resistance cassette. For *sven_2389,* the coding sequence was replaced with an *ori*T-containing viomycin resistance cassette. For *sven_2393*, the gene was initially deleted from a cosmid by replacement with an apramycin resistance cassette. The cassette was flanked by FRT sites, and was excised using FLP-mediated excision, leaving behind an 81 bp "scar" sequence (Gust et al., 2003). Mutant cosmids were introduced into the non-methylating *E. coli* strain ET12567/pUZ8002 prior to conjugation into wild type *S. venezuelae*. For the triple mutant, the Δ*sven_2389:*viomycin + Δ*sven_2393:*scar cosmid was introduced into the *sven_7281:*apramycin strain. Resulting exconjugants were screened for double-crossover recombinants. Correct replacement of *sven_7281*, *sven_2389*, and *sven_2393* were each confirmed using diagnostic PCRs (**Table 5.2**).

5.5.3 Light, fluorescence and scanning electron microscopy

Samples for light and fluorescence microscopy were obtained by growing *S. venezuelae* on MYM, YP or YPD agar for 1-14 days. For experiments with the *divIVA-mcherry* translational fusion (Schlimpert et al., 2016) cloned into pIJ10752, all images were obtained using the EVOS FL Auto Imaging System (Thermo Fischer Scientific) oil immersion objective (magnification ×100). When visualizing mCherry, we adjusted excitation levels to ensure controls strains (wild type *S. venezuelae* without pIJ10752) were not demonstrating detectable mCherry signals. For experiments using wild type *S. venezuelae* with constitutively expressed sfGFP or mCherry, images were obtained using a Leica dissecting microscope. Samples for scanning electron

microscopy (SEM) were grown on YP agar medium for 10 days. Strains were prepared and visualized using a TEMSCAN LSU scanning electron microscope as previously described (Haiser et al., 2009)

5.5.4 Fluorescence D-amino acid uptake experiments

Wild type *S. venezuelae* was grown on MYM agar medium for 12 hours or YP agar medium for up to 15 days. After incubation, 100 µL PBS solution (pH 7.4) containing 0.5 mM FDAA stock solution was added to the edge of each colony. Colonies were then incubated for 15 min at 30˚C, before being scraped into fresh PBS and gently resuspended. Cells were then covered with a PBS agar pad, and imaged using a Nikon Ti-E microscope (experiments with HADA or TADA FDAA's) or a BioRAD microscope (experiments with RF470 FDAA's, L-isomers and fluorescent wheat germ agglutinin).

5.5.5 Phylogenetic analyses

MreB protein sequences were aligned using ClustalW with default parameters and a BLOSUM matrix. Results were visualized as a rooted phylogenetic tree, with an unweighted pair group method with arithmetic mean clustering.

5.5.6 Transcriptional reporter assays

S. venezuelae strains containing pGUS-promoter constructs were grown overnight in MYM liquid medium, after which 5 µL were spotted to YP agar medium in 4-quadrant petri plates. Eight to ten replicates of each strain were spotted at a time, and plates were incubated for specific intervals. Colonies were flooded with 50 µL N,N-dimethylformamide solution containing 40 mg/mL X-gluc (5-bromo-4-chloro-3-indolyl-ß-D-glucoronic acid, BioShop). After flooding, plates were incubated for an additional 5 hours at 30˚C before imaging.

5.5.7 Colony wrinkling experiments

For analyses of colony ruggedness, the centre of each colony was marked, and 40 circumferential contours were drawn at regular intervals from the colony centre to the periphery. The distance between contours was plotted as steps from the colony centre. Pixels containing wrinkles were plotted and measured, and graphed as a function of steps from the colony centre. For core removal experiments, two sets of *S. venezuelae* were grown on YP agar medium, with four replicates per set. After 6 days incubation, the core was excised from one set using a sterile razor. The surface area of colonies for both sets was measured at intervals until day 13.

5.6 Tables

Table 5.1 Strains and constructs used in this study

Strain	Genotype, description, or use	Reference or source
Streptomyces venezuelae		
ATTC 10712		Gift from M. Buttner
	ATTC 10712 Δ*sven_2389::[vph-oriT]*	This work
	ATTC 10712 Δ*sven_2393::scar*	This work
	ATTC 10712 Δ*sven_7281::[aac(3)IV-oriT]*	This work
	ATTC 10712 Δ*sven_7281::[aac(3)IV-oriT]*	This work
Escherichia coli		
DH5α	Plasmid construction and general subcloning	Invitrogen
ET12567/pUZ8002	Generation of methylation-free plasmid DNA and conjugation into *Streptomyces*	(MacNeil et al., 1992; Paget et al., 1999)
BW25113/pIJ790	Construction of cosmid-based knockouts	(Gust et al., 2003)
Plasmids or cosmids		
4G01	*S. venezuelae* cosmid carrying *sven_1732*	Gift from M. Bibb and M. Buttner
6F06	*S. venezuelae* cosmid carrying *sven_2389* and *SVEN_2393*	Gift from M. Bibb and M. Buttner
3LI4	*S. venezuelae* cosmid carrying *sven_7281*	Gift from M. Bibb and M. Buttner
pIJ790	Temperature-sensitive plasmid carrying λ-RED genes	(Gust et al., 2003)
pIJ773	Plasmid carrying the apramycin knockout cassette	(Gust et al., 2003)
pIJ82	Integrating plasmid vector; complementation of mutant strains	Gift from H. Kieser
pSET152	Integrating plasmid vector	(Bierman et al., 1992)
pIJ6902	cloning plasmid containing the thiostrepton-inducible *tipA* promoter (*tipAp*), modified to include the *tipA* gene	(Huang et al., 2005)
pIJ10752	Plasmid carrying a *divIVA-mCherry* N-terminal translational fusion, based on pSET152	Gift from S. Schlimpert

pGUS	Plasmid carrying β-glucuronidase enzyme	(Myronovskyi et al., 2011)

Table 5.2. Oligonucleotides used in this study

Name	Sequence (5' to 3')	Use
SVEN1732 Up	ATATGGATCCGTCTTGCCGACTGCCGACG	Confirmation of Δ*1732* mutation
SVEN1732 Down	ATATGGATCCGCGAAGTGGGTGGCAGCTGG	Confirmation of Δ*1732* mutation; creation of inducible *divIVA* construct
SVEN1732 In	GACCGGCGGTCCGGATATGG	Confirmation of Δ*1732* mutation
SVEN1732Fwd	GCCGACTGCCGACGACTACGTAGAGGTGAAG AAGAGATGATTCCGGGGATCCGTCGACC	Creation of Δ*1732* strain; confirmation of Δ*1732* mutation
SVEN1732Rev	CCGACGGCTACGCGCTCAGCGCGCGAGCGCCC GCCGTCATGTAGGCTGGAGCTGCTTC	Creation of Δ*1732* strain; confirmation of Δ*1732* mutation
SVEN1732 IndUP	ATATCATATGCCGCTGACCCCCGAGGACG	Creation of inducible *divIVA* construct
TipAF	ATATAGATCTCTGACCGAGGTGGTTCCTCC	Creation of inducible *divIVA* construct
TipAR	ATACAGATCTGTCTCACCAAGACGCTGGTCG	Creation of inducible *divIVA* construct
DivIVAR-X	ATATTCTAGACGAGGAAGGCATCGACCTCG	Creation of pGUS:*divIVA* promoter construct
SVEN2389 Up	AGGCATATGAACGCCGATCC	Confirmation of Δ*2389* mutation
SVEN2389 Down	ATGTCCACCGTGATCAGTGC	Confirmation of Δ*2389* mutation
SVEN2389 In	ATCATCTTCTTCGCCTCCGC	Confirmation of Δ*2389* mutation
SVEN2389Fwd	GCACCACTCTCAGCCATGGGAAACAAGGGGAA CTCTATGATTCCGGGGATCCGTCGACC	Creation of Δ*2389* strain; confirmation of Δ*2389* mutation
SVEN2389Rev	GTGCGGTTGTTCTCTCGTGGGGCCGTACGGGT GGTGCTATGTAGGCTGGAGCTGCTTC	Creation of Δ*2389* strain; confirmation of Δ*2389* mutation
2389F-X	ATATTCTAGATTCCCGGGTCTCGTCTGAGC	Creation of pGUS:*2389* promoter construct
2389R-K	ATATGGTACCGCCGGTGTTGGTGTTGATGG	Creation of pGUS:*2389* promoter construct
2228F-X	ATATTCTAGAGCCGTGATTCTCCCGCTTCG	Creation of pGUS:*2228* promoter construct
2228R-K	ATATGGTACCCTCCGGTACGGGTGTTGACG	Creation of pGUS:*2228* promoter construct
SVEN2393 Up	ACCCCATTCGGGACTTTCGG	Confirmation of Δ*2393* mutation
SVEN2393 Down	CGATCTGCGGATCGAGGTGC	Confirmation of Δ*2393* mutation

SVEN2393 In	ACACGACCATCCGGGTACG	Confirmation of Δ*2393* mutation
SVEN2393Fwd	ACCGTCCGCCGTACCGTCCCGGCAAACTTGGC GATCATGATTCCGGGGATCCGTCGACC	Creation of Δ*2393* strain; confirmation of Δ*2393* mutation
SVEN2393Rev	TGACGGCGCTGCTGCCGACGGGGCTCCCGAG GTAGTTCATGTAGGCTGGAGCTGCTTC	Creation of Δ*2393* strain; confirmation of Δ*2393* mutation
2393F-X	ATATTCTAGAGGGTCTCGGTCTGTCTCGGC	Creation of pGUS:*2393* promoter construct
2393R-K	ATATGGTACCTCGTAGTCGCTGATCACACC	Creation of pGUS:*2393* promoter construct
SVEN7281 Up	ATATGGATCCGGCGACCTCACATCAGTACC	Confirmation of Δ*7281* mutation
SVEN7281 Down	ATATGGATCCTGCACGTCATCGGTGACTGG	Confirmation of Δ*7281* mutation
SVEN7281 In	GAGCTGGGAGTCCGTGTCGG	Confirmation of Δ*7281* mutation
SVEN7281Fwd	CGTATTCAGCGGGTCCGCAGGGAATGGACGG AAGCGATGATTCCGGGGATCCGTCGACC	Creation of Δ*7281* strain; Confirmation of Δ*7281* mutation
SVEN7281Rev	ACGGCTGACGGGCGGCCGGCTGACGGGCGGC CCCGGTCATGTAGGCTGGAGCTGCTTC	Creation of Δ*7281* strain; Confirmation of Δ*7281* mutation
7281F-X	ATATTCTAGAGGCGACCTCACATCAGTACC	Creation of pGUS:*7281* promoter construct
7281R-K	ATATGGTACCGAGCTGGGAGTCCGTGTCGG	Creation of pGUS:*7281* promoter construct
GUSAR2	TCGATACCGCAGTTCTCC	pGUS sequencing primer
FluorF	ATATGGATCCAGAAGGGAGCAATCATGTCCAA GGGCGAGGAGC	Creation of pIJ82:*ermE**:*sfGFP* construct
FluorR	ATATGGATCCTCACTTGTACAGCTCGTCC	Creation of pIJ82:*ermE**:*sfGFP* construct and pIJ82:*ermE**:*mCherry* construct
FluorFNew	ATATGGATCCAGAAGGGAGCAATCATGGTCTC CAAGGGCGAGG	Creation of pIJ82:*ermE**:*mCherry* construct

CHAPTER 6: GENERAL DISCUSSION AND FUTURE DIRECTIONS

6.1 RNA metabolism in *Streptomyces*

6.1.1 Summary of research – RNA metabolism

RNA processing and degradation are key components of regulation in bacteria. RNA molecules are cleaved by RNases, with *Streptomyces* species encoding a unique combination of RNases. We investigated the roles of RNase III and RNase J in rRNA metabolism in *S. venezuelae*. We found both enzymes were required for normal *S. venezuelae* development and antibiotic production. We found that these RNases were required for normal ribosome assembly, and showed RNase III was involved in rRNA processing. The loss of either RNase led to the formation of translationally inactive ribosome dimers, and sensitized mutant strains to ribosome-targeting antibiotics. We propose that the roles of these RNases in rRNA maturation and ribosome assembly are critical for the translation of large, multicistronic transcripts characteristic of antibiotic clusters (Chapter 2).

6.1.2 How do RNases affect antibiotic production in *Streptomyces*?

Streptomyces produce a plethora of antibiotics, and RNase III is required for antibiotic production in various *Streptomyces* species (Aceti and Champness, 1998; Gatewood et al., 2012; Huang et al., 2005; Lee et al., 2013). We assayed production levels of the antibiotic/chemotherapeutic compound jadomycin in *S. venezuelae* RNase mutant strains, and found jadomycin production was abolished in an *rnc* (RNase III) mutant. To determine whether this defect in jadomycin production was due to transcription abnormalities, we assessed the transcription levels of the jadomycin cluster in the *rnc* mutant versus wild type. The jadomycin cluster was minimally expressed in the *rnc* mutant, indicating that the failure of this mutant strain to produce jadomycin was due to a lack of expression (or reduced transcript stability) of the corresponding jadomycin genes.

It will be interesting to determine whether RNase III is required for the transcription of other biosynthetic clusters in *S. venezuelae*. RNA immunoprecipitation experiments coupled with RNA-seq experiments in *S. coelicolor* indicated RNase III associates with transcripts from at least 10% of genes (Gatewood et al., 2012). The widespread effects of RNase III on the *S. coelicolor* transcriptome led to the suggestion that the enzyme controls the production of various antibiotics not through one antibiotic-specific regulator, but through the pleiotropic effects of processing so many transcripts. Given the defective phenotype of our *S. venezuelae rnc* mutant (both in antibiotic production and sporulation), we hypothesize RNase III similarly plays widespread roles in mRNA processing. Additionally, hundreds of *cis*-acting antisense RNAs (asRNAs) have been identified in *Streptomyces* (Moody et al., 2013; Vockenhuber et al., 2011), and a recent study showed many asRNAs in *S. coelicolor* are located antisense to known binding targets of RNase III (Šetinová et al., 2018). Thus, we hypothesize various factors could contribute to aberrant antibiotic production in an *rnc* mutant background: widespread defects

in mRNA processing, defects in transcription/transcript stability, and as our work has demonstrated, defects in rRNA processing and ribosome assembly/activity. It seems that RNase III is generally required for antibiotic production in the streptomycetes, and a better understanding of its roles and regulatory targets could help elucidate antibiotic production pathways. RNA immunoprecipitation using catalytically inactivated RNase III coupled with RNA-seq experiments (focusing on both transcriptomic changes over the course of the *S. venezuelae* life cycle, and on direct targets through RNA stability assays) could be performed in *S. venezuelae*. This would generate a catalog of genes directly bound and affected by RNase III. Genes significantly bound or differentially expressed could be prioritized for further investigation, with a focus on their effects on antibiotic production.

Less is known about the function of RNase J in *Streptomyces*. In *S. coelicolor*, deleting *rnj* (RNase J) resulted in delayed production of actinorhodin, overproduction of undecylprodigiosin, and diminished production of calcium-dependent antibiotic compared to wild type (Bralley et al., 2014). How RNase J acts *in vivo* and affects antibiotic production in *Streptomyces* is unclear. Jadomycin production was reduced by 30% in our *rnj* mutant compared with wild type; however, the jadomycin cluster was not differentially expressed in the mutant strain relative to wild type. This indicated post-transcriptional factors must be at play, and we hypothesized that translational defects could account for reduced antibiotic production. Indeed, we found the *rnj* strain had defects in ribosome assembly, polysome activity and accumulated translationally inactive 100S ribosome dimers. Ribosome density is generally inversely correlated with transcript length. Many biosynthetic clusters including the jadomycin cluster, are organized as long operons, and consequently are expressed as long, polycistronic transcripts. We expect ribosome activity is already reduced on these long transcripts (Ciandrini et al., 2013; Valleriani et al., 2011), and we proposed *rnase* mutant strains with defective ribosomes would be further compromised in translational efficiency.

We cannot exclude the possibility that RNase J has widespread effects on mRNA metabolism, in the same way as RNase III in *S. coelicolor*. This idea is supported by the fact that our *rnj* mutant had various phenotypic defects, including delayed fragmentation and sporulation, and decreased melanin production. In *B. subtilis* and *H. pylori*, depletion of RNase J has widespread effects on mRNA metabolism, affecting the expression of 30% and 80% of all mRNAs, respectively (Mäder et al., 2008; Redko et al., 2016). There is virtually nothing known regarding the function of RNase J in *Streptomyces* antibiotic production pathways. RNA immunoprecipitation experiments with catalytically inactivated RNase J could identify cleavage targets, and while RNA-seq experiments (both over a developmental time course, and focusing on stability after inhibiting transcription with rifampicin) in an RNase J mutant background could provide insight into how RNase J affects the *Streptomyces* transcriptome. Furthermore, given that both RNase J and RNase III affect antibiotic production, it will be interesting to determine whether these RNases share cleavage targets and regulon members. For example, if both RNases target genes with known roles in antibiotic production, these targets could be prioritized for downstream investigation. Finally, given *Streptomyces* possess both RNase J and RNase E – two enzymes central to RNA metabolism in other bacteria – it will be important to determine whether these enzymes function independently, or participate in a single

degradosome complex. This could be examined using bacterial two-hybrid and co-immunoprecipitation experiments.

6.2 *Streptomyces* exploration: a new mode of bacterial development

6.2.1 Summary of research – exploration

It had always been thought that *Streptomyces* grew as static colonies, and that the *Streptomyces* life cycle encompasses distinct three cell types: vegetative hyphae, aerial hyphae and spores. We demonstrated *Streptomyces* can deviate from their classical life cycle via a novel mode of development termed 'exploration'. Explorer cells are motile and can rapidly traverse a wide range of abiotic surfaces. Exploration is further induced by a variety of factors, including interkingdom interactions and peptides. Exploring colonies raise the pH of their surroundings using a VOC, which we have determined is TMA. We found TMA can communicate this exploratory development to other streptomycetes, and can act as a competitive tool by reducing the survival of other microbes (Chapter 3).

As TMA raises the pH of the surrounding environment, nutrient availability is altered. In particular, a rise in pH significantly decreased iron solubility. As a consequence, microbes growing in the vicinity are starved of iron, and their survival is reduced. In contrast, *Streptomyces* explorer cells thrive in this alkaline, iron-depleted environment by secreting siderophores, and by upregulating siderophore transport clusters. We propose exploration is relentless and rapid as a consequence of a feedback loop, whereby exploration raises pH, iron availability is reduced, exploration is enhanced to scavenge for iron, this exploration stimulates further release of TMA, the pH of the surrounding environment rises, and the cycle continues (Chapter 4).

In addition to defining the environmental cues impacting exploration, we have also been probing the cellular mechanisms underlying exploration. *Streptomyces* grow by tip extension at the cell poles, and this mode of growth is driven by the protein DivIVA. Our data suggest that DivIVA is required during the initial phase of exploration, and becomes dispensable once exploration/colony expansion begins. Expansion of the explorer colonies appears to be achieved by a switch to lateral wall-mediated growth, driven by MreB proteins. We propose these two cooperating proteins drive the rapid growth and expansion of explorer cells (Chapter 5).

A unified summary of Chapters 3, 4 and 5 is presented in **Fig. 6.1**.

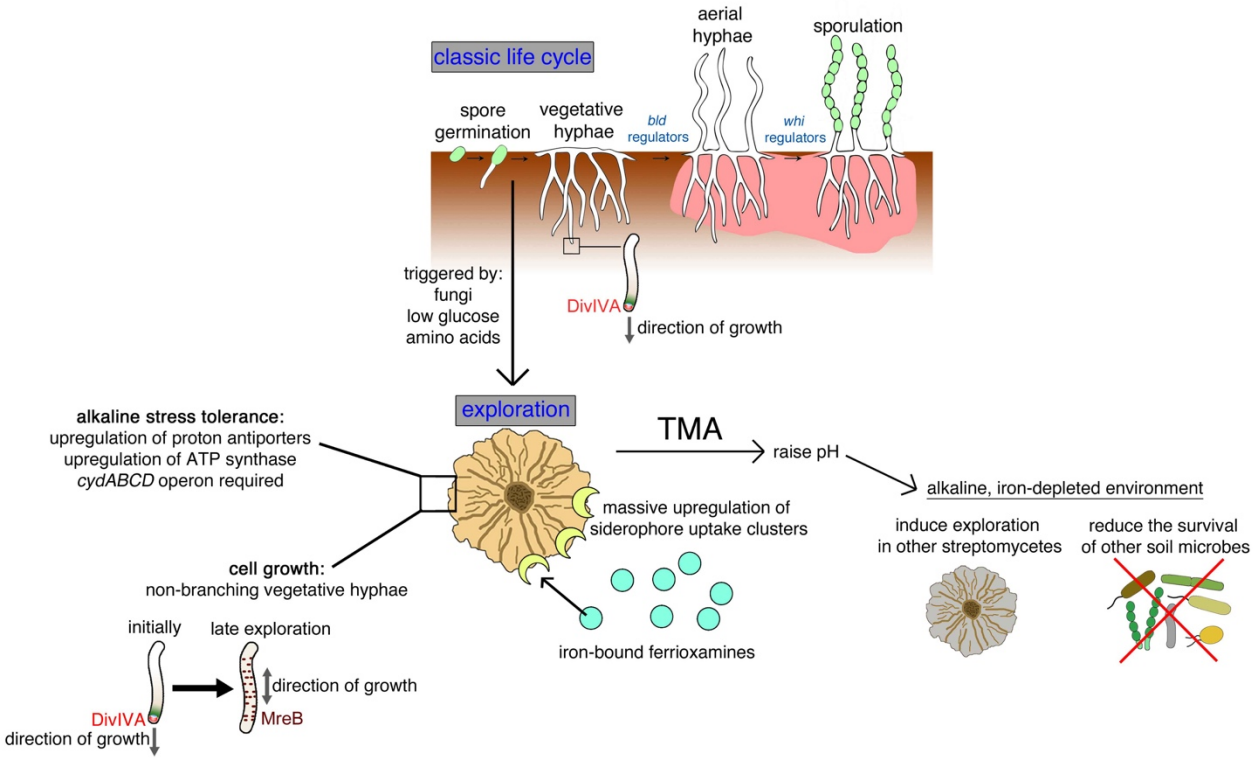

Fig. 6.1 Current model of *Streptomyces* exploration. Top: in the classic *Streptomyces* life cycle, a spore geminates, and germ tubes extend and develop into a dense network of branching vegetative hyphae. Hyphal growth occurs at the tips, and is directed by a polarisome complex governed by the protein DivIVA. In response to limited nutrients, aerial hyphae coated in a hydrophobic sheath rise into the air. Aerial hyphae then segment into chains of unigenomic spores. The transition from vegetative to aerial hyphae requires the *bld* regulators, and the transition from aerial hyphae to spores requires the *whi* regulators. Bottom: after spore germination, in response to low glucose (or fungi) and a rich amino acid source, *Streptomyces* can escape the classic life cycle. Here, *Streptomyces* grow as explorer cells, rapidly traversing solid surfaces. Right: explorer cells emit the airborne compound TMA, which raises the pH of the surrounding environment. TMA induces exploration in other streptomycetes. TMA also reduces environmental iron availability, effectively starving other microbes of iron. *Streptomyces* thrive in this iron-depleted environment by secreting iron-chelating compounds termed ferrioxamines, and through the upregulation of siderophore transport clusters. Left: at the molecular level, *Streptomyces* deal with the alkalinity of exploration by initiating an alkaline stress response, including upregulating proton antiporter clusters, upregulating the ATP synthase cluster, and requiring the activity of the cytochrome *bd* oxidase complex. At the cellular level, exploring colonies grow as non-branching vegetative hyphae. Growth is initially driven by DivIVA-mediated tip extension (in the same way as in classic growth), and is later driven by MreB-mediated lateral wall growth (or expansion).

6.2.2 The regulation of exploration

In chapter 2, we demonstrated that *S. venezuelae bld* mutants explore in the same way as wild type. Notably, this includes a *bldD* mutant strain. In the classic *Streptomyces* life cycle, BldD is considered to be a master repressor of *Streptomyces* development: it binds ~170 regions in the chromosome, and represses many sporulation genes during vegetative growth, including some of the other *bld* and *whi* regulators (den Hengst et al., 2010). Unlike most other *bld* mutants, *bldD* mutants fail to raise aerial hyphae, but instead of being blocked at vegetative growth, they bypass aerial hyphae growth altogether and proceed immediately to sporulation (Tschowri et al., 2014). Unexpectedly, during exploration, the *bldD* mutant grew as non-branching vegetative hyphae, and was phenotypically indistinguishable from wild type. This raises the exciting possibility that the pathways governing exploration may exist entirely outside of the defined *bld* and *whi* pathways. Other *bld* and *whi* mutants tested also explored in the same way as wild type, with the one exception being the *bldN* mutant strain. This strain explored more slowly than wild type. BldN is a sigma factor that directs the transcription of a number of genes including the developmental regulatory gene *bldM*. However, the *bldM* mutant explored in the same way as wild type, suggesting that the *bldN* deletion might affect exploration through other regulon members. New *bld* and *whi* genes have recently been characterized (Bush et al., 2017; Schumacher et al., 2018), and investigations into the exploratory capabilities of these strains should reveal whether there is any regulatory interplay between exploration and defined *bld* and *whi* pathways.

We are currently working to identify other regulatory pathways underlying exploration. We have conducted several rounds of chemical mutagenesis by screening for non-exploring colonies, followed by whole genome sequencing. The first round of screening led to the finding that the *cydABCD* operon was essential for exploration. Our second round of screening led us to identify an orphaned kinase (*sven_5238*) as being essential for exploration (unpublished). We are working to identify the associated signal transduction cascade, and are using a bacterial two-hybrid system to identify any associated proteins in the cell.

In addition to our mutagenesis experiments, we frequently observe exploring colony segments that escape from the main colony, and appear to 'hyperspread'. When we re-plate these hyperspreading lineages, they continue to spread faster than their wild type parent strain. This indicates genetic or epigenetic alterations that can be readily identified in exploring colonies. Whether there are simply many mutations that enhance exploration, or whether the prevalence of these 'hyperspreaders' is due to enhanced mutation rates in explorer cultures remains to be seen. Hypermutability could provide immediate competitive advantages at the expense of long-term fitness in bacterial populations (Billmyre et al., 2017; Couce et al., 2017). Future work will be aimed at taking advantage of these phenotypes to identify how these mutations result in enhanced exploration. The genomes of the hyperspreaders could be sequenced, alongside their wild type parents; it will be interesting to determine whether the mutated gene(s) encode repressors of exploration. In any case, the high frequency of hyperspreading segments suggests there are many more genes impacting exploration than we have defined to date.

6.2.3 Exploration as a form of motility

In the classic *Streptomyces* life cycle, spore dispersal serves as the sole means of colonizing new environments. *Streptomyces* explorer cells can rapidly traverse solid surfaces, and exploring colonies are phenotypically similar to sliding motility, which is defined as passive surface translocation powered by growth from the colony center and facilitated by a surfactant. We have preliminary evidence that exploring colonies produce a surfactant. When we scrape exploring cells away from their agar growth medium, the behaviour of oil droplets differs on this medium compared with equivalent but uninoculated agar medium. This suggests that explorer cells secrete a substance that alters the hydrophobic profile of the growth medium – a trait that is characteristic of amphipathic surfactant molecules. The identity of the surfactant, however, has remained elusive. We have not identified any obvious surfactant-encoding genes upregulated in exploring colonies. Additionally, attempts to identify the molecule using mass spectrometry have not been successful.

One line of investigating we are currently pursuing is whether the chaplin proteins promote exploration. *Streptomyces* produces two characterized surfactants: SapB and the chaplin proteins. In the classic life cycle, both surfactants coat the aerial hyphae, facilitating the emergence of these hyphae away from the aqueous colony surface and into the air (Capstick et al., 2007; Elliot et al., 2003). While most of the genes in the cluster directing SapB production are not expressed in exploring or static colonies, according to our RNA-seq data, some of the chaplins are significantly differentially expressed. Four of the chaplins (specifically, ChpH, ChpE, ChpG and ChpC) are significantly upregulated in exploring colonies versus static colonies. Intriguingly, our *bldN* mutant strain explores more slowly than wild type, and chaplin gene expression is controlled by BldN. Others in the lab have created chaplin mutant strains, and we have found some chaplin mutants have reduced exploratory capabilities. These data suggest that the chaplins could be the exploration-promoting surfactant. However, the chaplins may be involved in exploration in other ways. For example, chaplins form amyloid-like fibrils, and in other bacteria, equivalent amyloid proteins form an integral part of the extracellular matrix of biofilms (Serra et al., 2013). During our early SEM imaging we identified a web-like coating associated with some exploring cells. Others in the lab are working to determine whether this coating is analogous to a biofilm matrix, and whether this matrix is present in chaplin mutants.

If we find exploring colonies are encased in a matrix that is absent from classically growing *Streptomyces* cells, it would be an example of a 'motile biofilm'. Exploring colonies demonstrate properties of both motile bacteria and biofilms. Explorer cells can traverse abiotic surfaces, and we have found individual hyphae progress forwards without extending, suggestive of motility. At the same time, exploring colonies phenotypically resemble biofilms, including those formed by *B. subtilis* and *P. aeruginosa* (Patriquin et al., 2008; Wang et al., 2016). Motility and biofilm formation are typically thought of as entirely independent behaviours – many motile bacteria form non-motile aggregates held together by a biofilm matrix. It will be of interest to determine whether exploration indeed represents a motile biofilm. A definite claim of motility will likely require identification of the surfactant molecule. Additional mass spectrometry experiments aimed at identifying a fatty acid-type molecule should be performed. We could then attempt to

characterize the genes associated with production of the surfactant, and create mutations and determine whether exploration is impacted. If we can identify these genes, we could then bioinformatically determine whether they are exclusive to exploring streptomycetes. Additionally, the isolated/purified surfactant molecule could be tested for its ability to promote the exploration of non-exploring *S. venezuelae* mutants and of non-exploring wild streptomycete strains – although it is possible exploration could require more than just the addition of a surfactant molecule. At the same time, others in our lab are working to characterize the biofilm matrix by examining chaplin localization, alongside other imaging approaches (*e.g.* to detect eDNA, or different polysaccharides).

6.2.4 Potential applications of exploration

Beyond the implications for understanding fundamental aspects of bacterial growth and motility, it is conceivable that this novel mode of bacterial development could be exploited for translational applications. Every *Streptomyces* genome encodes 20-30 biosynthetic clusters, and there are thousands of *Streptomyces* species. Many creative approaches have been applied to stimulate the expression of these clusters, including: manipulating metabolic regulators, altering growth medium nutrient profiles, applying chemical stressors, and subjecting them to diverse interspecies interactions (Nai and Meyer, 2017). Given that exploration appears to be controlled entirely outside of the *bld* and *whi* regulatory pathways, it is possible antibiotic production during exploration may be controlled by distinct regulators. Experiments in our lab have shown some wild *Streptomyces* species produce more antibiotics when exploring, and this will be an interesting area for future investigation.

The application of exploration for agricultural purposes also holds interesting potential. Recent work has revealed that under drought conditions, the composition of the angiosperm plant root microbiome is substantially altered, with *Streptomyces* species being enriched (Fitzpatrick et al., 2018). We are investigating the possibility that these plant-associated *Streptomyces* species are capable of exploration, and are testing whether exploration could be used as a way of promoting plant-*Streptomyces* interactions. For example, it may be possible to exploit *Streptomyces*-plant interactions for the purposes of delivering anti-pathogen metabolites, by metabolically engineering exploring streptomycetes to produce valuable antibiotics or anti-fungal compounds. Others in the lab are currently investigating whether *S. venezuelae* exploring cells can coat plant roots in the same way that they traverse plastics and other surfaces. If so, we could test whether *Streptomyces*-associated plants are more resistant to plant pathogens, depending on the metabolites produced by the associated streptomycete. Alternatively, we have shown TMA produced by exploring colonies reduces the survival of other soil microbes, including the bacteria *B. subtilis* and *M. luteus*, and the fungus *S. cerevisiae*. It will be interesting to determine whether this VOC can also be used to inhibit the growth of plant pathogens. It should be noted that we do not know whether *Streptomyces* can explore in the soil, and we do not know whether exploration or the classic *Streptomyces* life cycle best represents the behaviour of *Streptomyces* in its natural environment. This needs to be a high priority for future investigations, and will require that we have appropriate molecular markers for detecting exploration in soil environments.

REFERENCES

Abràmoff, M.D., Hospitals, I., and Magalhães, P.J. (2004). Image processing with imageJ. Biophotonics Int. *11*, 33–42.

Abrudan, M.I., Smakman, F., Jan, A., Westhoff, S., and Miller, E.L. (2015). Socially mediated induction and suppression of antibiosis during bacterial coexistence. Proc. Natl. Acad. Sci. *112*, 11054–11059.

Aceti, D.J., and Champness, W.C. (1998). Transcriptional regulation of *Streptomyces coelicolor* pathway-specific antibiotic regulators by the *absA* and *absB* loci. J. Bacteriol. *180*, 3100–3106.

Adamidis, T., and Champness, W. (1992). Genetic analysis of *absB*, a *Streptomyces coelicolor* locus involved in global antibiotic regulation. J. Bacteriol. *174*, 4622–4628.

Ahmed, E., and Holmström, S.J.M. (2014). Siderophores in environmental research: Roles and applications. Microb. Biotechnol. *7*, 196–208.

Al-Bassam, M.M., Bibb, M.J., Bush, M.J., Chandra, G., and Buttner, M.J. (2014). Response regulator heterodimer formation controls a key stage in *Streptomyces* development. PLoS Genet. *10*, e1004554.

Ali, N., Herron, P.R., Evans, M.C., and Dyson, P.J. (2002). Osmotic regulation of the *Streptomyces lividans* thiostrepton-inducible promoter, *ptipA*. Microbiology *148*, 381–390.

Andrade-Domínguez, A., Salazar, E., Vargas-Lagunas, M.D.C., Kolter, R., and Encarnación, S. (2014). Eco-evolutionary feedbacks drive species interactions. ISME J. *8*, 1041–1054.

Arias, A.A., Lambert, S., Martinet, L., Adam, D., Tenconi, E., Hayette, M.P., Ongena, M., and Rigali, S. (2015). Growth of desferrioxamine-deficient *Streptomyces* mutants through xenosiderophore piracy of airborne fungal contaminations. FEMS Microbiol. Ecol. *91*, 1–9.

Arraiano, C.M., Andrade, J.M., Domingues, S., Guinote, I.B., Malecki, M., Matos, R.G., Moreira, R.N., Pobre, V., Reis, F.P., Saramago, M., et al. (2010). The critical role of RNA processing and degradation in the control of gene expression. FEMS Microbiol. Rev. *34*, 883–923.

Audrain, B., Létoffé, S., and Ghigo, J.-M. (2015). Airborne bacterial interactions: functions out of thin air. Front. Microbiol. *6*, 1–5.

Avalos, M., van Wezel, G.P., Raaijmakers, J.M., and Garbeva, P. (2018). Healthy scents: microbial volatiles as new frontier in antibiotic research? Curr. Opin. Microbiol. *45*, 84–91.

Baena-Monroy, T., Moreno-Maldonado, V., Franco-Martínez, F., Aldape-Barrios, B., Quindós, G., and Sánchez-Vargas, L.O. (2005). *Candida albicans, Staphylococcus aureus* and *Streptococcus*

mutans colonization in patients wearing dental prosthesis. Oral Med. Pathol. *10 Suppl 1*, 27–39.

Bagg, A., and Neilands, J.B. (1987). Molecular mechanism of regulation of siderophore-mediated iron assimilation. Microbiol. Rev. *51*, 509–518.

Baichoo, N., Wang, T., Ye, R., and Helmann, J.D. (2002). Global analysis of the *Bacillus subtilis* Fur regulon and the iron starvation stimulon. Mol. Microbiol. *45*, 1613–1629.

Banin, E., Vasil, M.L., and Greenberg, E.P. (2005). Iron and *Pseudomonas aeruginosa* biofilm formation. Proc. Natl. Acad. Sci. U. S. A. *102*, 11076–11081.

Bauer, E., Zimmermann, J., Baldini, F., Thiele, I., and Kaleta, C. (2017). BacArena: Individual-based metabolic modeling of heterogeneous microbes in complex communities. PLoS Comput. Biol. *13,* 1–22.

Bean, G.J., Flickinger, S.T., Westler, W.M., McCully, M.E., Sept, D., Weibel, D.B., and Amann, K.J. (2009). A22 disrupts the bacterial actin cytoskeleton by directly binding and inducing a low-affinity state in MreB. Biochemistry. *48*, 4852–4857.

Bean, H.D., Dimandja, J.-M.D., and Hill, J.E. (2012). Bacterial volatile discovery using solid phase microextraction and comprehensive two-dimensional gas chromatography–time-of-flight mass spectrometry. J. Chromatogr. *901*, 41–46.

Bentley, S., Chater, K., Cerdeño-Tárraga, a-M., Challis, G.L., Thomson, N.R., James, K.D., Harris, D.E., Quail, M. a, Kieser, H., Harper, D., et al. (2002). Complete genome sequence of the model actinomycete *Streptomyces coelicolor* A3(2). Nature *417*, 141–147.

Berendsen, B., Pikkemaat, M., Ro, P., Wegh, R., Sisseren, M. Van, Stolker, L., and Nielen, M. (2013). Occurrence of chloramphenicol in crops through natural production by bacteria in soil. J. Agric. Food Chem. *17*, 4004-4010.

Bergé, M., and Viollier, P.H. (2017). End-in-sight: cell polarization by the polygamic organizer PopZ. Trends Microbiol. *26*, 363–375.

Bernier, S.P., Létoffé, S., Delepierre, M., and Ghigo, J.M. (2011). Biogenic ammonia modifies antibiotic resistance at a distance in physically separated bacteria. Mol. Microbiol. *81*, 705–716.

Bertuzzi, M., Schrettl, M., Alcazar-Fuoli, L., Cairns, T.C., Munoz, A., Walker, L.A., Herbst, S., Safari, M., Cheverton, A.M., Chen, D., et al. (2014). The pH-responsive PacC transcription factor of *Aspergillus fumigatus* governs epithelial entry and tissue invasion during pulmonary aspergillosis. PLoS Pathog. *10*, 1-20.

Bibb, M.J., Domonkos, A., Chandra, G., and Buttner, M.J. (2012). Expression of the chaplin and rodlin hydrophobic sheath proteins in *Streptomyces venezuelae* is controlled by $\sigma^{(BldN)}$ and a

cognate anti-sigma factor, RsbN. Mol. Microbiol. *84*, 1033–1049.

Bierman, M., Logan, R., O'Brien, K., Seno, E.T., Nagaraja Rao, R., and Schoner, B.E. (1992). Plasmid cloning vectors for the conjugal transfer of DNA from *Escherichia coli* to *Streptomyces* spp. Gene *116*, 43–49.

Billmyre, R.B., Clancey, S.A., and Heitman, J. (2017). Natural mismatch repair mutations mediate phenotypic diversity and drug resistance in *Cryptococcus deuterogattii*. eLife *6*, 1–23.

Blanchard, A.E., and Lu, T. (2015). Bacterial social interactions drive the emergence of differential spatial colony structures. BMC Syst. Biol. *9*, 1-13.

Blin, K., Medema, M.H., Kazempour, D., Fischbach, M. a, Breitling, R., Takano, E., and Weber, T. (2013). antiSMASH 2.0--a versatile platform for genome mining of secondary metabolite producers. Nucleic Acids Res. *41*, 204-212.

Bos, L.D.J., Sterk, P.J., and Schultz, M.J. (2013). Volatile metabolites of pathogens: a systematic review. PLoS Pathog. *9*, 1–8.

Brachmann, C.B., Davies, A., Cost, G.J., Caputo, E., Li, J., Hieter, P., and Boeke, J.D. (1998). Designer deletion strains derived from *Saccharomyces cerevisiae* S288C: A useful set of strains and plasmids for PCR-mediated gene disruption and other applications. Yeast *14*, 115–132.

Bralley, P., Aseem, M., and Jones, G.H. (2014). SCO5745, a bifunctional RNase J ortholog, affects antibiotic production in *Streptomyces coelicolor*. J. Bacteriol. *196*, 1197–1205.

Briard, B., Heddergott, C., and Latgé, J. (2016). Volatile compounds emitted by *Pseudomonas aeruginosa* stimulate growth of the fungal pathogen *Aspergillus fumigatus*. mBio *7*, 1–5.

Britton, R. a, Wen, T., Schaefer, L., Pellegrini, O., Uicker, W.C., Mathy, N., Tobin, C., Daou, R., Szyk, J., and Condon, C. (2007). Maturation of the 5' end of *Bacillus subtilis* 16S rRNA by the essential ribonuclease YkqC/RNase J1. Mol. Microbiol. *63*, 127–138.

Brodersen, D.E., Clemons, W.M., Carter, a P., Morgan-Warren, R.J., Wimberly, B.T., and Ramakrishnan, V. (2000). The structural basis for the action of the antibiotics tetracycline, pactamycin, and hygromycin B on the 30S ribosomal subunit. Cell *103*, 1143–1154.

Brow, David A. and Noller, H.F. (1983). Protection of ribosomal implication RNA from Kethoxal in polyribosomes of specific sites in ribosome function. J. Mol. Biol. *163*, 27-46.

Burbank, L., Mohammadi, M., and Roper, M.C. (2015). Siderophore-mediated iron acquisition influences motility and is required for full virulence of the xylem-dwelling bacterial phytopathogen *Pantoea stewartii* subsp*. stewartii*. Appl. Environ. Microbiol. *81*, 139–148.

Bush, M.J., Bibb, M.J., Chandra, G., Findlay, K.C., and Buttner, M.J. (2013). Genes required for aerial growth, cell division , and chromosome segregation are targets of WhiA before sporulation in *Streptomyces venezuelae*. mBio *4*, 1–18.

Bush, M.J., Chandra, G., Findlay, K.C., and Buttner, M.J. (2017). Multi-layered inhibition of *Streptomyces* development: BldO is a dedicated repressor of *whiB*. Mol. Microbiol. *104*, 700–711.

Butcher, J., and Stintzi, A. (2013). The transcriptional landscape of *Campylobacter jejuni* under iron replete and iron limited growth conditions. PLoS One *8*, 1–16.

Bylund, G.O., Wipemo, L.C., Lundberg, L. a, and Wikström, P.M. (1998). RimM and RbfA are essential for efficient processing of 16S rRNA in *Escherichia coli*. J. Bacteriol. *180*, 73–82.

Cabeen, M.T., and Jacobs-Wagner, C. (2005). Bacterial cell shape. Nat. Rev. Microbiol. *3*, 601–610.

Caccamo, P.D., and Brun, Y. V. (2017). The molecular basis of noncanonical bacterial morphology. Trends Microbiol. *26*, 191–208.

Callaghan, A.J., Marcaida, M.J., Stead, J. A., McDowall, K.J., Scott, W.G., and Luisi, B.F. (2005). Structure of *Escherichia coli* RNase E catalytic domain and implications for RNA turnover. Nature *437*, 1187–1191.

Capstick, D.S., Willey, J.M., Buttner, M.J., and Elliot, M. A. (2007). SapB and the chaplins: connections between morphogenetic proteins in *Streptomyces coelicolor*. Mol. Microbiol. *64*, 602–613.

Carballido-Lopez, R. (2006). The bacterial actin-like cytoskeleton. Microbiol. Mol. Biol. Rev. *70*, 888–909.

Chang, S. A., Bralley, P., and Jones, G.H. (2005). The *absB* gene encodes a double strand-specific endoribonuclease that cleaves the read-through transcript of the *rpsO-pnp* operon in *Streptomyces coelicolor*. J. Biol. Chem. *280*, 33213–33219.

Chater, K.F. (2006). *Streptomyces* inside-out: a new perspective on the bacteria that provide us with antibiotics. Philos. Trans. R. Soc. Lond. B. Biol. Sci. *361*, 761–768.

Chater, K.F. (2016). Recent advances in understanding *Streptomyces*. F1000Research *5*, 1-16.

Chatfield, C.H., and Cianciotto, N.P. (2007). The secreted pyomelanin pigment of *Legionella pneumophila* confers ferric reductase activity. Infect. Immun. *75*, 4062–4070.

Chomczynski, P. (1987). Single-step method of RNA isolation by acid guanidinium extraction.

Anal. Biochem. *159*, 156–159.

Chuankun, X., Minghe, M., Leming, Z., and Keqin, Z. (2004). Soil volatile fungistasis and volatile fungistatic compounds. Soil Biol. Biochem. *36*, 1997–2004.

Ciandrini, L., Stansfield, I., and Romano, M.C. (2013). Ribosome traffic on mRNAs maps to gene ontology: genome-wide quantification of translation initiation rates and polysome size regulation. PLoS Comput. Biol. *9*, e1002866.

Claessen, D., Rink, R., De Jong, W., Siebring, J., De Vreugd, P., Boersma, F.G.H., Dijkhuizen, L., and Wosten, H.A.B. (2003). A novel class of secreted hydrophobic proteins is involved in aerial hyphae formation in *Streptomyces coelicolor* by forming amyloid-like fibrils. Genes Dev. *17*, 1714–1726.

Cohen, R.J., Jan, Y.N., Matricon, J., and Delbrück, M. (1975). Avoidance response, house response, and wind responses of the sporangiophore of *Phycomyces*. J. Gen. Physiol. *66*, 67–95.

Collins, M.D. (1987). Transfer of *Brevibacterium ammoniagenes* to the genus *Corynebacterium* as *Corynebacterium ammoniagenes* comb. nov. Int. J. Syst. Bacteriol. *37*, 442–443.

Condon, C., and Putzer, H. (2002). The phylogenetic distribution of bacterial ribonucleases. Nucleic Acids Res. *30*, 5339–5346.

Connolly, K., and Culver, G. (2009). Deconstructing ribosome construction. Trends Biochem. Sci. *34*, 256–263.

Cordovez, V., Carrion, V.J., Etalo, D.W., Mumm, R., Zhu, H., van Wezel, G.P., and Raaijmakers, J.M. (2015). Diversity and functions of volatile organic compounds produced by *Streptomyces* from a disease-suppressive soil. Front. Microbiol. *6*, 1–13.

Couce, A., Caudwell, L.V., Feinauer, C., Hindré, T., Feugeas, J.-P., Weigt, M., Lenski, R.E., Schneider, D., and Tenaillon, O. (2017). Mutator genomes decay, despite sustained fitness gains, in a long-term experiment with bacteria. Proc. Natl. Acad. Sci. *1,* 1–10.

Craciun, S., and Balskus, E.P. (2012). Microbial conversion of choline to trimethylamine requires a glycyl radical enzyme. Proc. Natl. Acad. Sci. U. S. A. *109*, 21307–21312.

Danecek, P., Auton, A., Abecasis, G., Albers, C. A., Banks, E., DePristo, M. A., Handsaker, R.E., Lunter, G., Marth, G.T., Sherry, S.T., et al. (2011). The variant call format and VCFtools. Bioinformatics *27*, 2156–2158.

Davis, D., Edwars, John, J., Mitchell, A.P., and Ibrahim, A.S. (2000). *Candida albicans* RIM101 pH response pathway is required for host-pathogen interactions. Infect. Immun. *68*, 5953–5959.

Deana, A., and Belasco, J.G. (2005). Lost in translation: the influence of ribosomes on bacterial mRNA decay. Genes Dev. *19*, 2526–2533.

Dempwolff, F., Reimold, C., Reth, M., and Graumann, P.L. (2011). *Bacillus subtilis* MreB orthologs self-organize into filamentous structures underneath the cell membrane in a heterologous cell system. PLoS One *6*, 1-9.

Deutscher, M.P. (2009). Maturation and degradation of ribosomal RNA in bacteria. Prog. Mol. Biol. Transl. Sci. *85*, 369–391.

Ditkowski, B., Holmes, N., Rydzak, J., Donczew, M., Bezulska, M., Ginda, K., Kedzierski, P., Zakrzewska-Czerwinska, J., Kelemen, G.H., and Jakimowicz, D. (2013). Dynamic interplay of ParA with the polarity protein, Scy, coordinates the growth with chromosome segregation in *Streptomyces coelicolor*. Open Biol. *3*, 1-13.

Domínguez-Escobar, J., Chastanet, A., Crevenna, A.H., Fromion, V., Wedlich-Söldner, R., and Carballido-López, R. (2011). Processive movement of MreB-associated cell wall biosynthetic complexes in bacteria. Science *80*, 225–228.

Donczew, M., Mackiewicz, P., Wróbel, A., Flärdh, K., Zakrzewska-Czerwińska, J., and Jakimowicz, D. (2016). ParA and ParB coordinate chromosome segregation with cell elongation and division during *Streptomyces* sporulation. Open Biol. *6*, 150263.

Doull, J.L. (1993). Production of a novel polyketide antibiotic, jadomycin B, by *S. venezuelae* following heat shock. J. Antibiot. (Tokyo). *46*, 869–871.

Doull, J.L., Singh, a K., Hoare, M., and Ayer, S.W. (1994). Conditions for the production of jadomycin B by *Streptomyces venezuelae* ISP5230: effects of heat shock, ethanol treatment and phage infection. J. Ind. Microbiol. *13*, 120–125.

Dunn, A.K., and Stabb, E. V. (2008). Genetic analysis of trimethylamine N-oxide reductases in the light organ symbiont *Vibrio fischeri* ES114. J. Bacteriol. *190*, 5814–5823.

Dupuis, S.N., Veinot, T., Monro, S.M. a, Douglas, S.E., Syvitski, R.T., Goralski, K.B., McFarland, S. a, and Jakeman, D.L. (2011). Jadomycins derived from the assimilation and incorporation of norvaline and norleucine. J. Nat. Prod. *74*, 2420–2424.

Durand, S., and Condon, C. (2018). RNases and helicases in Gram-positive bacteria. Microbiol. Spectr. *6*, 1-17.

Durand, S., Gilet, L., Bessières, P., Nicolas, P., and Condon, C. (2012). Three essential ribonucleases-RNase Y, J1, and III-control the abundance of a majority of *Bacillus subtilis* mRNAs. PLoS Genet. *8*, e1002520.

Edwards, D.H., and Errington, J. (1997). The *Bacillus subtilis* DivIVA protein targets to the division septum and controls the site specificity of cell division. Mol. Microbiol. *24*, 905–915.

Edwards, D.H., Thomaides, H.B., and Errington, J. (2000). Promiscuous targeting of *Bacillus subtilis* cell division protein DivIVA to division sites in *Escherichia coli* and fission yeast. EMBO J. *19*, 2719–2727.

Ehrlich, J., Gottlieb, D., Burkholder, P., Anderson, L., and Pridham, T.G. (1948). *Streptomyces venezuelae*, N. SP., the source of chloromycetin. J. Bacteriol. 467–477.

Elliot, M.A., Bibb, M.J., Buttner, M.J., and Leskiw, B.K. (2001). BldD is a direct regulator of key developmental genes in *Streptomyces coelicolor* A3(2). Mol. Microbiol. *40*, 257–269.

Elliot, M.A., Karoonuthaisiri, N., Huang, J., Bibb, M.J., Cohen, S.N., Kao, C.M., and Buttner, M.J. (2003). The chaplins: A family of hydrophobic cell-surface proteins involved in aerial mycelium formation in *Streptomyces coelicolo*r. Genes Dev. *17*, 1727–1740.

Elliot, M.A., Buttner, M.J., and Nodwell, J.R. (2008). Multicellular development in *Streptomyces*, in Myxobacteria: multicellularity and differentiation. Am. Soc. Microbiol. 419–439.

Even, S., Pellegrini, O., Zig, L., Labas, V., Vinh, J., Bréchemmier-Baey, D., and Putzer, H. (2005). Ribonucleases J1 and J2: two novel endoribonucleases in *B. subtili*s with functional homology to *E. coli* RNase E. Nucleic Acids Res. *33*, 2141–2152.

Farag, M.A., Song, G.C., Park, Y.-S., Audrain, B., Lee, S., Ghigo, J.-M., Kloepper, J.W., and Ryu, C.-M. (2017). Biological and chemical strategies for exploring inter- and intra-kingdom communication mediated via bacterial volatile signals. Nat. Protoc. *12*, 1359–1377.

Faure, L.M., Fiche, J.-B., Espinosa, L., Ducret, A., Anantharaman, V., Luciano, J., Lhospice, S., Islam, S.T., Tréguier, J., Sotes, M., et al. (2016). The mechanism of force transmission at bacterial focal adhesion complexes. Nature *539*, 530–535.

Figaro, S., Durand, S., Gilet, L., Cayet, N., Sachse, M., and Condon, C. (2013). *Bacillus subtilis* mutants with knockouts of the genes encoding ribonucleases RNase Y and RNase J1 are viable, with major defects in cell morphology, sporulation, and competence. J. Bacteriol. *195*, 2340–2348.

Fitzpatrick, C.R., Copeland, J., Wang, P.W., Guttman, D.S., Kotanen, P.M., and Johnson, M.T.J. (2018). Assembly and ecological function of the root microbiome across angiosperm plant species. Proc. Natl. Acad. Sci. 1-9.

Flärdh, K. (2003). Essential role of DivIVA in polar growth and morphogenesis in *Streptomyces coelicolor* A3(2). Mol. Microbiol. *49*, 1523–1536.

Flärdh, K., and Buttner, M.J. (2009). *Streptomyces* morphogenetics: dissecting differentiation in a filamentous bacterium. Nat. Rev. Microbiol. *7*, 36–49.

Flärdh, K., Richards, D.M., Hempel, A.M., Howard, M., and Buttner, M.J. (2012). Regulation of apical growth and hyphal branching in *Streptomyces*. Curr. Opin. Microbiol. *15*, 737–743.

Fu, G., Bandaria, J.N., Le Gall, A.V., Fan, X., Yildiz, A., Mignot, T., Zusman, D.R., and Nan, B. (2018). MotAB-like machinery drives the movement of MreB filaments during bacterial gliding motility. Proc. Natl. Acad. Sci. *115*, 2484-2489.

Gamow, R.I., and Bottger, B. (1982). Avoidance and rheotropic responses in *Phycomyces*. Evidence for an "avoidance gas" mechanism. J. Gen. Physiol. *79*, 835–848.

Garner, E.C., Bernard, R., Wang, W., Zhuang, X., Rudner, D.Z., and Mitchison, T. (2011). Circumferential motions of the cell wall synthesis machinery drive cytoskeletal dynamics in *B. subtilis*. Science. *333*, 222–225.

Gatewood, M.L., Bralley, P., Weil, M.R., and Jones, G.H. (2012). RNA-Seq and RNA immunoprecipitation analyses of the transcriptome of *Streptomyces coelicolor* identify substrates for RNase III. J. Bacteriol. *194*, 2228–2237.

Ginzburg, D, Steitz, A. (1975). The 30 S ribosomal precursor RNA from *Escherichia coli*. A primary transcript containing 23 S, 16 S, and 5 S sequences. J. Biol. Chem. *250*, 5647-5654.

Glick, R., Gilmour, C., Tremblay, J., Satanower, S., Avidan, O., Déziel, E., Greenberg, E.P., Poole, K., and Banin, E. (2010). Increase in rhamnolipid synthesis under iron-limiting conditions influences surface motility and biofilm formation in *Pseudomonas aeruginosa*. J. Bacteriol. *192*, 2973–2980.

Gravenbeek, M.L., and Jones, G.H. (2008). The endonuclease activity of RNase III is required for the regulation of antibiotic production by *Streptomyces coelicolor*. Microbiology *154*, 3547–3555.

Gunter, K., Toupet, C., and Schupp, T. (1993). Characterization of an iron-regulated promoter involved in Desferrioxamine B synthesis in *Streptomyces pilosus*: Repressor-binding site and homology to the diphtheria toxin gene promoter. J. Bacteriol. *175*, 3295–3302.

Guo, Y.P., Zheng, W., Rong, X.Y., and Huang, Y. (2008). A multilocus phylogeny of the *Streptomyces griseus* 16S rRNA gene clade: use of multilocus sequence analysis for streptomycete systematics. Int. J. Syst. Evol. Microbiol. *58*, 149–159.

Gust, B., Kieser, T., and Chater, K. (2002). REDIRECT technology: PCR-targeting system in *Streptomyces coelicolor*. John Innes Centre, UK.

Gust, B., Challis, G.L., Fowler, K., Kieser, T., and Chater, K.F. (2003). PCR-targeted *Streptomyces* gene replacement identifies a protein domain needed for biosynthesis of the sesquiterpene soil odor geosmin. Proc. Natl. Acad. Sci. U. S. A. *100*, 1541–1546.

Hagège, J.M., and Cohen, S.N. (1997). A developmentally regulated *Streptomyces* endoribonuclease resembles ribonuclease E of *Escherichia coli*. Mol. Microbiol. *25*, 1077–1090.

Haiser, H.J., Yousef, M.R., and Elliot, M. a (2009). Cell wall hydrolases affect germination, vegetative growth, and sporulation in *Streptomyces coelicolor*. J. Bacteriol. *191*, 6501–6512.

Hammes, W.P., and Neuhaus, F.C. (1974). On the mechanism of action of vancomycin: inhibition of peptidoglycan synthesis in *Gaffkya homari*. Antimicrob. Agents Chemother. *6*, 722–728.

Harshey, R.M. (2003). Bacterial motility on a surface: many ways to a common goal. Annu. Rev. Microbiol. *57*, 249–273.

Hartmann, Guido, Honikel, Kari Otto, Knusel, Fritz, Nuesch, J. (1967). The specific inhibition of the DNA-directed RNA synthesis by rifamycin. Biochim. Biophys. Acta *145*, 843–844.

Heichlinger, A., Ammelburg, M., Kleinschnitz, E.M., Latus, A., Maldener, I., Flärdh, K., Wohlleben, W., and Muth, G. (2011). The MreB-like protein Mbl of *Streptomyces coelicolor* A3(2) depends on MreB for proper localization and contributes to spore wall synthesis. J. Bacteriol. *193*, 1533–1542.

Helmann, J.D. (2014). Specificity of metal sensing: Iron and manganese homeostasis in *Bacillus subtilis*. J. Biol. Chem. *289*, 28112–28120.

Hempel, A.M., Wang, S.B., Letek, M., Gil, J.A., and Flärdh, K. (2008). Assemblies of DivIVA mark sites for hyphal branching and can establish new zones of cell wall growth in *Streptomyces coelicolor*. J. Bacteriol. *190*, 7579–7583.

den Hengst, C.D., Tran, N.T., Bibb, M.J., Chandra, G., Leskiw, B.K., and Buttner, M.J. (2010). Genes essential for morphological development and antibiotic production in *Streptomyces coelicolor* are targets of BldD during vegetative growth. Mol. Microbiol. *78*, 361–379.

Higo, A., Hara, H., Horinouchi, S., and Ohnishi, Y. (2012). Genome-wide distribution of AdpA, a global regulator for secondary metabolism and morphological differentiation in *Streptomyces*, revealed the extent and complexity of the AdpA regulatory network. DNA Res. *19*, 259–273.

Hindra, Pak, P., and Elliot, M. a (2010). Regulation of a novel gene cluster involved in secondary metabolite production in *Streptomyces coelicolor*. J. Bacteriol. *192*, 4973–4982.

Hoiczyk, E. (2000). A molecular motor for gliding motility in cyanobacteria. J. Phycol. *36*, 72.

Holden, V.I., and Bachman, M.A. (2015). Diverging roles of bacterial siderophores during infection. Metallomics *7*, 986–995.

Holmes, N.A., Walshaw, J., Leggett, R.M., Thibessard, A., Dalton, K.A., Gillespie, M.D., Hemmings, A.M., Gust, B., and Kelemen, G.H. (2013). Coiled-coil protein Scy is a key component of a multiprotein assembly controlling polarized growth in *Streptomyces*. Proc. Natl. Acad. Sci. U. S. A. *110*, 397-406.

Hopwood, D.A. (2007). *Streptomyces* in Nature and Medicine: the Antibiotic Makers (Oxford University Press).

Hosaka, T., Ohnishi-Kameyama, M., Muramatsu, H., Murakami, K., Tsurumi, Y., Kodani, S., Yoshida, M., Fujie, A., and Ochi, K. (2009). Antibacterial discovery in actinomycetes strains with mutations in RNA polymerase or ribosomal protein S12. Nat. Biotechnol. *27*, 462–464.

Hsu, Y.-P., Rittichier, J., Kuru, E., Yablonowski, J., Pasciak, E., Tekkam, S., Hall, E., Murphy, B., Lee, T.K., Garner, E.C., et al. (2017). Full color palette of fluorescent D-amino acids for in situ labeling of bacterial cell walls. Chem. Sci. *00*, 1–9.

Huang, J., Shi, J., Molle, V., Sohlberg, B., Weaver, D., Bibb, M.J., Karoonuthaisiri, N., Lih, C.-J., Kao, C.M., Buttner, M.J., et al. (2005). Cross-regulation among disparate antibiotic biosynthetic pathways of *Streptomyces coelicolor*. Mol. Microbiol. *58*, 1276–1287.

Hui, M.P., Foley, P.L., and Belasco, J.G. (2014). Messenger RNA degradation in bacterial cells. Annu. Rev. Genet. *11*, 537-559.

Ikeda, H., Ishikawa, J., Hanamoto, A., Shinose, M., Kikuchi, H., Shiba, T., Sakaki, Y., Hattori, M., and Omura, S. (2003). Complete genome sequence and comparative analysis of the industrial microorganism *Streptomyces avermitilis*. Nat. Biotechnol. *21*, 526–531.

Insam, H., and Seewald, M.S. A. (2010). Volatile organic compounds (VOCs) in soils. Biol. Fertil. Soils *46*, 199–213.

Izutsu, K., Wada, C., Komine, Y., Sako, T., Ueguchi, C., Nakura, S., and Wada, A. (2001). *Escherichia coli* ribosome-associated protein SRA, whose copy number increases during stationary phase. J. Bacteriol. *183*, 2765–2773.

Jakeman, D.L., Graham, C.L., Young, W., and Vining, L.C. (2006). Culture conditions improving the production of jadomycin B. J. Ind. Microbiol. Biotechnol. *33*, 767–772.

Jakeman, D.L., Bandi, S., Graham, C.L., Reid, T.R., Wentzell, J.R., and Douglas, S.E. (2009). Antimicrobial activities of jadomycin B and structurally related analogues. Antimicrob. Agents Chemother. *53*, 1245–1247.

Jarrell, K.F., and McBride, M.J. (2008). The surprisingly diverse ways that prokaryotes move. Nat. Rev. Microbiol. *6*, 466–476.

Jones, S.E., and Elliot, M.A. (2017). *Streptomyces* exploration: competition, volatile communication and new bacterial behaviours. Trends Microbiol. *25*, 1–10.

Jones, S.E., and Elliot, M.A. (2018). 'Exploring' the regulation of *Streptomyces* growth and development. Curr. Opin. Microbiol. *42*, 25–30.

Jones, L.J.F., Carballido-López, R., and Errington, J. (2001). Control of cell shape in bacteria: Helical, actin-like filaments in *Bacillus subtilis*. Cell *104*, 913–922.

Jones, S.E., Leong, V., Ortega, J., and Elliot, M. A. (2014). Development, antibiotic production, and ribosome assembly in *Streptomyces venezuelae* are impacted by RNase J and RNase III deletion. J. Bacteriol. *196*, 4253-4267.

Jones, S.E., Ho, L., Rees, C.A., Hill, J.E., Nodwell, J.R., and Elliot, M.A. (2017). *Streptomyces* exploration is triggered by fungal interactions and volatile signals. eLife *6*, 1–21.

Joyce, G., Williams, K.J., Robb, M., Noens, E., Tizzano, B., Shahrezaei, V., and Robertson, B.D. (2012). Cell division site placement and asymmetric growth in Mycobacteria. PLoS One *7*, 1–8.

Kaberdin, V.R., Singh, D., and Lin-Chao, S. (2011). Composition and conservation of the mRNA-degrading machinery in bacteria. J. Biomed. Sci. *18*, 1-12.

Kai, M., Haustein, M., Molina, F., Petri, A., Scholz, B., and Piechulla, B. (2009). Bacterial volatiles and their action potential. Appl. Microbiol. Biotechnol. *81*, 1001–1012.

Kang, C.M., Nyayapathy, S., Lee, J.Y., Suh, J.W., and Husson, R.N. (2008). Wag31, a homologue of the cell division protein DivIVA, regulates growth, morphology and polar cell wall synthesis in mycobacteria. Microbiology *154*, 725–735.

Kato, T., Yoshida, H., Miyata, T., Maki, Y., Wada, A., and Namba, K. (2010). Structure of the 100S ribosome in the hibernation stage revealed by electron cryomicroscopy. Structure *18*, 719–724.

Kawai, Y., Asai, K., and Errington, J. (2009). Partial functional redundancy of MreB isoforms, MreB, Mbl and MreBHp in cell morphogenesis of *Bacillus subtilis*. Mol. Microbiol. *73*, 719–731.

Kawai, Y., Mercier, R., and Errington, J. (2014). Bacterial cell morphogenesis does not require a preexisting template structure. Curr. Biol. *24*, 863–867.

Kearns, D.B. (2010). A field guide to bacterial swarming motility. Nat. Rev. Microbiol. *8*, 634–644.

Kelemen, G.H., Buttner, M.J., and Buttnert, M.J. (1998). Initiation of aerial mycelium formation

in *Streptomyces*. Curr. Opin. Microbiol. *1*, 656–662.

Kieser, T., Bibb, M.J., Buttner, M.J., Chater, K.F., and Hopwood, D.A. (2000). Practical *Streptomyces* Genetics (Norwich, England: The John Innes Foundation).

Kim, K., Lee, S., and Ryu, C.-M. (2013). Interspecific bacterial sensing through airborne signals modulates locomotion and drug resistance. Nat. Commun. *4*, 1-12.

Kliewer, W. (1965). Changes of concentration of glucose, fructose and total soluble solids in flowers and berries of *Vitis Vinifera*. Am. J. Enol. Vitic. *16,* 101–110.

Kodani, S., Hudson, M.E., Durrant, M.C., Buttner, M.J., Nodwell, J.R., and Willey, J.M. (2004). The SapB morphogen is a lantibiotic-like peptide derived from the product of the developmental gene *ramS* in *Streptomyces coelicolor*. Proc. Natl. Acad. Sci. U. S. A. *101*, 11448–11453.

Kois-Ostrowska, A., Strzalka, A., Lipietta, N., Tilley, E., Zakrzewska-Czerwinska, J., Herron, P., and Jakimowicz, D. (2016). Unique function of the bacterial chromosome segregation machinery in apically growing *Streptomyces* - targeting the chromosome to new hyphal tubes and its anchorage at the tips. PLoS Genet. *12*, 1–25.

Kolter, R. (2012). Old meets new: using interspecies interactions to detect secondary metabolite production in Actinomycetes. Methods Enzymol. *517*, 89-109.

Könönen, E., and Wade, W.G. (2015). *Actinomyces* and related organisms in human infections. Clin. Microbiol. Rev. *28*, 419–442.

Krokowski, D., Gaccioli, F., Majumder, M., Mullins, M.R., Yuan, C.L., Papadopoulou, B., Merrick, W.C., Komar, A. A., Taylor, D.J., and Hatzoglou, M. (2011). Characterization of hibernating ribosomes in mammalian cells. Cell Cycle *10*, 2691–2702.

Krulwich, T.A., Sachs, G., and Padan, E. (2011). Molecular aspects of bacterial pH sensing and homeostasis. Nat. Rev. Microbiol. *9*, 330–343.

Kuru, E., Hughes, H.V., Brown, P.J., Hall, E., Tekkam, S., Cava, F., Pedro, M.A. De, Brun, Y. V, and Vannieuwenhze, M.S. (2012). *In situ* probing of newly synthesized peptidoglycan in live bacteria with fluorescent D-amino acids. Angew. Chemie *51,* 12519–12523.

Kuru, E., Lambert, C., Rittichier, J., Till, R., Ducret, A., Derouaux, A., Gray, J., Biboy, J., Vollmer, W., VanNieuwenhze, M., et al. (2017). Fluorescent D-amino-acids reveal bi-cellular cell wall modifications important for *Bdellovibrio bacteriovorus* predation. Nat. Microbiol. *2*, 1–10.

Laalami, S., Zig, L., and Putzer, H. (2014). Initiation of mRNA decay in bacteria. Cell. Mol. Life Sci. *71*, 1799–1828.

Lambert, T. (2012). Antibiotics that affect the ribosome. Rev. Sci. Tech. *31*, 57–64.

Lambert, S., Traxler, M.F., Craig, M., Maciejewska, M., Ongena, M., van Wezel, G.P., Kolter, R., and Rigali, S. (2014). Altered desferrioxamine-mediated iron utilization is a common trait of bald mutants of *Streptomyces coelicolor*. Met. Integr. Biometal Sci. *6*, 1390–1399.

Langmead, B., and Salzberg, S.L. (2012). Fast gapped-read alignment with Bowtie 2. Nat. Methods *9*, 357–359.

Lee, K., and Cohen, S.N. (2003). A *Streptomyces coelicolor* functional orthologue of *Escherichia coli* RNase E shows shuffling of catalytic and PNPase-binding domains. Mol. Microbiol. *48*, 349–360.

Lee, J.-H., Gatewood, M.L., and Jones, G.H. (2013). RNase III is required for actinomycin production in *Streptomyces antibioticus*. Appl. Environ. Microbiol. *79*, 6447–6451.

Lehnik-Habrink, M., Lewis, R.J., Mäder, U., and Stülke, J. (2012). RNA degradation in *Bacillus subtilis*: an interplay of essential endo- and exoribonucleases. Mol. Microbiol. *84*, 1005–1017.

Lenarcic, R., Halbedel, S., Visser, L., Shaw, M., Wu, L.J., Errington, J., Marenduzzo, D., and Hamoen, L.W. (2009). Localisation of DivIVA by targeting to negatively curved membranes. EMBO J. *28*, 2272–2282.

Leong, V., Kent, M., Jomaa, A., and Ortega, J. (2013). *Escherichia coli rimM* and *yjeQ* null strains accumulate immature 30S subunits of similar structure and protein complement. RNA *19*, 789–802.

Letek, M., Ordóñez, E., Vaquera, J., Margolin, W., Flärdh, K., Mateos, L.M., and Gil, J.A. (2008). DivIVA is required for polar growth in the MreB-lacking rod-shaped actinomycete *Corynebacterium glutamicum*. J. Bacteriol. *190*, 3283–3292.

Létoffé, S., Audrain, B., Bernier, S.P., Delepierre, M., and Ghigo, J.M. (2014). Aerial exposure to the bacterial volatile compound trimethylamine modifies antibiotic resistance of physically separated bacteria by raising culture medium pH. mBio *5*, 1–12.

Li, H., Handsaker, B., Wysoker, A., Fennell, T., Ruan, J., Homer, N., Marth, G., Abecasis, G., and Durbin, R. (2009). The sequence alignment/map format and SAMtools. Bioinformatics *25*, 2078–2079.

Li, Z., Pandit, S., and Deutscher, M.P. (1999). RNase G (CafA protein) and RNase E are both required for the 5’ maturation of 16S ribosomal RNA. EMBO J. *18*, 2878–2885.

Li de la Sierra-Gallay, I., Zig, L., Jamalli, A., and Putzer, H. (2008). Structural insights into the dual activity of RNase J. Nat. Struct. Mol. Biol. *15*, 206–212.

Lugtenberg, B.J.J., Kravchenko, L. V, and Simons, M. (1999). Tomato seed and root exudate sugars: composition, utilization by *Pseudomonas* biocontrol strains and role in rhizosphere colonization. Environ. Microbiol. *1*, 439–446.

Lyons, N. A., and Kolter, R. (2015). On the evolution of bacterial multicellularity. Curr. Opin. Microbiol. *24*, 21–28.

Mackie, G. A. (2013). RNase E: at the interface of bacterial RNA processing and decay. Nat. Rev. Microbiol. *11*, 45–57.

MacNeil, D.J., Gewain, K.M., Ruby, C.L., Dezeny, G., Gibbons, P.H., and MacNeil, T. (1992). Analysis of *Streptomyces avermitilis* genes required for avermectin biosynthesis utilizing a novel inte- gration vector. Gene *111*, 61–68.

Mäder, U., Zig, L., Kretschmer, J., Homuth, G., and Putzer, H. (2008). mRNA processing by RNases J1 and J2 affects *Bacillus subtilis* gene expression on a global scale. Mol. Microbiol. *70*, 183–196.

Madhugiri, R., and Evguenieva-Hackenberg, E. (2009). RNase J is involved in the 5'-end maturation of 16S rRNA and 23S rRNA in *Sinorhizobium meliloti*. FEBS Lett. *583*, 2339–2342.

Maguire, B. A. (2009). Inhibition of bacterial ribosome assembly: a suitable drug target? Microbiol. Mol. Biol. Rev. *73*, 22–35.

Marsili, E., Baron, D.B., Shikhare, I.D., Coursolle, D., Gralnick, J.A., and Bond, D.R. (2008). *Shewanella* secretes flavins that mediate extracellular electron transfer. Proc. Natl. Acad. Sci. *105*, 3968–3973.

Mathy, N., Bénard, L., Pellegrini, O., Daou, R., Wen, T., and Condon, C. (2007). 5'-to-3' exoribonuclease activity in bacteria: role of RNase J1 in rRNA maturation and 5' stability of mRNA. Cell *129*, 681–692.

Matsuno, K., and Sonenshein, A. L. (1999). Role of SpoVG in asymmetric septation in *Bacillus subtilis*. J. Bacteriol. *181*, 3392–3401.

Mazza, P., Noens, E.E., Schirner, K., Grantcharova, N., Mommaas, a M., Koerten, H.K., Muth, G., Flärdh, K., van Wezel, G.P., and Wohlleben, W. (2006). MreB of *Streptomyces coelicolor* is not essential for vegetative growth but is required for the integrity of aerial hyphae and spores. Mol. Microbiol. *60*, 838–852.

McClure, R., Balasubramanian, D., Sun, Y., Bobrovskyy, M., Sumby, P., Genco, C. A., Vanderpool, C.K., and Tjaden, B. (2013). Computational analysis of bacterial RNA-Seq data. Nucleic Acids Res. *41*, 1-16.

McCormick, J.R., and Flärdh, K. (2012). Signals and regulators that govern *Streptomyces* development. FEMS Microbiol. Rev. *36*, 206–231.

McCrindle, S.L., Kappler, U., and McEwan, A.G. (2005). Microbial dimethylsulfoxide and trimethylamine-N-oxide respiration. Advances in Microbial Phys., *50*, 147–201.

McMillan, D.G.G., Velasquez, I., Nunn, B.L., Goodlett, D.R., Hunter, K.A., Lamont, I., Sander, S.G., and Cook, G.M. (2010). Acquisition of iron by alkaliphilic *Bacillus* species. Appl. Environ. Microbiol. *76*, 6955–6961.

McVittie, A. (1974). Ultrastructural studies on sporulation in wild-type and white colony mutants of *Streptomyces coelicolor*. J. Gen. Microbiol. *81*, 291–302.

Meniche, X., Otten, R., Siegrist, M.S., Baer, C.E., Murphy, K.C., Bertozzi, C.R., and Sassetti, C.M. (2014). Subpolar addition of new cell wall is directed by DivIVA in mycobacteria. Proc. Natl. Acad. Sci. *111*, 3243–3251.

Mignot, T., and Zusman, D.R. (2007). Evidence that focal adhesion complexes power bacterial gliding motility. Science. *315*, 853-856.

Miles, S., Carpenter, B.M., Gancz, H., and Merrel, D.S. (2010). *Helicobacter pylori* Fur regulation appears unconserved across species. J. Microbiol. *48*, 378–386.

Mitri, S., and Foster, K.R. (2013). The genotypic view of social interactions in microbial communities. Annu. Rev. Genet. *47*, 247–273.

Miyata, M., and Hamaguchi, T. (2016). Prospects for the gliding mechanism of *Mycoplasma mobile*. Curr. Opin. Microbiol. *29*, 15–21.

Modolell, J., and Vázquez (1977). The inhibition of ribosomal translocation by viomycin. Eur. J. Biochem. *81*, 491–497.

Mohanty, B.K., and Kushner, S.R. (2016). Regulation of mRNA decay in bacteria. Annu. Rev. Microbiol. *70*, 25–44.

Mohanty, B.K., and Kushner, S.R. (2018). Enzymes involved in posttranscriptional RNA metabolism in gram-negative bacteria. Microbiol. Spectr. *11*, 1–16.

Molle, V., Palframan, W.J., Findlay, K.C., and Buttner, M.J. (2000). WhiD and WhiB, homologous proteins required for different stages of sporulation in *Streptomyces coelicolor* A3(2). J. Bacteriol. *182*, 1286–1295.

Moody, M.J., Young, R. A, Jones, S.E., and Elliot, M. A (2013). Comparative analysis of non-coding RNAs in the antibiotic-producing *Streptomyces* bacteria. BMC Genomics *14*, 1-17.

Morales, D.K., Grahl, N., Okegbe, C., Dietrich, L.E.P., Jacobs, N.J., and Hogan, A. (2013). Control of *Candida albicans* metabolism and biofilm formation by *Pseudomonas aeruginosa* Phenazines. mBio *4*, 1–9.

Murakami, T., Holt, T.G., and Thompson, C.J. (1989). Thiostrepton-induced gene expression in *Streptomyces lividans*. J. Bacteriol. *171*, 1459–1466.

Myronovskyi, M., Welle, E., Fedorenko, V., and Luzhetskyy, A. (2011). β-Glucuronidase as a sensitive and versatile reporter in actinomycetes. Appl. Environ. Microbiol. *77*, 5370–5383.

Nai, C., and Meyer, V. (2017). From axenic to mixed cultures: technological advances accelerating a paradigm shift in microbiology. Trends Microbiol. *26*, 538–554.

Nett, M., Ikeda, H., and Moore, B.S. (2009). Genomic basis for natural product biosynthetic diversity in the actinomycetes. Nat. Prod. Rep. *26*, 1362–1384.

Nicholson, A.W. (2013). Ribonuclease III mechanisms of double-stranded RNA cleavage. Wiley Interdiscip. Rev. RNA *5*, 31–48.

Nicol, G.W., Leininger, S., Schleper, C., and Prosser, J.I. (2008). The influence of soil pH on the diversity, abundance and transcriptional activity of ammonia oxidizing archaea and bacteria. Environ. Microbiol. *10*, 2966–2978.

Niehus, R., Picot, A., Oliveira, N.M., Mitri, S., and Foster, K.R. (2017). The evolution of siderophore production as a competitive trait. Evolution (N. Y). *71*, 1443–1455.

Nikolaev, N., and Silengo, L. (1973). A role for ribonuclease III in processing of ribosomal ribonucleic acid and messenger ribonucleic acid precursors in *Escherichia coli*. J. Biol. Chem. *248*, 7967-7949.

Nishimura, K., Hosaka, T., Tokuyama, S., Okamoto, S., and Ochi, K. (2007). Mutations in *rsmG*, encoding a 16S rRNA methyltransferase, result in low-level streptomycin resistance and antibiotic overproduction in *Streptomyces coelicolor* A3(2). J. Bacteriol. *189*, 3876–3883.

O'Meara, T.R., Xu, W., Selvig, K.M., O'Meara, M.J., Mitchell, A.P., and Alspaugh, J.A. (2014). The *Cryptococcus neoformans* Rim101 transcription factor directly regulates genes required for adaptation to the host. Mol. Cell. Biol. *34*, 673–684.

Ohlsen, K.L., Grimsley, J.K., and Hoch, J. A. (1994). Deactivation of the sporulation transcription factor Spo0A by the Spo0E protein phosphatase. Proc. Natl. Acad. Sci. U. S. A. *91*, 1756–1760.

Ojha, A., and Hatfull, G.F. (2007). The role of iron in *Mycobacterium smegmatis* biofilm formation: the exochelin siderophore is essential in limiting iron conditions for biofilm formation but not for planktonic growth. Mol. Microbiol. *66*, 468–483.

Okamoto, S., Lezhava, A., Hosaka, T., Okamoto-hosoya, Y., and Ochi, K. (2003). Enhanced expression of S-adenosylmethionine synthetase causes overproduction of actinorhodin in *Streptomyces coelicolor* A3 (2). J. Bacteriol. *185*, 601–609.

Oliveria, N.M., Martinez-Garcia, E., Xavier, J., Durham, W.M., Kolter, R., Kim, W., and Foster, K.R. (2015). Biofilm formation as a response to ecological competition. PLOS Biol. *13*, e1002191.

Padan, E., Bibi, E., Ito, M., and Krulwich, T.A. (2005). Alkaline pH homeostasis in bacteria: New insights. Biochim. Biophys. Acta - Biomembr. *1717*, 67–88.

Paget, M.S., Chamberlin, L., Atrih, A., Foster, S.J., and Buttner, M.J. (1999). Evidence that the extracytoplasmic function sigma factor sigmaE is required for normal cell wall structure in *Streptomyces coelicolor A3*(2). J. Bacteriol. *181*, 204–211.

Palková, Z., Janderová, B., Gabriel, J., Zikánová, B., Pospísek, M., and Forstová, J. (1997). Ammonia mediates communication between yeast colonies. Nature *390*, 532–536.

Patin, N. V, Duncan, K.R., Dorrestein, P.C., and Jensen, P.R. (2015). Competitive strategies differentiate closely related species of marine actinobacteria. ISME J. *10*, 1–13.

Patriquin, G.M., Banin, E., Gilmour, C., Tuchman, R., Greenberg, E.P., and Poole, K. (2008). Influence of quorum sensing and iron on twitching motility and biofilm formation in *Pseudomonas aeruginosa*. J. Bacteriol. *190*, 662–671.

Pelchovich, G., Omer-Bendori, S., and Gophna, U. (2013). Menaquinone and iron are essential for complex colony development in *Bacillus subtilis*. PLoS One *8*, 1–14.

Peleg, A.Y., Hogan, D. a, and Mylonakis, E. (2010). Medically important bacterial-fungal interactions. Nat. Rev. Microbiol. *8*, 340–349.

Price, B., Adamidis, T., Kong, R., and Champness, W. (1999). A *Streptomyces coelicolor* antibiotic regulatory gene, *absB*, encodes an RNase III homolog. J. Bacteriol. *181*, 6142-6151.

Proshkin, S., Rahmouni, A. R., Mironov, A., and Nudler, E. (2010). Cooperation between translating ribosomes and RNA polymerase in transcription elongation. Science *328*, 504–508.

Przybyla-Zawislak, B., Gadde, D.M., Ducharme, K., and McCammon, M.T. (1999). Genetic and biochemical interactions involving tricarboxylic acid cycle (TCA) function using a collection of mutants defective in all TCA cycle genes. Genetics *152*, 153–166.

Qin, D., and Fredrick, K. (2013). Analysis of polysomes from bacteria. Methods Enzymol. *530*, 159–172.

Ramamurthi, K.S., Lecuyer, S., Stone, H.A., and Losick, R. (2009). Geometric cue for protein

localization in a bacterium. Science (80). *323*, 1354–1357.

Ratzke, C., and Gore, J. (2018). Modifying and reacting to the environmental pH can drive bacterial interactions. PLoS Biol. *16*, 1–20.

Redko, Y., Galtier, E., Arnion, H., Darfeuille, F., Sismeiro, O., and Reuse, H. De (2016). RNase J depletion leads to massive changes in mRNA abundance in *Helicobacter pylori*. RNA Biol. *6286*, 243-253.

Rees, C.A., Smolinska, A., and Hill, J.E. (2016). The volatile metabolome of *Klebsiella pneumoniae* in human blood. J. Breath Res. *10*, 27101-27113.

Richards, D.M., Hempel, A.M., Flärdh, K., Buttner, M.J., and Howard, M. (2012). Mechanistic basis of branch-site selection in filamentous bacteria. PLoS Comput. Biol. *8*, 1-8.

Robinson, J.T. (2012). Integrated genomics viewer. Nat. Biotechnol. *29*, 24–26.

Roemer, T., Jiang, B., Davison, J., Ketela, T., Veillette, K., Breton, A., Tandia, F., Linteau, A., Sillaots, S., Marta, C., et al. (2003). Large-scale essential gene identification in *Candida albicans* and applications to antifungal drug discovery. Mol. Microbiol. *50*, 167–181.

Romano, J.D., and Kolter, R. (2005). *Pseudomonas - Saccharomyces* Interactions: influence of fungal metabolism on bacterial physiology and survival. J. Bacteriol. *187*, 940–948.

Rousk, J., Bååth, E., Brookes, P.C., Lauber, C.L., Lozupone, C., Caporaso, J.G., Knight, R., and Fierer, N. (2010). Soil bacterial and fungal communities across a pH gradient in an arable soil. ISME J. *4*, 1340–1351.

S Brooks, M., J Burdock, T., and E Ghaly, A. (2012). Changes in cell structure, morphology and activity of *Streptomyces venezuelae* during the growth, shocking and jadomycin production stages. J. Microb. Biochem. Technol. *4*, 63–75.

Salje, J., van den Ent, F., de Boer, P., and Löwe, J. (2011). Direct membrane binding by bacterial actin MreB. Mol. Cell *43*, 478–487.

Scherlach, K., Graupner, K., and Hertweck, C. (2013). Molecular bacteria-fungi interactions: effects on environment, food, and medicine. Annu. Rev. Microbiol. *67*, 375–397.

Schlimpert, S., Flärdh, K., and Buttner, M. (2016). Fluorescence time-lapse imaging of the complete *S. venezuelae* life cycle using a microfluidic device. J. Vis. Exp. *108,* 1–10.

Schmidt, R., Cordovez, V., de Boer, W., Raaijmakers, J., and Garbeva, P. (2015). Volatile affairs in microbial interactions. ISME J. *42,* 1–7.

Schmidt, R., Etalo, D.W., de Jager, V., Gerards, S., Zweers, H., de Boer, W., and Garbeva, P.

(2016). Microbial small talk: volatiles in fungal-bacterial interactions. Front. Microbiol. *6*, 1-12.

Schmitt, M.P., and Holmes, R.K. (1991). Iron-dependent regulation of diphtheria toxin and siderophore expression by the cloned *Corynebacterium diphtheriae* repressor gene *dtxR* in *C. diphtheriae* C7 strains. Infect. Immun. *59*, 1899–1904.

Schöller, C., Gurtler, H., Pedersen, R., Molin, S., and Wilkins, K. (2002). Volatile metabolites from Actinomycetes. J. Agric. Food Technol. *50*, 2615-2621.

Schroeckh, V., Scherlach, K., Nützmann, H.-W., Shelest, E., Schmidt-Heck, W., Schuemann, J., Martin, K., Hertweck, C., and Brakhage, A. A. (2009). Intimate bacterial-fungal interaction triggers biosynthesis of archetypal polyketides in *Aspergillus nidulans*. Proc. Natl. Acad. Sci. U. S. A. *106*, 14558–14563.

Schulz, S., and Dickschat, J.S. (2007). Bacterial volatiles: the smell of small organisms. Nat. Prod. Rep. *24*, 814–842.

Schumacher, M.A., Den Hengst, C.D., Bush, M.J., Le, T.B.K., Tran, N.T., Chandra, G., Zeng, W., Travis, B., Brennan, R.G., and Buttner, M.J. (2018). The MerR-like protein BldC binds DNA direct repeats as cooperative multimers to regulate *Streptomyces* development. Nat. Commun. *9*, 1–12.

Sello, J.K., and Buttner, M.J. (2008). The gene encoding RNase III in *Streptomyces coelicolor* is transcribed during exponential phase and is required for antibiotic production and for proper sporulation. J. Bacteriol. *190*, 4079–4083.

Serra, D.O., Richter, A.M., and Hengge, R. (2013). Cellulose as an architectural element in spatially structured *Escherichia coli* biofilms. J. Bacteriol. *195*, 5540–5554.

Serrano, R., Bernal, D., Simón, E., and Ariño, J. (2004). Copper and iron are the limiting factors for growth of the yeast *Saccharomyces cerevisiae* in an alkaline environment. J. Biol. Chem. *279*, 19698–19704.

Šetinová, D., Šmídová, K., Pohl, P., Music, I., and Bobek, J. (2018). RNase III-binding-mRNAs revealed novel complementary transcripts in *Streptomyces*. Front. Microbiol. *8*, 1–12.

Shaddox, T.W., Unruh, J.B., Kruse, J.K., and Restuccia, N.G. (2016). Solubility of iron, manganese, and magnesium sulfates and glucoheptonates in two alkaline soils. Soil Sci. Soc. Am. J. *80*, 765-770.

Shahbabian, K., Jamalli, A., Zig, L., and Putzer, H. (2009). RNase Y, a novel endoribonuclease, initiates riboswitch turnover in *Bacillus subtilis*. EMBO J. *28*, 3523–3533.

Shi, H., Bratton, B.P., Gitai, Z., and Huang, K.C. (2018). How to build a bacterial cell: MreB as the

foreman of *E. coli* construction. Cell *172*, 1294–1305.

Shirtliff, M.E., Peters, B.M., and Jabra-Rizk, M.A. (2009). Cross-kingdom interactions: *Candida albicans* and bacteria. FEMS Microbiol. Lett. *299*, 1–8.

Shrout, J.D. (2015). A fantastic voyage for sliding bacteria. Trends Microbiol. *23*, 1–3.

Srivastava, A. K., and Schlessinger, D. (1988). Coregulation of processing and translation: mature 5' termini of *Escherichia coli* 23S ribosomal RNA form in polysomes. Proc. Natl. Acad. Sci. U. S. A. *85*, 7144–7148.

Stamatakis, A. (2006). RAxML-VI-HPC: Maximum likelihood-based phylogenetic analyses with thousands of taxa and mixed models. Bioinformatics *22*, 2688–2690.

Strahl, H., Bürmann, F., and Hamoen, L.W. (2014). The actin homologue MreB organizes the bacterial cell membrane. Nat. Commun. *5*, 1–11.

Stubbendieck, R.M., and Straight, P.D. (2016). Multifaceted interfaces of bacterial competition. J. Bacteriol. *198*, 2145-2155.

Surovtsev, I. V., and Jacobs-Wagner, C. (2018). Subcellular organization: a critical feature of bacterial cell replication. Cell *172*, 1271–1293.

Tagami, K., Nanamiya, H., Kazo, Y., Maehashi, M., Suzuki, S., Namba, E., Hoshiya, M., Hanai, R., Tozawa, Y., Morimoto, T., et al. (2012). Expression of a small (p)ppGpp synthetase, YwaC, in the ppGpp mutant of *Bacillus subtilis* triggers YvyD-dependent dimerization of ribosome. Microbiology Open *1*, 115–134.

Tanaka, Y., Komatsu, M., Okamoto, S., Tokuyama, S., Kaji, A., Ikeda, H., and Ochi, K. (2009). Antibiotic overproduction by *rpsL* and *rsmG* mutants of various actinomycetes. Appl. Environ. Microbiol. *75*, 4919–4922.

Taverniti, V., Forti, F., Ghisotti, D., and Putzer, H. (2011). *Mycobacterium smegmatis* RNase J is a 5'-3' exo-/endoribonuclease and both RNase J and RNase E are involved in ribosomal RNA maturation. Mol. Microbiol. *82*, 1260–1276.

van Teeffelen, S., Wang, S., Furchtgott, L., Huang, K.C., Wingreen, N.S., Shaevitz, J.W., and Gitai, Z. (2011). The bacterial actin MreB rotates, and rotation depends on cell-wall assembly. Proc. Natl. Acad. Sci. *108*, 15822–15827.

Tenson, T., Lovmar, M., and Ehrenberg, M. (2003). The mechanism of action of macrolides, lincosamides and streptogramin B reveals the nascent peptide exit path in the Ribosome. J. Mol. Biol. *330*, 1005–1014.

Thom, G., and Prescott, C.D. (1997). The selection *in vivo* and characterization of an RNA recognition motif for spectinomycin. Bioorg. Med. Chem. *5*, 1081–1086.

Tillotson, R.D., Wösten, H.A.B., Richter, M., and Willey, J.M. (1998). A surface active protein involved in aerial hyphae formation in the filamentous fungus *Schizophillum* commune restores the capacity of a bald mutant of the filamentous bacterium *Streptomyces coelicolor* to erect aerial structures. Mol. Microbiol. *30*, 595–602.

Traag, B.A., and van Wezel, G.P. (2008). The SsgA-like proteins in actinomycetes: small proteins up to a big task. Antonie van Leeuwenhoek, Int. J. Gen. Mol. Microbiol. *94*, 85–97.

Trauner, A., Lougheed, K.E. a, Bennett, M.H., Hingley-Wilson, S.M., and Williams, H.D. (2012). The dormancy regulator DosR controls ribosome stability in hypoxic mycobacteria. J. Biol. Chem. *287*, 24053–24063.

Traxler, M.F., and Kolter, R. (2015). Natural products in soil microbe interactions and evolution. Nat. Prod. Rep. *00*, 1–15.

Traxler, M.F., and Watrous, J.D. (2013). Interspecies interactions stimulate diversification of the *Streptomyces coelicolor* secreted metabolome. mBio 1-12, *4*.

Traxler, M.F., Seyedsayamdost, M.R., Clardy, J., and Kolter, R. (2012). Interspecies modulation of bacterial development through iron competition and siderophore piracy. Mol. Microbiol. *86*, 628–644.

Tschowri, N., Schumacher, M.A., Schlimpert, S., Chinnam, N.B., Findlay, K.C., Brennan, R.G., and Buttner, M.J. (2014). Tetrameric c-di-GMP mediates effective transcription factor dimerization to control *Streptomyces* development. Cell *158*, 1136–1147.

Tu, D., Blaha, G., Moore, P.B., and Steitz, T. A. (2005). Structures of MLSBK antibiotics bound to mutated large ribosomal subunits provide a structural explanation for resistance. Cell *121*, 257–270.

Tunca, S., Barreiro, C., Sola-Landa, A., Coque, J.J.R., and Martín, J.F. (2007). Transcriptional regulation of the desferrioxamine gene cluster of *Streptomyces coelicolor* is mediated by binding of DmdR1 to an iron box in the promoter of the *desA* gene. FEBS J. *274*, 1110–1122.

Tyc, O., Zweers, H., de Boer, W., and Garbeva, P. (2015). Volatiles in inter-specific bacterial interactions. Front. Microbiol. *6*, 1-15.

Ueta, M., Yoshida, H., Wada, C., Baba, T., Mori, H., and Wada, A. (2005). Ribosome binding proteins YhbH and YfiA have opposite functions during 100S formation in the stationary phase of *Escherichia coli*. Genes Cells *10*, 1103–1112.

Ueta, M., Wada, C., and Wada, A. (2010). Formation of 100S ribosomes in *Staphylococcus aureus* by the hibernation promoting factor homolog SaHPF. Genes Cells *15*, 43–58.

Ueta, M., Wada, C., Daifuku, T., Sako, Y., Bessho, Y., Kitamura, A., Ohniwa, R.L., Morikawa, K., Yoshida, H., Kato, T., et al. (2013). Conservation of two distinct types of 100S ribosome in bacteria. Genes Cells *18*, 554–574.

Valleriani, A., Zhang, G., Nagar, A., Ignatova, Z., and Lipowsky, R. (2011). Length-dependent translation of messenger RNA by ribosomes. Phys. Rev. E. Stat. Nonlin. Soft Matter Phys. *83*, 1-4.

Ventura, M., Canchaya, C., Tauch, A., Chandra, G., Fitzgerald, G.F., Chater, K.F., and van Sinderen, D. (2007). Genomics of Actinobacteria: tracing the evolutionary history of an ancient phylum. Microbiol. Mol. Biol. Rev. *71*, 495–548.

Viegas, S.C., Silva, I.J., Saramago, M., Domingues, S., and Arraiano, C.M. (2011). Regulation of the small regulatory RNA MicA by ribonuclease III: a target-dependent pathway. Nucleic Acids Res. *39*, 2918–2930.

Vockenhuber, M.-P., Sharma, C.M., Statt, M.G., Schmidt, D., Xu, Z., Dietrich, S., Liesegang, H., Mathews, D.H., and Suess, B. (2011). Deep sequencing-based identification of small non-coding RNAs in *Streptomyces coelicolor*. RNA Biol. *8*, 468–477.

Wada A., Akira, Igarashi, K., Shoko, Y. Aimoto, and S. Ishihama, A. (1995). Ribosome modulation factor: stationary growth phase-specific inhibitor of ribosome functions from *Escherichia coli*. Biochem and Biophys. Research comm. *214*, 410–417.

Wada, A., Yamazaki, Y., Fujita, N., and Ishihama, A. (1990). Structure and probable genetic location of a “ribosome modulation factor” associated with 100S ribosomes in stationary-phase *Escherichia coli* cells. Proc. Natl. Acad. Sci. U. S. A. *87*, 2657–2661.

Wang, L. (2003). Control of growth, secondary metabolism and sporulation in *Streptomyces venezuelae* ISP5230 by *jadW1*, a member of the *afsA* family of gamma-butyrolactone regulatory genes. Microbiology *149*, 1991–2004.

Wang, C., Wang, Z., Qiao, X., Li, Z., Li, F., Chen, M., Wang, Y., Huang, Y., and Cui, H. (2013). Antifungal activity of volatile organic compounds from *Streptomyces alboflavus* TD-1. FEMS Microbiol. Lett. *341*, 45–51.

Wang, L., Yu, Y., He, X., Zhou, X., Deng, Z., Chater, K.F., and Tao, M. (2007). Role of an FtsK-like protein in genetic stability in *Streptomyces coelicolor* A3(2). J. Bacteriol. *189*, 2310–2318.

Wang, L., Tian, X., Wang, J., Yang, H., Fan, K., Xu, G., Yang, K., and Tan, H. (2009). Autoregulation

of antibiotic biosynthesis by binding of the end product to an atypical response regulator. Proc. Natl. Acad. Sci. U. S. A. *106*, 8617–8622.

Wang, X., Koehler, S.A., Wilking, J.N., Sinha, N. N., Cabeen, M.T., Srinivasan, S., Seminara, A., Rubinstein, S., Sun, Q., Brenner, M.P., et al. (2016). Probing phenotypic growth in expanding *Bacillus subtilis* biofilms. Appl. Microbiol. Biotechnol. *100*, 4607–4615.

Wargo, M.J., and Hogan, D. a (2006). Fungal--bacterial interactions: a mixed bag of mingling microbes. Curr. Opin. Microbiol. *9*, 359–364.

Westhoff, S., van Wezel, G., and Rozen, D. (2017). Distance dependent danger responses in bacteria. Curr. Opin. Microbiol. *36*, 95–101.

Westphal, H., and Crouch, R.J. (1975). Cleavage of adenovirus messenger RNA and of 28S and 18S ribosomal RNA by RNase III. Proc. Natl. Acad. Sci. U. S. A. *72*, 3077–3081.

Wheatley, R.E. (2002). The consequences of volatile organic compound mediated bacterial and fungal interactions. Antonie Van Leeuwenhoek *81*, 357–364.

Wilkins, K., and Schöller, C. (2009). Volatile organic metabolites from selected *Streptomyces* strains. Actinomycetologica *23*, 27–33.

Willemse, J., Borst, J.W., De Waal, E., Bisseling, T., and Van Wezel, G.P. (2011). Positive control of cell division: FtsZ is recruited by SsgB during sporulation of *Streptomyces*. Genes Dev. *25*, 89–99.

Wilson, D.N. (2014). Ribosome-targeting antibiotics and mechanisms of bacterial resistance. Nat. Rev. Microbiol. *12*, 35–48.

Wolanski, M., Donczew, R., Kois-Ostrowska, A., Masiewicz, P., Jakimowicz, D., and Zakrzewska-Czerwinska, J. (2011). The level of AdpA directly affects expression of developmental genes in *Streptomyces coelicolor*. J. Bacteriol. *193*, 6358–6365.

Wright, P.R., Richter, A.S., Papenfort, K., Mann, M., Vogel, J., Hess, W.R., Backofen, R., and Georg, J. (2013). Comparative genomics boosts target prediction for bacterial small RNAs. Proc. Natl. Acad. Sci. U. S. A. *110*, 3487-3496.

Xu, W., Huang, J., and Cohen, S.N. (2008). Autoregulation of AbsB (RNase III) expression in *Streptomyces coelicolor* by endoribonucleolytic cleavage of *absB* operon transcripts. J. Bacteriol. *190*, 5526–5530.

Xu, W., Huang, J., Lin, R., Shi, J., and Cohen, S.N. (2010). Regulation of morphological differentiation in *S. coelicolor* by RNase III (*absB*) cleavage of mRNA encoding the AdpA transcription factor. Mol. Microbiol. *75*, 781–791.

Yamanaka, K., Oikawa, H., Ogawa, H.O., Hosono, K., Shinmachi, F., Takano, H., Sakuda, S., Beppu, T., and Ueda, K. (2005). Desferrioxamine E produced by *Streptomyces* griseus stimulates growth and development of *Streptomyces tanashiensis*. Microbiology *151*, 2899–2905.

Yamazaki, H., Ohnishi, Y., and Horinouchi, S. (2003). Transcriptional switch on of *ssgA* by A-factor, which is essential for spore septum formation in *Streptomyces griseus*. J. Bacteriol. *185*, 1273–1283.

Yang, K., Han, L., He, J., Wang, L., and Vining, L.C. (2001). A repressor-response regulator gene pair controlling jadomycin B production in *Streptomyces venezuelae* ISP5230. Gene *279*, 165–173.

Yoon, V., and Nodwell, J.R. (2014). Activating secondary metabolism with stress and chemicals. J. Ind. Microbiol. Biotechnol. *41*, 415–424.

Yoshida, H., Maki, Y., Kato, H., Hisao, F., Izutsu, K., Wada, C., and Wada, A. (2002). The ribosome modulation factor (RMF) binding site on the 100S ribosome of *Escherichia coli*. J. Biol. Chem. *132*, 983–989.

Zhang, Y., Pan, G., Zou, Z., Fan, K., Yang, K., and Tan, H. (2013). JadR*-mediated feed-forward regulation of cofactor supply in jadomycin biosynthesis. Mol. Microbiol. *90*, 884–897.

Zheng, J.-T. (2005). Cytotoxic activities of new jadomycin derivatives. J Antibiot *58*, 405–408.

Zheng, J.-T., Wang, S.-L., and Yang, K.-Q. (2007). Engineering a regulatory region of jadomycin gene cluster to improve jadomycin B production in *Streptomyces venezuelae*. Appl. Microbiol. Biotechnol. *76*, 883–888.

Zhou, X., Halladin, D.K., and Theriot, J.A. (2016). Fast mechanically driven daughter cell separation is widespread in Actinobacteria. mBio *7*, 1–6.

Zhu, Y., Jameson, E., Crosatti, M., Schäfer, H., Rajakumar, K., Bugg, T.D.H., and Chen, Y. (2014). Carnitine metabolism to trimethylamine by an unusual Rieske-type oxygenase from human microbiota. Proc. Natl. Acad. Sci. U. S. A. *111*, 4268–4273.